Nitric oxide signalling and the regulation of cardiac repolarisation

Thesis submitted for the degree of

Doctor of Philosophy

at the University of Leicester

by

Rachel Caves BSc

Department of Cell Physiology and Pharmacology

University of Leicester

2014

Abstract   **Rachel Caves**

Nitric oxide signalling and the regulation of cardiac repolarisation

Nitric oxide (NO) signalling has been recently linked with cardiac repolarisation. Studies from isolated heart preparations have demonstrated a protective effect from ventricular fibrillation following vagus nerve stimulation, which is NO-dependent. Genome-wide association studies have linked NO signalling components to arrhythmias. A role for NO signalling has also been described in the diurnal variation of cardiac muscle responses to sympathetic stimulation. The cellular and molecular mechanisms for NO regulation of ventricular repolarisation by cGMP-dependent signalling were investigated using BAY 60-2770, a novel NO/haem-independent soluble guanylyl cyclase (sGC) activator and compared with the NO donor SNAP. Experiments were performed on guinea pig isolated left ventricular myocytes. Cellular cGMP was selectively quantified by radioimmunoassay. Action potentials and the slow (I_{Ks}) and rapid (I_{Kr}) delayed rectifier K^+ currents were recorded using the perforated patch-clamp technique. BAY 60-2770 applied under basal conditions, modestly increased cellular cGMP levels and shortened action potential duration (APD), but failed to modulate I_{Ks} or I_{Kr}. In contrast, SNAP failed to modulate APD despite greater increases in cGMP compared with BAY 60-2770. When phosphodiesterases (PDEs) were inhibited, BAY 60-2770 increased cGMP levels much more, prolonged APD and inhibited I_{Ks} (but not I_{Kr}).The mechanism for inhibition of I_{Ks} did not involve protein kinase G. These results demonstrate that PDE activity suppresses elevations of cGMP in response to sGC activation, and also compartmentalises cGMP-dependent signalling. Thus, PDEs uncouple changes in cGMP levels from ion channels located at the sarcolemma. In addition, APD shortening in response to isoprenaline exhibited diurnal variation, with greater shortening in active compared to resting period myocytes. However, this effect was not blocked by nitric oxide synthase inhibition.

In conclusion, NO signalling pathways may be able to regulate cardiac repolarisation through a cGMP-dependent mechanism, but PDEs act to limit these responses in the healthy myocardium.

Acknowledgements

Contents

Chapter 3. Responses of cellular cGMP levels and action potentials to modulation of cGMP-dependent signalling in guinea pig ventricular myocytes   74

Publications

In addition to the work presented in this thesis, I've contributed to two publications studying I_{Kr} pharmacology. In brief, I determined the potency of human ether-a-go-go related gene (hERG) blocker analogues and investigated the effect of a drug that reorganises the endoplasmic reticulum, on hERG currents in human embryonic kidney cells stably expressing hERG channels.

Cavalli, A., Buonfiglio, R., Ianni, C., Masetti, M., Ceccarini, L., **Caves, R.**, Chang, M.W., Mitcheson, J.S., Roberti, M., Recanatini, M., 2012. Computational design and discovery of "minimally structured" hERG blockers. *Journal of Medicinal Chemistry*. **55**, 4010-4014.

Varadarajan, S., Bampton, E.T., Smalley, J.L., Tanaka, K., **Caves, R.E.**, Butterworth, M., Wei, J., Pellecchia, M., Mitcheson, J., Gant, T.W., Dinsdale, D., Cohen, G.M., 2012. A novel cellular stress response characterised by a rapid reorganisation of membranes of the endoplasmic reticulum. *Cell Death and Differentiation*. **19,** 1896-1907.

Abstracts:

Physiological Society Meeting, Manchester, UK, September 2012 (presentation and poster)
The role of cGMP dependent nitric oxide signalling on cardiac repolarisation in adult guinea pig ventricular myocytes.

Biophysical Society 57th Annual Meeting, Philadelphia, Pennsylvania, February 2013 (poster)
The role of cGMP dependent nitric oxide signalling on cardiac repolarisation in adult guinea pig ventricular myocytes.

International Union of Physiological Sciences (IUPS) Meeting, Birmingham, UK, July 2013 (poster)
Differential regulation of slow and rapid delayed rectifier potassium currents by cGMP dependent nitric oxide signalling pathways in isolated adult guinea pig ventricular myocytes.

Biophysical Society 58th Annual Meeting, San Francisco, California, February 2014 (poster)
Differential regulation of slow and rapid delayed rectifier potassium currents by cGMP dependent nitric oxide signalling pathways in isolated adult guinea pig ventricular myocytes.

Authors: Rachel E. Caves, Kieran E. Brack, André Ng, John S. Mitcheson

Abbreviations

^{125}I	*iodine-125*
8-Br-cGMP	*8-bromo-cyclic guanosine monophosphate*
AC	*adenylyl cyclase*
ACh	*acetylcholine*
ANOVA	*analysis of variance*
AP	*action potential*
APD	*action potential duration*
APD$_{90}$	*action potential duration to 90% repolarisation*
ATP	*adenosine triphosphate*
BAY 60-2770	*(4-({{(4-carboxybutyl)[2-(5-fluoro-2-{[4'(trifluoromethyl)bi phenyl-4-yl]methoxy} phenyl)ethyl]amino}methyl)benzoic acid)*
BH$_4$	*tetrahydrobiopterin*
BSA	*albumin from bovine serum*
CaM	*calmodulin*
cAMP	*cyclic adenosine monophosphate*
CAPON	*carboxy-terminal PDZ ligand of neuronal nitric oxide synthase*
cGMP	*cyclic guanosine monophosphate*
CNB	*cyclic nucleotide binding*
DAF-2 DA	*4,5-diaminofluorescein diacetate*
DI	*diastolic interval*
DMSO	*dimethyl sulfoxide*
DPM	*disintegrations per minute*
DPPX	*dipeptidyl-aminopeptidase-like protein 6*
e$^-$	*electron*
E4031	*N-[4-[[1-[2-(6-Methyl-2-pyridinyl)ethyl]-4-piperidinyl]carbonyl]phenyl] methane sulfonamide dihydrochloride*
ECC	*excitation-contraction coupling*
EDTA	*ethylene diamine tetraacetic acid*

EGTA	*ethylene glycol tetraacetic acid*
E_K	*equilibrium potential for potassium*
E_{Na}	*equilibrium potential for sodium*
eNOS	*endothelial nitric oxide synthase/NOS3*
FAD	*flavin adenine dinucleotide*
FMN	*flavin mononucleotide*
FSK	*forskolin*
GTP	*guanosine triphosphate*
H105	*histidine 105*
H89	*N-[2-(p-Bromocinnamylamino)ethyl]-5-isoquinoline sulfonamide dihydrochloride*
hERG	*human ether-a-go-go related gene*
IBMX	*3-isobutyl-1-methylxanthine*
IC_{50}	*half maximal inhibitory concentration*
$I_{Ca,L}$	*L-type calcium current*
I_{CNG}	*cyclic nucleotide-gated current*
I_{K1}	*inward rectifier potassium current*
I_{Kr}	*rapid delayed rectifier potassium current*
I_{Ks}	*slow delayed rectifier potassium current*
I_{Kur}	*ultra-rapid delayed rectifier potassium current*
I_{Na}	*sodium current*
iNOS	*inducible nitric oxide synthase/NOS2*
ISO	*isoprenaline*
I_{To}	*transient outward potassium current*
I-V	*current-voltage*
JNJ 303	*2-(4-Chlorophenoxy)-2-methyl-N-[5 [(methylsulfonyl) amino]tricycle [3.3.1.13,7]dec-2-yl]-propanamide*
KChIP2	*K_v channel-interacting protein 2*
Klf15	*krüppel-like factor 15*

KT5823	*(9S,10R,12R)-2,3,9,10,11,12-Hexahydro-10-methoxy-2,9-dimethyl-1-oxo-9,12-epoxy-1H-diindolo[1,2,3-fg:3',2',1'-kl]pyrrolo[3,4-i][1,6]benzodiazocine-10-carboxylic acid, methyl ester*
L-NNA	*N-Nitro-L-arginine*
LQTS	*long QT syndrome*
MinK	*minimal potassium channel*
MiRP1	*minK-related peptide 1*
MLC	*myosin light chain*
MLCK	*myosin light chain kinase*
MLCP	*myosin light chain phosphatase*
mRNA	*messenger ribonucleic acid*
NADPH	*nicotinamide adenine dinucleotide phosphate-oxidase*
nNOS	*neuronal nitric oxide synthase/NOS1*
NO	*nitric oxide*
NOS	*nitric oxide synthase*
ns	*no significance*
ODQ	*1H-[1,2,4]Oxadiazolo[4,3-a]quinoxalin-1-one*
$ONOO^-$	*peroxynitrite*
PAS	*Per-Arnt-Sim*
PDE	*phosphodiesterase*
PDZ	*post-synaptic density-protein, discs-large, ZO-1*
PIP_2	*phosphatidylinositol 4,5-bisphosphate*
PKA	*protein kinase A/cAMP-dependent protein kinase*
PKG	*protein kinase G/cGMP-dependent protein kinase*
PLB	*phospholamban*
QT_c	*QT interval corrected for heart rate*
RIA	*radioimmunoassay*
SEM	*standard error of the mean*
SERCA	*sarcoplasmic/endoplasmic reticulum calcium ATPase*
sGC	*soluble guanylyl cyclase*
SNAP	*S-nitroso-N-acetylpenicillamine*

SR	*sarcoplasmic reticulum*
TCA	*trichloroacetic acid*
VF	*ventricular fibrillation*
VNS	*vagus nerve stimulation*

Chapter 1

Introduction

1.1 Nitric oxide signalling

1.1.1 Nitric oxide synthesis

Nitric oxide (NO) is a free radical gaseous signalling molecule that has localised effects due to high reactivity with iron-containing haem groups, and other free radicals (Tamargo *et al.*, 2010(1)). NO diffuses quickly from its source and is oxidised to nitrite and nitrate, thus ceasing signalling. Therefore, synthesis of NO must occur rapidly and on demand under physiological conditions (Miller & Megson, 2007).

NO synthesis occurs when nitric oxide synthase (NOS) enzymes catalyse the conversion of L-arginine into L-citrulline (Ziolo *et al.*, 2008). The metabolic pathway of NO synthesis also requires multiple co-factors which include, nicotinamide adenine dinucleotide phosphate-oxidase (NADPH), flavin adenine dinucleotide (FAD), flavin mononucleotide (FMN), tetrahydrobiopterin (BH_4), haem and O_2 (Zhou & Zhu, 2009). Three distinct isoforms of NOS are expressed in the heart, nNOS (neuronal), iNOS (inducible) and eNOS (endothelial) which are also known as NOS1, NOS2 and NOS3 respectively (Ziolo *et al.*, 2008). The activity and expression of nNOS and eNOS differs from that of iNOS. All three isoforms can bind calmodulin (CaM) which in turn binds Ca^{2+}. However, the activities of nNOS and eNOS are Ca^{2+}-dependent, in contrast to the Ca^{2+}-independent activity of iNOS. In the healthy heart, nNOS and eNOS are constitutively expressed (Brahmajothi & Campbell, 1999), whereas iNOS expression is induced by an increase in cytokines under pathophysiological conditions (Arstall *et al.*, 1999). nNOS is expressed in cardiac myocytes and cardiac autonomic nerves whereas eNOS is expressed in coronary vascular endothelium, endocardium and to a lesser extent in cardiac myocytes (Tamargo *et al.*, 2010(1)). In addition, the expression of nNOS and eNOS is compartmentalised in specific microdomains of myocytes with nNOS

localised at the sarcoplasmic recticulum (SR) membrane (Xu *et al.*, 1999) and eNOS localised at the sarcolemma t-tubule caveolae (Feron *et al.*, 1996). Similarities exist between the structure of eNOS and nNOS and the process of NO production. The structure of nNOS will be discussed in further detail as nNOS is the predominant source of NO in cardiac myocytes. Active nNOS exists as a homodimer and each monomer is comprised of a C-terminal reductase domain and an N-terminal oxygenase domain which are linked by a CaM binding motif (Zhang *et al.*, 2014). Binding sites for NADPH, FAD and FMN are located on the reductase domain. Whereas, the oxygenase domain contains binding sites for L-arginine, haem and BH_4 and is where NO production occurs. The oxidation of NADPH to $NADP^+$ generates an electron (e^-) which is transported from the reductase domain to iron (Fe) in the oxygenase domain via FAD and FMN (Figure 1.1). This process is facilitated by the binding of CaM which acts as an allosteric activator of nNOS (Zhou & Zhu, 2009). CaM dissociates from nNOS in the presence of low concentrations of intracellular Ca^{2+} which slows down the flow of electrons between FAD and FMN and renders nNOS inactive (Matsuda & Iyanagi, 1999). Thus, intracellular Ca^{2+} concentration is the predominant regulator of nNOS activity. However, the activity of nNOS can also be regulated by other mechanisms, such as phosphorylation (Song *et al.*, 2004; Rameau *et al.*, 2004). As a monomer nNOS is inactive and dimerisation requires binding of BH_4 and L-arginine. BH_4 binding is fundamental as it plays a role in stabilising the dimer, protects NOS from proteolysis, increases the affinity for L-arginine and provides an electron which is vital for the conversion of L-arginine into L-citrulline (Munzel *et al.*, 2005). Zinc (Zn) also helps to stabilise the dimer by binding to the oxygenase domain of each monomer to prevent uncoupling (Zou *et al.*, 2002), as shown in Figure 1.1, B. However, NOS uncouples under pathophysiological conditions resulting in the generation of superoxide (O_2^-) and peroxynitrite ($ONOO^-$) as electrons are diverted to O_2 as opposed to L-arginine. The non-selective NOS inhibitor N-Nitro-L-arginine (L-NNA) antagonises the electron transfer to L-arginine or O_2 and therefore inhibits NO and O_2^- production, in coupled and uncoupled NOS respectively (Munzel *et al.*, 2005). L-NNA is a widely used inhibitor of NOS and was used in subsequent experiments.

Figure 1.1
Nitric oxide synthase structure and the pathway for nitric oxide synthesis.
Nitric oxide synthase has a C-terminal reductase domain with NADPH, FAD and FMN binding sites and an N-terminal oxygenase domain with L-arginine (ARG), haem and BH_4 binding sites. These domains are separated by a calmodulin (CaM) binding motif which facilitates electron (e^-) flow from NADPH to iron (Fe). BH_4 donates an electron which plays a fundamental role in the conversion of L-arginine and O_2 into L-citrulline and NO. Zinc (Zn) binding to the oxygenase domain helps to stabilise the dimer. (A) Representation of a NOS monomer and the pathway involved in NO synthesis. The post-synaptic density-protein, discs-large, ZO-1 *(*PDZ) domain can bind regulatory proteins such as CAPON (carboxy-terminal PDZ ligand of nNOS). Taken from Zhang *et al.* (2014). (B) Representation of coupled dimeric NOS and uncoupled monomeric NOS, which produce NO and O_2^- respectively. Modified from Munzel *et al.* (2005).
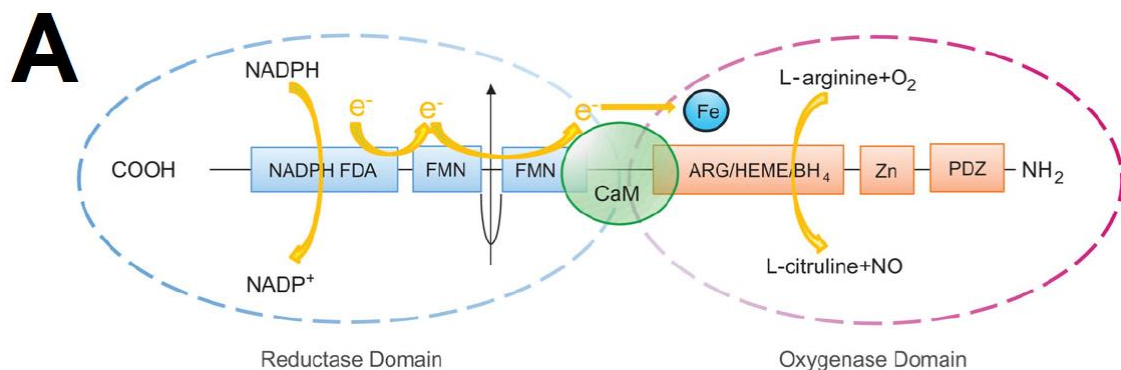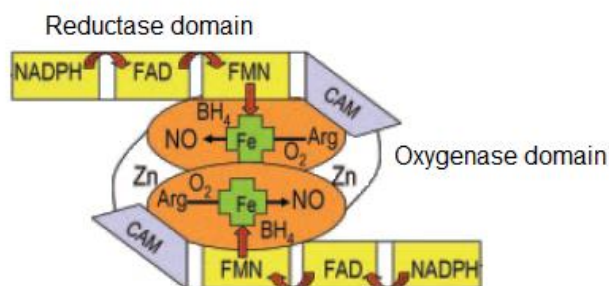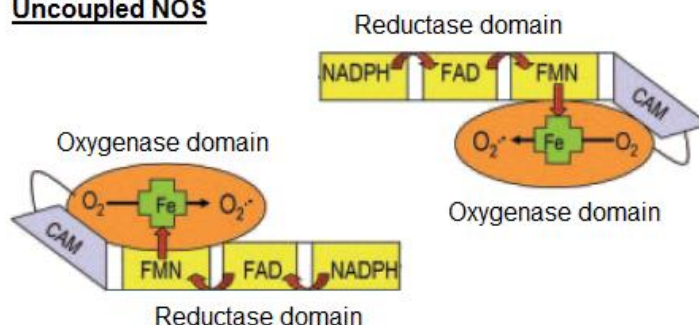
1.1.2 Nitric oxide donor drugs

The importance of NO as a signalling molecule was emphasised when it was identified as the endothelium-derived relaxing factor in the 1980's (Palmer *et al.*, 1987). Compounds that release NO have been used as therapeutic medications long before the discovery of NO as a signalling molecule. However, the therapeutic use of NO gas is limited due to the risk of oxidation. Therefore, a more suitable method of delivery is via molecular carriers known as NO donors, which stabilise NO until release (Miller & Megson, 2007). During recent decades, research into NO signalling has grown extensively and a variety of NO donor drugs have been developed, but few are used routinely in clinical practice. The two types of NO donors used clinically are organic nitrates and nitroprusside. These differ as organic nitrates are pro-drugs whereby an enzymatic reaction of denitration is required to release NO, whereas nitroprusside releases NO without metabolism (Iachini Bellisarii *et al.*, 2012).

Organic nitrates, such as glyceryl trinitrate and isosorbide mononitrate/dinitrate are the most common NO donor drugs used clinically nowadays (Iachini Bellisarii *et al.*, 2012). The main therapeutic effects are through vasodilation of diseased blood vessels which improves blood flow and the symptoms associated with diseases such as angina and heart failure. A disadvantage of organic nitrates is that prolonged use leads to the development of tolerance. Preventing tolerance requires cease of use periodically, which proves problematic especially in chronic cases (Miller & Megson, 2007). In addition, organic nitrates improve symptoms but fail to have long term beneficial effects or reduce mortality rates. In contrast to organic nitrates, nitroprusside is used clinically in extreme cases of hypertension, and causes vasodilation independently of the endothelium. The relative stability of nitroprusside means that release of NO does not occur spontaneously, there is a requirement for light or sulphur-containing reducing agents found within tissues (Grossi & D'Angelo, 2005). In addition, rare cases of cyanidosis have been associated with prolonged use due to release of cyanide groups contained within the structure.

NO hybrid drugs are another type of NO donor. NO hybrid drugs are novel compounds which incorporate NO into the structure of established and clinically used drugs for an additional beneficial effect (Miller & Megson, 2007). Nonsteroidal anti-inflammatory drugs such as aspirin, are used as a prophylactic to prevent heart attacks, strokes and blood clot formation. However, it is known that gastrointestinal tract problems are a frequent side-effect of long term aspirin use. Nitroaspirins retain the pharmacological properties of aspirin and counteract the side-effects on the gastrointestinal tract (Fiorucci *et al.*, 2004). NO and nitrate have also been incorporated into other drugs such as statins, which are used to decrease cholesterol levels, captopril which is an angiotensin-converting enzyme inhibitor used to treat hypertension and nicorandil which is used to prevent and treat angina. The number of coronary events in angina patients was decreased by nicorandil (IONA Study Group, 2002), which is an improvement over current organic nitrate use.

Other NO donor drugs which are used experimentally with the potential for future therapeutic use include S-nitrosothiols and diazeniumdiolates also known as NONOates. Under physiological conditions, NONOates decompose spontaneously. Accurate prediction of the release rate of NO can be achieved as the rate of decomposition is not increased by thiols or tissue (Morley & Keefer, 1993). Tissue-independent release of NO is proposed as an explanation for the lack of tolerance associated with the use of NONOates. S-nitrosothiols are characterised by an NO group bonded to a thiol group by a single chemical bond which breaks down under physiological conditions to generate NO and a disulphide (Al-Sa'doni & Ferro, 2000). Light, heat, enzymes and other thiol groups are among the multiple factors with the capability of releasing NO from S-nitrosothiols (Miller & Megson, 2007). Lack of tolerance, tissue specificity and dose-dependent inhibition of platelets with no vascular effect are major advantages associated with the use of S-nitrosothiols (de Belder *et al.*, 1994). S-nitroso-N-acetylpenicillamine (SNAP) is a widely used S-nitrosothiol and was used in subsequent experiments. The chemical structure of SNAP is shown in Figure 1.2.

Figure 1.2
Chemical structure of the nitric oxide donor SNAP. The NO group is circled, bonded to the sulphur atom of a thiol group by a single covalent bond. Modified from Miller & Megson, (2007).
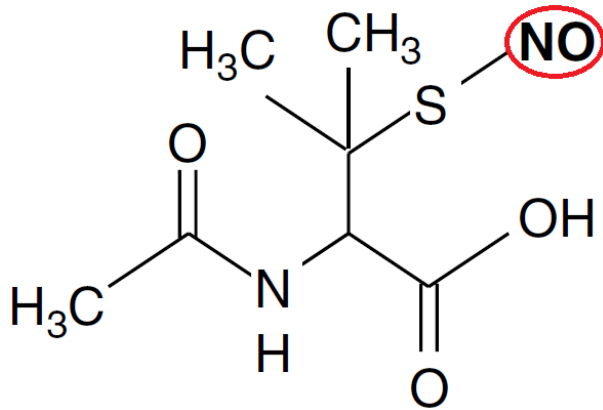
1.1.3 cGMP-dependent nitric oxide signalling

Two distinct types of NO signalling pathways have been widely described, one of which is cyclic guanosine monophosphate (cGMP)-dependent and another which is cGMP-independent (Ziolo *et al.*, 2008) and will be discussed in later sections. A summary of NO signalling is shown in Figure 1.3. In cGMP-dependent NO signalling, NO binds to the haem group of soluble guanylyl cyclase (sGC) resulting in its activation. Activation of sGC catalyses the conversion of guanosine triphosphate (GTP) into cGMP, thus increasing cGMP levels. cGMP is an important second messenger that directly activates protein kinase G (PKG) and can indirectly regulate protein kinase A (PKA) via cyclic nucleotide phosphodiesterases (PDEs) and cyclic adenosine monophosphate (cAMP). Protein kinases mediate the effects of cyclic nucleotides by phosphorylating protein targets, such as ion channels and proteins involved in excitation-contraction coupling (ECC). Hydrolysis of cyclic nucleotides by PDEs ceases signalling.

Figure 1.3

Nitric oxide signalling pathways. NOS catalyses the conversion of L-arginine into L-citrulline and NO and is under the regulation of the autonomic nervous system. NO signalling can be mediated via cGMP-dependent or cGMP-independent pathways. cGMP-dependent NO signalling activates sGC, increases cGMP and directly activates PKG. PKA activity can also be indirectly regulated via PDEs and cAMP. cGMP-independent NO signalling occurs by reaction with superoxide to generate $ONOO^-$ or through the process of S-nitrosylation. cGMP-dependent and cGMP-independent NO signalling regulates the activity of ion channels and ECC proteins.
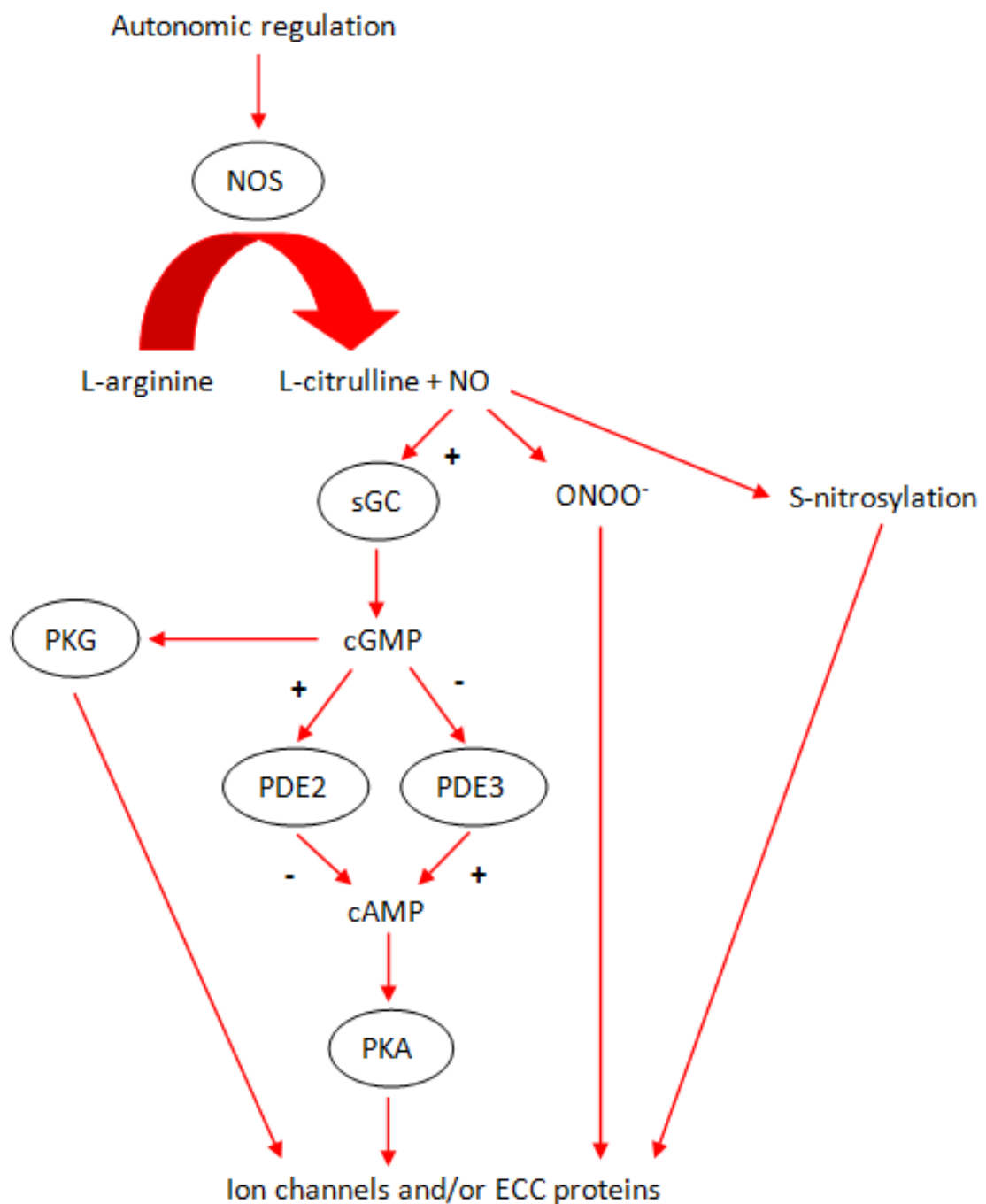
1.1.3.1 Soluble guanylyl cyclase

Soluble guanylyl cyclase (sGC) is an important target for therapeutic and experimental interventions. The structural features of sGC and its activation by NO are summarised in Figure 1.4. sGC is a heterodimeric NO receptor that catalyses the conversion of GTP into cGMP (Krumenacker *et al.*, 2004). A single α and β subunit dimerise to form sGC (Harteneck *et al.*, 1990). The α and β subunits each exist as two isoforms, α_1 and α_2, and β_1 and β_2 (Harteneck *et al.*, 1991; Russwurm *et al.*, 1998; Yuen *et al.*, 1990). In humans the most abundant sGC dimer is $\alpha_1\beta_1$ (Munzel *et al.*, 2005). The isoforms are expressed throughout the body but display differential tissue distribution. The levels of expression of α_1 and β_1 are high in many tissues, including the heart (Budworth *et al.*, 1999; Nakane *et al.*, 1990). The subunits of sGC consist of three distinct domains, an N-terminal regulatory domain, a central dimerisation domain and a C-terminal catalytic domain (Andreopoulos & Papapetropoulos, 2000). The N-terminal domain binds to haem, a heterocyclic prosthetic group containing a central iron (Fe) atom that binds NO. The single haem group is orientated between the α and β subunits, thus dimerisation is necessary prior to haem binding. The β_1 subunit contains a key residue, histidine 105 (H105) that is important in haem binding and NO sensitivity. Mutation of H105 results in haem deficiency and NO unresponsiveness. H105 is integral because when NO binds to the haem group of sGC, Fe^{2+} is moved out of the porphyrin plane slightly and the bond between H105 and Fe^{2+} is broken (Wedel *et al.*, 1994) (Figure 1.4, B). This forms a nitrosyl haem complex and a conformational change in the receptor that influences the catalytic domain and causes an increase in sGC activity (Pyriochou & Papapetropoulos, 2005). The central domain contains the dimerisation region, of which the only known function is the combining of the α and β subunits to form a heterodimer (Wilson & Chinkers, 1995). Dimerisation is also fundamental for catalytic activity as the residues that are involved in recognition of the substrate are spread over the C-terminal catalytic domains of both subunits (Wedel *et al.*, 1995). The C-terminal catalytic domain is highly conserved with other cyclase enzymes, and is responsible for binding GTP and converting it into cGMP (Koesling, 1999).

Figure 1.4
Soluble guanylyl cyclase structure and activation by nitric oxide.
(A) Representation of the structure of sGC. A heterodimer consisting of α and β subunits each comprised of an N-terminal regulatory domain containing a haem group with a central Fe^{2+} that binds NO, a central dimerisation domain and a C-terminal catalytic domain that catalyses the conversion of GTP into cGMP. Modified from Andreopoulos & Papapetropoulos, (2000). (B) Representation of the activation of sGC by NO. In its inactive state sGC exists as a five membered ring structure and Fe^{2+} is bound to histidine 105 (His) a residue found on the β_1 subunit. Upon NO binding to Fe^{2+} a six membered structure is formed. In its active form the bond between histidine 105 and Fe^{2+} is broken forming a five membered nitrosyl haem complex. Modified from Bellamy & Garthwaite, (2002).
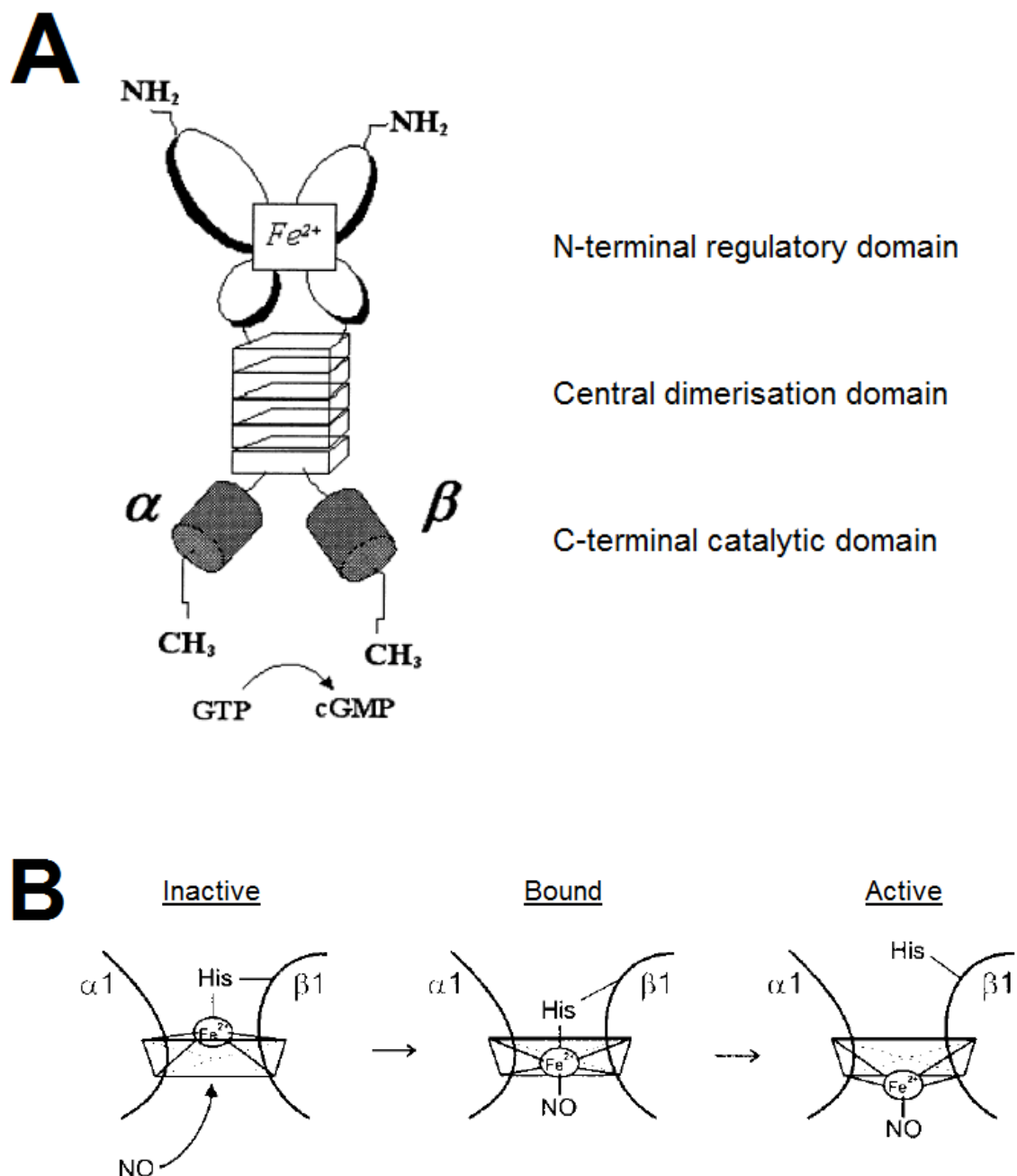
1.1.3.1.1 Soluble guanylyl cyclase inhibition

In order to distinguish sGC-mediated signalling from other signalling pathways it is useful to have a selective inhibitor of sGC. A compound that has fulfilled this role is 1H-[1,2,4]oxadiazolo-[4,3-a]quinoxalin-1-one also known as ODQ. ODQ binds to the haem group of sGC in competition with NO and inhibits sGC by oxidising the haem group (Lies *et al.*, 2013). Although, NO can bind to both ferrous/Fe^{2+} and ferric/Fe^{3+} haem, the affinity for NO binding is considerably higher for ferrous haem. In addition, the release of H105 upon NO binding and the subsequent conformational change is prominent only in sGC with ferrous haem (Fritz *et al.*, 2011). Therefore, oxidised ferric sGC is unresponsive to NO binding. The mechanisms involved in the regulation of sGC by ODQ and NO are summarised in Figure 1.5.

A study by Zhao *et al.* (2000) investigated the molecular mechanism by which ODQ inhibits sGC. The effect of ODQ on recombinant sGC was determined using electronic absorption spectroscopy and by measuring sGC activity. Upon application of ODQ, the electronic absorption spectra showed that the Soret peak shifted from 431 nm to 392 nm. This is characteristic of oxidation of the ferrous haem to ferric haem, which is consistent with other studies. The basal activity of sGC was not altered by ODQ, up to concentrations of 100 µM. However, ODQ inhibited NO-stimulated sGC activity. ODQ-oxidised sGC could be reduced by application of reducing agents and subsequent NO-stimulated sGC activity was identical to that prior to oxidation by ODQ. This evidence and the lack of effect on basal sGC activity further suggests that inhibition by ODQ is due to oxidation of haem as opposed to an effect on the catalytic domain. Since haem is oxidised by the loss of one electron, the presence of an organic radical was investigated. Upon ODQ application, an organic radical was detected, which is likely to be a protein-based radical or an ODQ radical due to the direct transfer of one electron from sGC to ODQ.

Figure 1.5
A mechanistic model of soluble guanylyl cyclase regulation by ODQ and nitric oxide through redox reactions. Ferrous/Fe^{II} haem (1) binds ODQ resulting in oxidation to ferric/Fe^{III} haem (2) and the generation of an ODQ radical. NO can bind but not activate ferric/Fe^{III} haem (3) which can be reduced back to ferrous/Fe^{II} haem (1) by reducing agents. Ferrous/Fe^{II} haem (1) can also bind NO to form a ferrous-nitrosyl haem complex (4) breaking the bond with histidine 105 (His). Modified from Zhao *et al.* (2000).
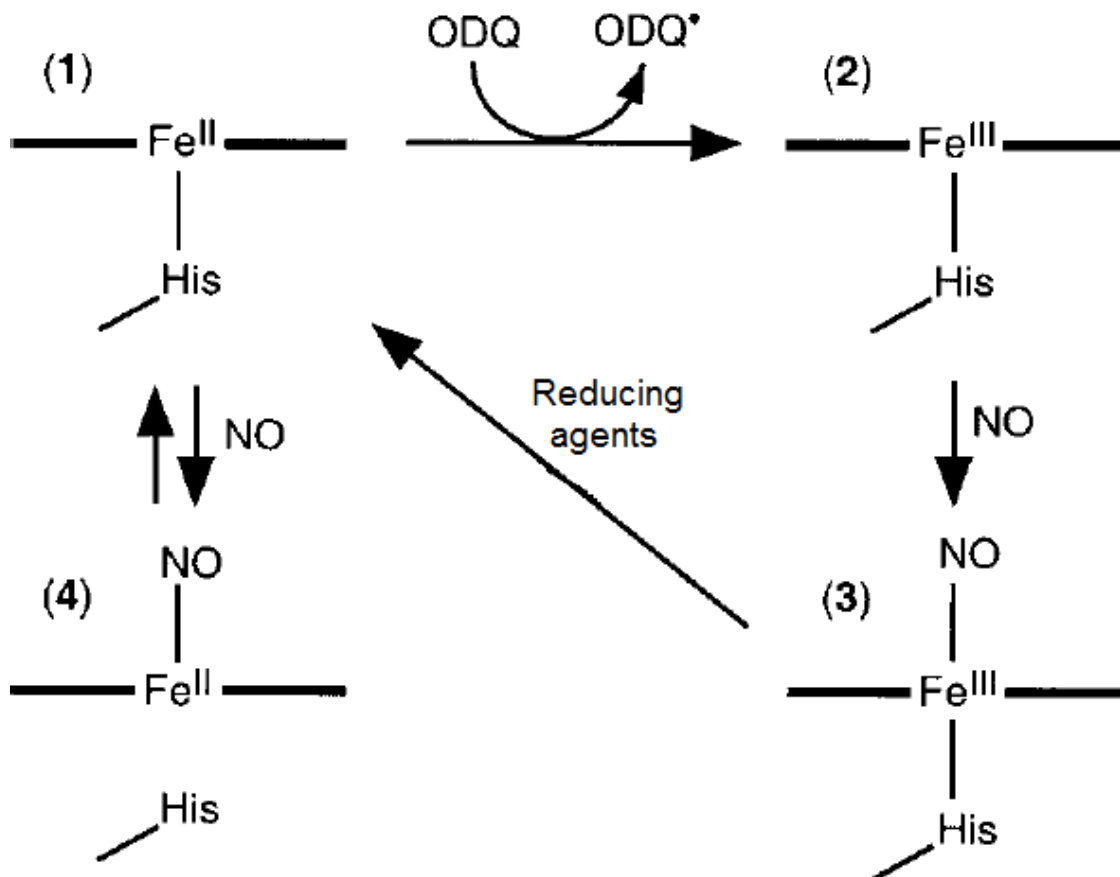
1.1.3.1.2 Soluble guanylyl cyclase activators and stimulators

As previously described, sGC can exist in two different states, a reduced ferrous NO-sensitive state and an oxidised ferric NO-insensitive state, which through the loss of haem can also become haem-free (Tamargo *et al.*, 2010(2)). cGMP-dependent NO signalling becomes disrupted in a range of cardiovascular diseases in which oxidative stress plays a role, such as heart failure. This is likely due to an increase in oxidised/haem-free NO-insensitive sGC, among other factors such as a decrease in NO synthesis or availability, and an increase in cGMP degradation by PDEs (Schmidt *et al.*, 2009). Therefore, drugs which can activate sGC in a NO/haem-independent manner may have potential for future therapeutic use (Tamargo *et al.*, 2010(2)). Two different types of drugs, haem-dependent sGC stimulators and haem-independent sGC activators, have been developed to investigate this. These drugs differ as haem-dependent sGC stimulators enhance the NO sensitivity of sGC in its reduced ferrous state, whereas haem-independent sGC activators activate oxidised/haem-free NO-insensitive sGC (Schmidt *et al.*, 2009). BAY 58-2667 also known as cinaciguat, is a novel and potent NO/haem-independent sGC activator developed by Bayer AG, which binds to the haem binding pocket of sGC. The amino acid residues histidine 105, tyrosine 135 and arginine 139 located in the haem binding pocket have been identified as fundamental residues involved in sGC activation by BAY 58-2667 and haem binding (Schmidt *et al.*, 2004).

An *in-vitro* study on purified sGC by Stasch *et al.* (2002) provides evidence that BAY 58-2667 activates sGC in a haem-independent manner. Ultra violet spectroscopy found that upon NO application, the Soret peak characteristically shifted to a lower wavelength which is indicative of NO binding to haem. However, there was no change with the application of BAY 58-2667, suggesting it does not bind to haem. Furthermore, BAY 58-2667 activated sGC after removal of haem by detergents and oxidation of haem by ODQ. Interestingly, BAY 58-2667-induced sGC activity was higher in the presence of ODQ. BAY 58-2667 and ODQ in combination, resulted in a potent concentration-dependent increase in sGC activity. Receptor binding studies indicated that submicromolar

concentrations of BAY 58-2667 were sufficient for saturation of binding to sGC, in the presence of ODQ. The maximum saturation decreased by half in the absence of ODQ. As BAY 58-2667 is a weaker activator of sGC compared to NO, a higher concentration of BAY 58-2667 is required to exert similar effects to organic nitrates. However, concentrations as low as 1 nM produced physiologically relevant increases in cGMP and the effects are longer lasting due to a low clearance and long half-life which is therapeutically promising. Animal models and clinical trials have demonstrated that BAY 58-2667 increases cardiac output, decreases blood pressure by potent vasodilation, is cardioprotective similar to ischaemic preconditioning and inhibits platelet aggregation (Lapp *et al.*, 2009; Krieg *et al.*, 2009; Stasch *et al.*, 2002). In phase II clinical trials on patients with acute decompensated heart failure, BAY 58-2667 unloaded the heart but also a caused substantial decrease in blood pressure (Erdmann *et al.*, 2013). Hypotension is a concerning side-effect associated with use of BAY 58-2667. Therefore, although BAY 58-2667 can improve symptoms and does not induce tolerance, these trials have failed to provide substantial evidence on safety and the effectiveness in long term outcome, such as mortality (Tamargo *et al.*, 2010(2)). As an alternative to BAY 58-2667, Bayer AG kindly provided a closely related chemical analogue BAY 60-2770. The chemical structures of the novel NO/haem-independent sGC activators are shown in Figure 1.6. An *in-vitro* study on purified sGC by Knorr *et al.* (2008) demonstrated that BAY 60-2770 shared similar characteristics with BAY 58-2667. The application of 0.0001 to 10 µM concentrations of BAY 60-2770 increased sGC activity between 2 and 53 fold over basal activity, in a concentration-dependent manner. BAY 60-2770-induced increases in sGC activity were potentiated at all concentrations in the presence of 10 µM ODQ. The activity of sGC increased substantially by 176 fold with 10 µM BAY 60-2770, in combination with ODQ. Furthermore, haem-free sGC was also activated by BAY 60-2770 in the absence and presence of ODQ. In the presence of ODQ, 10 µM BAY 60-2770 increased sGC activity dramatically by 242 fold. However, ODQ failed to potentiate the response to BAY 60-2770 in haem-free sGC. BAY 60-2770 was used as a novel NO/haem-independent sGC activator in subsequent experiments to investigate the role of cGMP-dependent signalling pathways in cardiac repolarisation.

Figure 1.6
Chemical structures of NO/haem-independent soluble guanylyl cyclase activators BAY 58-2667 and BAY 60-2770. The additional structural features of BAY 60-2770 are circled. Modified from Schmidt *et al.* (2009).
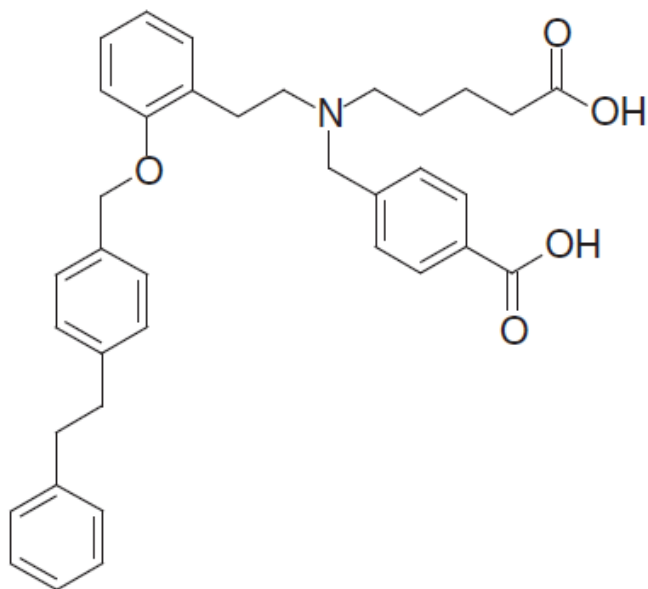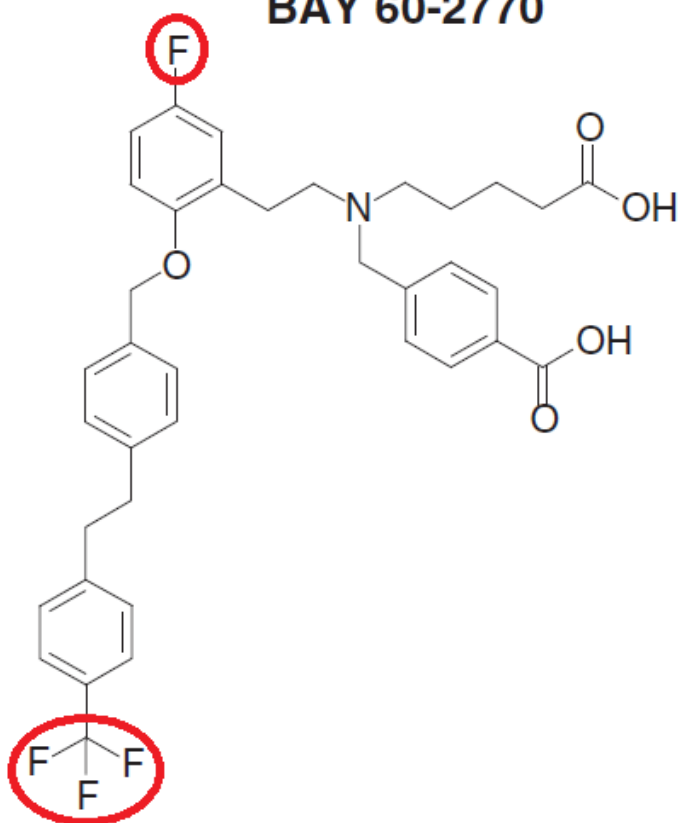
1.1.3.2 Phosphodiesterases

Phosphodiesterases (PDEs) are responsible for the degradation of cGMP but also play an integral role in the compartmentalisation of cGMP signalling which allows signal specificity. PDEs are classified into eleven broad families that differ in multiple ways, including substrate specificity, regulation and tissue expression (Maurice *et al.*, 2003). PDEs 1, 2, 3, 10 and 11 hydrolyse both cAMP and cGMP, thus have dual substrate specificity (Bender & Beavo, 2006). In contrast, PDEs 4, 7 and 8 specifically hydrolyse cAMP, and PDEs 5, 6 and 9 are cGMP-specific (Maurice *et al.*, 2003). At least seven subtypes of PDEs have been described in the heart PDEs 1-5, 8 and 9 (Zaccolo & Movsesian, 2007). PDE5 is the most widely studied, as selective PDE5 inhibition with sildenafil is a potential treatment for heart failure (Guazzi *et al.*, 2011). In heart failure patients and animal models, cGMP degradation is increased due to an increase in PDE5 expression (Pokreisz *et al.*, 2009; Lu *et al.*, 2010). In contrast, human cardiac myocytes have relatively low expression levels of PDE5 under normal physiological conditions (Takimoto *et al.*, 2005(1)). Cardiac PDEs can also be inhibited non-selectively by 3-isobutyl-1-methylxanthine (IBMX). IBMX is known to inhibit PDEs 1-5 by binding to and interacting with conserved residues within a common active site sub-pocket. Huai *et al.* (2004) found that the majority of IBMX binding residues were highly conserved between PDEs 4 and 5. However, it has been proposed that some cardiac PDEs are insensitive to inhibition by IBMX. Wang *et al.* (2008(3)) found that the catalytic domain of PDE8A1 was IBMX insensitive, with an IC_{50} of 700 μM. Additionally, PDE9A also exhibits IBMX insensitivity (Fisher *et al.*, 1998; Soderling *et al.*, 1998). Despite this, IBMX is a widely used cardiac PDE inhibitor and was used in subsequent experiments. In addition to differences in expression and sensitivity to inhibitors, PDEs are also differentially regulated. PDE1 is stimulated by Ca^{2+}-CaM and PDEs 2 and 5 are stimulated by cGMP (Zhang & Kass, 2011). In contrast, PDE3 is inhibited by cGMP (Miller & Yan, 2010). Since PDEs 2 and 3 are differentially regulated by cGMP but also hydrolyse cAMP, this allows cross-talk between cGMP and cAMP signalling. Thus elevation of cGMP can increase levels of cAMP in some cells and decrease it in others, depending on the cell-

specific expression levels of PDEs. The regulation, substrate specificity and expression of PDE isoforms is summarised in Figure 1.7.

Changes in cyclic nucleotide levels regulate protein kinase activity. Protein kinases are enzymes that modulate the activity of proteins through phosphorylation. Target proteins include the L-type Ca^{2+} channel, phospholamban (PLB), the ryanodine receptor and contractile proteins, all of which play key roles in ECC (Fischmeister *et al.*, 2005). Protein kinase G is an important effector molecule for cGMP. In addition, cGMP can also directly activate cGMP-gated cation channels. However, these channels are not expressed in the cardiovascular system but are often used as an experimental tool to investigate cGMP signalling (Tsai & Kass, 2009). Classically, cGMP is viewed as the second messenger for the parasympathetic regulation of the heart and acts in opposition to cAMP signalling. Thus, cGMP and cAMP signalling are closely interlinked but have contrasting effects.

1.1.3.3 Protein kinase G

Protein kinase G (PKG), also known as cGMP-dependent protein kinase, mediates many effects of cGMP. PKG modulates the activity of proteins by phosphorylating serine and threonine residues and is thus known as a serine/threonine kinase (Takimoto, 2012). PKG exists in three isoforms, PKG-Iα, PKG-Iβ and PKG-II. Different genes encode PKG-I and PKG-II, whereas PKG-Iα and PKG-Iβ are splice variants of a single gene (Wernet *et al.*, 1989). PKG-I is highly expressed in vascular smooth muscle cells and endothelial cells, with lower expression levels in cardiac myocytes (Draijer *et al.*, 1995; Mery *et al.*, 1991). However, PKG-I is the predominant isoform in the cardiovascular system, whereas PKG-II expression is found largely in the brain, kidney and intestine (Uhler, 1993; Jarchau *et al.*, 1994).

PKG-I and PKG-II have a homodimeric structure, with two identical monomer subunits. Figure 1.8 summarises the structural features of PKG. On each subunit, three different functional domains can be found, an N-terminal domain, a regulatory domain and a C-terminal catalytic domain (Takimoto, 2012). The N-

terminal domain is involved in high affinity dimerisation and also inhibits the catalytic domain in the absence of cGMP. These features are governed by the leucine/isoleucine zipper motif and the auto-inhibitory contacts, which overlap with the auto-phosphorylation subdomain (Richie-Jannetta *et al.*, 2003; Monken & Gill, 1980). The structural features of the regulatory domain include two allosteric binding sites for cGMP (Lincoln *et al.*, 1977) and the C-terminal catalytic domain contains an adenosine triphosphate (ATP) binding site that is essential for phosphotransferase activity. cGMP binding induces a change in conformation and auto-phosphorylation. This in turn increases the affinity for further cGMP binding and relieves the inhibition on the catalytic domain, resulting in PKG activation (Francis *et al.*, 2010). PKG is then able to phosphorylate target proteins such as PDE5. Phosphorylation of PDE5 leads to an increase in cGMP hydrolysis and a subsequent decrease in cGMP levels. PKG-mediated phosphorylation of PDE5 is an important negative feedback mechanism in cGMP-dependent signalling (Corbin *et al.*, 2000) and may also be important for compartmentalising cGMP within particular cellular regions.

To investigate PKG-mediated signalling, membrane-permeable analogues of cGMP are commonly used tools. In fact, some cGMP analogues activate PKG more effectively than cGMP. However, others bind to the allosteric sites without causing a substantial increase in catalytic activity, and are therefore used as PKG inhibitors as they prevent cGMP binding. The use of cGMP analogues is advantageous as they are resistant to hydrolysis compared to cGMP and direct activation of PKG allows circumvention of other parts of the signalling pathway (Francis *et al.*, 2010). 8-bromo-cyclic guanosine monophosphate (8-Br-cGMP) is a widely used PKG-activating cGMP analogue and was used in subsequent experiments. Protein kinase inhibitors include (9*S*,10*R*,12*R*)-2,3,9,10,11,12-Hexahydro-10-methoxy-2,9-dimethyl-1-oxo-9,12-epoxy-1*H*-diindolo[1,2,3-*fg*:3',2',1'-*kl*]pyrrolo[3,4-*i*][1,6]benzodiazocine-10-carboxylic acid, methyl ester (KT5823) and N-[2-(p-Bromocinnamylamino)ethyl]-5-isoquinoline sulfonamide dihydrochloride (H89) which were also used in experiments to inhibit PKG and PKA respectively. Both inhibitors compete with ATP for the binding site on the catalytic domain (Gambaryan *et al.*, 2012; Hidaka & Kobayashi, 1992).

Figure 1.7
Summary of phosphodiesterase isoform regulation, substrate specificity and expression in the heart. PDE1 is regulated by Ca^{2+}-CaM, PDE2 is stimulated by cGMP and PDE3 is inhibited by cGMP. PDEs 1-3 have dual substrate specificity, whereas PDEs 4 and 8 specifically hydrolyse cAMP and PDEs 5 and 9 specifically hydrolyse cGMP. PDEs 1-5, 8 and 9 are all expressed in cardiac tissue. Modified from Takimoto, (2012).

PDE isoform	Regulation/ substrate specificity	Cardiac expression
PDE1	Ca^{2+}/CaM regulated, Dual specificity	Yes
PDE2	cGMP-stimulated, Dual specificity	Yes
PDE3	cGMP-inhibited, Dual specificity	Yes
PDE4	cAMP-specific	Yes
PDE5	cGMP-specific	Yes
PDE8	cAMP-specific	Yes
PDE9	cGMP-specific	Yes

Figure 1.8
Protein kinase G structure and activation by cGMP. Representation of the structure of protein kinase G. A homodimer consisting of two identical subunits each comprised of an N-terminal domain with a leucine zipper motif and overlapping auto-inhibitory and auto-phosphorylation sites, a regulatory domain with two allosteric cGMP binding sites and a C-terminal catalytic domain where the catalytic site is located. Modified from Francis *et al*. (2010).
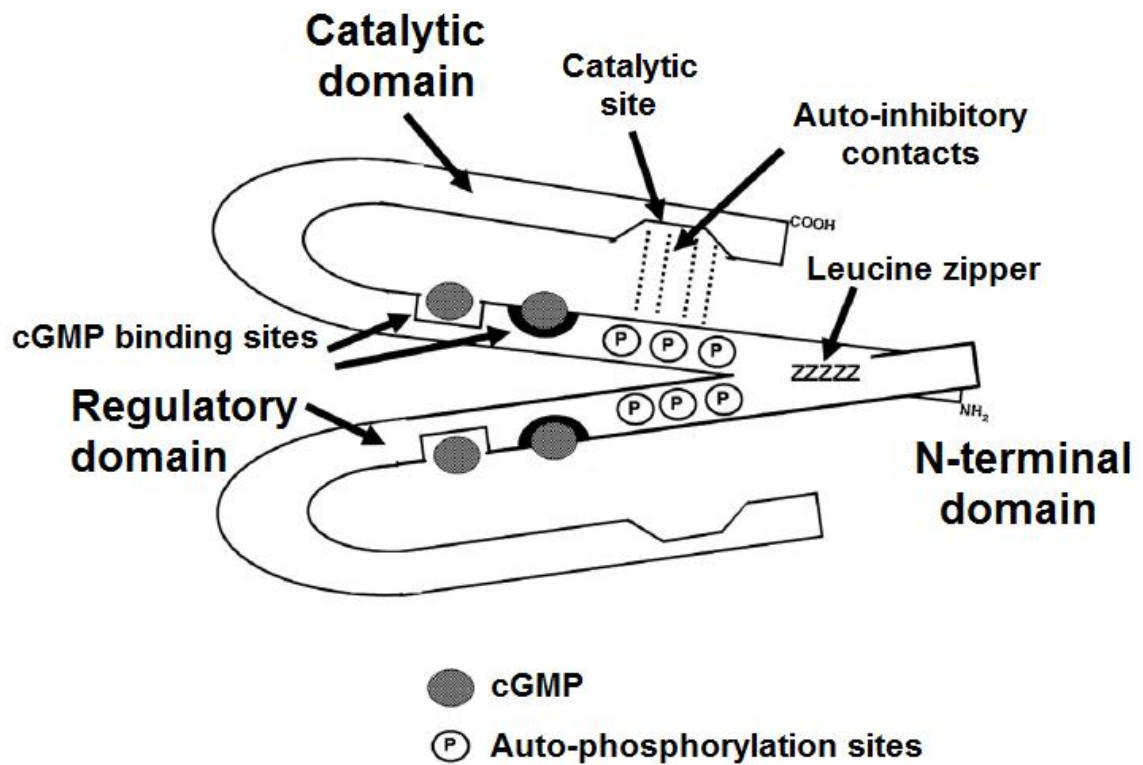
1.1.4 cGMP-independent nitric oxide signalling

NO can also exert effects via cGMP-independent signalling pathways. For instance, NO can react with superoxide to generate peroxynitrite (Stamler, 1994). However, the primary mechanism involved in cGMP-independent NO signalling is S-nitrosylation (Ziolo *et al.*, 2008). S-nitrosylation is a reversible form of protein modification that involves the conversion of a thiol group into an S-nitrosothiol. A thiol group contains a sulphur-hydrogen covalent bond which is broken during S-nitrosylation and the hydrogen atom is replaced by an NO group. In addition, NO groups can be transferred between thiols or between a transition metal and a thiol by transnitrosylation (Gonzalez *et al.*, 2009). S-nitrosylation is reversed by denitrosylation, which involves enzymes such as S-nitrosoglutathione reductase and thioredoxin reductase (Lima *et al.*, 2010).

Cysteine, an amino acid found in proteins such as ion channels, contains a thiol group. Therefore, ion channel activity can be modulated by S-nitrosylation of cysteine residues. S-nitrosylation also regulates proteins involved in ECC, such as ryanodine receptors which release Ca^{2+} from the SR. Cardiac ryanodine receptors contain multiple thiol sites that can undergo S-nitrosylation, resulting in a progressive increase in activity and Ca^{2+} efflux due to an increase in opening probability (Xu *et al.*, 1998; Stoyanovsky *et al.*, 1997). Under pathophysiological conditions, S-nitrosylation may be a cardioprotective mechanism against irreversible oxidation (Sun *et al.*, 2007).

S-nitrosylated proteins can be detected and quantified by a variety of techniques, of which the biotin switch technique is the most widely used (Gonzalez *et al.*, 2009). This technique involves blocking free thiol groups with methyl groups upon the application of a methylating agent. Ascorbate is then applied to reduce the S-nitrosylated thiols to free thiol groups, which are subsequently labelled with a thiol-specific biotinylating agent. Finally, an anti-biotin antibody is used to detect the biotin labelled thiol groups, which were originally S-nitrosylated (Sun & Murphy, 2010). Therefore, this technique can detect which proteins are S-nitrosylated and also quantify the relative amounts of S-nitrosylated thiol groups present within a protein.

1.1.5 The role of nitric oxide signalling in vasodilation

NO signalling exerts multiple physiological effects, of which vascular dilation is the most widely characterised. Maintaining vascular tone is fundamental in the regulation of blood pressure and becomes disrupted under pathophysiological conditions such as hypertension and atherosclerosis. The intricate balance of vasoconstrictor and vasodilator signalling governs vascular tone (Surks, 2007). The discovery of NO as the endothelium-derived relaxing factor (Palmer *et al.*, 1987), gave rise to a new era of research investigating the role of NO signalling under physiological and pathophysiological conditions in various tissues (Loscalzo, 2013).

The NO/sGC/cGMP/PKG signalling pathway has been found to be important in mediating vasodilation (Arnold *et al.*, 1977; Rapoport & Murad, 1983; Archer *et al.*, 1994). The contraction and relaxation of vascular smooth muscle is linked to the phosphorylation and dephosphorylation of the myosin light chain (MLC) which regulates the ATPase activity of myosin and cross-bridge cycling. Myosin light chain kinase (MLCK) and myosin light chain phosphatase (MLCP) phosphorylate and dephosphorylate MLC respectively. Dephosphorylation of MLC by MLCP favours relaxation (Somlyo & Somlyo, 1994). PKG has been proposed to activate MLCP, thus mediating vasodilation (Surks *et al.*, 1999; Lee *et al.*, 1997; Wu *et al.*, 1996).

NO-mediated effects are primarily protective, such as anti-atherosclerosis, in which eNOS-derived NO inhibits vascular smooth muscle cell proliferation and platelet aggregation and adhesion (Cornwell *et al.*, 1994; Radomski *et al.*, 1990). Thus, atherosclerosis is initiated and accelerated under conditions in which NO is reduced (Munzel *et al.*, 2005). Under normal physiological conditions, picomolar to nanomolar concentrations of NO are sufficient to exert physiological effects (Miller & Megson, 2007).

1.1.6 The role of nitric oxide signalling in the heart

The role of NO signalling within cardiac muscle is less clear, but is important in the regulation of excitation-contraction coupling (ECC) and β-adrenergic signalling (Ziolo et al., 2008). During exercise, metabolic demands increase which results in a multitude of physiological changes, one of which is an increase in contractility. Contractility is linked to the electrical activity by ECC and in turn ECC is predominantly regulated by β-adrenergic signalling. Interestingly, contractility is differentially influenced by nNOS and eNOS due to differences in localisation and signalling targets (Ziolo, 2008). ECC is a highly co-ordinated sequence of events that begins with excitation of individual cardiac myocytes and ends with contraction of the whole heart. During cardiac myocyte excitation, action potentials are triggered by activation of voltage-gated Na^+ channels, Na^+ influx and depolarisation of the cell membrane. This is turn activates L-type Ca^{2+} channels on the sarcolemma resulting in Ca^{2+} influx. A further increase in intracellular Ca^{2+} is triggered due to Ca^{2+}-induced Ca^{2+} release, in which Ca^{2+} is released from stores within the SR via ryanodine receptors (Valdeolmillos et al., 1989). Cardiac myocyte contraction is initiated when Ca^{2+} binds to troponin C causing a conformational change of the troponin-tropomyosin complex on the thin myofilaments, revealing myosin binding sites on actin and allowing myosin cross-bridge cycling to occur. Conversely, myocyte relaxation is initiated when cytosolic Ca^{2+} falls, due to Ca^{2+} being pumped into the SR by the SR Ca^{2+} ATPase (SERCA) and removed from the cell by the sarcolemma Na^+/Ca^{2+} exchanger (Bers, 2002). Classic β-adrenergic signalling is mediated by $β_1$- and $β_2$-adrenergic G-protein coupled receptors. $β_1$- and $β_2$-adrenergic receptors couple to $G_{αs}$ which stimulates adenylyl cyclase (AC), increasing cAMP and activating PKA resulting in an increase in contractility. However, the discovery and characterisation of the $β_3$-adrenergic receptor in the human heart has been shown to decrease contractility (Gauthier et al., 1996). $β_3$-adrenergic receptor activation occurs at high catecholamine concentrations, suggesting it plays an important protective role during sympathetic overstimulation by antagonising $β_1$- and $β_2$-adrenergic receptor activity (Moens et al., 2010). However, increased $β_3$-adrenergic receptor

expression in failing human hearts compared to non-failing hearts has been proposed to be detrimental by exacerbating the effects of heart failure (Moniotte *et al.*, 2001). The β_3-adrenergic receptor couples with and activates eNOS, thus its effects are mediated by NO (Saraiva & Hare, 2006). Cawley *et al.* (2011) demonstrated that application of a β_3-selective adrenergic receptor agonist (BRL37344) elicited a negative inotropic (force of contraction) effect in wild-type mice but had no effect in sGC_{α_1} subunit deficient mice. Thus, establishing a role for the cGMP-dependent β_3-adrenergic signalling pathway. β-adrenergic receptors can also be stimulated non-selectively by the widely used agonist isoprenaline (ISO), which was used in this study.

1.1.6.1 Physiological nitric oxide signalling in the heart

1.1.6.1.1 Physiological relevance of nNOS signalling

Differential regulation of contractility by nNOS and eNOS are due to differences in subcellular localisation and signalling targets. Under normal physiological conditions, nNOS is localised to the SR and co-immunoprecipitates with the ryanodine receptor (Xu *et al.*, 1999; Barouch *et al.*, 2002). The ryanodine receptor is integral for Ca^{2+}-induced Ca^{2+} release from the SR during ECC. In a study on myocytes from nNOS knockout mice, Gonzalez *et al.* (2007) reported an increase in Ca^{2+} leak from ryanodine receptors and an elevation in diastolic Ca^{2+} levels, which correlated with a more arrhythmic phenotype compared to wild-type myocytes. nNOS knockout myocytes exhibited a decrease in S-nitrosylation of the ryanodine receptor, suggesting that S-nitrosylation is important in normal ryanodine receptor function. Another target for nNOS signalling is phospholamban (PLB), which regulates the activity of the SERCA. SERCA is inhibited by unphosphorylated PLB and phosphorylation relieves this inhibition. Wang *et al.* (2008(1)) found that inhibition of nNOS in wild-type mice reduced PLB phosphorylation and decreased contraction in both unstimulated and β-adrenergic receptor stimulated myocytes. In contrast, contraction was unaffected by nNOS inhibition in myocytes from PLB knockout mice. This suggests that nNOS is important for phosphorylation of PLB, and that PLB is

integral to the nNOS-mediated stimulatory effect on contraction. In a separate study, Barouch *et al.* (2002) also found that nNOS knockout mice exhibited a depressed inotropic response to β-adrenergic receptor stimulation with ISO compared with wild-type mice. Xanthine oxidoreductase, an enzyme which generates superoxide, is another nNOS signalling target. nNOS co-immunoprecipitates with and inhibits xanthine oxidoreductase. An increase in superoxide production was found in hearts from nNOS knockout mice and these myocytes also exhibited suppressed contractility (Khan *et al.*, 2004). Overall, these studies suggest that nNOS has a stimulatory effect on contractility and plays a role in reducing oxidative stress which would otherwise lead to suppressed contractility.

1.1.6.1.2 Physiological relevance of eNOS signalling

The localisation, signalling targets and physiological effects of eNOS differs from that of nNOS. Under normal physiological conditions eNOS is localised to the sarcolemma caveolae and co-immunoprecipates with caveolin-3 (Feron *et al.*, 1996). Brahmajothi & Campbell, (1999) found that eNOS also co-localises with superoxide dismutase, which catalyses superoxide decomposition, thus reducing the generation of peroxynitrite and oxidative stress. In addition, eNOS and superoxide dismutase expression varied within the left ventricular wall, with higher expression in epicardial compared to endocardial myocytes. In contrast to nNOS, eNOS has been widely reported to attenuate contractility in response to β-adrenergic receptor stimulation. Barouch *et al.* (2002) found that eNOS knockout mice exhibited an enhanced inotropic response to β-adrenergic receptor stimulation with ISO compared with wild-type mice. In a converse approach, Massion *et al.* (2004) found that cardiac-specific overexpression of eNOS attenuated the inotropic response to ISO compared with wild-type mice. Overall, these studies suggest that eNOS has an inhibitory effect on contractility. eNOS signalling may also act to protect against arrhythmias. The L-type Ca^{2+} channel and the slow delayed rectifier K^+ channel may also be important signalling targets for eNOS signalling, and regulate action potential duration. Bai *et al.* (2005) have shown that the L-type Ca^{2+} current ($I_{Ca,L}$) was

Figure 1.9
Physiological nNOS and eNOS signalling in cardiac myocytes. nNOS
(NOS1) is expressed in the sarcoplasmic reticulum (SR) where it co-localises
with ryanodine receptors (RyR) and xanthine oxidoreductase (XO). nNOS-
derived NO, signals predominantly through cGMP-independent signalling
by S-nitrosylation (S-NO) or by reacting with superoxide (O_2^-) to form
peroxynitrite ($ONOO^-$). Phospholamban (PLB) is regulated by peroxynitrite and
the L-type Ca^{2+} channel by S-nitrosylation. eNOS (NOS3) is expressed in the
caveolae where it co-localises with caveolin-3 (CAV-3) and superoxide
dismutase (SOD). eNOS-derived NO, signals through cGMP-dependent and
cGMP-independent signalling and regulates the L-type Ca^{2+} channel by S-
nitrosylation and phosphorylation (P), and the Ca^{2+} sensitivity of the
myofilaments by phosphorylation. eNOS has been shown to enhance I_{Ks}, but
the underlying mechanism is unclear. Modified from Ziolo *et al.* (2008).
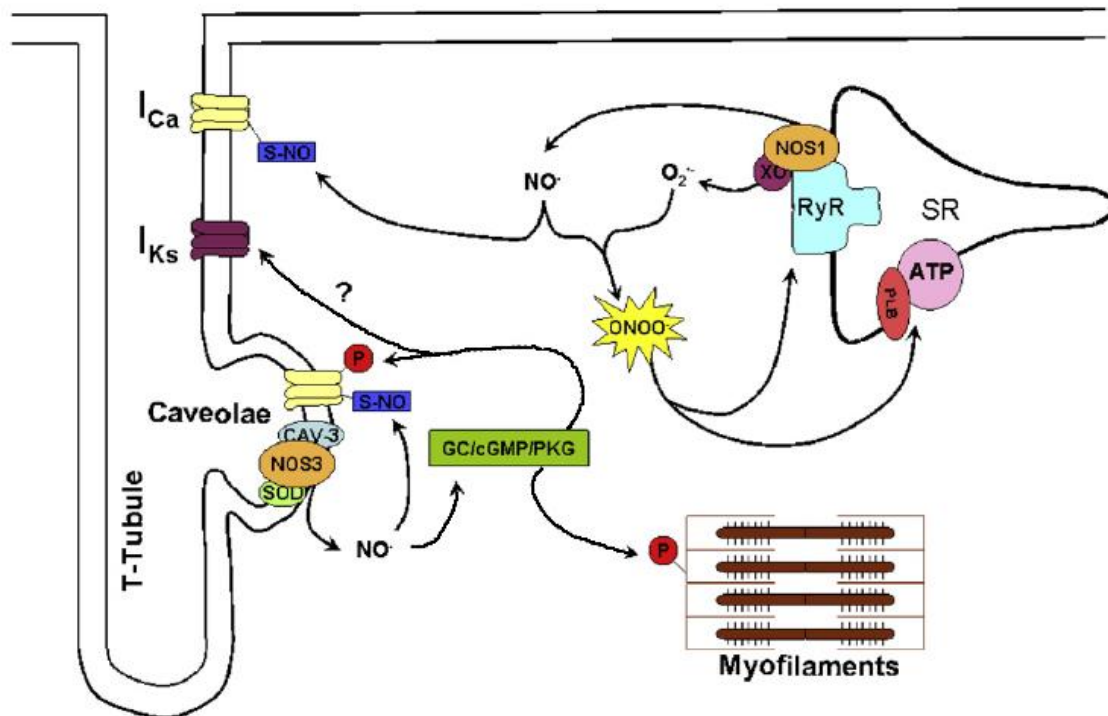
inhibited and the slow delayed rectifier K$^+$ current (I_{Ks}) was enhanced by stimulation of eNOS. Wang *et al.* (2008(2)) demonstrated that under β-adrenergic receptor stimulation, myocytes from eNOS knockout mice had prolonged action potential duration and an increase in early and delayed after depolarisations compared to wild-type mice. In addition, similar effects were observed by eNOS inhibition in wild-type myocytes. These studies suggest that eNOS signalling plays an important cardioprotective role against arrhythmia.

In summary, the evidence from transgenic mice indicated that nNOS-derived NO has a stimulatory effect and eNOS-derived NO has an inhibitory effect on ECC. It has been proposed that S-nitrosylation is the predominant signalling mechanism for nNOS, whereas eNOS signalling occurs primarily via cGMP (Hammond & Balligand, 2012). The localisation and signalling targets of nNOS and eNOS are summarised in Figure 1.9.

1.1.6.2 Nitric oxide signalling in the diseased heart

1.1.6.2.1 Pathophysiological alterations to nNOS signalling

NO signalling becomes disrupted under pathophysiological conditions such as hypertrophy, heart failure and ischaemia. In animal models and human heart failure, the expression of nNOS increases and nNOS translocates from the SR to the sarcolemma and localises with caveolin-3 (Damy *et al.*, 2004). Since nNOS normally co-immunoprecipitates with ryanodine receptors and xanthine oxidoreductase in the SR, regulation of these effectors is altered. S-nitrosylation of ryanodine receptors is reduced thus increasing the likelihood of irreversible oxidation and activation. This causes Ca^{2+} leak and a decrease in the Ca^{2+} stored in the SR. In addition, the inhibition of xanthine oxidoreductase is lost upon nNOS translocation, which increases superoxide production and contributes to oxidative stress. Furthermore, following translocation, nNOS exerts eNOS-like effects such as attenuating β-adrenergic mediated increases in contraction (Bendall *et al.*, 2004; Damy *et al.*, 2003). Similar to heart failure, nNOS undergoes translocation to the sarcolemma during ischaemia and targets the L-type Ca^{2+} channel. This may account for the increased S-nitrosylation of

Ca$_v$1.2 channels reported during ischaemia. Translocation of nNOS may be a cardioprotective mechanism to inhibit $I_{Ca,L}$ and help to protect against Ca^{2+} overload injury (Sun *et al.*, 2006).

1.1.6.2.2 Pathophysiological alterations to eNOS signalling

In contrast to nNOS, expression levels of eNOS decrease in animal models and human hypertrophy and heart failure. Damy *et al.* (2004) found that expression and activity of eNOS was decreased in patients with dilated cardiomyopathy. Using the spontaneously hypertensive rat as an animal model of hypertrophy, Bayraktutan *et al.* (1998) reported reduced expression and activity of eNOS in cardiac myocytes from hypertensive rats compared with normotensive rats. In addition, eNOS was unaltered in endothelial cells, suggesting tissue-selective downregulation of eNOS in hypertrophy. In a study on eNOS knockout mice, Buys *et al.* (2007) found that cardiac-specific restoration of eNOS attenuated hypertrophic remodelling, following transverse aortic constriction. This was characterised by less thickening of the left ventricular wall and improved contractile function compared to eNOS knockout mice. Similarly, Ruetten *et al.* (2005) demonstrated that pressure overload-induced left ventricular hypertrophy was greater in eNOS knockout mice compared to wild-type mice. Overall, these studies suggest that eNOS may play a protective role in limiting hypertrophic remodelling. Uncoupling of eNOS occurs under pathophysiological conditions such as hypertrophy, heart failure, ischaemia and atherosclerosis in addition to a reduction in eNOS expression. Uncoupling enhances superoxide production and subsequent generation of peroxynitrite (Munzel *et al.*, 2005). Peroxynitrite can then exacerbate uncoupling by oxidising BH$_4$, a NOS co-factor integral in dimerisation and the binding and conversion of L-arginine (Milstien & Katusic, 1999). Takimoto *et al.* (2005(2)) reported that eNOS uncoupling in mice was prevented by treatment with BH$_4$. Furthermore, the administration of the B vitamin folic acid improves BH$_4$ stability and increases the regeneration of BH$_4$ from BH$_2$, an oxidised and inactive form (Moens *et al.*, 2008). Treatment with BH$_4$ proved beneficial in hypertrophic mice and pre-treatment with folic acid reduced NOS uncoupling. Increasing eNOS activity by increasing expression or

reducing uncoupling are potential targets for the treatment of hypertrophy and heart failure (Umar & van der Laarse, 2010).

1.1.6.2.3 Pathophysiological iNOS signalling

The expression of iNOS is induced by an increase in the levels of cytokines and therefore occurs only under pathophysiological conditions (Arstall *et al.*, 1999). iNOS-dependent signalling is typically viewed as detrimental to the heart, and is mediated by cGMP-dependent and cGMP-independent pathways. However, cGMP-independent signalling is predominant and peroxynitrite is likely to be the main iNOS-derived signalling molecule. This is because iNOS is high output unlike the other isoforms of NOS, and therefore uncoupling is probable due to BH_4 depletion (Ziolo *et al.*, 2008). Thus, coupled and uncoupled iNOS produce NO and superoxide respectively which can subsequently combine to form peroxynitrite. Peroxynitrite exerts a deleterious effect on contraction via multiple signalling targets, one such target is SERCA. Lokuta *et al.* (2005) demonstrated that SERCA activity was directly inactivated through nitration in human failing hearts. In addition, peroxynitrite activates phosphatases which decreases PLB phosphorylation and also reduces SERCA activity (Ziolo *et al.*, 2008). As a result, contraction is attenuated due to a decrease in Ca^{2+} loading from the SR. Mungrue *et al.* (2002) found that overexpression of iNOS in mice, resulted in the development of hypertrophy, heart failure and sudden death due to cardiac remodelling by an increase in peroxynitrite production. In a study by Zhang *et al.* (2007) on wild-type and iNOS-deficient mice, hypertrophy was induced by the transverse aortic constriction procedure. In wild-type hearts, iNOS expression and hypertrophy was observed and development of hypertrophy was decreased by inhibition of iNOS. In contrast, substantially less hypertrophy was observed in the iNOS-deficient mice, suggesting that iNOS plays a role in the development of hypertrophy. iNOS is also involved in heart failure. A study by Drexler *et al.* (1998) found a high level of iNOS expression and activity in left ventricular tissue from patients with end-stage heart failure. The activity of iNOS (in the presence of EGTA) was determined using a citrulline assay and was found to be inversely proportional to the force of contraction in response to β-adrenergic receptor stimulation with ISO. High iNOS expression levels are also

found in response to myocardial infarction. Feng *et al.* (2001) showed that contractility and mortality rates were improved in iNOS knockout mice compared to wild-type, following myocardial infarction induced by left coronary artery ligation. This suggests that iNOS has a detrimental effect on myocardial infarction-induced survival. Interestingly, iNOS has a cardioprotective role in the context of ischaemia/reperfusion injury by reducing oxygen radicals which play a role in injury via the proposed mitochondrial permeability transition pore. West *et al.* (2008) induced ischaemia by coronary occlusion in wild-type mice and transgenic mice with upregulated iNOS. Following ischaemia and reperfusion, iNOS transgenic hearts exhibited a decreased infarct size and an improved contractile recovery. Therefore, not all iNOS-mediated NO signalling is detrimental.

1.2 Cardiac electrophysiology

1.2.1 The ventricular action potential

NO signalling is important in the regulation of ECC, which begins with an action potential (AP) and concludes with contraction of the heart. APs originate in the sinoatrial node and pass through the heart in a co-ordinated manner to the ventricles. The ventricular AP differs from most APs in other excitable cells due to a characteristic plateau phase that results in a prolonged duration of around 300 ms in humans. Subsequently, prolonged refractory periods limit AP firing frequency and heart rate, provide time for contractile relaxation and refilling with blood and are protective against arrhythmia. Therefore, the features of the ventricular AP are fundamental for function.

Species differences in ventricular AP morphology and duration exist, which is an important consideration when selecting an animal model. These differences are due to the relative contributions of repolarising currents, such as the transient outward K^+ current (I_{To}), the rapid (I_{Kr}) and slow (I_{Ks}) delayed rectifier K^+ currents and the inward rectifier K^+ current (I_{K1}). In intermediate and large mammals such as guinea pig, rabbit and dog, the ventricular AP has a "spike

and dome" morphology as shown in Figure 1.10, A. This is due to delayed repolarisation predominantly by I_{Kr}, I_{Ks} and I_{K1}. I_{Kr} and I_{Ks} are slow to activate, resulting in slow repolarisation and a longer duration. In contrast, in small mammals like the mouse, the ventricular AP lacks the elevated plateau phase and therefore has a "triangular" morphology as shown in Figure 1.10, A. The predominant current involved in repolarisation is I_{To} which activates rapidly and is large in amplitude, resulting in fast repolarisation and a shorter duration (Rosati *et al.*, 2008). However, I_{To} is still an important repolarising current in other species, like humans and rabbits, but is absent in guinea pigs (Wang *et al.*, 1999; Varro *et al.*, 1993). Guinea pigs also differ from rabbits and humans as repolarisation is largely mediated by I_{Ks} (Lu *et al.*, 2001). The ventricular AP also differs across the ventricles of a single species. AP morphology and duration shows regional heterogeneity between the endocardium, midmyocardium and epicardium due to differences in K^+ channel expression.

1.2.2 The ionic basis of the ventricular action potential

1.2.2.1 The inward rectifier potassium current

The resting membrane potential of ventricular myocytes is close to -90 mV. This is because the membrane of the ventricular myocytes has a high permeability for K^+ ions whilst being relatively impermeable to other ions. As a result, the membrane potential is driven towards the equilibrium potential for K^+ (E_K) which is typically -90 mV. However, the membrane is not solely permeable to K^+, thus the resting membrane potential is typically slightly positive to E_K (Hibino *et al.*, 2010). The current responsible for establishing the resting membrane potential is known as the inward rectifier potassium current (I_{K1}), passed by $K_{ir}2.1$ channels that are constitutively open and expressed in ventricular myocytes and largely absent in pacemaker cells (Zobel *et al.*, 2003; Nakamura *et al.*, 1998; Cho *et al.*, 2003; Shinagawa *et al.*, 2000). I_{K1} is a strong inward rectifier, meaning that current is passed preferentially in the inward direction compared to the outward direction. This can be observed experimentally in voltage clamp

Figure 1.10
Species variation in ventricular action potential morphology and duration.
(A) Ventricular APs recorded from mouse, guinea pig and canine ventricular
myocytes. Mouse ventricular APs have a shorter duration and lack a plateau
phase in contrast to guinea pig and canine ventricular APs. Modified from
Rosati *et al*. (2008). (B) Representation of a human ventricular AP and the
currents underlying each phase. Modified from Nerbonne & Kass, (2005).
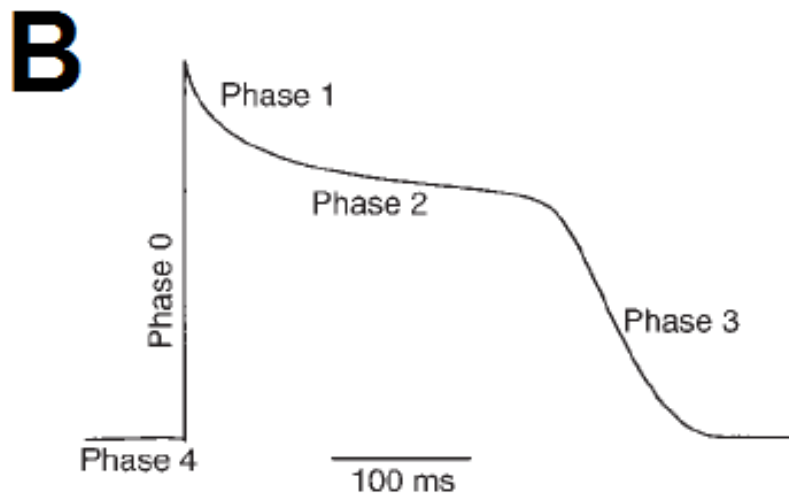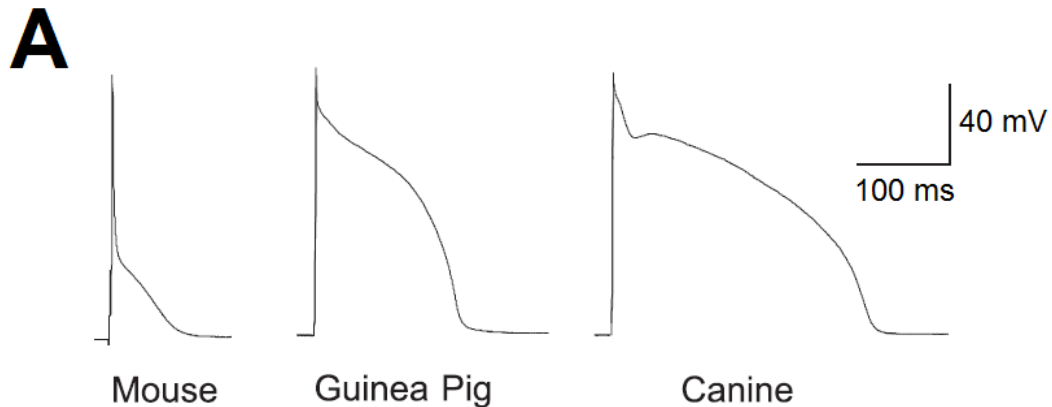
experiments. At potentials negative to E_K there is a large amplitude sustained inward current whereas at potentials positive to E_K there is a smaller amplitude outward current (Gomez *et al.*, 2009). Physiologically, the membrane potential is never more negative than E_K, thus current is always outward (Nerbonne & Kass, 2005). I_{K1} contribution during the phases of the AP is shown in Figure 1.10, B. I_{K1} is large at rest and towards the latter stage of repolarisation, as shown by phases 4 and 3 respectively. In contrast, during depolarisation at membrane potentials positive to -20 mV, I_{K1} is smaller due to voltage-dependent block of the channels by Mg^{2+} and polyamines (Ficker *et al.*, 1994; Fakler *et al.*, 1995). Therefore, during phases 0, 1 and 2, in which the AP upstroke, early repolarisation and plateau occur, a high proportion of I_{K1} channels are blocked (Gomez *et al.*, 2009). However, during the latter stage of phase 3 repolarisation, I_{K1} increases. Therefore, I_{K1} is fundamental in underlying the resting membrane potential and the final stage of repolarisation. This has been shown experimentally, by membrane potential depolarisation and prolongation of phase 3 repolarisation upon the application of Ba^{2+} which is known to block I_{K1} channels (Giles & Imaizumi, 1988; Imoto *et al.*, 1987).

1.2.2.2 The sodium current

APs originate in the sinoatrial node, the pacemaker region of the heart, whereby an AP is initiated by spontaneous depolarisation of the membrane potential to the AP threshold potential (Irisawa *et al.*, 1993). The spread of depolarisation is passed to neighbouring cardiac myocytes and throughout the rest of the heart via gap junctions (Jansen *et al.*, 2010). In the ventricle, membrane depolarisation leads to the rapid opening of $Na_v1.5$ channels, once the membrane potential exceeds the threshold for activation, which is typically -55 mV (Nerbonne & Kass, 2005). This results in a fast inward Na^+ current (I_{Na}) which drives the membrane potential towards the equilibrium potential for Na^+ (E_{Na}), which is typically close to +70 mV. Depolarisation of the membrane initiates the rapid upstroke of the ventricular AP, as shown by phase 0 in Figure 1.10, B. However, the membrane potential does not reach E_{Na} because the

membrane is not perfectly selective for Na^+ and a few milliseconds after activation the Na^+ channels become inactivated. The channels recover from inactivation as the membrane potential repolarises but I_{Na} remains small, contributing to an increased threshold for activation which prevents the triggering of another AP. The time course of I_{Na} during the phases of the AP is shown in Figure 1.10, B.

1.2.2.3 The transient outward potassium current

Membrane depolarisation also activates the transient outward K^+ current (I_{To}). I_{To} underlies the "notch" phase of the ventricular AP whereby there is a rapid but only partial repolarisation, shown as phase 1 in Figure 1.10, B. Although I_{To} is relatively large in amplitude, partial repolarisation occurs because I_{To} only activates in response to a large depolarisation and then inactivates rapidly (Niwa & Nerbonne, 2010). The time course of I_{To} during the phases of the AP is shown in Figure 1.10, B. I_{To} is comprised of fast and slow components. $I_{To\ fast}$ is conducted by channels composed of $K_v4.2$ and $K_v4.3$ α subunits and $I_{To\ slow}$ by $K_v1.4$ α subunits (Brahmajothi $et\ al.$, 1999). Human I_{To} is mediated by channels composed of $K_v4.3$ α subunits and K_v channel-interacting protein 2 (KChIP2) β subunits (Akar $et\ al.$, 2004; Decher $et\ al.$, 2001). However, channels comprised of these subunits fail to reproduce the exact electrophysiological properties of native I_{To}. Dipeptidyl-aminopeptidase-like protein 6 (DPPX) has been proposed as an additional β subunit in human I_{To} channels. DPPX modifies inactivation kinetics resulting in current that is more characteristic of native I_{To} (Radicke $et\ al.$, 2005). In addition, there are regional variations in I_{To} across the ventricles. APs from the epicardium and midmyocardium exhibit a larger notch, which is reflective of greater I_{To} compared to the endocardium (Brahmajothi $et\ al.$, 1999; Rosati $et\ al.$, 2001). As previously described, I_{To} is absent in guinea pig ventricular myocytes. Addition of mathematically modelled I_{To} results in a dramatic change in the morphology and duration of the guinea pig ventricular AP, whereby it more closely resembles that of the mouse (Rosati $et\ al.$, 2008).

1.2.2.4 The L-type calcium current

Membrane depolarisation also activates the L-type Ca^{2+} current ($I_{Ca,L}$) which plays a fundamental role in the plateau phase of the ventricular AP, shown as phase 2 in Figure 1.10, B. There is little change in the membrane potential during this phase due to a balance between inward depolarising currents and outward repolarising currents. $I_{Ca,L}$ is the primary inward depolarising current during the plateau phase and is conducted by $Ca_V1.2$ channels in human cardiac myocytes (Catterall *et al.*, 2005). The characteristics of $I_{Ca,L}$ include activation only by strong depolarisation, typically positive to -20 mV, and the long lasting nature of the current due to L-type Ca^{2+} channels inactivating slowly. L-type Ca^{2+} channel activation is slower than Na^+ channel activation, thus $I_{Ca,L}$ does not contribute significantly to the AP upstroke (Nerbonne & Kass, 2005). $I_{Ca,L}$ contribution during the phases of the AP is shown in Figure 1.10, B. Following activation, L-type Ca^{2+} channels subsequently undergo voltage-dependent and Ca^{2+}-dependent inactivation (Best & Kamp, 2012). The intricate balance of the plateau phase is disrupted by inactivation of $I_{Ca,L}$ and an increase in repolarising K^+ currents. $I_{Ca,L}$ can be inhibited with the dihydropyridine class of drugs, such as nisoldipine.

1.2.2.5 The delayed rectifier potassium currents

Several K^+ currents underlie the repolarisation phase of the ventricular AP, shown as phase 3 in Figure 1.10, B. The delayed rectifier K^+ currents are fundamental in repolarisation and are named based on the rate of activation, ultra-rapid (I_{Kur}), rapid (I_{Kr}) and slow (I_{Ks}). The delayed rectifier K^+ channels share the same basic structure as other voltage-gated K^+ channels, a tetramer comprised of four pore-forming α subunits. Each subunit consists of six α helical transmembrane spanning domains, known as S1-S6, and intracellular N and C termini. The voltage sensing domains are S1-S4, with the S4 domain functioning as the primary voltage sensor due to positively charged lysine or arginine residues. The S5-S6 domains from each of the four subunits assemble

together centrally to form the pore and the selectivity filter of the channel (Vandenberg *et al.*, 2004). The structural features of I_{Kr} and I_{Ks} channels are shown in Figures 1.11 and 1.13.

1.2.2.5.1 The ultra-rapid delayed rectifier potassium current

The ultra-rapid delayed rectifier K^+ current (I_{Kur}) is conducted by $K_v1.5$ channels in humans and is solely present in the atria (Feng *et al.*, 1997; Van Wagoner *et al.*, 1997; Gaborit *et al.*, 2007). Repolarisation of ventricular myocytes does not involve I_{Kur}, as demonstrated by no contribution during the phases of the ventricular AP in Figure 1.10, B. In atrial myocytes, I_{Kur} is a relatively large amplitude outward current which activates very rapidly and is largely non-inactivating (Du *et al.*, 2003). Thus, I_{Kur} contributes to rapid, early repolarisation in the atrial AP, which has a very different morphology compared to the ventricular AP (Nerbonne & Kass, 2005).

1.2.2.5.2 The rapid delayed rectifier potassium current

The rapid delayed rectifier K^+ current (I_{Kr}) is conducted by $K_v11.1$ channels encoded by the human ether-a-go-go related gene (hERG), also known as KCNH2 (Sanguinetti *et al.*, 1995; Trudeau *et al.*, 1995). I_{Kr} is a small amplitude current which contradictory to its name, activates relatively slowly, albeit faster than I_{Ks}. Despite this, I_{Kr} is fundamental in the plateau and repolarisation phases of the ventricular AP, shown as phases 2 and 3 in Figure 1.10, B. Although the basic structural features of I_{Kr} channels are shared with other voltage-gated K^+ channels, the gating properties of I_{Kr} channels are unusual. For typical voltage-gated K^+ channels activation is fast and inactivation is slow. Conversely, I_{Kr} channel activation/deactivation is slow and inactivation/recovery from inactivation is fast, due to the kinetics of the activation and inactivation gates respectively (Zhou *et al.*, 1998). The gating properties of I_{Kr} channels in response to depolarisation and repolarisation are shown in Figure 1.12. At the resting membrane potential, shown as phase 4 in Figure 1.10, B a high

proportion of I_{Kr} channels are deactivated, thus I_{Kr} is absent. Upon initiation of an AP, membrane depolarisation activates I_{Kr} channels resulting in a slow increase in I_{Kr} due to the slow opening of the activation gate. However, due to the fact that I_{Kr} channels slowly activate and also rapidly inactivate, I_{Kr} is small during the plateau phase of the ventricular AP. As the membrane potential becomes more negative during repolarisation, I_{Kr} increases further and peaks, as channels rapidly recover from inactivation but also begin to slowly deactivate (Hancox *et al.*, 1998). This results in a window of current which is fundamental in repolarisation of the ventricular AP.

Reproducing the exact electrophysiological properties of native I_{Kr} with recombinant protein expression has proven difficult. It is widely reported that the properties of hERG1a channels are similar to native I_{Kr} but not identical. The hERG1a α subunit isoform was the first isoform identified in the human heart. However, additional isoforms have since been identified and include hERG1b, hERGuso and hERG1buso (Lees-Miller *et al.*, 1997; Kupershmidt *et al.*, 1998; Guasti *et al.*, 2008). As a result, a heterotetrameric channel comprised of at least two different α subunits with slightly modified electrophysiological properties to hERG1a channels has been proposed to make up the native I_{Kr} channel (Jones *et al.*, 2004). The hERG1b isoform has a shorter N-terminus compared with hERG1a and can form homotetrameric channels or co-assemble with hERG1a to form heterotetrameric channels. An increase in current density, faster activation and faster deactivation are associated with co-expression with hERG1b (Larsen *et al.*, 2008). The electrophysiological properties of heterotetrameric hERG1a and hERG1b channels resemble native I_{Kr} more closely. hERGuso is a splice variant that differs in the C-terminus amino acid sequence and hERG1buso differs from hERG1a in both the N and C termini. The N-terminus and C-terminus contain the Per-Arnt-Sim (PAS) and cyclic nucleotide binding (CNB) domains respectively, which play a role in the trafficking of the protein (Jonsson *et al.*, 2012). Functional channels cannot be formed from hERGuso and hERG1buso alone. Co-expression of hERGuso or hERG1buso with hERG1a or hERG1b decreases current density. Furthermore,

hERG1a and hERG$_{USO}$ co-expression accelerates activation (Kupershmidt *et al.*, 1998). Structural features of hERG1 α subunits are shown in Figure 1.11.

Native I$_{Kr}$ may differ from hERG1 currents as I$_{Kr}$ channels may comprise a modulatory β subunit. KCNE2, also known as minK-related peptide 1 (MiRP1), belongs to a family of K$^+$ channel β subunits consisting of five different members. KCNE subunits have a single transmembrane spanning domain, an extracellular N-terminus and an intracellular C-terminus (Abbott, 2012). These subunits co-assemble with K$^+$ channel α subunits, as a functional conducting ion channel cannot be formed from KCNE subunits alone (Eldstrom & Fedida, 2011). Co-expression with KCNE2 has been reported to modulate multiple K$^+$ currents, including those that underlie I$_{To}$ (Zhang *et al.*, 2001), I$_{Ks}$ (Toyoda *et al.*, 2006; Jiang *et al.*, 2009) and I$_{Kr}$ (Abbott *et al.*, 1999). KCNE2 was originally proposed to be the missing subunit of I$_{Kr}$ channels. Co-assembly of hERG and KCNE2 subunits was predicted to replicate the exact electrophysiological properties of native I$_{Kr}$. This does not appear to be the case, and there are inconsistences in the findings from studies in this field. Furthermore, the expression of KCNE2 in the ventricle is controversial. High expression levels of KCNE2 have been reported in the purkinje fibres, sinoatrial node and atria, with very little expression in the ventricle (Pourrier *et al.*, 2003; Yu *et al.*, 2001). However, some studies have detected greater expression levels in the ventricle, which exceed those found in the atria (Jiang *et al.*, 2004; Zhang *et al.*, 2012). Another reason native I$_{Kr}$ may be different from hERG1 currents is modulation by kinases such as protein kinase C and PKA and possibly other second messenger signalling pathways (Heath & Terrar, 2000; Wang *et al.*, 2009). I$_{Kr}$ can be inhibited experimentally with a range of potent and selective inhibitors, including the widely used inhibitor N-[4-[[1-[2-(6-Methyl-2-pyridinyl)ethyl]-4-piperidinyl]carbonyl]phenyl] methane sulfonamide dihydrochloride (E4031) (Heath & Terrar, 1996).

Figure 1.11
The structural differences between hERG α subunit isoforms.
Representation of hERG α subunit isoform structure. All α subunit isoforms are
comprised of six α helical transmembrane spanning domains (S1-S6) and
intracellular N and C termini. S1-S4 are the voltage sensing domains with S4 as
the primary voltage sensor and S5-S6 function as the pore forming domains. All
isoforms contain a cyclic nucleotide binding (CNB) domain (although it is
incomplete in hERG$_{USO}$ and hERG1b$_{USO}$). hERG1b and hERG1b$_{USO}$ have an
altered N-terminus that lacks the Per-Arnt-Sim (PAS) domain. Taken from
Jonsson *et al.* (2012).
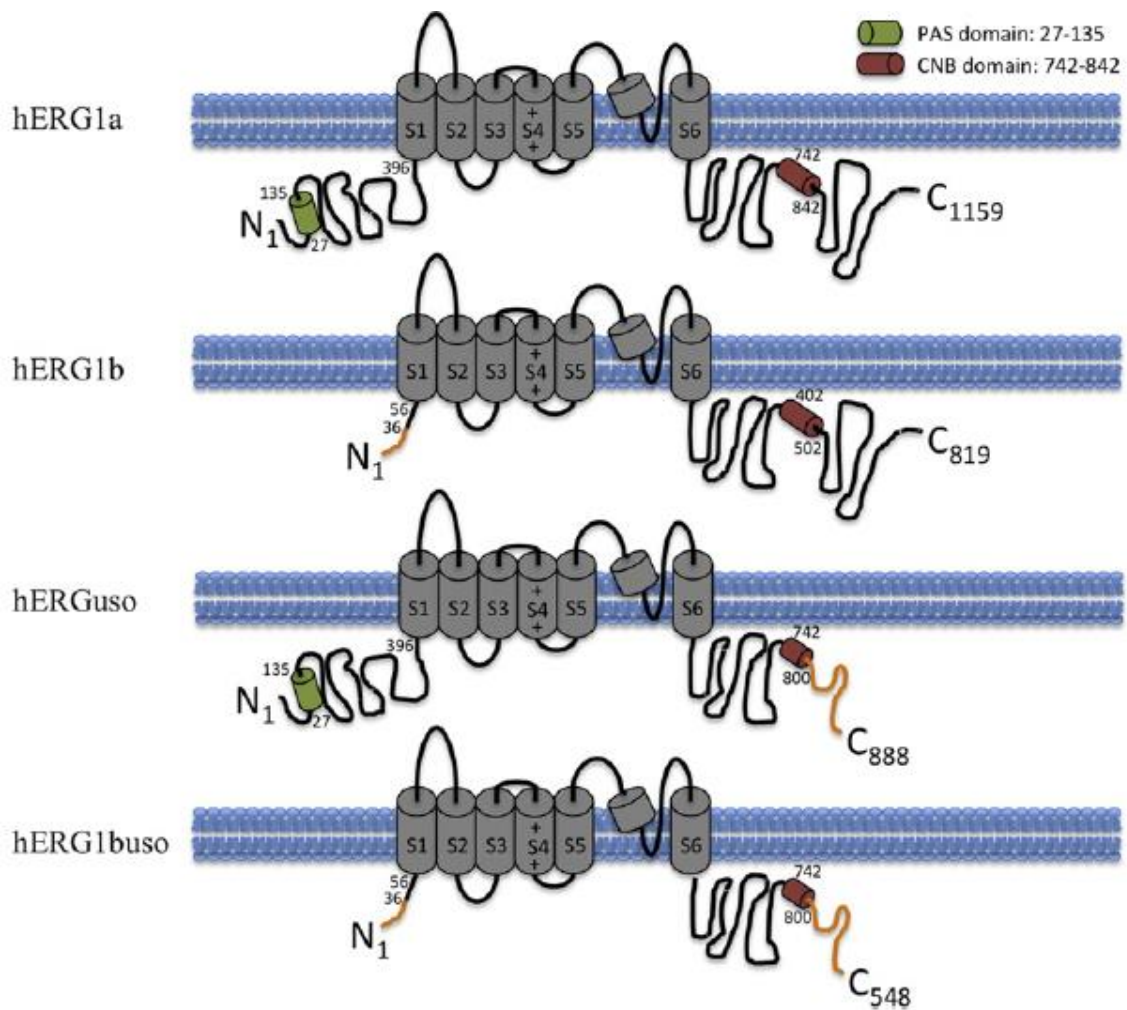
Figure 1.12

The gating properties of I_{Kr} channels. Representation of the voltage- and time-dependent gating kinetics of a single I_{Kr} channel. At negative membrane potentials the channel is deactivated. With depolarisation the activation gate opens slowly and the inactivation gate closes rapidly. Therefore, at positive membrane potentials the channel is non-conducting. With repolarisation the inactivation gate opens rapidly and the activation gate closes slowly. Therefore, the I_{Kr} channel is open for a limited period of time during repolarisation. Modified from Sanguinetti & Tristani-Firouzi, (2006).
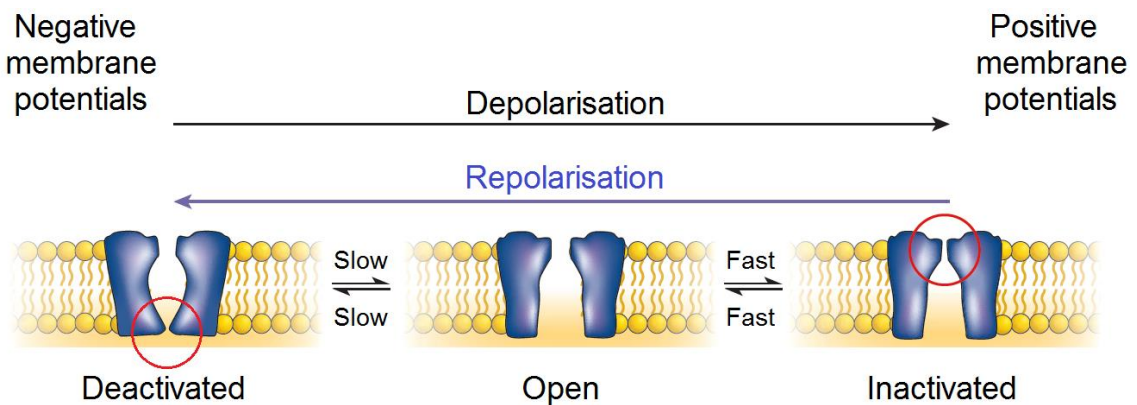
1.2.2.5.3 The slow delayed rectifier potassium current

The slow delayed rectifier K^+ current (I_{Ks}) activates more slowly than I_{Kr} in response to membrane depolarisation and is a fundamental repolarising current, especially during β-adrenergic receptor stimulation. I_{Ks} is conducted by $K_v7.1$ pore forming subunits that co-assemble with the minK (minimal K^+ channel) β subunit (Barhanin *et al.*, 1996; Sanguinetti *et al.*, 1996). The time course of I_{Ks} during the phases of the AP is shown in Figure 1.10, B. The inactivation kinetics of I_{Ks} and I_{Kr} differ, as $K_v7.1$ inactivation is suppressed by the accessory minK β subunit. Furthermore, minK alters channel gating by slowing activation and increasing single channel conductance (Barhanin *et al.*, 1996). The minK subunit was initially named because it consists of a single transmembrane spanning domain and was thought to be the minimal sequence required for a K^+ channel (Hausdorff *et al.*, 1991; Honore *et al.*, 1991). I_{Ks} was originally thought to be conducted by minK β subunits alone, but it is now known that I_{Ks} channels are heteromultimeric proteins composed of both $K_v7.1$ (encoded by *KCNQ1*) and minK (encoded by *KCNE1*). The assembly of four α subunits into a tetramer forms the pore of the channel and this complex is associated with additional minK β subunits. Although $K_v7.1$ α subunits alone can form a functional channel, co-assembly with minK results in electrophysiological properties which more closely resemble native I_{Ks} (Tristani-Firouzi & Sanguinetti, 2003). Co-assembly is also fundamental for function as minK increases the sensitivity of the I_{Ks} channel for phosphatidylinositol 4,5-bisphosphate (PIP_2) which is required for I_{Ks} activation (Li *et al.*, 2011). The relative and absolute expression levels of the subunits appear to differ between species, with higher expression of $K_v7.1$ in humans and higher expression of minK in guinea pigs (Zicha *et al.*, 2003). The increased minK expression in guinea pigs may account for the larger amplitude and slower rate of activation of I_{Ks} in guinea pigs compared to humans. As guinea pig ventricular myocytes lack I_{To} it is likely that I_{Ks} and I_{Kr} are the predominant repolarising currents. Enhancement of I_{Ks}, due to PKA-dependent phosphorylation of $K_v7.1$, is fundamental in the shortening of action potential duration (APD) during β-

adrenergic receptor stimulation (Marx *et al.*, 2002). I_{Ks} can be inhibited with 2-(4-Chlorophenoxy)-2-methyl-*N*-[5 [(methylsulfonyl) amino]tricycle [3.3.1.13,7]dec-2-yl]-propanamide (JNJ 303) (Towart *et al.*, 2009) and was used in subsequent experiments.

Figure 1.13

The structural features of I_{Ks} channels. (A) Representation of a single $K_v7.1$ α subunit and a single minK β subunit that co-assemble to form an I_{Ks} channel. The $K_v7.1$ α subunit consists of six transmembrane spanning domains, represented as 1-6, and intracellular N and C termini. The minK β subunit consists of a single transmembrane spanning domain, an extracellular N-terminus and an intracellular C-terminus. (B) Representation of the proposed heteromultimeric structure of the I_{Ks} channel comprised of four $K_v7.1$ α subunits and four minK β subunits. Transmembrane spanning domains 5 and 6 from each α subunit form the pore of the channel. Modified from Jost *et al.* (2007).
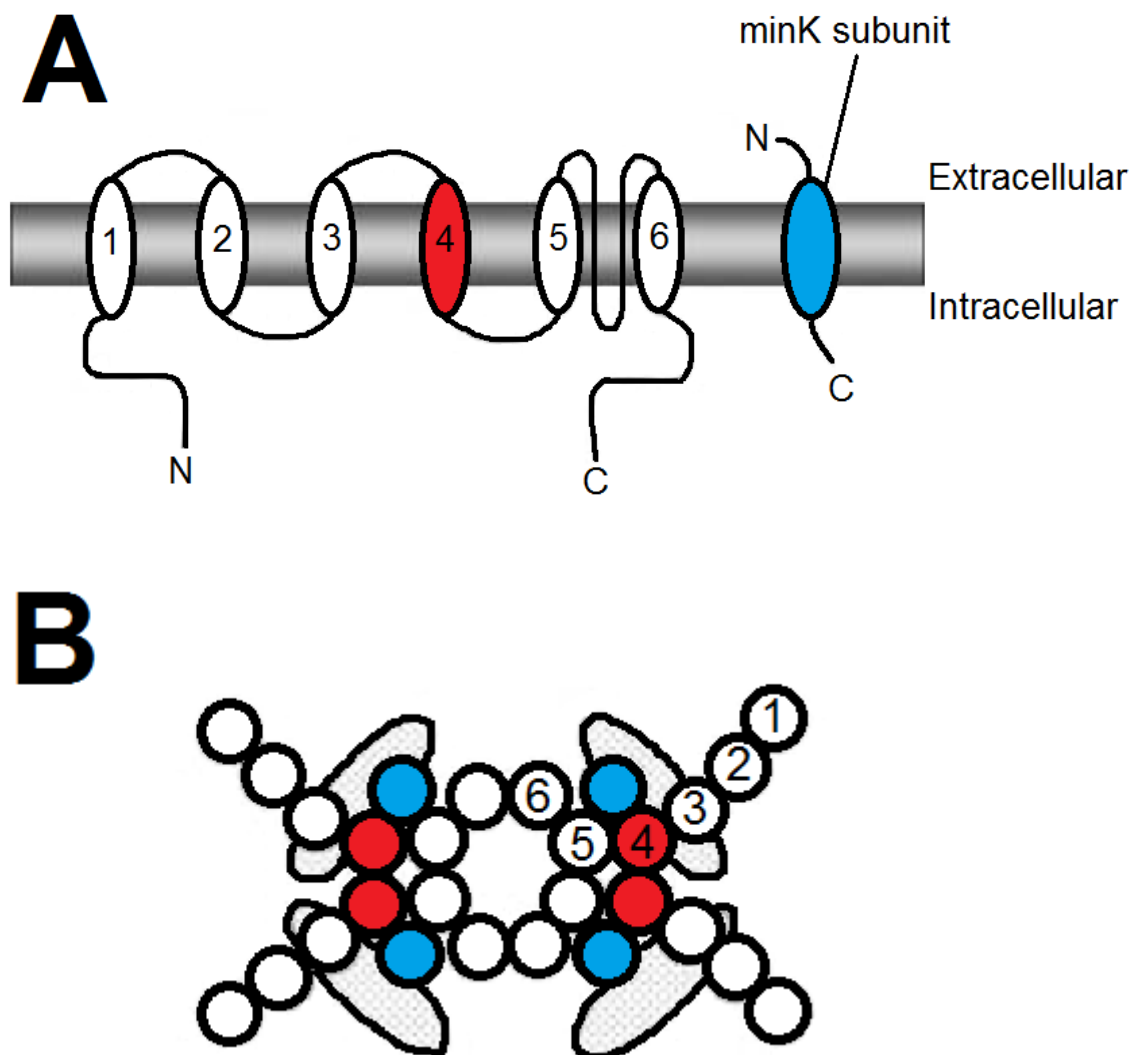
1.2.3 Cardiac electrophysiology abnormalities

Abnormalities in cardiac repolarisation are associated with an increased risk of arrhythmia and sudden cardiac death. In some cases, the risk of cardiovascular events can be predicted by the QT interval, which is a measure of ventricular repolarisation (Post *et al.*, 2007). The QRS complex and the T wave are characteristic features of an electrocardiogram during a cardiac cycle, which indicate spread of depolarisation and repolarisation respectively (Sanguinetti & Tristani-Firouzi, 2006). The time between the start of the Q wave and the end of the T wave is used to determine the QT interval, as shown in Figure 1.14, A. Abnormalities in the QT interval can lead to short QT syndrome and long QT syndrome (LQTS), which can both be arrhythmogenic. LQTS is characterised by prolonged repolarisation and can be classified into congenital and drug-induced LQTS. Drug-induced LQTS is caused by a diverse range of drugs, most of which cause this side-effect by blocking I_{Kr} channels. Withdrawal of drugs from the market and routine testing of new drugs against hERG channel block means that drug-induced LQTS is uncommon (Sanguinetti & Mitcheson, 2005). Congenital LQTS is caused by inherited genetic mutations of ion channels underlying the cardiac AP. The three most common genetic subgroups of congenital LQTS are LQT1, 2 and 3 (Schwartz & Ackerman, 2013). LQT1 and 2 are caused by mutations in *KCNQ1* and *KCNH2* genes that encode $K_v7.1$ and $K_v11.1$ channels respectively (Wang *et al.*, 1996; Curran *et al.*, 1995). All LQTS associated K^+ channel mutations result in a loss of function, a subsequent decrease in I_{Ks} or I_{Kr} and prolonged repolarisation (Sanguinetti & Tristani-Firouzi, 2006). In contrast, LQT3 is due to mutations in the *SCN5A* gene that encodes $Na_v1.5$ channels. Mutations lead to a gain of function and a subsequent increase in I_{Na} usually due to reduced inactivation (Bennett *et al.*, 1995). Thus, LQTS and delayed repolarisation can result in after depolarisations and increases the risk of arrhythmias, such as torsade de pointes as shown in Figure 1.14, B. Torsade de pointes can lead to ventricular fibrillation and sudden cardiac death. Research has established links between NO signalling, the QT interval and regulation of cardiac electrophysiology and aims to prevent and treat arrhythmias in patients.

Figure 1.14

The electrocardiogram QT interval can predict the risk of torsade de pointes arrhythmias. (A) Representation of normal (orange) and abnormal (green) electrocardiogram traces for a single cardiac cycle. The QRS complex and the T wave indicate ventricular depolarisation and repolarisation respectively. The abnormal trace displays a prolongation between the start of the Q wave and the end of the T wave, referred to as the QT interval. (B) Representation of an electrocardiogram trace showing an arrhythmia known as torsade de pointes, which is commonly associated with long QT syndrome. Modified from Sanguinetti & Tristani-Firouzi, (2006).
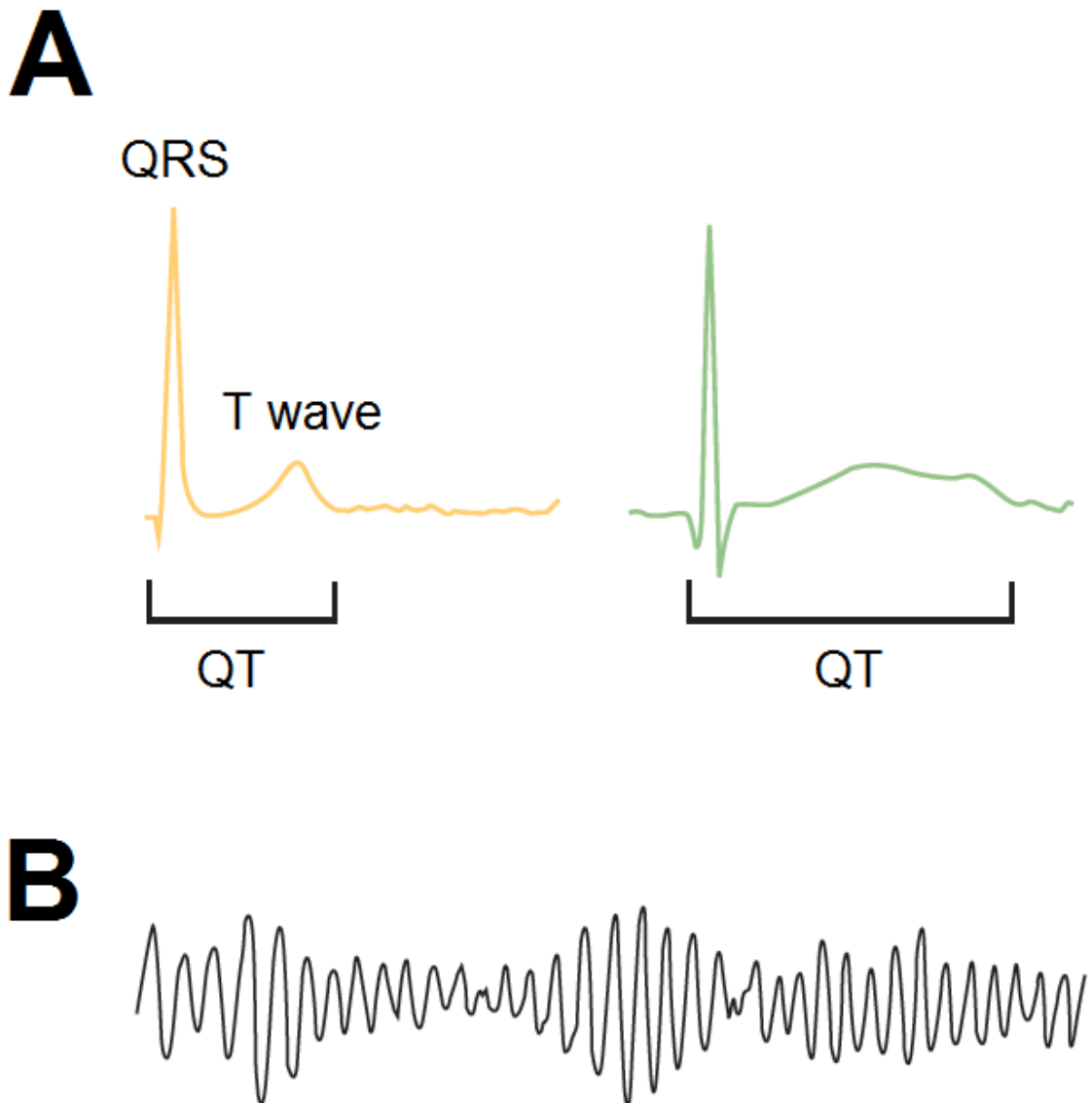
1.3 Cardiac electrophysiology and nitric oxide signalling

1.3.1 Regulation of ventricular repolarisation by nitric oxide signalling

It is widely known that NO signalling plays an important role in the heart. However, research investigating the effect of NO signalling on the ionic currents underlying the ventricular AP is lacking or inconclusive. Research in this field has predominantly used NO donors to stimulate NO signalling which has disadvantages and could explain inconsistencies in the findings. NO donors can stimulate both cGMP-dependent and cGMP-independent signalling pathways, may not release physiologically relevant concentrations of NO and are dependent on the presence of reduced haem for sGC activation. Inconsistencies could also be due to differences in the model system or species and the experimental conditions used.

I_{Na} is fundamental in the depolarisation of the ventricular AP but can also play a role in ventricular repolarisation, such as in LQT3. Therefore, the effect of NO signalling on I_{Na} and its role in repolarisation is important. Research has found that I_{Na} can be inhibited and enhanced by NO signalling and is therefore inconclusive. Ahmmed *et al.* (2001) reported that application of NO solution and the NO donor SNAP inhibited I_{Na} in mouse and guinea pig ventricular myocytes. This inhibitory effect was also mimicked by application of membrane-permeable analogues of cGMP and cAMP. Interestingly, inhibition of both sGC and PKA was required to prevent the inhibitory effect on I_{Na}. Therefore, inhibition of I_{Na} was mediated by a cGMP-dependent pathway also involving PKA. In addition, application of a thiol-reducing agent did not reverse the inhibition of I_{Na} which suggests that the effect was not dependent on S-nitrosylation. In contrast, Ahern *et al.* (2000) found that application of NO donors or ionomyocin, which increases endogenous NO production by activating NOS, enhanced I_{Na} and resulted in a late persistent Na^+ current in rat ventricular myocytes. Enhancement of I_{Na} was blocked by the application of a thiol-alkylating agent which prevents S-nitrosylation. Therefore, enhancement of I_{Na} was mediated by

a cGMP-independent pathway involving S-nitrosylation. In conclusion, I_{Na} appears to be inhibited by cGMP-dependent NO signalling and enhanced by cGMP-independent NO signalling.

The majority of research investigating the effect of NO signalling on cardiac ionic currents has focused on $I_{Ca,L}$ (Abi-Gerges *et al.*, 2002; Imai *et al.*, 2001; Wahler & Dollinger, 1995; Mery *et al.*, 1993; Mery *et al.*, 1996; Vandecasteele *et al.*, 1998; Wang *et al.*, 2000; Kirstein *et al.*, 1995; Wang *et al.*, 1998). Results have demonstrated that NO signalling can inhibit, enhance or have no effect on atrial and ventricular $I_{Ca,L}$. In many studies no effect was observed unless $I_{Ca,L}$ was previously stimulated with ISO or IBMX, or NOS activity was stimulated with L-arginine. Thus, the findings have been inconsistent and inconclusive. However, overall the research suggests that NO signalling predominantly inhibits ventricular $I_{Ca,L}$ and this has been shown to be mediated by a cGMP-dependent pathway in a number of studies. Additionally, it also appears that $I_{Ca,L}$ can be enhanced by cGMP-independent NO signalling. Campbell *et al.* (1996) found that the application of the NO donor SIN-1 could both inhibit and enhance basal $I_{Ca,L}$ in ferret ventricular myocytes. SIN-1 consistently inhibited basal $I_{Ca,L}$ in the presence of superoxide dismutase, which degrades superoxide thus reducing the formation of peroxynitrite and favouring cGMP-dependent signalling. Furthermore, the application of the cGMP analogue 8-Br-cGMP, also inhibited basal $I_{Ca,L}$. Whereas the application of S-nitrosothiol NO donors enhanced basal $I_{Ca,L}$ by a cGMP-independent pathway. In contrast, Grushin *et al.* (2008) reported that the application of the NO donor nitroprusside or 8-Br-cGMP had no effect on basal $I_{Ca,L}$ in rat ventricular myocytes. However, in the presence of the endogenous NOS substrate L-arginine, nitroprusside and 8-Br-cGMP both inhibited $I_{Ca,L}$. Additionally, inhibition of $I_{Ca,L}$ was blocked in the presence of the sGC inhibitor ODQ and the PKG inhibitor KT5823. Using a converse approach to decrease NO, Gallo *et al.* (1998) demonstrated that the application of NOS inhibitors enhanced basal $I_{Ca,L}$ in guinea pig ventricular myocytes and this effect was blocked in the presence of L-arginine. In a subsequent study, Gallo *et al.* (2001) demonstrated that application of an NO

scavenger or ODQ also enhanced $I_{Ca,L}$ in guinea pig ventricular myocytes. These studies suggest that basal NO levels inhibit $I_{Ca,L}$, as a decrease in basal NO was associated with an enhancement of $I_{Ca,L}$. In contrast, Abi-Gerges *et al*. (2001) reported that an increase in NO levels with multiple NO donors including SNAP had no effect on basal or ISO-stimulated $I_{Ca,L}$ in rat ventricular myocytes. However, the NO donor DEANO did inhibit ISO-stimulated $I_{Ca,L}$ and the effect was antagonised by ODQ and KT5823. These findings were in contrast to a previous study by Abi-Gerges *et al*. (1997) whereby SNAP inhibited ISO-stimulated $I_{Ca,L}$ in frog ventricular myocytes and was antagonised by ODQ. However, this inconsistency could be due to species differences. Similarly, Levi *et al*. (1994) found that the application of the NO donor nitroprusside had no effect on basal $I_{Ca,L}$ in guinea pig ventricular myocytes. However, IBMX-stimulated $I_{Ca,L}$ was inhibited by nitroprusside or the intracellular application of cGMP. In summary, ventricular $I_{Ca,L}$ appears to be inhibited by cGMP-dependent NO signalling and enhanced by cGMP-independent NO signalling.

A limited number of studies have investigated the regulation of the repolarising K^+ currents by NO signalling, albeit fewer on native currents in ventricular myocytes. Gomez *et al*. (2008) reported that NO solution and NO donors including SNAP inhibited $K_v4.3$ currents expressed in Chinese hamster ovary cells. As I_{To} is predominantly mediated by $K_v4.3$ channels in humans this suggests that NO signalling may inhibit I_{To}, although this has not been confirmed in ventricular myocytes.

Research indicates that I_{Kr} may also be inhibited by NO. Taglialatela *et al*. (1999) found that hERG currents expressed in Xenopus oocytes were enhanced by the application of a NOS inhibitor and inhibited by the application of L-arginine. Furthermore, the application of multiple NO donors including SNAP also had an inhibitory effect which was blocked by an NO scavenger but not ODQ. The application of ODQ or 8-Br-cGMP also had no effect on basal hERG currents. This suggests that the inhibitory effect of NO signalling on hERG currents was not mediated by a cGMP-dependent pathway. In contrast,

Mewe et $al.$ (2010) reported that 8-Br-cGMP inhibited ERG1a/1b and ERG1b currents expressed in human embryonic kidney cells. The inhibitory effect of 8-Br-cGMP was absent in the presence of a PKG inhibitor. In addition, 8-Br-cGMP also inhibited I_{Kr} in atrial mouse myocytes but had no effect on I_{Kr} recorded from ventricular mouse myocytes. Overall these studies are inconclusive as to whether NO signalling regulates I_{Kr}. The effect of NO signalling on native I_{Kr} in ventricular myocytes is unclear.

In contrast to I_{To} and I_{Kr}, NO signalling has been reported to enhance I_{Ks}. Bai et $al.$ (2004) demonstrated that the application of the NO donor nitroprusside enhanced I_{Ks} in guinea pig ventricular myocytes. I_{Ks} enhancement was barely suppressed by ODQ but was reversed by a reducing agent. This suggests that a cGMP-independent signalling pathway mediated the enhancement of I_{Ks}. Similarly, Asada et $al.$ (2009) found that the application of the NO donor SNAP enhanced KCNQ1/KCNE1 currents expressed in human embryonic kidney cells by S-nitrosylation. However, enhancement only occurred when cells were co-transfected with CaM. There is a lack of clarity in the literature on the regulation of native I_{Ks} by physiologically relevant levels of NO.

I_{K1} may also be enhanced by NO signalling. Gomez et $al.$ (2009) demonstrated that $K_{ir}2.1$ current expressed in Chinese hamster ovary cells was enhanced by the application of the NO donor SNAP. $K_{ir}2.1$ channels are proposed to be the major isoform that mediate I_{K1} in ventricular myocytes. Additionally, the enhancement of the $K_{ir}2.1$ current was unaffected by ODQ but was prevented in the presence of a reducing agent. $K_{ir}2.1$ current enhancement was found to be due to an increase in the opening probability of the channels as a result of S-nitrosylation.

In summary, NO signalling appears to differentially regulate the ionic currents underlying the ventricular AP and is dependent on whether NO is derived from cGMP-dependent or cGMP-independent signalling pathways. Current research suggests I_{Na} and $I_{Ca,L}$ are inhibited by cGMP-dependent NO signalling and

enhanced by cGMP-independent NO signalling. I_{To} and I_{Kr} may also be inhibited by NO signalling but the mechanism is unclear. In contrast, I_{Ks} and I_{K1} appear to be enhanced by NO signalling, in particular by cGMP-independent signalling pathways. However, research in this field is far from conclusive and requires further investigation. Findings thus far may not be that relevant physiologically, as stimulation of NO signalling with NO donors is flawed.

1.3.2 The QT interval, arrhythmia and nitric oxide signalling

NO signalling has only recently been linked with the QT interval (Aarnoudse *et al.*, 2007; Eijgelsheim *et al.*, 2009; Kao *et al.*, 2009; Tomas *et al.*, 2010). The potential link between the QT interval and NO was discovered by genome-wide association studies which screen the genome of many individuals in order to identify common genetic variants called single nucleotide polymorphisms that are associated with a particular disease. Arking *et al.* (2006) identified in the general population, that extremely long or short QT intervals were associated with a common genetic variant in the *NOS1AP* gene that encodes carboxy-terminal PDZ ligand of nNOS (CAPON). CAPON is an adaptor protein that binds to the post-synaptic density-protein, discs-large, ZO-1 (PDZ) domain located in the oxygenase domain of nNOS/NOS1 (Zhou & Zhu, 2009). Thus, the PDZ domain is important in protein recruitment and the assembly of signalling complexes, and it is proposed that CAPON regulates the subcellular location of nNOS (Tamargo *et al.*, 2010(1)). A study by Crotti *et al.* (2009) reported that in a LQTS population, the occurrence of symptoms and a greater probability of sudden cardiac death were also linked with *NOS1AP* variants. These studies suggested that NO signalling might play an important role in the regulation of the QT interval and cardiac repolarisation. Furthermore, Chang *et al.* (2008) found that adenoviral-mediated overexpression of CAPON in guinea pig ventricular myocytes resulted in a shortening of APD through a mechanism involving inhibition of $I_{Ca,L}$ and enhancement of I_{Kr}. Pre-treatment with the NOS inhibitor L-NAME reversed these effects. In addition, CAPON overexpression was also associated with an up-regulation of nNOS protein levels, an enhancement of nNOS activity and a modest increase in NO generation.

Therefore, it is likely that the effects of CAPON overexpression were mediated by a nNOS signalling pathway.

NO signalling has also been linked with protection against arrhythmias such as ventricular fibrillation (VF). Susceptibility to VF can be predicted from the electrical restitution properties of the heart. Electrical restitution is the relationship between APD and the diastolic interval (DI), which is the time between APs. This relationship is not linear and is plotted from experimental data as a curve, known as a restitution curve. At short DIs, small changes in the DI result in profound changes in APD forming the steep component of the restitution curve. Whereas, changes in APD are small at long DIs, forming the plateau phase of the curve (Franz, 2003). The maximum slope of the restitution curve is used to predict the risk of arrhythmia, with a steeper slope associated with a greater chance of the initiation of VF (Ng *et al.*, 2007). Brack *et al.* (2007) have shown that NO signalling plays an important role in the protective effect of vagus nerve stimulation (VNS) against induction of VF in an isolated Langendorff perfused rabbit heart with intact dual autonomic innervation. VF was induced by high frequency current pulses. The amplitude of the current was increased until the threshold for VF was reached and a sustained VF was observed. Monophasic APs were recorded from the ventricle by a recording electrode positioned on the surface of the heart. Restitution curves and the VF threshold were determined with no nerve stimulation and during VNS. VNS flattened the slope of the restitution curve and increased the threshold for inducing VF. However, the slope became steeper with VNS in the presence of L-NNA (a NOS inhibitor) and closely resembled the slope observed with no nerve stimulation. In addition, an increase in the VF threshold was no longer observed. The effects of NOS inhibition could be reversed by out competing L-NNA with the NOS substrate L-arginine. In summary, the protective effects of VNS were lost by inhibiting NO synthesis, suggesting these effects are likely mediated by NO signalling. In a subsequent study, Brack *et al.* (2009) demonstrated in the same preparation that NO was released and detected in the ventricle during VNS, using the NO fluorescent indicator 4,5-diaminofluorescein diacetate (DAF-2 DA). DAF-2 DA fluorescence increased during VNS and was inhibited by perfusion with L-NNA or an nNOS-specific

inhibitor. L-NNA also reduced background fluorescence. Vagal innervation of the ventricle and its role in ventricular function remains a controversial topic. However, these studies provide evidence that VNS increases NO in the ventricles and that this plays a fundamental role in the protection against arrhythmia.

1.4 Diurnal variation of cardiac electrophysiology

The oscillation of biological processes with a 24 hour cycle is referred to as a circadian rhythm (Jeyaraj *et al.*, 2012). Circadian rhythms are co-ordinated by a biological clock and are believed to anticipate and prepare organisms for the transitions between active and resting periods. Multiple physiological parameters within the cardiovascular system exhibit time of day variation. For instance during the daytime, heart rate and blood pressure are higher with a peak in the morning, and lower at night during sleep (Takeda & Maemura, 2011).

Interestingly, the occurrence of sudden cardiac death displays distinct diurnal variation. Sudden cardiac death is defined as unexpected death within one hour of the onset of symptoms, and accounts for a significant proportion of cardiac associated deaths (Mahmoud *et al.*, 2011). Muller *et al.* (1987) found a low incidence of sudden cardiac death during the night and a prominent increase in the number of cases from 7 to 11 AM. A primary peak was observed between 10 and 11 AM and a secondary peak between 5 and 6 PM. The pattern in circadian variation resembles that reported for myocardial infarction. A clear relationship has been demonstrated between the time of awakening and the incidence of sudden cardiac death, as opposed to a link with morning alone (Willich *et al.*, 1992). Sudden cardiac death is often caused by ventricular fibrillation resulting from ventricular tachycardia. It has been proposed that an increase in sympathetic nervous system activity might increase electrical instability and lead to an arrhythmic event which can result in sudden cardiac death (Muller *et al.*, 1987).

Hohnloser *et al.* (1993) investigated diurnal variation of ventricular repolarisation in response to changes in heart rate in patients with ventricular arrhythmia. Heart rate, uncorrected QT interval and ventricular ectopic activity displayed distinct circadian patterns. Heart rate and the occurrence of ventricular ectopics exhibited a similar pattern, with the lowest measurements at 5 AM, which increased at 6 AM, peaked at noon and decreased throughout the remainder of the day. However, heart rate remained relatively high during the morning with a substantial decrease in the evening. Conversely, uncorrected QT intervals peaked a few hours prior to 6 AM, decreased thereafter and started to increase at 6 PM. Therefore, QT intervals are longer during sleep. The autonomic nervous system also displays diurnal variation and has long been proposed to influence the QT interval. Bexton *et al.* (1986) showed that the circadian pattern of QT intervals corrected for heart rate (QT_c) differed between innervated and denervated hearts. Pacemaker patients with normally innervated hearts displayed distinct diurnal changes in the QT_c interval, with a profound shortening between 6 and 9 AM. However, in transplant patients with denervated hearts, the circadian pattern was blunted and the pronounced change in the morning was absent. This study suggests that the autonomic nervous system plays an important role in the diurnal changes of the QT_c interval. Furthermore, Honda *et al.* (2013) investigated the influence of parasympathetic and sympathetic nervous activity on diurnal variation of the QT_c interval in marmosets. QT_c interval prolongation during the dark period was blocked by atropine, a muscarinic receptor antagonist which suppresses parasympathetic activity. Conversely, QT_c interval shortening during the light period was blocked by propranolol, a β-adrenergic receptor antagonist which suppresses sympathetic activity. This suggests that the parasympathetic nervous system prolongs and the sympathetic nervous system shortens the QT_c interval, during the dark and light periods respectively. Therefore, an increase in the activity of the sympathetic nervous system during the transition from resting to active may increase the susceptibility to arrhythmias by modulating repolarisation.

The QT interval is a measure of ventricular repolarisation. Recently, diurnal variations have been detected in the expression of genes and proteins associated with the K^+ channels that underlie repolarisation. Yamashita *et al*. (2003) investigated cardiac K^+ channel gene expression in rat hearts at periodic intervals during the day. Circadian variation in the expression of $K_v4.2$ and $K_v1.5$ genes was discovered. Expression levels increased for both genes by almost two fold throughout the course of the day. The expression and current density of $K_v4.2$ peaked during the light period (when rats are resting) whereas $K_v1.5$ troughed. These diurnal patterns were partially inverted by reversal of light conditions. Therefore, this suggests that light is a fundamental parameter governing diurnal variation of the repolarising K^+ currents I_{To} and I_{Kur}. The generation of I_{To} is dependent on the expression of the β subunit KChIP2 (Kuo *et al*., 2001). The mechanism behind the diurnal variation of I_{To} was studied by Jeyaraj *et al*. (2012) in mice. KChIP2 was identified as a target of the transcription factor krüppel-like factor 15 (Klf15). Expression of *Klf15*, *KChIP2* and *Kcnd2* (which encodes $K_v4.2$), were all found to display circadian variation. Klf15 null mice and gain of function Klf15-Tg mice were used to examine the effect of Klf15 on the diurnal variation and expression of KChIP2 and Kcnd2. In Klf15 null mice, KChIP2 lacked diurnal variation and the circadian rhythm of Kcnd2 was shifted. Additionally, KChIP2 and Kcnd2 expression decreased. Klf15 null mice had decreased I_{To}, prolonged APD and prolonged QT intervals, whereas the reverse was the case in Klf15-Tg mice. The circadian rhythm of the QT interval was lost and an increased vulnerability to ventricular arrhythmia was observed for both Klf15 null and Klf15-Tg mice compared to wild-type. Spontaneous arrhythmias were detected in Klf15-Tg mice but had to be induced in Klf15 null mice. In summary, this study provides molecular evidence that links circadian rhythms, repolarisation by I_{To} and ventricular arrhythmia susceptibility.

Diurnal variation of ECC through regulation of NO signalling has also been demonstrated. Collins & Rodrigo, (2010) investigated whether multiple ECC parameters including Ca^{2+} transients, cell shortening and $I_{Ca,L}$ density exhibited diurnal variation in rat left ventricular myocytes. Paradoxically, cell shortening was greater in resting period myocytes, whereas $I_{Ca,L}$ density was greater in

active period myocytes, under basal conditions. However, both Ca^{2+} transients and $I_{Ca,L}$ density responded more strongly to β-adrenergic receptor stimulation with ISO, in resting than active period myocytes. To investigate if NO signalling played a role in the response to ISO, NOS was inhibited with L-NNA. L-NNA increased $I_{Ca,L}$ density in response to ISO in active period myocytes but had little effect in resting period myocytes. Furthermore, arrhythmic activity in response to ISO was greater in resting period myocytes and inhibition of nNOS increased arrhythmic activity in response to ISO in active period myocytes but had no effect in resting period myocytes. In addition, active period myocytes had a higher expression of nNOS than resting period myocytes. Therefore, NOS-dependent signalling exhibited diurnal variation, and suppressed ECC and arrhythmic activity in active but not resting period myocytes.

The study of diurnal variation of the ionic currents underlying the ventricular AP is in its infancy. Studies in this field have used mouse and rat models, in which ventricular APD is short and repolarisation is mediated predominantly by I_{To} and I_{K1}. What happens to the delayed rectifier K^+ currents, which are fundamental in determining ventricular APD in larger mammals is unknown.

1.5 Aims

The overall aim of this PhD was to explore the regulation of repolarisation by cGMP-dependent NO signalling in guinea pig isolated left ventricular myocytes. The vast majority of research in this field has used NO donors which are likely to release high concentrations of NO that are not physiological. NO donors can also activate cGMP-independent signalling pathways. I opted to solely activate the cGMP-dependent pathway in a physiologically relevant manner with the novel NO/haem-independent sGC activator BAY 60-2770. I also chose to use the perforated patch-clamp technique to minimise changes to the intracellular signalling environment of the myocytes. Other reagents known to modulate cGMP-dependent signalling were also used to modulate the activity of sGC, PDEs, PKG and PKA. The main aims were to characterise the effects of BAY 60-2770 on cellular cGMP levels, APD and delayed rectifier K^+ current amplitude. Literature on the modulation of the ventricular AP and its underlying ionic currents by NO signalling is inconclusive and has thus far focused predominantly on $I_{Ca,L}$. There is little research investigating the regulation of the delayed rectifier K^+ currents by NO signalling, especially native I_{Ks} and I_{Kr} in ventricular myocytes. Therefore, the experiments conducted, aimed to address this gap in the literature, particularly in light of recent studies associating ventricular arrhythmias with NO signalling (Arking *et al.*, 2006; Crotti *et al.*, 2009; Brack *et al.*, 2007; Brack *et al.*, 2009).

Repolarisation of the ventricular AP is modulated by β-adrenergic receptor activity. In addition, the QT interval, a measure of ventricular repolarisation, is widely reported to exhibit diurnal variation. Furthermore, the autonomic nervous system has been proposed to influence the diurnal variation of ventricular repolarisation and is also known to regulate the activity of NOS. Therefore, a further aim was to study whether ventricular repolarisation and cell shortening responses to β-adrenergic receptor stimulation, and inhibition of NOS activity, exhibited diurnal variation in guinea pig isolated left ventricular myocytes.

Chapter 2
Materials and Methods

2.1 Guinea pig housing

Adult male Dunkin Hartley guinea pigs (Harlan Laboratories) were housed in environmentally controlled rooms prior to experiments. Guinea pigs are active during daylight hours and are therefore diurnal as opposed to nocturnal. The majority of animals were housed in light controlled rooms with lights on at 6 AM and off at 6 PM. Culling was carried out at 8:30 AM, therefore these animals were in an active period (Figure 2.1). An exception was one group of guinea pigs used in experiments investigating diurnal variation (refer to chapter 5). These guinea pigs were housed in an opposing 12 hour light cycle, with lights on at 6 PM and off at 6 AM, for a minimum of three weeks prior to experiments and throughout the course of experiments. Therefore, these experimental animals were in a resting period when culled (Figure 2.1). Light controlled conditions were used because light is the main parameter responsible for setting the circadian clock. Culling of the animal is proposed to stop the cycling of the circadian clock at its current state (Collins & Rodrigo, 2010).

2.2 Isolation of guinea pig ventricular myocytes

Guinea pigs were culled by cervical dislocation in accordance with Home Office regulations. Most animals were culled rapidly and humanely, without sedation under Home Office project licence authority. However, in some experiments hypnorm (1 ml kg^{-1}, VetaPharma Ltd) and hypnovel (1 ml kg^{-1}, Roche Ltd) were administered to induce sedation prior to cervical dislocation. The majority of guinea pigs were 500-780 g, as animals over 550 g are reported to have fully developed vagal innervation and NO signalling (Herring *et al.*, 2000). However, guinea pigs of 370-490 g were used in some experiments (three week period from February to March 2013). Immediately after culling of the guinea pig, the heart was excised and submerged in cold Ca^{2+}-free Tyrode that contained (in mM) 135 NaCl, 4 KCl, 1 $MgCl_2$, 0.33 NaH_2PO_4, 5 Na^+ pyruvate, 10 glucose, 10

HEPES, pH 7.4 (adjusted with NaOH). In later isolation procedures, 0.5 mM ethylene glycol tetraacetic acid (EGTA) was added to the Ca^{2+}-free Tyrode to improve the yield and viability of the myocytes. The aorta was cannulated and retrogradely perfused with Ca^{2+}-free Tyrode for 4-6 minutes via Langendorff apparatus (Figure 2.2), whilst excess tissue surrounding the heart was removed. The heart was then perfused with Ca^{2+}-free Tyrode that contained 1.04 mg ml^{-1} collagenase (type I), 0.62 mg ml^{-1} protease (type XIV) and 1.67 mg ml^{-1} albumin from bovine serum (BSA) for 7-15 minutes (referred to as enzyme solution). After 1-2 minutes of perfusion, the enzyme solution was collected and recirculated (Figure 2.2, red dashed lines). Enzyme solution perfusion time was judged independently for each isolation procedure, based on an initial rapid and considerable decrease in the rigidity of the heart, followed by gradual softening. The heart was perfused finally with Ca^{2+}-free Tyrode for 1-2 minutes. In initial isolation procedures, the heart was instead perfused with normal Tyrode, that contained (in mM) 135 NaCl, 4 KCl, 2 $CaCl_2$, 1 $MgCl_2$, 0.33 NaH_2PO_4, 5 Na^+ pyruvate, 10 glucose, 10 HEPES, pH 7.4 (adjusted with NaOH). This was abandoned due to improved yield and viability of the isolated myocytes following perfusion with Ca^{2+}-free Tyrode. Tyrode and enzyme solution were maintained at 37^oC, bubbled with 100% oxygen and perfused at a rate of 10 ml $minute^{-1}$. The left ventricle was removed from the heart, dissected into smaller pieces and added to a flask that contained 5-10 ml normal Tyrode. The flask was bubbled with oxygen and placed into a water bath set at 37^oC and shaken mechanically to aid the dispersion of cells from the tissue into suspension. At periodic intervals the tissue was separated from the cell suspension, resuspended in normal Tyrode and returned to the water bath. This process was repeated until a decrease in rod shaped quiescent myocytes was observed, or until the cardiac tissue had fully dissociated. The cell suspensions were filtered using a sieve and left to sediment. Following formation of a loose pellet, the supernatant was discarded and the cell pellet was resuspended in normal Tyrode. The cell suspensions were left to sediment for a second time. Following reformation of the pellet, the supernatant was discarded and the cell pellets were resuspended in normal Tyrode and transferred to labelled petri dishes for use in patch-clamp experiments.

Figure 2.1
Representation of the light controlled guinea pig housing conditions.
Active guinea pigs induced by lights on between 6 AM and 6 PM. Resting
guinea pigs induced by an opposing 12 hour light cycle with lights off between 6
AM and 6 PM. Cull at 8:30 AM indicated by the vertical dashed line.
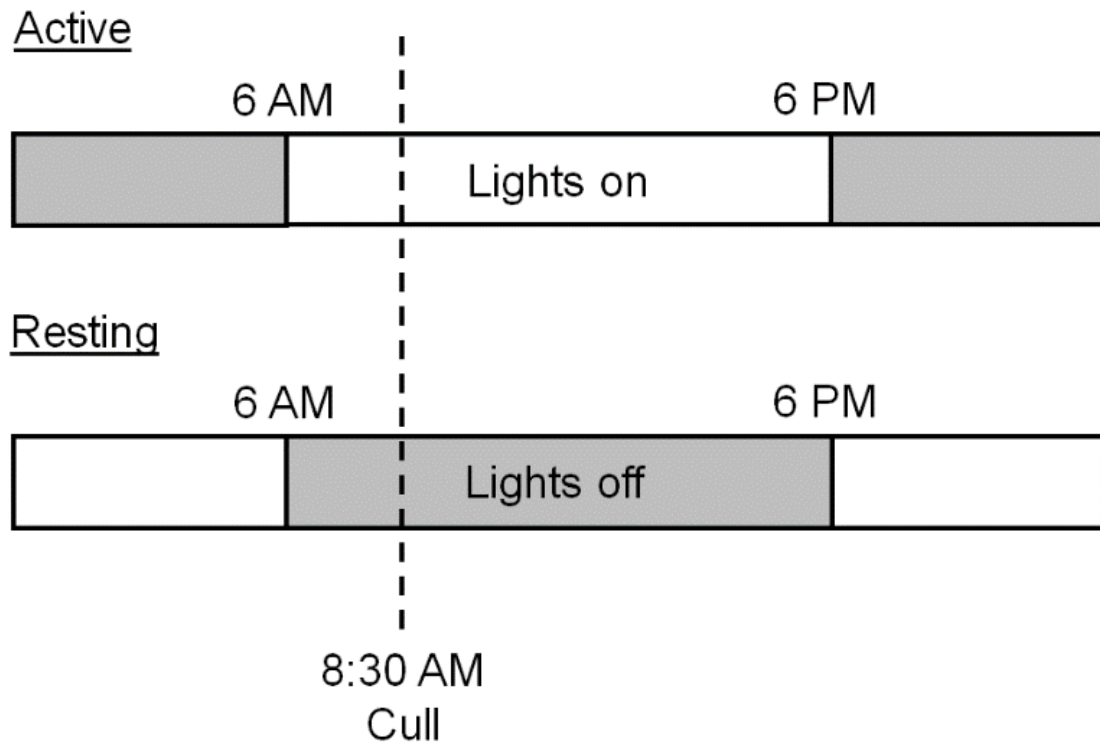
Figure 2.2

Representation of the Langendorff apparatus used to isolate guinea pig ventricular myocytes. Solutions were maintained at 37°C by heated water jackets and pumped through a heat exchange coil to the cannulated heart by a peristaltic pump. Enzyme solution was collected and recirculated to the reservoir via a different line by the peristaltic pump (red dashed lines).
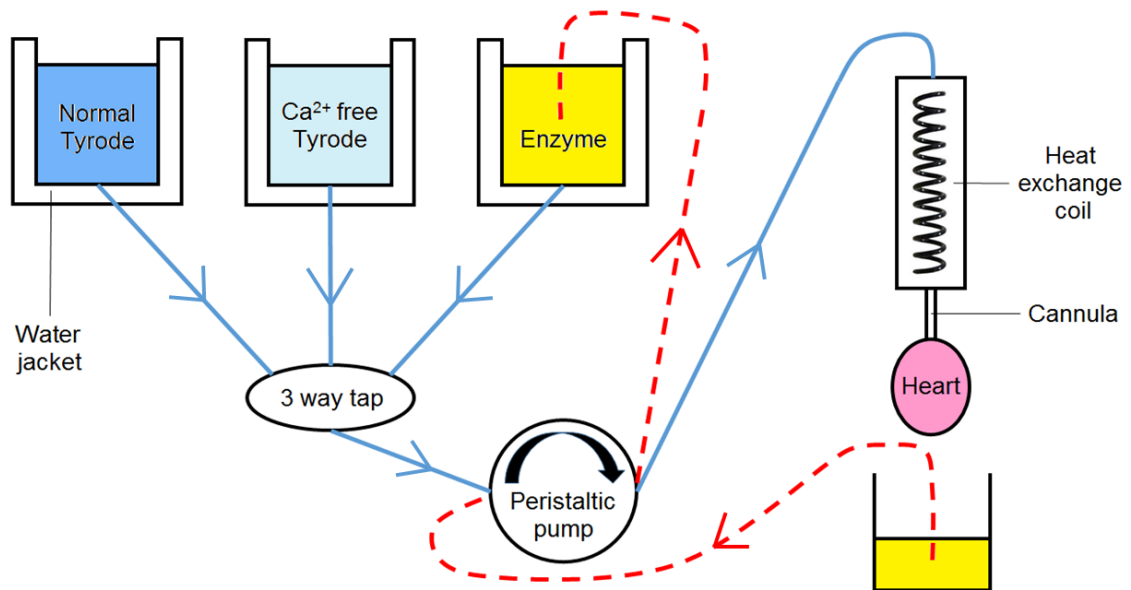
2.3 Electrophysiology

2.3.1 Electrophysiology apparatus

Myocytes were placed in a recording chamber and superfused with normal Tyrode using a peristaltic pump (Gilson) at a flow rate of 3-4 ml minute^{-1}. The perfusion line contained a bubble trap to prevent air flow caused by switching solutions. Solutions were warmed to 35-37°C by a Peltier heat exchange device (University of Leicester workshop) before flow into the recording chamber. A suction tube connected to another pump, removed solution and air from the recording chamber and was positioned to maintain the level of solution. The myocytes and electrode in the recording chamber were viewed using phase contrast microscopy. The microscope (Eclipse TE300, Nikon) was supported on an anti-vibration table, to prevent external vibrations from disrupting electrical access between the electrode and myocyte. The electrode was secured to a headstage (Axon CV203BU, Molecular Devices) and moved around the recording chamber in three planes by a micromanipulator (MX7600, Siskiyou). The solution in the recording chamber was connected to the ground input of the headstage via an agar bridge in 3 M KCl and silver chloride (AgCl) pellet assembly. The agar bridge minimised the transfer of potentially toxic Ag/AgCl to the recording chamber whilst still providing a low resistance and stable electrical connection. A Faraday cage was used to shield the apparatus from external electric fields and therefore minimise electrical noise.

2.3.2 Patch-clamp recording techniques

The patch-clamp technique was used to measure membrane ionic current, which is the flow of ions across a cell membrane. A command potential was set and the membrane potential of the myocyte was maintained or clamped at this voltage. Any difference between the membrane potential and the command potential was detected by the feedback amplifier and current was injected to maintain the voltage at the command potential. Therefore, the current across

the cell membrane was equal but opposite to the current injected. A single electrode measured the membrane potential and injected current.

Perforated and ruptured patch-clamp are two commonly used techniques to record currents from cells. In both techniques, an electrode is touched onto the cell membrane and a high resistance gigaohm seal is formed. The perforated patch-clamp technique uses pore-forming antibiotics such as amphotericin B to perforate the patch of membrane beneath the electrode tip and gain electrical access to the cell (Figure 2.3). Whereas, the ruptured patch-clamp technique uses suction to rupture the patch of membrane beneath the electrode tip (Figure 2.4). An advantage of the perforated patch-clamp technique is the maintenance of the cytosolic components, as the amphotericin B pores are only permeable to small monovalent ions and impermeable to larger ions and molecules. In the ruptured patch-clamp technique, the cytosol is dialysed by the intracellular solution in the electrode and is associated with current 'run-down' due to reductions in channel activity. To avoid this phenomenon, recordings were obtained using the perforated patch-clamp technique. However, potential disadvantages included less electrical access to the cell and a longer time required to gain sufficient access.

2.3.3 Perforated patch-clamp of guinea pig ventricular myocytes

Electrodes were made using borosilicate standard wall unfilamented glass (Harvard Apparatus) pulled by a micropipette puller (P-97 Flaming/Brown, Sutter Instrument Company) to a resistance of 1.5-2.5 MΩ. Electrodes were tip-filled by 2-3 mm with amphotericin B-free intracellular solution and back filled with intracellular solution that contained 0.48 mg ml^{-1} amphotericin B. For voltage clamp recordings the intracellular solution contained (in mM): 30 KCl, 110 L-aspartic acid K$^+$ salt, 5 MgCl$_2$, 10 HEPES, pH 7.2 (adjusted with KOH). For current clamp recordings the intracellular solution contained (in mM): 10 NaCl, 20 KCl, 110 L-aspartic acid K$^+$ salt, 5 MgCl$_2$, 10 HEPES, pH 7.2 (adjusted with KOH). All solutions containing amphotericin B were prepared from stock solutions on each experimental day, protected from light and placed on ice.

Amphotericin B stock solution 60 mg ml^{-1} was prepared in dimethyl sulfoxide (DMSO), sonicated and stored at -20°C for use within one week. Intracellular Ca^{2+} was not buffered with Ca^{2+} chelators, which enabled Ca^{2+} levels to change in a physiologically relevant manner. Amphotericin B diffused quickly to the electrode tip and prevented seal formation. Another potential concern was that amphotericin B could be ejected over cells which could make them 'leaky' and depolarised. Therefore, as a preventative measure, minimal positive pressure was applied before seal formation, and rapid seal formation was vital. Following formation of a gigaohm seal, electrical access to the myocyte was gained by increased pore formation in the membrane over time, as observed by the increased amplitude and faster decay rate of the capacitance transients (Figure 2.3, B). Typically, transients formed within a few minutes and took up to 20 minutes to reach an acceptable access resistance, which was monitored using whole cell capacitance and series resistance parameters on the voltage clamp amplifier. Once the series resistance was <15 MΩ with series resistance compensation at 60-70%, the electrical access was deemed sufficient to start to make recordings and the experiment commenced. Series resistance was monitored at periodic intervals during voltage clamp experiments. In the majority of recordings, series resistance was 5-15 MΩ with >60% compensation. Under these experimental conditions a 1 nA current would cause a maximum voltage error of 15 mV. The majority of delayed rectifier K$^+$ currents recorded were less than 0.3 nA. Data with a series resistance >25 MΩ was excluded.

2.3.4 Recording solutions

Guinea pig ventricular myocytes were superfused with normal Tyrode, that contained (in mM): 135 NaCl, 4 KCl, 2 CaCl$_2$, 1 MgCl$_2$, 0.33 NaH$_2$PO$_4$, 5 Na$^+$ pyruvate, 10 glucose, 10 HEPES, pH 7.4 (adjusted with NaOH) warmed to 35-37°C. Intracellular solutions were stored at -20°C and kept on ice during experimental days. Reagents were made up as stock solutions, typically in DMSO or water/Tyrode, stored at -20°C or 4°C accordingly and diluted to the required concentration in normal Tyrode on the day of the experiment. DMSO concentration did not exceed 0.1%.

Figure 2.3
Representation of the perforated patch-clamp technique. (A) Diagram showing increased amphotericin B pore formation in the myocyte membrane with time. (B) Increased capacitance transient amplitude and faster decay rate with time. Modified from Axopatch 200B Patch Clamp Theory and Operation.
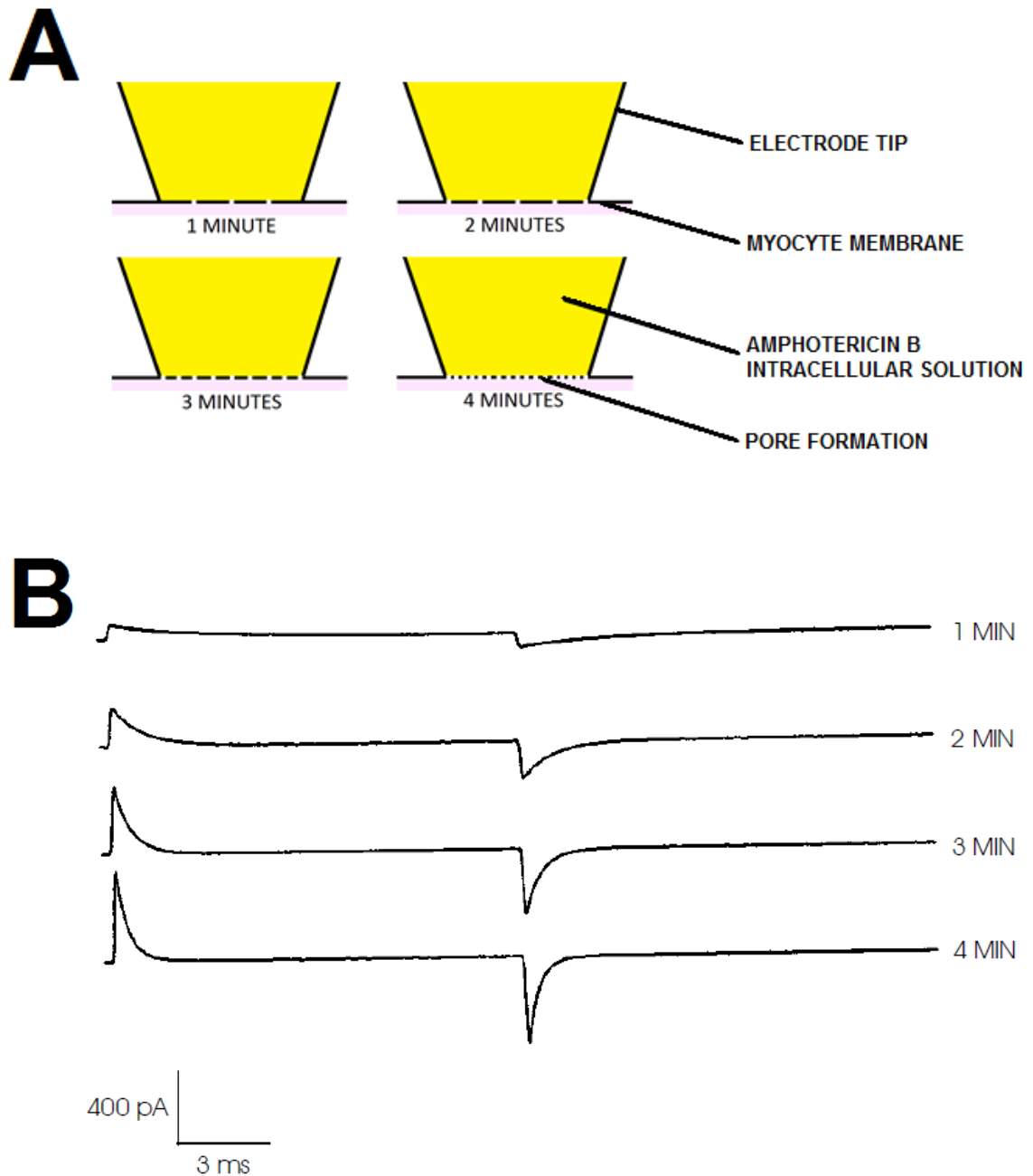
Figure 2.4
Representation of the ruptured patch-clamp technique. (A) Diagram showing application of suction to rupture the myocyte membrane and go whole-cell. (B) Current traces at indicated stages of the procedure. Taken from Axopatch 200B Patch Clamp Theory and Operation.
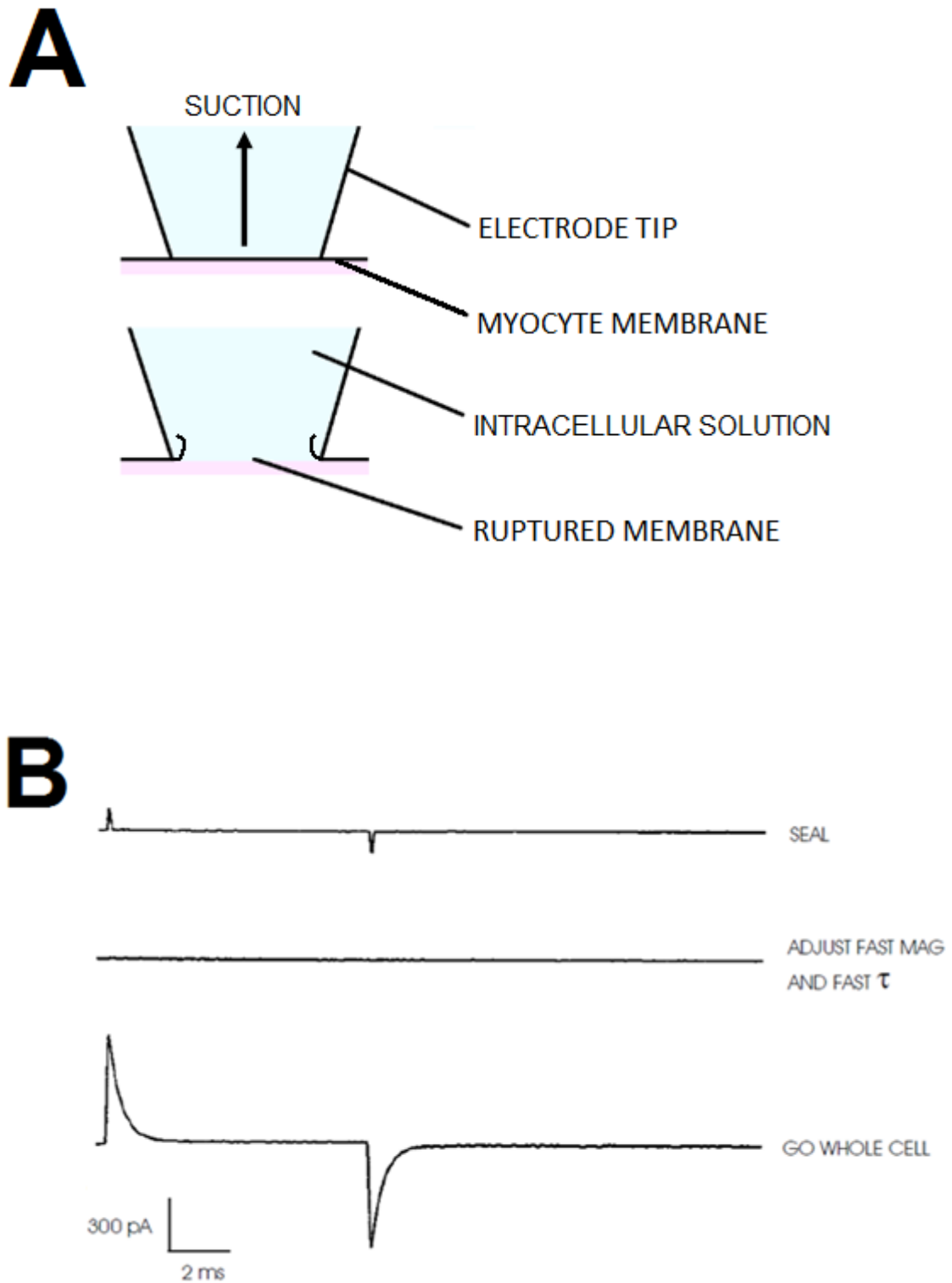
2.3.5 Data acquisition

Electrophysiological recordings were acquired using an amplifier (Axopatch 200B, Molecular Devices), an analogue to digital converter (1322A or 1440A Digidata, Molecular Devices) and Clampex software (versions 8.2 and 10.2, Molecular Devices). For voltage clamp experiments, the current and voltage signals were filtered at 5 kHz and recorded for off-line analysis at a sampling frequency of 2 kHz. For current clamp experiments, the low pass filter frequency was 5 kHz and the sampling frequency 5 kHz. A pipette voltage offset of -13 mV was applied for perforated patch-clamp recordings to counteract a junction potential of 13 mV at the electrode tip, due to a difference in the concentrations and mobilities of anions and cations between the intracellular electrode solution and the extracellular Tyrode solution. The ion concentrations and experimental conditions were input into the junction potential calculator within the Clampex software and used to determine the junction potential.

2.3.5.1 Perforated patch-clamp action potential recordings from guinea pig ventricular myocytes

APs in guinea pig isolated left ventricular myocytes were stimulated by 2 ms current pulses applied via the recording electrode. Current pulse amplitude was increased incrementally until the threshold for triggering an AP was reached (Figure 2.5). Following determination of the threshold, current pulses of 1.2 times the threshold were applied at 2 Hz.

2.3.5.2 Perforated patch-clamp recordings of delayed rectifier potassium currents from guinea pig ventricular myocytes

The delayed rectifier K^+ currents, I_{Ks} and I_{Kr} were recorded selectively from guinea pig isolated left ventricular myocytes by using a combination of a specific voltage protocol and pharmacological inhibitors to isolate each current. The voltage protocol (Figure 2.6) had a holding potential of -80 mV, followed by a depolarising step to -50 mV to inactivate channels conducting the fast Na^+

current (I_{Na}) and then to +40 mV for 500 ms to activate I_{Ks} and I_{Kr}. I_{Ks} and I_{Kr} tail currents were elicited upon repolarisation to -50 mV due to the characteristically slow deactivation kinetics of these channels and the outward driving force for K^+ efflux. Voltage pulses were separated by 4000 ms. A holding potential of -80 mV was used because cells were stable at this potential, which is close to the zero current potential. When holding at -40 mV or -50 mV, cells became unstable and Ca^{2+} overloaded.

A voltage protocol designed to elicit tail currents was used because the window of opportunity to measure I_{Kr} was small. At +40 mV, hERG channels were predominantly inactivated. A high proportion of channels had the activation gate open and the inactivation gate closed, thus channel opening probability was low which resulted in very little current. The step from +40 mV to -50 mV utilised the particular kinetics of channel gating and allowed current to be measured whilst channels quickly recovered from inactivation and slowly deactivated, as is characteristic at negative membrane potentials. Therefore, tail currents were representative of the proportion of channels activated at +40 mV. I_{Ks} is also characterised by a slow time course for channel activation and deactivation, although I_{Ks} does not inactivate. The same voltage protocol was used to measure I_{Ks}.

I_{Ks} and I_{Kr} were isolated and recorded selectively by using pharmacological inhibitors to inhibit contaminating currents. The L-type Ca^{2+} current ($I_{Ca,L}$) was inhibited with 10 μM nisoldipine, and inward Ca^{2+} influx on the Na^+/Ca^{2+} exchanger was minimised by using a low intracellular Na^+ concentration. I_{Ks} and I_{Kr} were inhibited with 1 μM JNJ 303 and 1 μM E4031 respectively. JNJ 303 and E4031 in combination at these concentrations, resulted in complete inhibition of the tail current which indicated that these were the only contributing currents.

Figure 2.5

Stimulation of guinea pig ventricular action potentials. The amplitude of current pulses was increased incrementally until an AP was triggered. (A) An AP was triggered in the black trace but not in the preceding blue, green and red traces. (B) Expansion of dashed box in A, to show membrane potential responses to current stimuli.
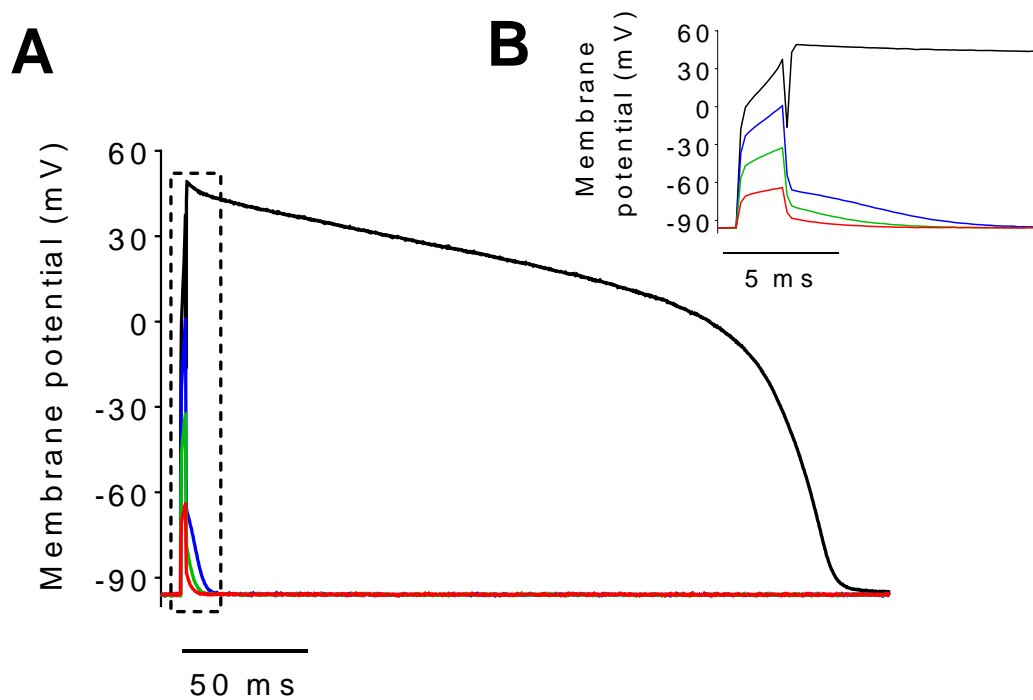
Figure 2.6
Representation of the voltage protocol applied to guinea pig left ventricular myocytes to measure I$_{Ks}$ and I$_{Kr}$. The voltage protocol had holding potential of -80 mV, followed by depolarising steps to -50 mV and +40 mV for 500 ms and repolarising steps to -50 mV and -80 mV.
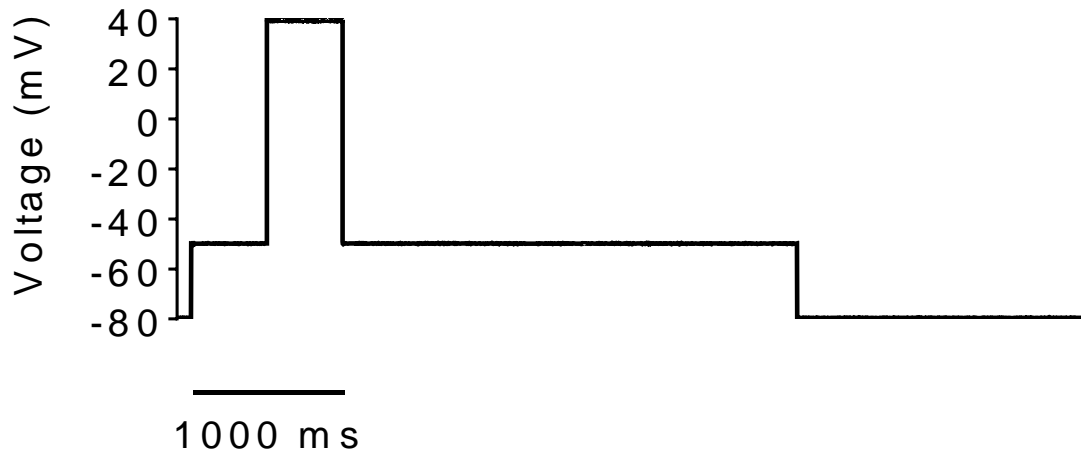
2.3.5.3 Edge detection recordings from guinea pig ventricular myocytes

Video based edge detection is a technique used to detect changes in the position of a cell edge in contracting cells by using changes in contrast around the periphery of the cell when imaged by phase contrast microscopy. An edge detector (Crescent Electronics), video camera and monitor were used to visualise and detect changes in myocyte edge position with cell contraction during AP stimulation.

A myocyte was positioned so it was visible on the monitor and the settings on the edge detector were used to place a cursor on one end of the myocyte at the interface between the edge of the myocyte and the background where contrast was maximal. A cursor could not be placed on each end of the myocyte due to the field of view being smaller than the length of the myocyte with the x40 objective used in the microscope. Thus, the amount of movement at one end of the cell (single ended cell shortening) could be measured but not cell length. The voltage signal of the device was digitised and recorded in parallel with the AP and current stimulus signals for off-line analysis.

2.3.6 Data analysis and statistical analysis

APs were analysed using Clampfit (version 10.2, Molecular Devices) or Tracan software developed locally by Dr Noel Davies (University of Leicester) using Microsoft Visual Studio and National Instruments Measurement Studio Library.

Using Clampfit, the decay time from 100% to 10% function was used to measure AP duration to 90% repolarisation (APD_{90}). A cursor was placed on the AP peak and the time of the cursor was noted, this cursor indicated 0% repolarisation. Another cursor was placed on the resting membrane potential after the AP, this cursor indicated 100% repolarisation. The peak amplitude was determined from a number of similar consecutive APs. The time of AP upstroke was measured using the time of maximum rise slope function. The time from AP upstroke to AP peak was measured and added onto the decay time from 0% to

90% repolarisation to account for variability in the time from upstroke to peak between APs.

Similarly, Tracan automatically measured the time from AP upstroke threshold to AP peak and added this onto the time from AP peak to 90% repolarisation. Clampfit files were imported into Tracan, a cursor was placed after the stimulus artefact and the AP upstroke threshold was typically set at -20 mV but varied up to +20 mV for some cells. Unlike the Clampfit analysis, APD_{90} was measured using the peak for each individual AP. To test the accuracy of the Clampfit analysis against Tracan, APD_{90} in a number of cells were analysed using both methods and a maximum difference of 1 ms was found. Mean APD_{90} under each experimental condition was obtained by averaging 20 consecutive steady-state APs.

I_{Ks} and I_{Kr} tail current amplitude was analysed by measuring the difference between the amplitude of the peak of the tail current and the end of the pulse at -50 mV when the tail current had deactivated. The mean amplitude from a 10 ms and 30 ms window at the peak and end were used respectively. Mean I_{Ks} and I_{Kr} tail current amplitude under each experimental condition was obtained by averaging 5 consecutive steady-state current traces.

Myocyte edge detection changes during AP stimulation were analysed using the peak measurement function in Clampfit. The difference in amplitude between the peak and the baseline was measured. A search region set from shortly before a change occurred to shortly after the return to baseline was used to measure the peak amplitude. The baseline amplitude was measured using the mean value from a 10 ms window. Mean cell shortening amplitude under each experimental condition was obtained by averaging 20 consecutive steady-state traces.

Prism (versions 5.0 and 6.0, GraphPad Software) was used to plot data and perform statistical analysis. All data are presented as mean ± standard error of the mean (SEM). Significance was tested for using a paired two-tailed t test or

repeated measures or ordinary one-way or two-way analysis of variance (ANOVA). Sidak's multiple comparisons test was used to compare pre-selected pairs of means and Dunnett's multiple comparison test was used to compare all means to one experimental condition, such as control. P values are presented as * for $p<0.05$, ** for $p<0.01$, *** for $p<0.001$ and no significance (ns) for $p>0.05$.

2.4 cGMP radioimmunoassay

A competitive binding radioimmunoassay (RIA) was used to determine changes in cGMP concentration following modulation of cGMP-dependent signalling in guinea pig ventricular myocytes. The assay was based on competition between unlabelled cGMP and iodine-125 (^{125}I) labelled cGMP for binding sites on a cGMP-specific antibody. The quantity of ^{125}I labelled cGMP and antibody were fixed, therefore the concentration of unlabelled cGMP present in test samples was inversely proportional to the amount of radiolabelled ligand bound to the antibody and could be quantified from a standard curve generated with known cGMP concentrations.

Guinea pig isolated ventricular myocytes in a suspension of normal Tyrode were plated in equal volume on 24 well plates and incubated with test reagents for 10 minutes at 37°C. The incubation was stopped by the application of ice cold 1 M trichloroacetic acid (TCA) which lysed the myocytes and solubilised the cGMP. Degradation of cGMP was minimised by the addition of 10 mM ethylene diamine tetraacetic acid (EDTA), which chelated Ca^{2+} and inhibited Ca^{2+}-dependent phosphodiesterase activity. TCA-solubilised cGMP was separated and extracted from the samples using a 1:1 mixture of tri-n-octylamine and 1,1,2-Trichloro-1,2,2-trifluoroethane. The samples were then neutralised with 60 mM $NaHCO_3$ and the cGMP was acetylated with 20 µl triethylamine 99% and 10 µl acetic anhydride to increase the sensitivity of the assay. A cGMP-specific antibody (GE Healthcare) and 5-10 µl ^{125}I cGMP (Perkin Elmer) were diluted with 8-10 ml and 4-5 ml of 50 mM sodium acetate buffer + 0.2% BSA, pH 6.2 respectively. The diluted cGMP antibody was placed

on ice which prevented denaturation and retained the binding capacity of the antibody, and the BSA prevented non-specific binding of the antibody to surfaces. The samples were incubated with 50 µl diluted [125]I cGMP and 100 µl diluted cGMP antibody. Addition of 100 mM potassium phosphate buffer + 0.2% BSA, pH 6.2 charcoal suspension to samples bound the 'free' cGMP and stopped the incubation. Centrifugation pelleted the charcoal and separated it from the antibody-bound cGMP. Radioactivity was counted using a 3 minute ^{125}I count program on a liquid scintillation counter. The sample counts were interpolated from a standard curve generated from cGMP standards with known cGMP concentrations.

2.4.1 cGMP radioimmunoassay data analysis and statistical analysis

Prism (versions 5.0 and 6.0, GraphPad Software) was used analyse and plot data and perform statistical analysis. The concentrations of the cGMP standards used in the RIA were input as log values with the corresponding disintegrations per minute (DPM) values. The DPM values for the samples were also input. Data was analysed with the nonlinear regression (curve fit) function and fit with sigmoidal dose-response (variable slope) and least squares (ordinary) fit. Unknown values were interpolated from the standard curve. Interpolated log [cGMP] for the sampes were then analysed with the inverse of log equation $B=10^{\wedge}A$, where A is the log [cGMP] and B is [cGMP]. [cGMP] in the sample was then calculated by multiplying [cGMP] from the previous equation by K, a multiplication factor, using the $C=K^{x}B$ equation. The multiplication factor was calculated due to dilution of the sample with other reagents in the RIA procedure. The mean [cGMP] under each experimental condition was calculated and divided by the mean [cGMP] in control wells that contained untreated cells under basal conditions, to express values as a fold change over control.

Changes in cGMP were expressed as a fold change relative to control because [cGMP] could not be normalised accurately to protein concentration [protein], as is typical. Firstly, the myocytes plated on 24 well plates contained both live and

dead myocytes. A protein assay would detect total [protein], and would therefore not be an accurate representation of [cGMP] relative solely to the live myocytes which responded to the test reagents. In addition, the proportion of live to dead myocytes varied between each assay due to the quality of the myocyte isolation procedure. Secondly, total protein for each sample was difficult to obtain because a proportion of the myocytes adhered to the surface of the well and a proportion remained in suspension. This varied between wells and thus between experimental conditions. Therefore, normalisation to [protein], would introduce errors to the results. It was decided that the most appropriate way to express cGMP levels was as a fold change relative to control wells, to normalise for differences in cell number and viability but not for [protein]. All data are presented as mean ± SEM. Significance was tested for using an unpaired two-tailed t test or one-way ANOVA. Sidak's and Dunnett's multiple comparison tests were used as described previously. Statistical significance is presented as described previously.

Figure 2.7
cGMP radioimmunoassay summary flow diagram.
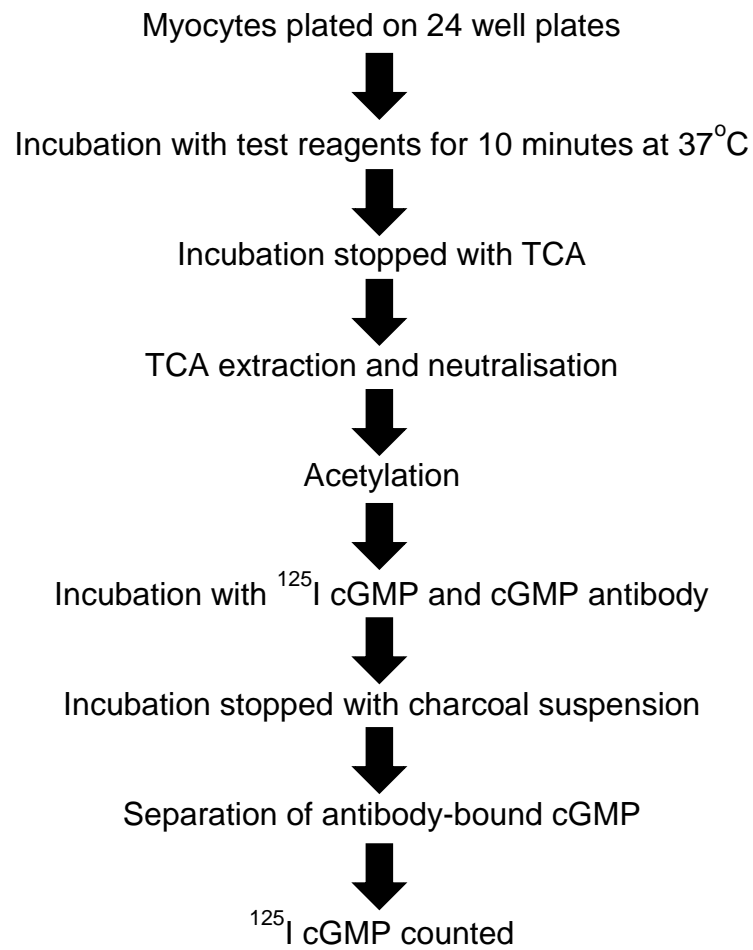
Myocytes plated on 24 well plates

⬇

Incubation with test reagents for 10 minutes at 37°C

⬇

Incubation stopped with TCA

⬇

TCA extraction and neutralisation

⬇

Acetylation

⬇

Incubation with ^{125}I cGMP and cGMP antibody

⬇

Incubation stopped with charcoal suspension

⬇

Separation of antibody-bound cGMP

⬇

^{125}I cGMP counted

Chapter 3

Responses of cellular cGMP levels and action potentials to modulation of cGMP-dependent signalling in guinea pig ventricular myocytes

3.1 Introduction

Two distinct types of NO signalling pathway have been widely described. Those which are dependent on cGMP and those which are cGMP-independent. In cGMP-dependent signalling, NO binds to the haem group of sGC causing activation and an increase in cGMP levels (Ziolo *et al.*, 2008). Cyclic nucleotide PDEs are responsible for the degradation of cGMP and also play an important role in signal compartmentalisation (Evgenov *et al.*, 2006). sGC is a key component of the cGMP-dependent signalling pathway. Under physiological conditions sGC is believed to exist in two different forms. A reduced haem-containing NO-sensitive sGC and an oxidised/haem-free NO-insensitive sGC (Evgenov *et al.*, 2006). *In-vitro* studies have shown the existence of oxidised/haem-free sGC and it is believed that this form also exists *in-vivo*, especially under pathophysiological conditions (Schmidt *et al.*, 2009).

NO donors such as SNAP, are commonly used to stimulate NO signalling pathways through the release of NO. However, the use of NO donors has disadvantages. Firstly, NO donors activate cGMP-independent signalling pathways, through S-nitrosylation and peroxynitrite production, in addition to activating cGMP-dependent signalling. Secondly, NO donors may not release physiologically relevant concentrations of NO. Thirdly, NO donors are dependent on the presence of haem for sGC activation. Novel NO/haem-independent sGC activators have been recently developed, including BAY 60-2770 which preferentially activates oxidised/haem-free sGC in a NO-independent manner (Stasch *et al.*, 2011). This was important to the study as there was concern that haem may be oxidised or lost in myocytes due to the isolation procedure.

The objective was to induce physiologically relevant changes in cGMP and investigate the effect of solely modulating cGMP-dependent signalling

pathways. Therefore, as a sGC activator, BAY 60-2770 was a useful tool, with significant advantages over NO donors. Cellular cGMP levels in guinea pig ventricular myocytes were measured to determine the effectiveness of BAY 60-2770 as an activator of sGC. The effects of BAY 60-2770 were characterised and changes in cGMP were compared with other reagents known to modulate cGMP levels. In order to determine the role played by cGMP-dependent signalling on cardiac repolarisation, the effects of BAY 60-2770 on guinea pig ventricular APs were also characterised. Guinea pig ventricular APs share many properties with human ventricular APs, such as a relatively long duration that is profoundly stimulation frequency-dependent, similar morphology and reliance on delayed rectifier K^+ currents for repolarisation (Rosati *et al.*, 2008). Therefore, the guinea pig was used as a model animal in preference to rat or mouse animal models which do not share these same features.

3.2 Results

3.2.1 Changes in cellular cGMP levels in response to modulation of cGMP-dependent signalling

Cyclic nucleotide signalling in cardiac myocytes is complex and involves interplay between synthesis by cyclases, degradation by PDEs and subsequent interlinked regulation of cGMP and cAMP signalling pathways. In these experiments a highly specific cGMP assay was used to quantify changes in cellular cGMP levels in guinea pig isolated ventricular myocytes in response to modulation of cGMP-dependent signalling.

Guinea pig ventricular myocytes were incubated with test reagents for 10 minutes at $37^{o}C$. Samples were then assayed in a competitive binding RIA, incubated with ^{125}I labelled cGMP and a cGMP-specific antibody and counted for antibody bound ^{125}I labelled cGMP. Counts were inversely proportional to the concentration of unlabelled cGMP present in test samples and were interpolated from a standard curve generated from known cGMP concentrations. Changes in cGMP were expressed as a fold change over control, untreated myocytes.

3.2.1.1 The effect of soluble guanylyl cyclase activation by BAY 60-2770 and SNAP on cellular cGMP levels

BAY 60-2770 (BAY) is a novel NO/haem-independent sGC activator, whereas SNAP is a NO donor. Therefore, BAY and SNAP activate sGC in different ways to increase cGMP. The aim of this experiment was to investigate and compare the effect of BAY and SNAP on cellular cGMP levels, and the concentration-dependence of these responses. SNAP was used as a positive control, as it releases high levels of NO that activate sGC. It has been shown that stimulation with SNAP increases cGMP levels in rat ventricular myocytes (Castro *et al.*, 2010).

BAY increased cGMP levels above control, at 1 and 10 µM concentrations (Figure 3.1). However, no change was observed in response to 0.1 µM BAY ($P>0.05$). In contrast, 1 and 10 µM BAY modestly but significantly increased cGMP by 2.2 ± 0.29 fold (n=8) and 2.7 ± 0.22 fold (n=4) respectively ($P<0.001$). The response to 1 µM BAY was significantly different to 0.1 µM ($P<0.05$) but not 10 µM ($P>0.05$), suggesting a concentration-dependent response to BAY and a maximal response with 1 µM.

SNAP also increased cGMP above control levels at 1, 10 and 100 µM concentrations (Figure 3.1). However, the modest 1.6 ± 0.22 fold change (n=3) with 1 µM SNAP was not significantly different to cGMP under control conditions ($P>0.05$). In contrast, substantial changes of 24 ± 5.6 fold (n=4) and 19 ± 3.7 fold (n=8) were observed with 10 and 100 µM SNAP respectively ($P<0.001$). The response to 10 µM SNAP was significantly different to 1 µM ($P<0.05$) but not 100 µM ($P>0.05$), suggesting a concentration-dependent response to SNAP and a maximal response with 10 µM.

Figure 3.1

BAY 60-2770 and SNAP induce concentration-dependent increases in cellular cGMP levels. Mean ± SEM fold changes in cGMP over control in response to BAY and SNAP. Reagents were applied to guinea pig ventricular myocytes for 10 minutes at 37°C. Samples were prepared in duplicate or triplicate from the number of hearts indicated in each bar. Statistical analysis performed with one-way ANOVA with Dunnett's multiple comparisons tests. Statistical significance, P<0.05, P<0.01 and P<0.001 presented as *, ** and *** respectively. No statistical significance presented as ns.
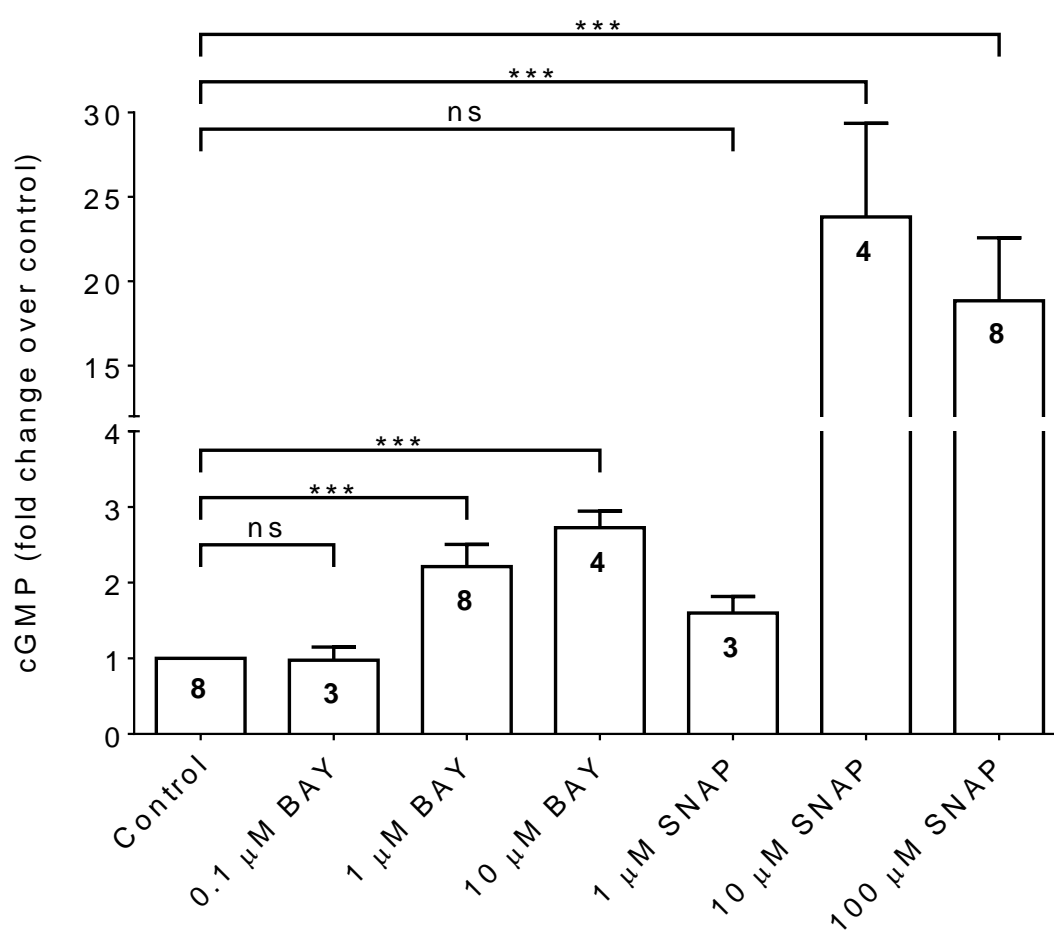
3.2.1.2 The effect of phosphodiesterase inhibition on basal cGMP and the responses to BAY 60-2770 and SNAP

3-isobutyl-1-methylxanthine (IBMX) is a widely used non-selective PDE inhibitor. Since PDEs are responsible for degrading cGMP, PDE activity may suppress cGMP levels under basal conditions and in response to BAY and SNAP. The aim of this experiment was to investigate and compare the effect of PDE inhibition alone and in combination with BAY and SNAP on cellular cGMP levels.

PDE inhibition with 100 µM IBMX significantly increased cGMP by 2.5 ± 0.23 fold (n=6) over control levels (P<0.001) (Figure 3.2). This suggests that sGC had constitutive activity, as cGMP levels increased in the absence of exogenous sGC activation.

In the presence of IBMX, activation of sGC with either BAY or SNAP, increased cGMP above the response to IBMX alone (Figure 3.2). However, the modest 4.4 ± 0.89 fold change (n=3) and 5.2 ± 0.69 fold change (n=3) with 0.1 µM BAY and 1 µM SNAP respectively were not significantly different to IBMX (P>0.05). Whereas, modest but significant increases of 7.1 ± 0.76 fold (n=7) and 8.7 ± 1.4 fold (n=4) were observed with 1 µM BAY (P<0.01) and 10 µM BAY (P<0.001) respectively. In contrast, 10 and 100 µM SNAP increased cGMP substantially, by 42 ± 11 fold (n=4) and 34 ± 6.4 fold (n=7) respectively (P<0.01).

IBMX significantly increased cGMP levels in response to 0.1, 1 and 10 µM BAY over BAY alone (Figure 3.3). In the absence of IBMX, a 0.97 ± 0.17 fold change (n=3) was observed in response to 0.1 µM BAY which increased to 4.4 ± 0.89 fold (n=3) in combination with IBMX (P<0.05). Whereas, a change from 2.2 ± 0.29 fold (n=8) to 7.1 ± 0.76 fold (n=7) was observed for 1 µM BAY (P<0.001). The response to 10 µM BAY also increased in the presence of IBMX, from 2.7 ± 0.22 fold (n=4) to 8.7 ± 1.4 fold (n=4) (P<0.001). This suggests that in the absence of PDE inhibition, cGMP produced by sGC was rapidly degraded, which resulted in smaller fold changes in cGMP under basal conditions and in response to sGC activation.

Figure 3.2
PDE inhibition increases cellular cGMP levels under basal conditions, with a further increase in cGMP when sGC was activated by BAY 60-2770 and SNAP. Mean ± SEM fold changes in cGMP over control in response to 100 µM IBMX and BAY and SNAP in the presence of IBMX. Statistical analysis performed with an unpaired two-tailed t test for control and a one-way ANOVA with Dunnett's multiple comparisons tests for BAY and SNAP. (Refer to Figure 3.1 legend for further detail).
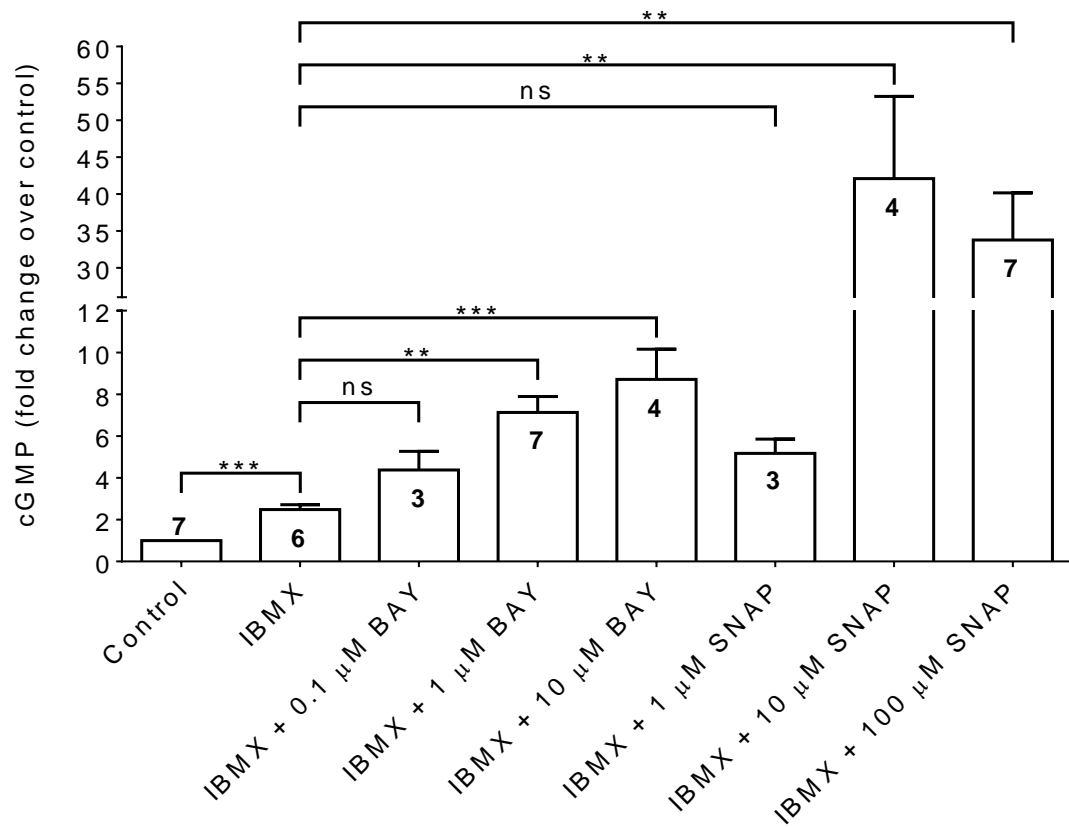
Figure 3.3

PDE inhibition and sGC activation increases cellular cGMP levels over sGC activation alone by BAY 60-2770. Mean ± SEM fold changes in cGMP over control in response to BAY in the absence and presence of 100 µM IBMX. Statistical analysis performed with one-way ANOVA with Sidak's multiple comparisons tests. (Refer to Figure 3.1 legend for further detail).
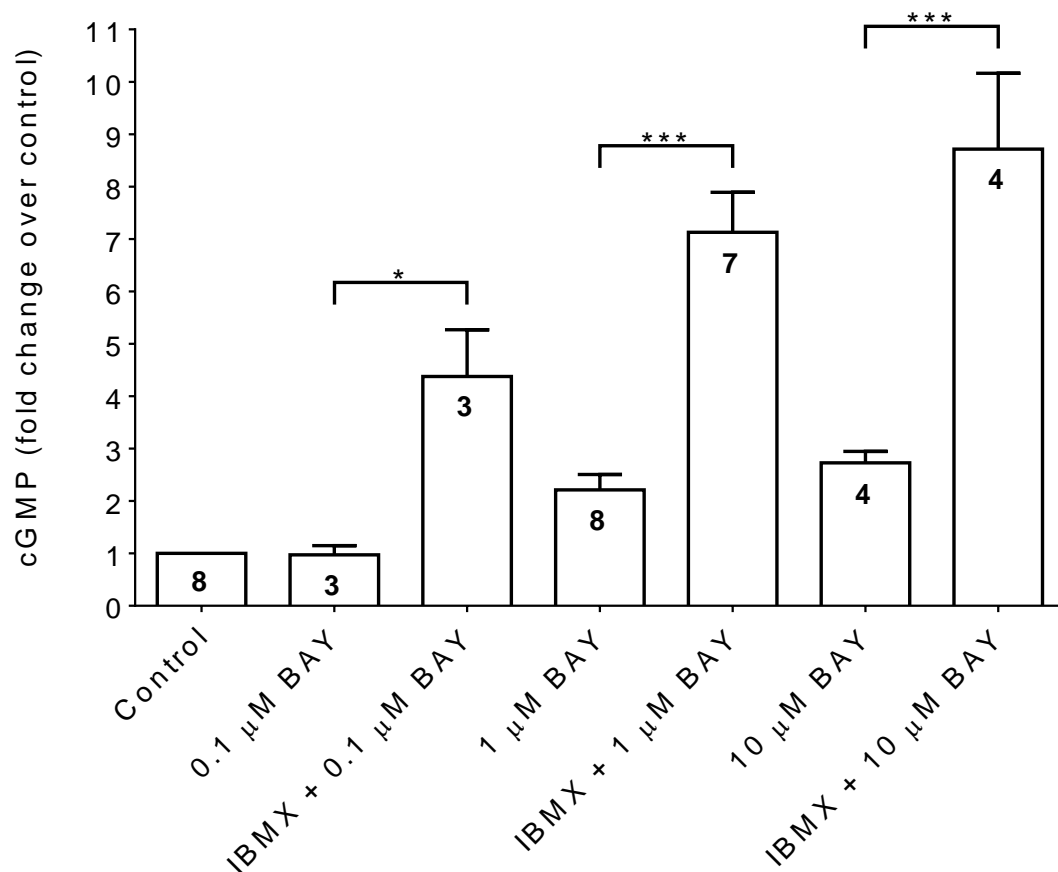
3.2.1.3 The effect of ODQ on cGMP responses to BAY 60-2770 and SNAP

1H-[1,2,4]Oxadiazolo[4,3-a]quinoxalin-1-one (ODQ) is a widely used selective inhibitor of sGC. However, previous reports on isolated co-recombinant sGC have demonstrated that ODQ acts synergistically with BAY to potentiate the activation of sGC (Knorr *et al.*, 2008). The aim of this experiment was to investigate and compare the effect of ODQ on cGMP responses to BAY and SNAP.

Application of 10 µM ODQ alone decreased cGMP to 0.75 ± 0.20 fold (n=3) compared with control levels (Figure 3.4). Although this decrease was not statistically significant (P>0.05), it suggests that ODQ inhibits the constitutive activity of sGC to some extent. However, cGMP may also be produced by other pathways including particulate guanylyl cyclase.

ODQ had opposing effects on the cGMP responses to BAY and SNAP. The response to BAY was potentiated by ODQ, whereas the response to SNAP was partially inhibited by ODQ (Figure 3.4). A 2.2 ± 0.29 fold change (n=8) was observed in response to 1 µM BAY, which increased profoundly to 28 ± 9.6 fold (n=4) in combination with ODQ (P<0.05). In the presence of IBMX, the response to 1 µM BAY also increased in combination with ODQ from 7.1 ± 0.76 fold (n=7) to 59 ± 17 fold (n=4) (P<0.001). In contrast, a 19 ± 3.7 fold change (n=8) was observed in response to 100 µM SNAP, which decreased to 3.2 ± 0.44 fold (n=3) in combination with ODQ. However, this substantial decrease in cGMP was not statistically significant (P>0.05). In the presence of IBMX, the response to 100 µM SNAP also decreased in combination with ODQ from 34 ± 6.4 fold (n=7) to 12 ± 3.7 fold (n=3) (P<0.05). This suggests differential modulation of sGC by ODQ for BAY and SNAP as opposing cGMP responses were observed. Importantly, a profound increase in cGMP was observed in response to BAY + ODQ. This combination of reagents was used in subsequent electrophysiology experiments.

Figure 3.4

ODQ potentiated the cellular cGMP response to BAY 60-2770 and inhibited the response to SNAP. Mean ± SEM fold changes in cGMP over control in response to 1 µM BAY, 100 µM SNAP, 10 µM ODQ and 100 µM IBMX in combination as indicated. Statistical analysis performed with an unpaired two-tailed t test for ODQ and a one-way ANOVA with Sidak's multiple comparisons tests for BAY and SNAP. (Refer to Figure 3.1 legend for further detail).
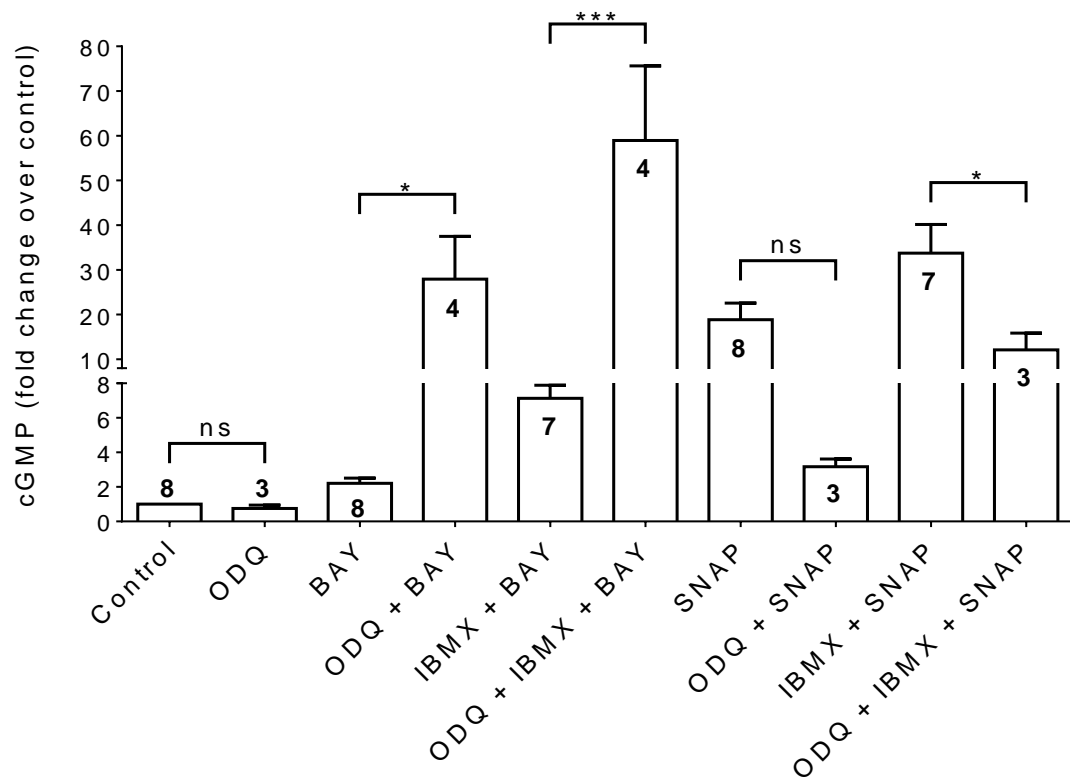
3.2.1.4 The effect of phosphodiesterase 5 inhibition on cGMP responses to BAY 60-2770 and SNAP

Phosphodiesterase 5 (PDE5) is highly expressed in guinea pig ventricular myocytes (Johnson *et al.*, 2012) and is a cGMP-specific PDE. Thus, PDE5 is an important regulator of cGMP levels and can be selectively inhibited by sildenafil. Compartmentalisation of cyclic nucleotide signalling pathways by specific PDEs has been widely described (Fischmeister *et al.*, 2006; Castro *et al.*, 2006; Castro *et al.*, 2010). To further investigate the role of PDEs in signal compartmentalisation, PDE5 was selectively inhibited as opposed to non-selective PDE inhibition with IBMX. The aim of this experiment was to investigate and compare the effect of sildenafil on cGMP responses to BAY and SNAP in contrast to IBMX.

PDE5 inhibition with 100 nM sildenafil did not alter cGMP over control levels ($P>0.05$) (Figure 3.5). This was in contrast to the 2.5 ± 0.23 fold change (n=6) observed in response to 100 µM IBMX ($P<0.01$) (Figure 3.2). This suggests that PDE5 was not primarily responsible for the degradation of cGMP produced by constitutive sGC activity.

Sildenafil also had no effect on cGMP responses to BAY or SNAP ($P>0.05$) (Figure 3.5). The response to 1 µM BAY was increased in combination with sildenafil, although the modest change was not statistically significant over BAY alone. This was in contrast to a significant increase of 7.1 ± 0.76 fold (n=7), in response to 1 µM BAY in combination with 100 µM IBMX ($P<0.05$). In the presence of sildenafil, the response to 100 µM SNAP was not altered over SNAP alone. This was in contrast to a large increase of 34 ± 6.4 fold (n=7), in combination with IBMX. However, the response to SNAP was not significantly different between sildenafil and IBMX ($P>0.05$). This suggests that PDE5 makes little contribution to the cGMP elevations induced by BAY and SNAP. At least at the cellular level, PDE5 did not appear to influence cGMP synthesised by sGC.

Figure 3.5
PDE5 inhibition did not modulate the cellular cGMP responses to BAY 60-2770 and SNAP. Mean ± SEM fold changes in cGMP over control in response to 100 nM sildenafil, 100 µM IBMX, 1 µM BAY and 100 µM SNAP in combination as indicated. Statistical analysis performed with unpaired two-tailed t tests for control and IBMX, and one-way ANOVA with Dunnett's multiple comparisons tests for BAY and SNAP. (Refer to Figure 3.1 legend for further detail).
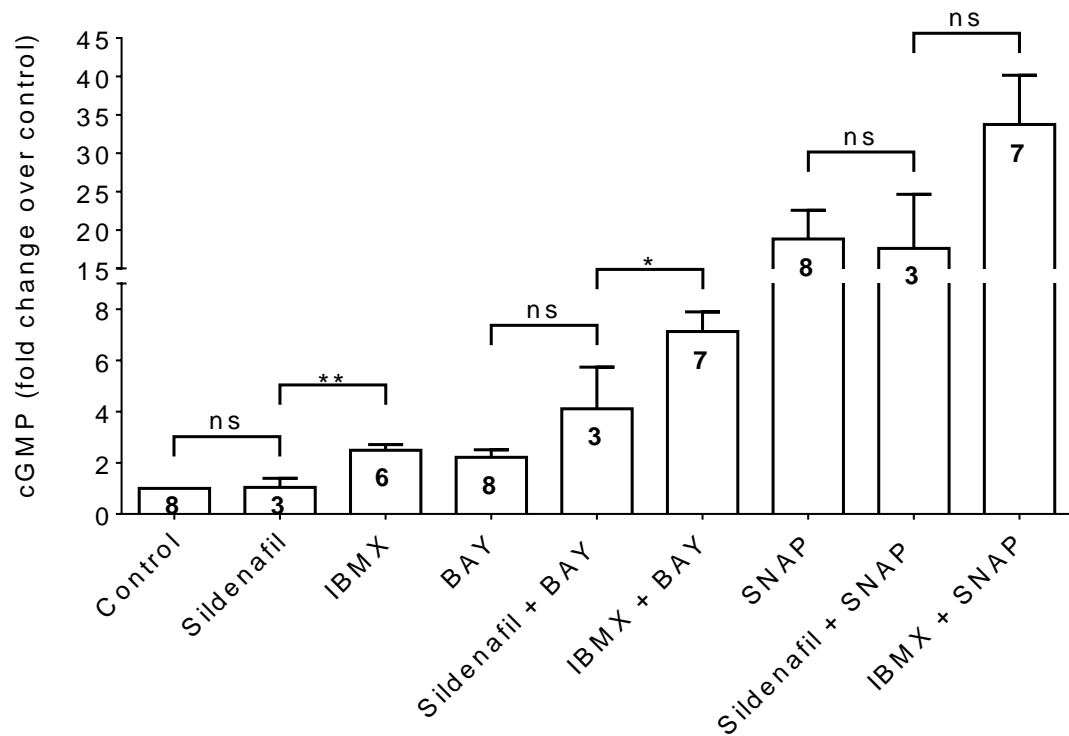
3.2.1.5 Comparison of cGMP responses to acetylcholine, isoprenaline and forskolin with BAY 60-2770

The results so far indicate that BAY activates sGC and increases cellular cGMP levels. However, the cGMP responses to BAY were modest compared with the NO donor SNAP. The aim of this experiment was to investigate the cGMP responses to physiologically relevant modulators of cGMP levels and compare the responses with BAY.

Acetylcholine (ACh) acts as an agonist at ACh receptors located on the sarcolemma of cardiac myocytes. Isoprenaline (ISO) is a β-adrenergic receptor agonist that stimulates β_1-, β_2- and β_3-adrenergic receptors. Stimulation of ACh and β_3-adrenergic receptors are coupled to nitric oxide synthase (NOS) activation, increased NO synthesis, activation of sGC and an increase in cGMP. In addition, ACh and β_3-adrenergic receptor stimulation inhibits adenylyl cyclase (AC) activity via the inhibitory G-protein $G_{\alpha i}$, which modulates cGMP via the interplay with cAMP and a change in the cAMP:cGMP. In contrast, stimulation of $\beta_{1/2}$-adrenergic receptors by ISO, and AC activation by forskolin (FSK) modulates cGMP via interplay with cAMP. ACh, ISO and FSK were applied at 1 μM, 30 nM and 30 μM respectively, concentrations that produce robust physiological responses.

ACh, ISO and FSK increased cGMP by 1.5 ± 0.31 fold (n=4), 1.4 ± 0.13 fold (n=4) and 3.1 ± 0.5 fold (n=3) respectively over control levels (Figure 3.6). These changes were not significantly different to the 2.2 ± 0.29 fold change (n=8) in response to 1 μM BAY (P>0.05). PDE inhibition with 100 μM IBMX increased the ACh, ISO and FSK responses to 5.3 ± 1.2 fold (n=5) (P<0.05), 6.3 ± 0.84 fold (n=5) (P<0.001) and 12 ± 2.3 fold (n=5) (P<0.05) respectively, compared to in the absence of IBMX. The ACh and ISO responses in the presence of IBMX were not significantly different to the 7.1 ± 0.76 fold change (n=7) in response to IBMX + BAY. In contrast, the large increase in cGMP in response to IBMX + FSK was significantly different (P<0.05). The responses to ACh, ISO and FSK were not altered by 10 μM ODQ (P>0.05). Whereas, ODQ

greatly potentiated the response to BAY by 28 ± 9.6 fold (n=4). Thus, the cGMP response to ODQ + BAY was significantly different to the ACh, ISO and FSK responses in the presence of ODQ (P<0.05).

This suggests that cGMP levels in response to ACh, ISO and FSK in the absence and presence of IBMX were comparable with BAY, with the exception of IBMX + FSK which responded with a markedly greater increase in cGMP. However, the potentiated response to BAY in combination with ODQ was not comparable with ACh, ISO and FSK.

3.2.1.6 The assay is highly specific for cGMP over cAMP

Cellular levels of cAMP are far higher than cGMP, and the fold changes in cAMP in response to some of the reagents tested were far greater than for cGMP. Therefore, it was important that the assay was highly selective for cGMP over cAMP. The specificity of the assay was investigated. On two occasions, cAMP standards with high concentrations of non-labelled cAMP (200 and 400 pmol, corresponding to several orders of magnitude higher than cGMP) were assayed. If the cGMP antibody in the assay was binding cAMP, then this would have resulted in low DPM values because it out competed the labelled cGMP. The DPM values for the cAMP containing samples were 888, 918, 981 and 1004 corresponding to 11.6, 10.5, 17.7 and 17.0 fmol for the 200 pmol cAMP standards and 672, 677, 908, 904 corresponding to 24.0, 23.5, 20.5, 20.7 fmol for the 400 pmol cAMP standards. Thus, detection of cAMP was 11,765-19,048 times smaller than the known concentration of cAMP, showing that the assay had high specificity for cGMP.

Figure 3.6
Comparability of cellular cGMP responses to BAY 60-2770 with ACh, ISO and FSK. Mean ± SEM fold changes in cGMP over control in response to 1 µM BAY, 1 µM ACh, 30 nM ISO, 30 µM FSK, 100 µM IBMX and 10 µM ODQ in combination as indicated. Statistical analysis performed with one-way ANOVA with Dunnett's multiple comparisons tests. (Refer to Figure 3.1 legend for further detail).
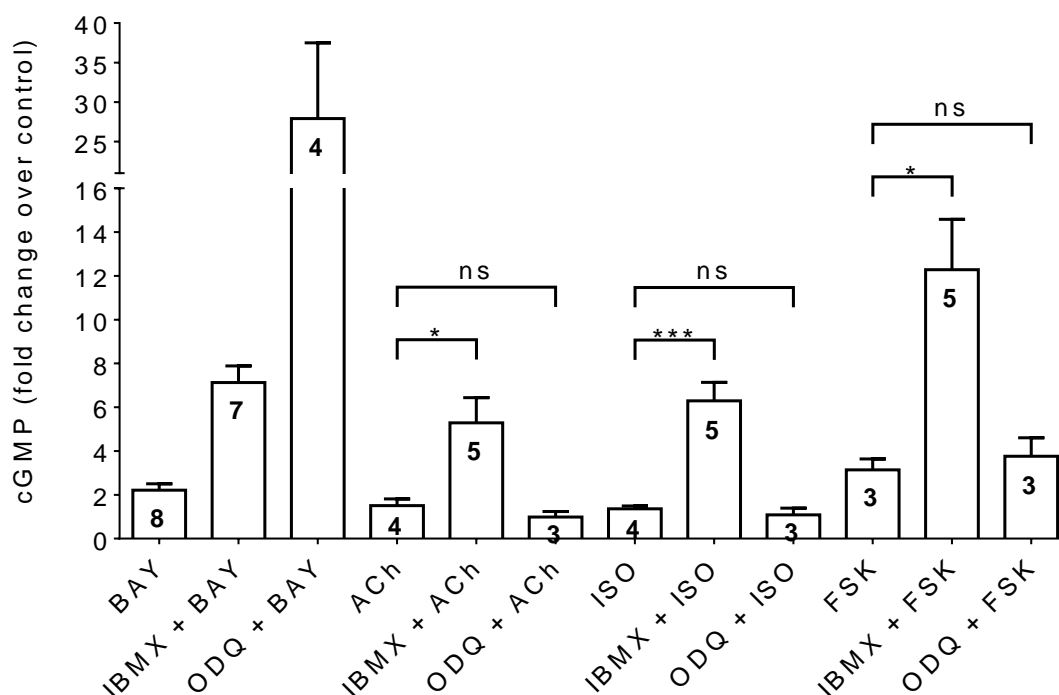
Figure 3.7
The assay is highly specific for cGMP over cAMP. (A and B) Representative cGMP standard curves from two separate assays. Disintegrations per minute (DPM) values are plotted against $\log_{10}$ [cGMP] (in fmol) for known cGMP standards. Individual symbols represent mean DPM values from duplicate cGMP standards. The curves were fit with a sigmoidal dose-response (variable slope) and least squares (ordinary fit) function (solid lines). DPM values for the 200 pmol and 400 pmol cAMP standards are shown interpolated from the standard curve and indicated by the red and blue dashed lines respectively.
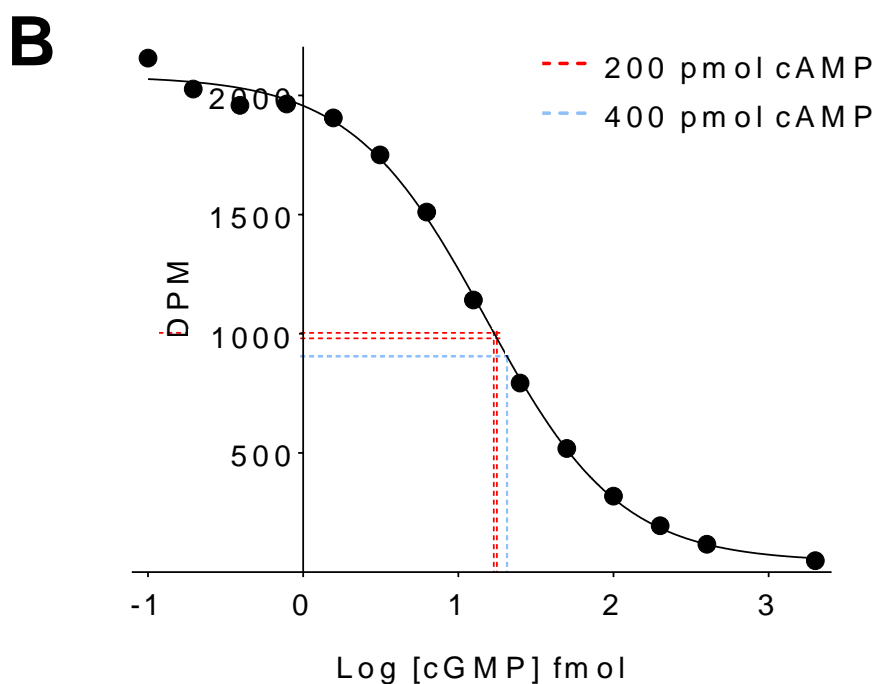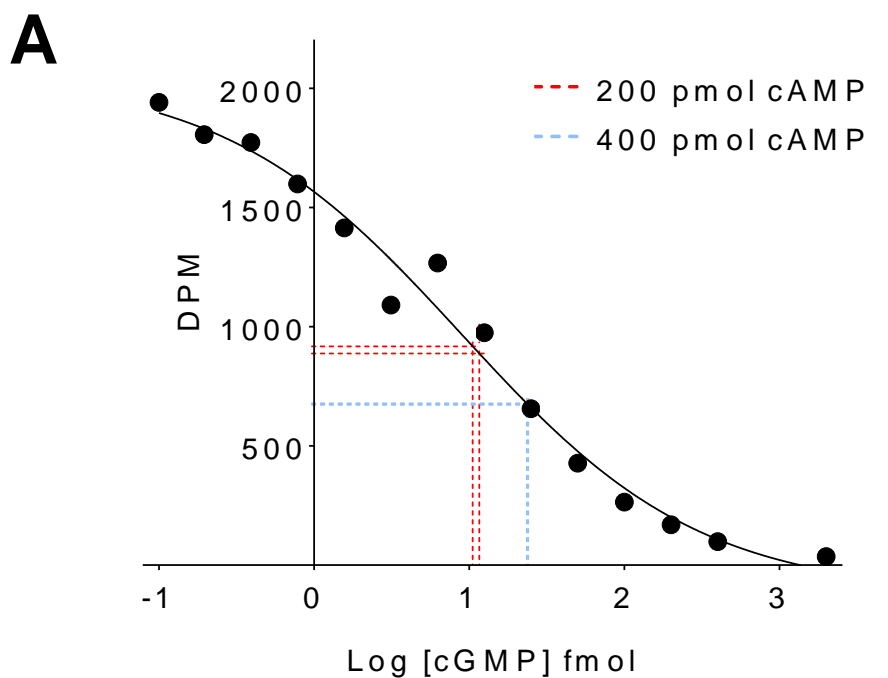
3.2.2 The perforated patch-clamp technique provided stable conditions for action potential measurement

The ruptured patch-clamp technique is often associated with 'run-down' of recordings over time, because the cytosol is dialysed by the intracellular solution in the electrode which results in reductions in channel activity. Thus, there is a lack of continuity between experimental conditions with time. The perforated patch-clamp technique is designed to overcome this problem. The aim of this experiment was to investigate the stability of action potential duration (APD) over time whilst using the perforated patch-clamp technique.

Representative ventricular APs recorded from a single guinea pig left ventricular myocyte during the course of an experiment are shown in Figure 3.8, A. The mean resting membrane potential was -92.4 mV. During stimulation of an AP, the membrane potential became more positive with an extremely rapid AP upstroke. The AP upstroke time and AP peak membrane potential had mean values of 2.4 ms and +46.4 mV respectively. The AP peak was followed by a short lasting plateau phase whereby the membrane potential remained relatively stable, typically for <20 ms before repolarisation. During repolarisation, the membrane potential became more negative, with an initial slow phase and a rapid final phase and returned to the resting membrane potential. Figure 3.8, B shows measurements of the action potential duration to 90% repolarisation (APD_{90}) from the same cell during the course of an experiment. Initially, APD_{90} was relatively extended during AP stimulation. APD_{90} was 328 ms, 10 seconds after first stimulated, rapidly decreased during the first minute, reached a steady-state duration of 217 ms in 2 minutes and remained stable thereafter. The initial decrease in APD_{90} during AP stimulation was due to the physiological process of electrical restitution. Thus, APD remained stable for long periods of time whilst using the perforated patch-clamp technique, which allowed continuity between experimental conditions over time and longer duration experiments.

Figure 3.8
Action potentials were stable when measured using the perforated patch-clamp technique. (A) Representative APs recorded from a guinea pig left ventricular myocyte at indicated time intervals after the first AP stimulation. Experiments were performed at $37^{o}C$ and cells were stimulated at 2 Hz with 2 ms current pulses applied via the electrode. (B) Time course of APD_{90}. Individual symbols represent measurement from a single AP.
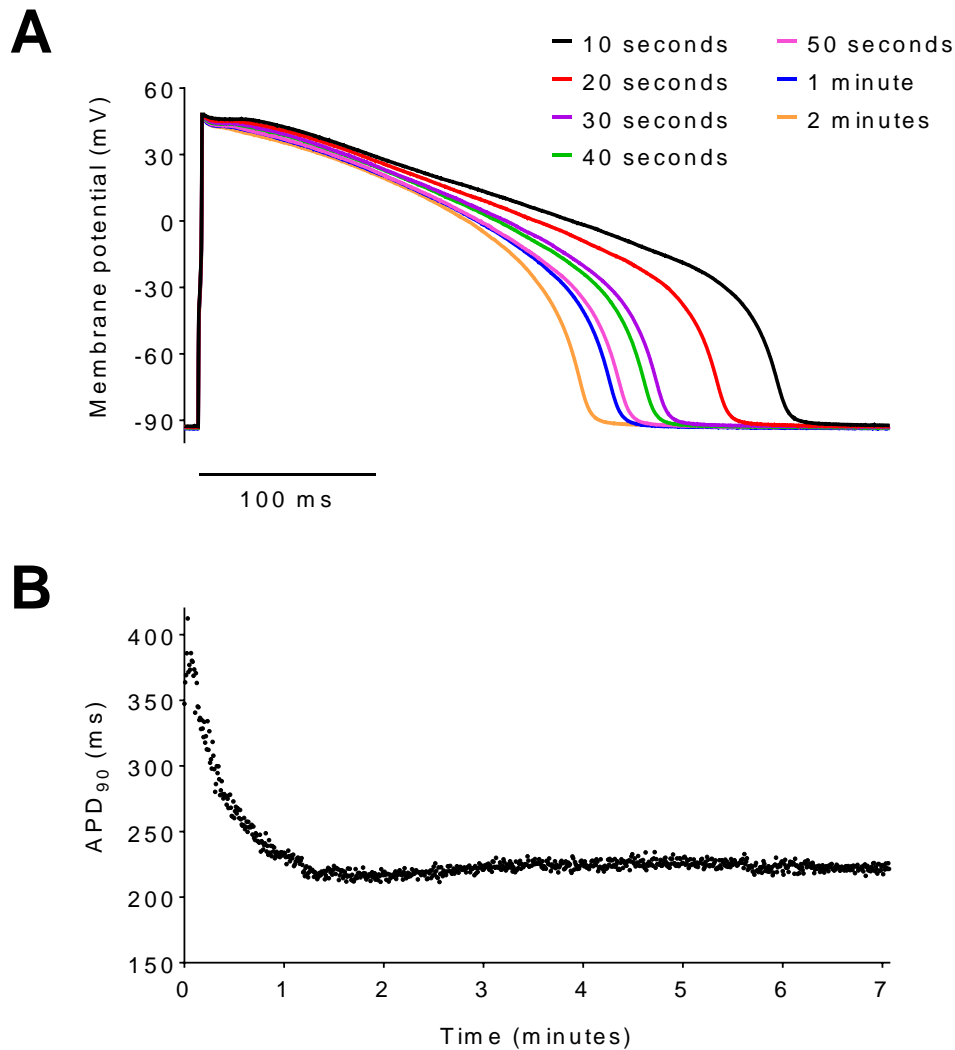
3.2.3 Responses of action potentials to modulation of cGMP-dependent signalling

3.2.3.1 The effect of soluble guanylyl cyclase activity on action potentials

Results from the previous section showed that the novel sGC activator BAY elevated cellular cGMP levels by comparable amounts to ACh and ISO. Additionally, cGMP could be profoundly increased by BAY + ODQ and the NO donor SNAP. Also, the changes in cGMP levels in response to BAY and SNAP were increased by non-selective PDE inhibition with IBMX.

The following experiments investigated whether APs were modulated under these experimental conditions. APs were stimulated at 2 Hz and recorded from single guinea pig isolated left ventricular myocytes. In all experiments, APD was given time to reach steady-state prior to superfusion with test reagents and in between test reagents. APD_{90} was measured and compared between experimental conditions. The aim of these experiments was to investigate the effect of sGC activity modulation by 10 µM ODQ and 1 µM BAY on APs.

Inhibition of basal sGC activity with ODQ did not modulate APs. Representative APs and APD_{90} time course are shown in Figure 3.9. No change in APD or AP morphology was observed in ODQ (Figure 3.9, A). APD_{90} remained relatively stable throughout the course of the experiment, with no profound changes during ODQ application (Figure 3.9, B). Mean APD_{90} was 261 ± 8.7 ms (n=5) in control and remained unchanged at 261 ± 8.1 ms (n=5) in response to ODQ (P>0.05) (Figure 3.9, D). This suggests that ODQ-mediated inhibition of sGC activity did not modulate APD, under basal conditions.

In contrast, activation of sGC with BAY modulated APs and shortened APD. Representative APs and APD_{90} time course are shown in Figure 3.10. APD was shortened by BAY by acceleration of repolarisation (Figure 3.10, A). APD_{90} decreased within 3 minutes of BAY application and reached a relatively steady-state within 5 minutes, although fluctuations in APD were observed (Figure

3.10, B). BAY decreased mean APD_{90} to 210 ± 5.2 ms (n=7) from 221 ± 7.0 ms (n=7) in control (P<0.01) (Figure 3.10, D). Co-application of BAY and ODQ dramatically potentiated sGC activity, which resulted in a profound increase in cGMP levels compared to BAY application alone (Figure 3.4). Despite this, co-application of BAY and ODQ had no effect on APD or AP morphology over BAY alone (Figure 3.10, A). APD_{90} remained relatively stable with no profound changes during ODQ application (Figure 3.10, B). Mean APD_{90} remained unchanged at 211 ± 10 ms (n=7) in response to BAY + ODQ which was not significantly different to BAY alone (P>0.05) (Figure 3.10, D). Mean APD_{90} responses to BAY and BAY + ODQ were significantly different to control (P<0.01) and the response to BAY was not reversed by wash off (Figure 3.10, D).

Regulation of repolarisation by BAY was most likely due to activation of the slow or rapid delayed rectifier K^+ currents, I_{Ks} and I_{Kr}, as the early phases of the AP were marginally altered during BAY application. Importantly, ODQ had no additional effect over BAY alone, despite the profound potentiation of sGC activity measured in the cGMP assay (Figure 3.4).

Figure 3.9

ODQ did not modulate APs under basal conditions. (A) Representative APs recorded from a guinea pig left ventricular myocyte at 37°C in control and 10 μM ODQ. Each AP was averaged from 20 consecutive APs after reaching steady-state (indicated by vertical dashed lines in B). (B) Time course of APD$_{90}$ responses before and during ODQ application (indicated by horizontal bar). Individual symbols represent measurement from a single AP. (C) APD$_{90}$ from individual myocytes under each condition. Data points from individual cells linked by a continuous line. (D) Mean ± SEM APD$_{90}$. Number of cells indicated in each bar. Statistical analysis performed with a paired two-tailed t test.
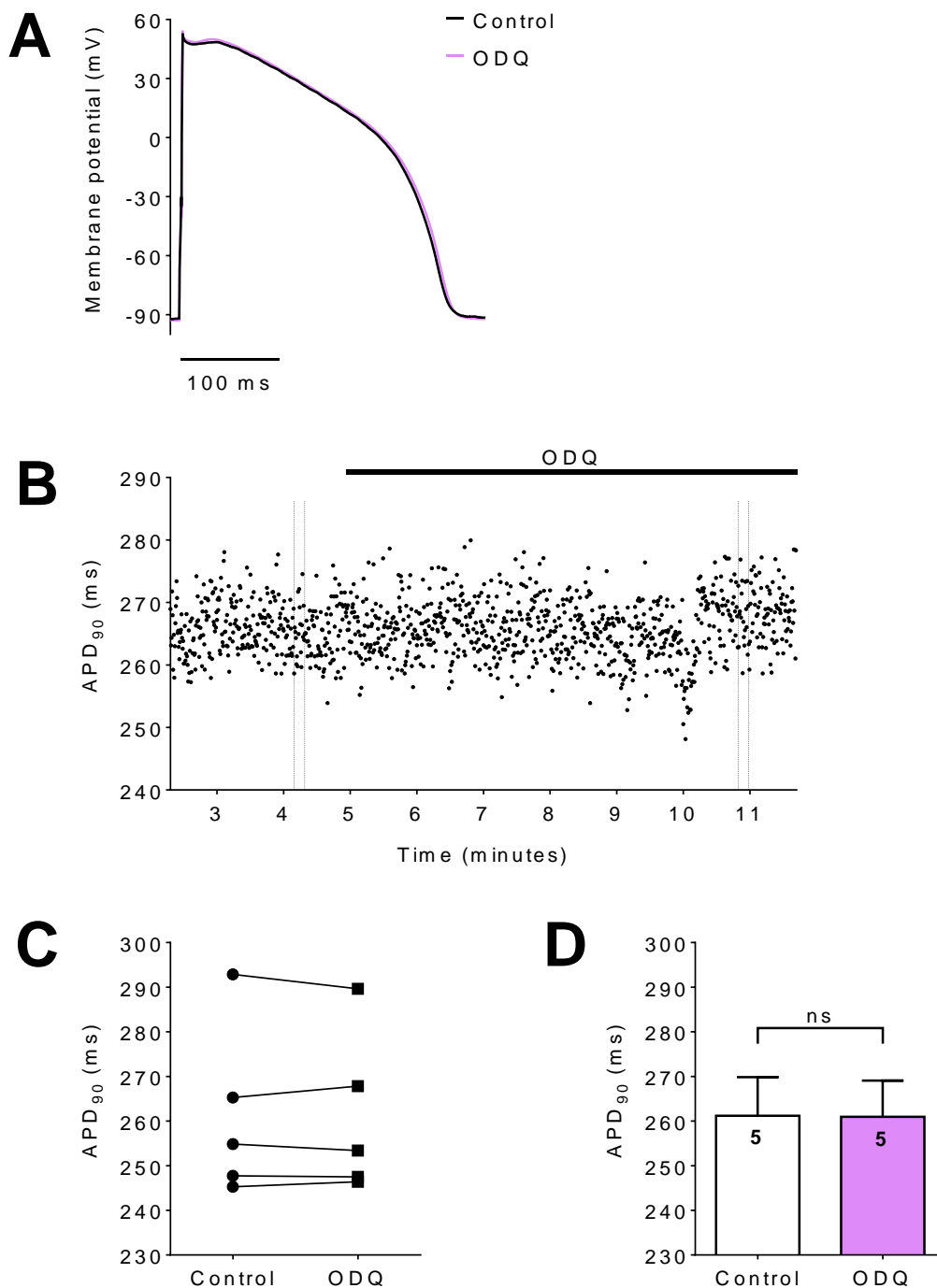
Figure 3.10

BAY 60-2770 shortened APD under basal conditions, with no further modulation by ODQ. (A) Representative APs recorded in control, 1 µM BAY and BAY + 10 µM ODQ. (B) Time course of APD_{90} responses before and during BAY and ODQ application. (C) APD_{90} from individual myocytes under each condition. (D) Mean ± SEM APD_{90}. Number of cells indicated in each bar. Statistical analysis performed with repeated measures one-way ANOVA with Sidak's multiple comparisons test. (Refer to Figure 3.9 legend for further detail).
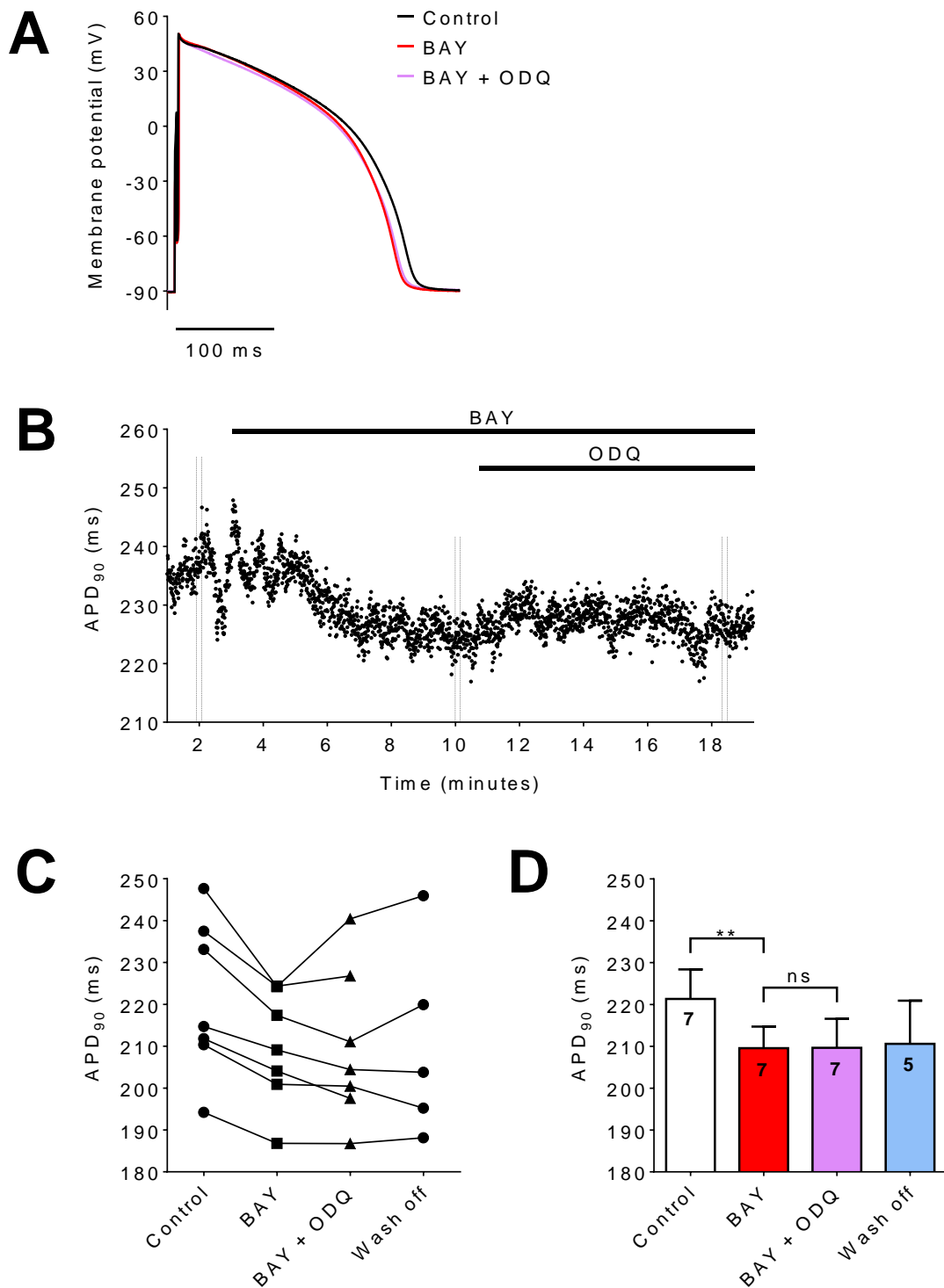
3.2.3.2 The effect of phosphodiesterase inhibition on the modulation of repolarisation by BAY 60-2770

The AP responses to sGC activation were relatively minor, despite earlier results showing substantial elevations in cellular cGMP levels, with BAY + ODQ in particular. The aim of this experiment was to investigate whether PDEs were responsible for suppressing responses to BAY, by using 100 µM IBMX to non-selectively inhibit PDE activity.

Inhibition of PDE activity with IBMX, shortened APD by a profound acceleration of repolarisation compared to control and also elevated the plateau phase, suggesting augmentation of $I_{Ca,L}$ (Figure 3.11, A). Within 1 minute of IBMX application, APD_{90} rapidly decreased and reached steady-state within 3 minutes (Figure 3.11, B). Mean APD_{90} decreased to 184 ± 9.8 ms (n=7) in response to IBMX, from 259 ± 7.3 ms (n=7) in control (P<0.01) (Figure 3.11, D). Interestingly, application of 1 µM BAY in the presence of IBMX, prolonged APD by slowing down repolarisation (Figure 3.11, A). A slow increase in APD_{90} was observed within 2 minutes of BAY application which reached steady-state within 5 minutes (Figure 3.11, B). Mean APD_{90} increased to 200 ± 10 ms (n=7) in response to IBMX + BAY and recovered to 256 ± 6.6 ms (n=7) in wash off (P<0.05) (Figure 3.11, D). Mean APD_{90} responses to IBMX and IBMX + BAY were significantly different to control (P<0.01), and were fully reversible as no significant difference was found between control and wash off (P>0.05). This suggests that under PDE inhibition, sGC activation prolongs APD, the opposite effect to BAY under basal conditions. Thus, there were differential effects of sGC activation in the absence and presence of PDE activity.

In a sub-population of myocytes, BAY did not modulate APs when PDEs were inhibited (Figure 3.12). IBMX modulated APD and AP morphology as previously described. APD_{90} decreased in response to IBMX, remained unchanged in response to IBMX + BAY and partially recovered in wash off (Figure 3.12, C). The number of cells were too small for statistical analysis. However, it suggests that there may be heterogeneity in responses to sGC activation.

Figure 3.11

BAY 60-2770 prolonged APD when PDEs were inhibited. (A) Representative APs recorded in control, 100 μM IBMX and IBMX + 1 μM BAY. (B) Time course of APD_{90} responses before and during IBMX and BAY application. (C) APD_{90} from individual myocytes under each condition. (D) Mean ± SEM APD_{90}.

Number of cells indicated in each bar. Statistical analysis performed with repeated measures one-way ANOVA with Sidak's multiple comparisons test. (Refer to Figure 3.9 legend for further detail).
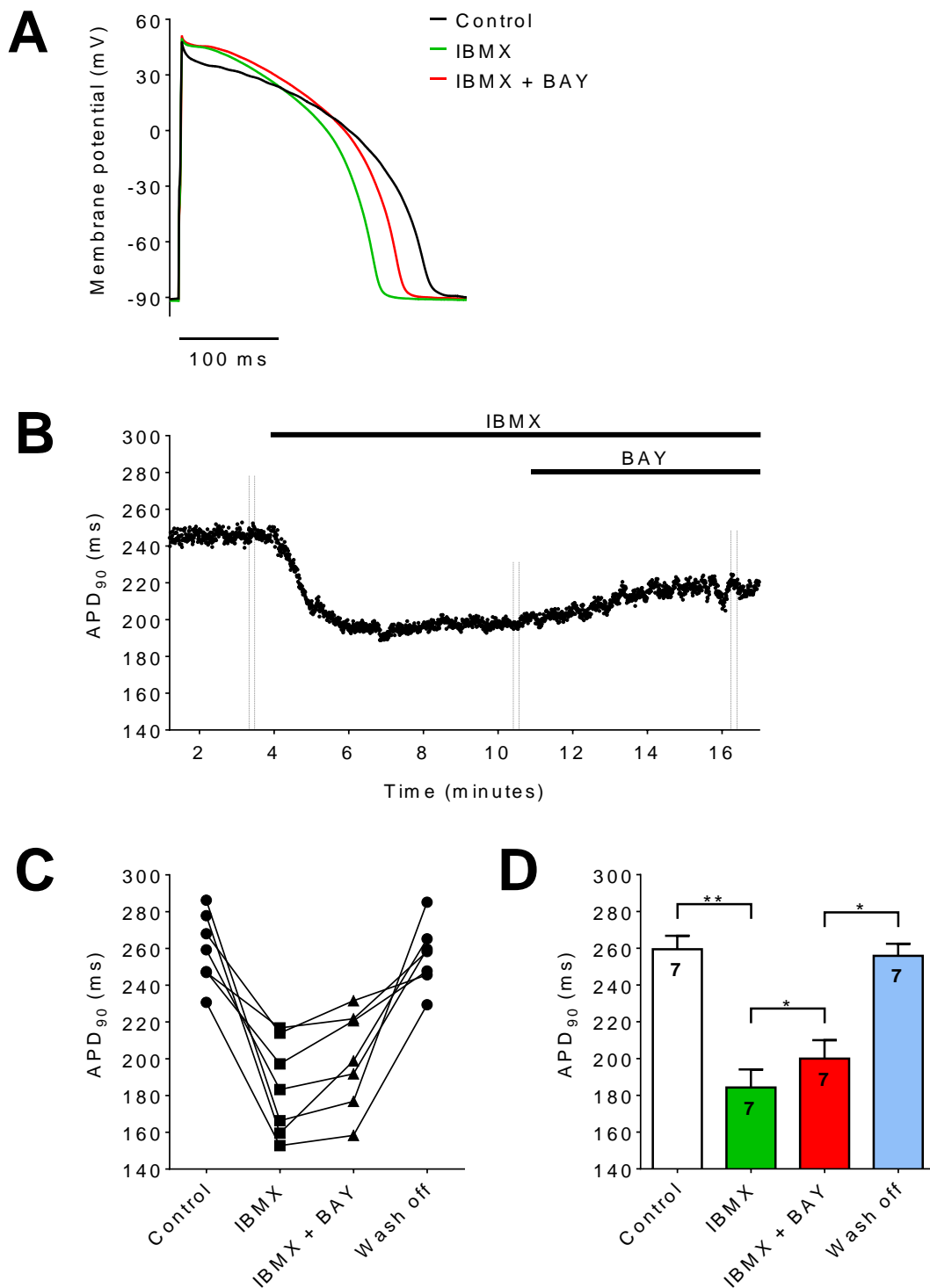
Figure 3.12

In a proportion of myocytes, BAY 60-2770 did not modulate APs when PDEs were inhibited. (A) Representative APs recorded in control, 100 μM IBMX and IBMX + 1 μM BAY. (B) Time course of APD_{90} responses before and during IBMX and BAY application. (C) APD_{90} from individual myocytes under each condition. (Refer to Figure 3.9 legend for further detail).
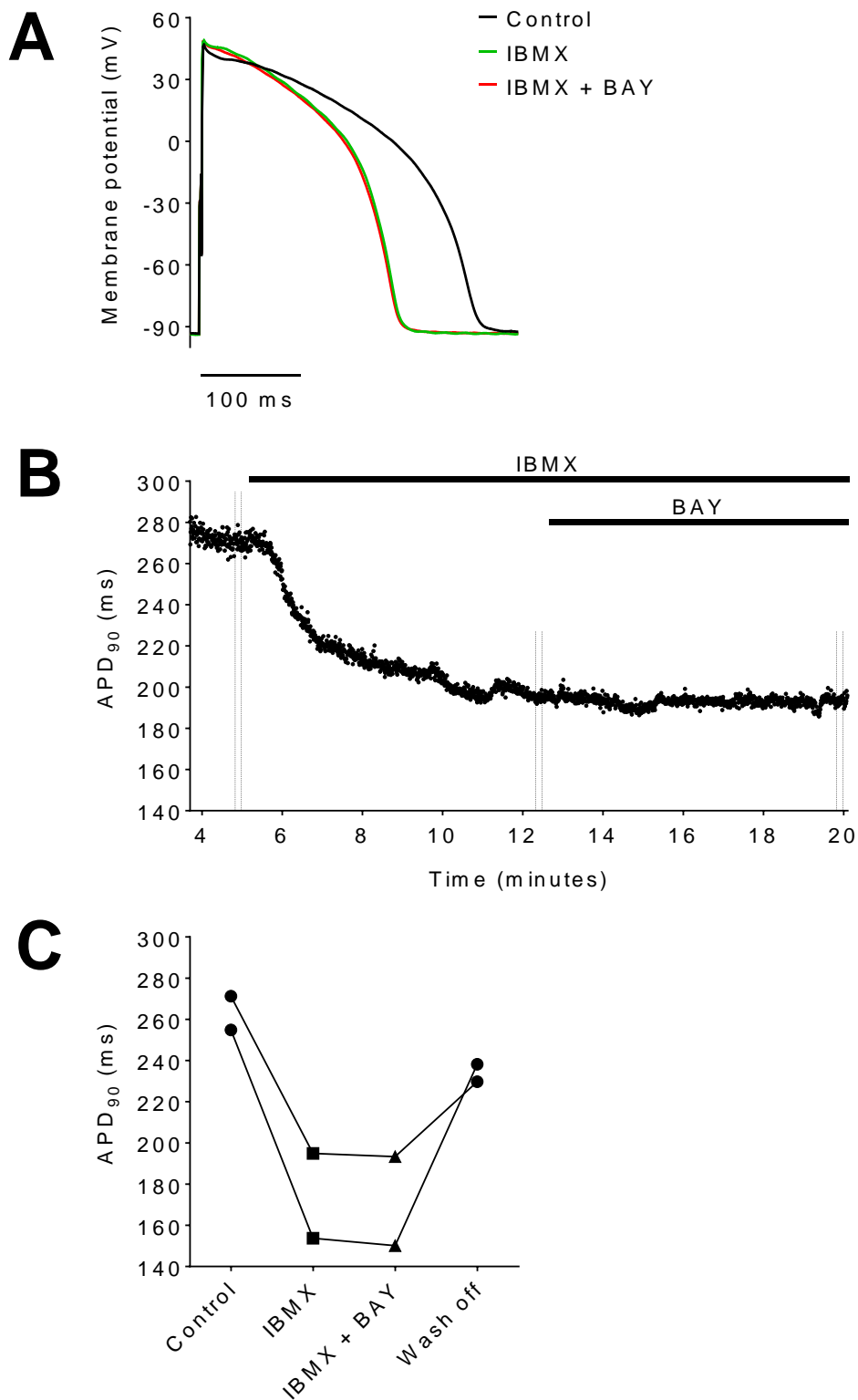
3.2.3.3 The effect of a protein kinase A inhibitor on the modulation of repolarisation by BAY 60-2770

cGMP and cAMP signalling pathways are interlinked. Changes in cGMP levels can alter the activity of phosphodiesterase 2 (PDE2) and phosphodiesterase 3 (PDE3) and since most PDEs are non-selective this can modulate levels of cAMP. The aim of this experiment was to investigate whether responses to sGC activation were mediated by changes in cAMP signalling. Thus, protein kinase A (PKA), an important effector of cAMP was inhibited with 3 μM N-[2-(p-Bromocinnamylamino)ethyl]-5-isoquinolinesulfonamide dihydrochloride (H89).

PKA inhibition with H89 prolonged APD and modulated AP morphology. APs exhibited a triangular morphology and the membrane potential of the plateau phase became more negative compared to control (Figure 3.13, A). A rapid increase in APD_{90} was observed within 1 minute of H89 application and reached steady-state within 3 minutes (Figure 3.13, B). H89 significantly increased mean APD_{90} to 268 ± 10 ms (n=7) from 224 ± 6.0 ms (n=7) in control (P<0.01) (Figure 3.13, D). IBMX had the same effect on APD and AP morphology as previously described and decreased mean APD_{90} to 195 ± 7.1 ms (n=7) compared to H89 alone (P<0.001) (Figure 3.13, D), despite H89 supposedly inhibiting PKA. BAY also had the same effect on APD and AP morphology as previously described and increased mean APD_{90} to 217 ± 12 ms (n=7), compared to H89 + IBMX (P<0.05) (Figure 3.13, D). In wash off, mean APD_{90} recovered to 227 ± 6.2 ms (n=5). Mean APD_{90} responses to H89 and H89 + IBMX were significantly different to control (P<0.01), (P<0.05), whereas there was no significant difference between control and H89 + IBMX + BAY (P>0.05) (Figure 3.13, D).

Importantly, H89 had no effect on the response to IBMX (Figure 3.13). This suggests that at this concentration, H89 did not fully and selectively inhibit PKA and may have blocked K^+ channels resulting in changes in AP morphology. The response to BAY was also not inhibited by H89. However, conclusions cannot be drawn from these experiments as H89 is not selective or potent enough.

Figure 3.13

BAY 60-2770 prolonged APD when PDEs were inhibited and a PKA inhibitor was applied. (A) Representative APs recorded in control, 3 μM H89, H89 + 100 μM IBMX and H89 + IBMX + 1 μM BAY. (B) Time course of APD_{90} responses before and during H89, IBMX and BAY application. (C) APD_{90} from individual myocytes under each condition. (D) Mean ± SEM APD_{90}. Number of cells indicated in each bar. Statistical analysis performed with repeated measures one-way ANOVA with Sidak's multiple comparisons test. (Refer to Figure 3.9 legend for further detail).
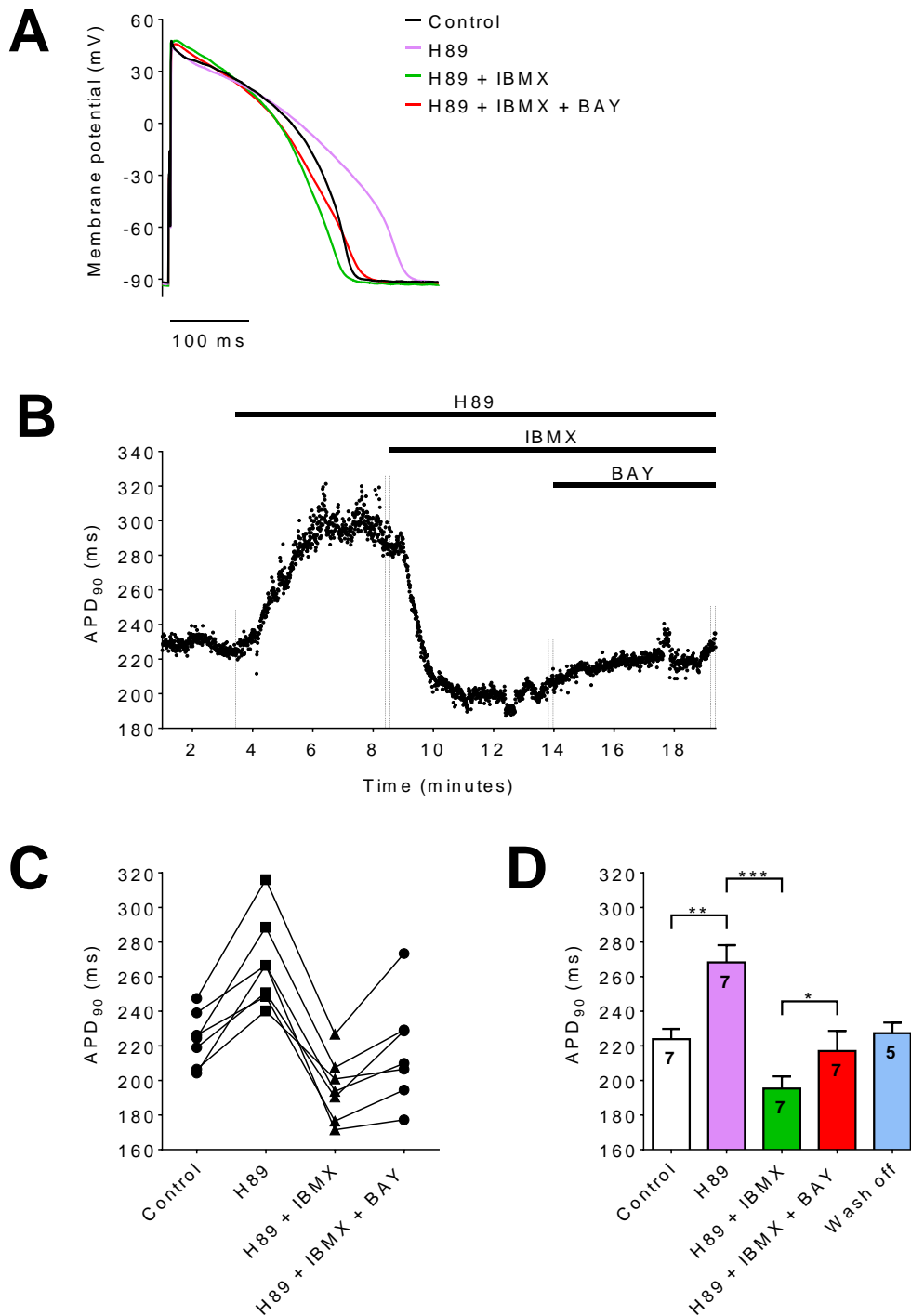
3.2.3.4 The effect of soluble guanylyl cyclase activation by the nitric oxide donor SNAP on action potentials

The physiological agonist of sGC is NO. However, NO can also exert effects via cGMP-independent signalling, such as S-nitrosylation of proteins. The aim of this experiment was to compare AP responses to BAY and the NO donor SNAP, which caused a robust elevation in cGMP levels (Figures 3.1 and 3.2).

Surprisingly, 100 µM SNAP did not modulate APs under basal conditions or when PDEs were inhibited. Representative APs and APD_{90} time courses are shown in Figures 3.14 and 3.15. Under basal conditions, no change in APD or AP morphology was observed in SNAP (Figure 3.14, A). APD_{90} remained relatively stable throughout the course of the experiment, with no profound changes during SNAP application (Figure 3.14, B). Mean APD_{90} remained unchanged at 235 ± 16 ms (n=5) in response to SNAP, compared to 232 ± 14 ms (n=5) in control (P>0.05) (Figure 3.14, D).

IBMX had the same effect on APD and AP morphology as previously described and decreased mean APD_{90} to 169 ± 9.0 ms (n=5) from 247 ± 3.1 ms (n=5) in control (P<0.01) (Figure 3.15, D). In the presence of IBMX, no change in APD or AP morphology was observed in SNAP (Figure 3.15, A). APD_{90} remained relatively stable with no profound changes during SNAP application (Figure 3.15, B). Mean APD_{90} remained unchanged at 171 ± 9.6 ms (n=5) in response to IBMX + SNAP compared to IBMX alone (P>0.05) (Figure 3.15, D).

This suggests that unlike BAY, sGC activation with the NO donor SNAP did not modulate APD in the absence or presence of PDE inhibition. Thus, SNAP and BAY act differently.

Figure 3.14

SNAP did not modulate APs under basal conditions. (A) Representative APs recorded in control and 100 μM SNAP. (B) Time course of APD_{90} responses before and during SNAP application. (C) APD_{90} from individual myocytes under each condition. (D) Mean ± SEM APD_{90}. Number of cells indicated in each bar. Statistical analysis performed with repeated measures one-way ANOVA with Sidak's multiple comparisons test. (Refer to Figure 3.9 legend for further detail).
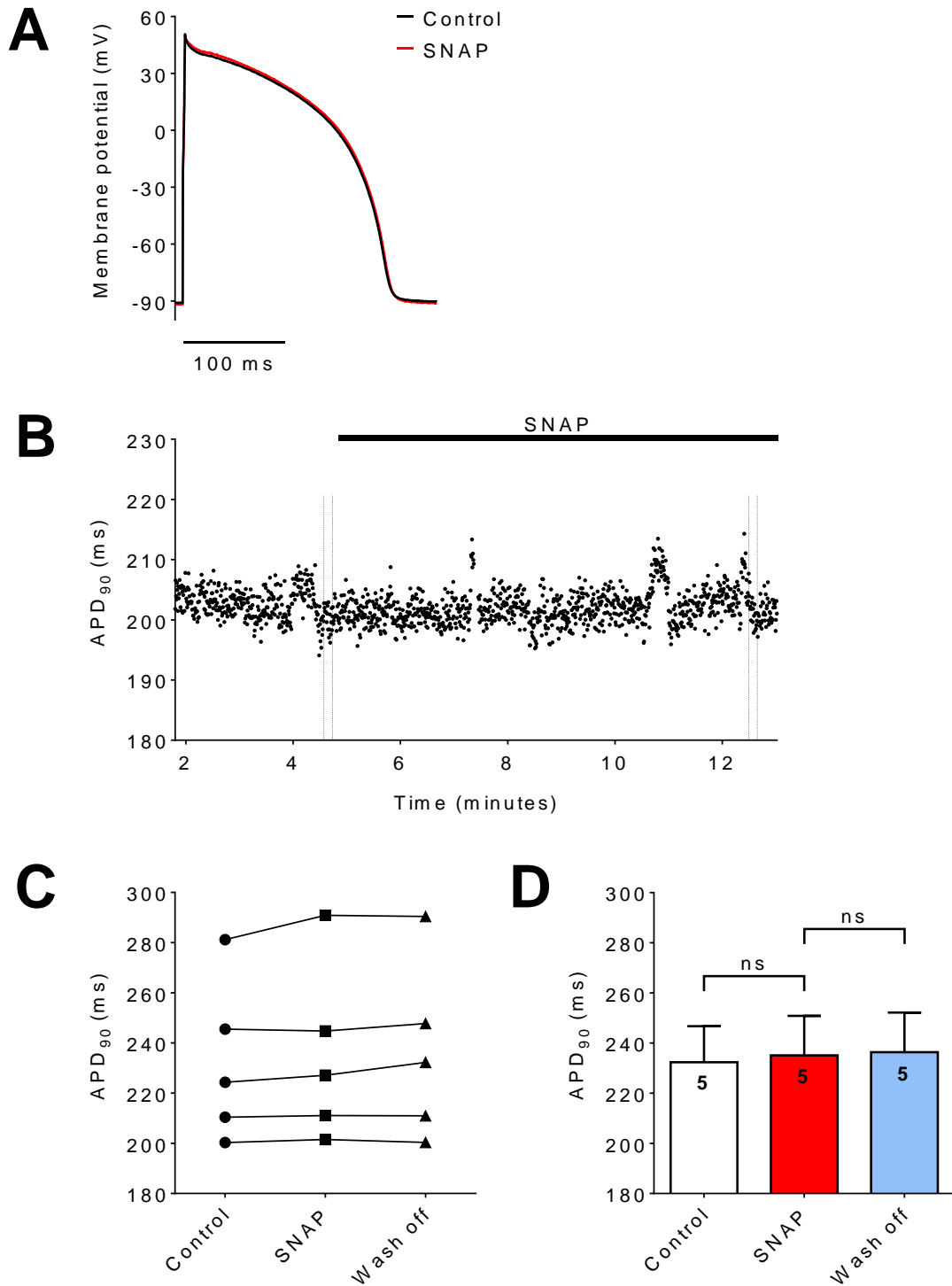
Figure 3.15

SNAP did not modulate APs when PDEs were inhibited. (A) Representative APs recorded in control, 100 µM IBMX and IBMX + 100 µM SNAP. (B) Time course of APD_{90} responses before and during IBMX and SNAP application. (C) APD_{90} from individual myocytes under each condition. (D) Mean ± SEM APD_{90}. Number of cells indicated in each bar. Statistical analysis performed with repeated measures one-way ANOVA with Sidak's multiple comparisons test. (Refer to Figure 3.9 legend for further detail).
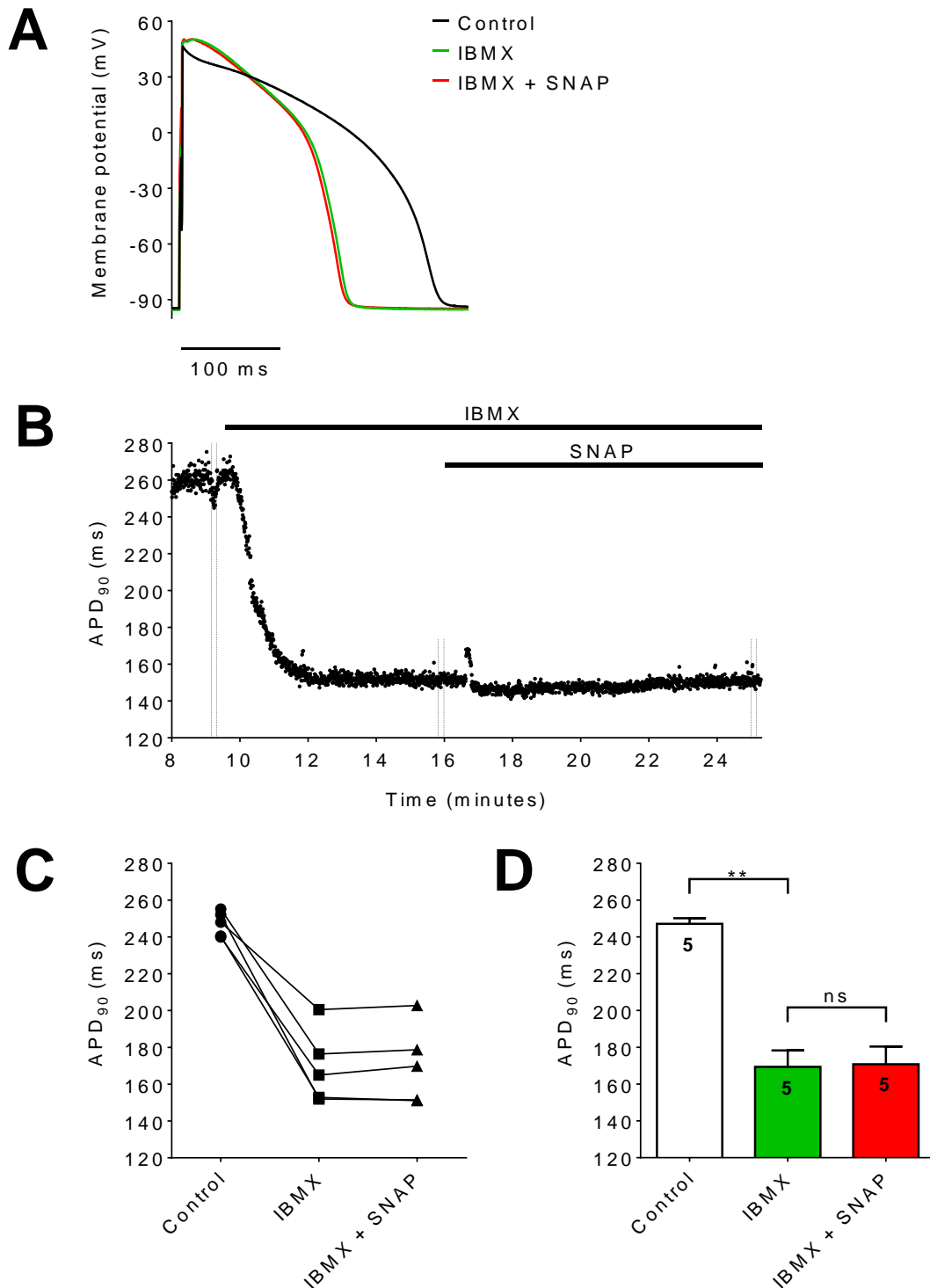
Chapter 4

Responses of delayed rectifier potassium currents to modulation of cGMP-dependent signalling in guinea pig left ventricular myocytes

4.1 Introduction

The delayed rectifier K^+ currents play a vital role in cardiac repolarisation. Repolarisation of the human ventricular AP occurs as a result of activation of multiple currents, which include the transient outward K^+ current (I_{To}), the delayed rectifier K^+ currents and the inward rectifier K^+ current (I_{K1}). Human myocytes exhibit three distinct types of delayed rectifier K^+ currents which are named according to the time course of activation. The ultra-rapid, rapid and slow delayed rectifier K^+ currents are known as I_{Kur}, I_{Kr} and I_{Ks} respectively. Channels conducting I_{Kur} are expressed in human atrial myocytes but not in human ventricular myocytes (Gaborit *et al.*, 2007). I_{Kr} and I_{Ks} are vital for controlling and terminating the plateau phase of the ventricular AP.

The guinea pig was used as a model animal due to similarities with humans in ventricular AP properties, as previously described. In addition, guinea pig ventricular repolarisation is highly dependent on I_{Kr} and I_{Ks} channels, as in humans. Mouse or rat animal models have little I_{Kr} and I_{Ks}, and the predominant repolarising currents are I_{To} and I_{K1} (Rosati *et al.*, 2008). Thus, although not perfect, the guinea pig is a suitable animal model to investigate modulation of the delayed rectifier K^+ currents by cGMP-dependent signalling.

Previous experiments had shown that sGC activation with BAY 60-2770 shortened APD when applied on its own (refer to Figure 3.10). On the other hand, when PDEs were inhibited to block cGMP hydrolysis, then BAY 60-2770 prolonged APD (refer to Figure 3.11). In both cases, the changes to the AP occurred during the late plateau phase, rather than during the notch, early plateau or final repolarisation phases. While this did not rule out effects on other channels, it suggested that the delayed rectifier K^+ currents were the most likely

currents to be modulated by BAY 60-2770. Therefore, the objectives were to investigate the effects on I_{Kr} and I_{Ks} of BAY 60-2770 and other reagents known to modulate cGMP-dependent signalling in guinea pig isolated left ventricular myocytes.

4.2 Results

4.2.1 Recording delayed rectifier potassium currents

4.2.1.1 Unstable currents recorded using I-V protocols

The perforated patch-clamp technique was used for all voltage clamp recordings to minimise alterations to intracellular constituents and ensure continuity between experimental conditions with time. The delayed rectifier K^+ currents were initially recorded from single guinea pig isolated left ventricular myocytes using a current-voltage (I-V) relationship protocol that stepped to a number of different test potentials. This type of protocol is widely used to study voltage-dependent properties of the current, such as the voltage-dependence of activation.

The initial I-V protocol had a holding potential of -40 mV that was used to inactivate the fast I_{Na}, followed by a depolarising step to a test potential for 500 ms and a final step back to the -40 mV holding potential. The test potentials ranged from -30 mV to +60 mV and were increased in 10 mV increments from negative to positive potentials (Figure 4.1, A) at start-start intervals of 10 seconds. Unfortunately, use of this I-V protocol was commonly associated with myocytes becoming Ca^{2+} overloaded, which was reflected in the instability of the currents recorded and the observation of contractile waves passing along the length of the cell when viewed down the microscope. A representation of the I-V protocol and the corresponding family of current traces are shown in Figure 4.1. The instability and fluctuations of the tail current and the current during the test potential in response to a number of different test potentials is shown in red to highlight the effect on current amplitude and time course (Figure 4.1, B). As a result, current amplitude could not be measured accurately. In these experiments, the intracellular solution contained 10 mM NaCl. Under these conditions, the reversal potential for the Na^+/Ca^{2+} exchanger was calculated as -42 mV. Therefore, at voltages positive to the reversal potential, the exchanger would be reversed resulting in Ca^{2+} influx which could result in the myocytes becoming Ca^{2+} overloaded. The aim was to avoid using Ca^{2+} chelators to buffer

intracellular Ca^{2+}. In subsequent experiments, NaCl was excluded from the intracellular solution to reduce the likelihood of Ca^{2+} overloading, on the basis that 1 mM Na^+ altered the Na^+/Ca^{2+} exchanger reversal potential to +141 mV.

A modified I-V protocol was designed with a holding potential of -80 mV to further reduce the likelihood of Ca^{2+} overloading and increase the stability of recordings. A subsequent step to -50 mV for 500 ms was designed to inactivate I_{Na} prior to stepping to test potentials. The maximum test potential was also altered from +60 mV to +40 mV, as the currents often became Ca^{2+} overloaded at the most positive test potentials, which could then affect the stability and quality of subsequent currents recorded. A representation of the I-V protocol and the corresponding family of current traces over time are shown in Figure 4.2. Sustained outward current was observed at -80 mV and -50 mV due to I_{K1}. A transient inward current was observed at the beginning of each test potential due to activation of the $I_{Ca,L}$, followed by an outward current that increased in amplitude typically to several hundred pA. This outward current was predominantly due to activation of I_{Ks} but also I_{Kr}. Upon repolarisation to -50 mV an outward tail current was observed that peaked within a few milliseconds and then decayed with a slow time course to a steady-state. With each 10 mV increase in the test potential, the tail current and the current during the test potential increased in amplitude. The current measured over time at the +40 mV test potential is shown in red (Figure 4.2, B-E). The tail current was measured by the difference in amplitude between the peak and the end of the potential at -50 mV (after 3 seconds, the whole pulse is not shown in Figure 4.2) when the tail current had deactivated. At the start of the experiment the tail current amplitude in response to the +40 mV test potential was 264 pA. A decrease in amplitude was observed over time, to 257 pA after 2 minutes 25 seconds, 228 pA after 6 minutes 4 seconds and 197 pA after 12 minutes 32 seconds (Figure 4.2, B-E). Therefore, overall a 25% decrease in the tail current was observed. The decrease in current was deemed unacceptable, thus a different approach to recording the delayed rectifier K^+ currents was required.

Figure 4.1

Ca²⁺ overloaded currents recorded using an I-V protocol with a -40 mV holding potential. (A) Representation of the applied I-V protocol. The voltage protocol had a holding potential of -40 mV and stepped to a test potential for 500 ms, which ranged from -30 mV to + 60 mV and increased in 10 mV increments from negative to positive potentials. (B) Representative family of current traces recorded from the same guinea pig left ventricular myocyte at 37°C in response to the I-V protocol. Some selected traces affected by Ca²⁺ overload are shown in red for clarity. The zero current level is indicated by the horizontal dashed line. Currents were recorded in 10 µM nisoldipine to inhibit $I_{Ca,L}$.
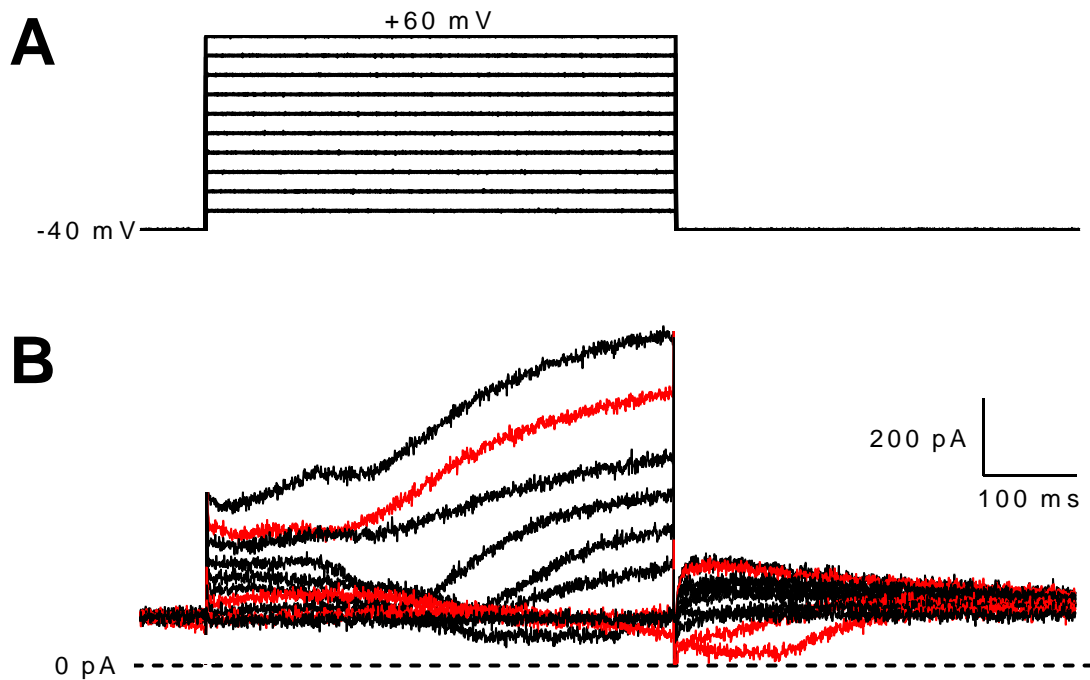
Figure 4.2
Slow 'run-down' of tail current amplitudes with repetitive application of the I-V protocol. (A) Representation of the modified I-V protocol. The voltage protocol had a holding potential of -80 mV, stepped to -50 mV for 500 ms, followed by a 500 ms test potential and a second step to -50 mV. Test potentials ranged from -40 mV to +40 mV and increased in 10 mV increments from negative to positive potentials. (B-E) Representative family of current traces recorded from the same guinea pig left ventricular myocyte at $37^{o}C$ in response to the I-V protocol at the time intervals indicated. Current during the +40 mV test potential and the subsequent tail current is shown in red. The zero current level is indicated by the horizontal dashed lines. Currents were recorded in 10 µM nisoldipine to inhibit $I_{Ca,L}$.
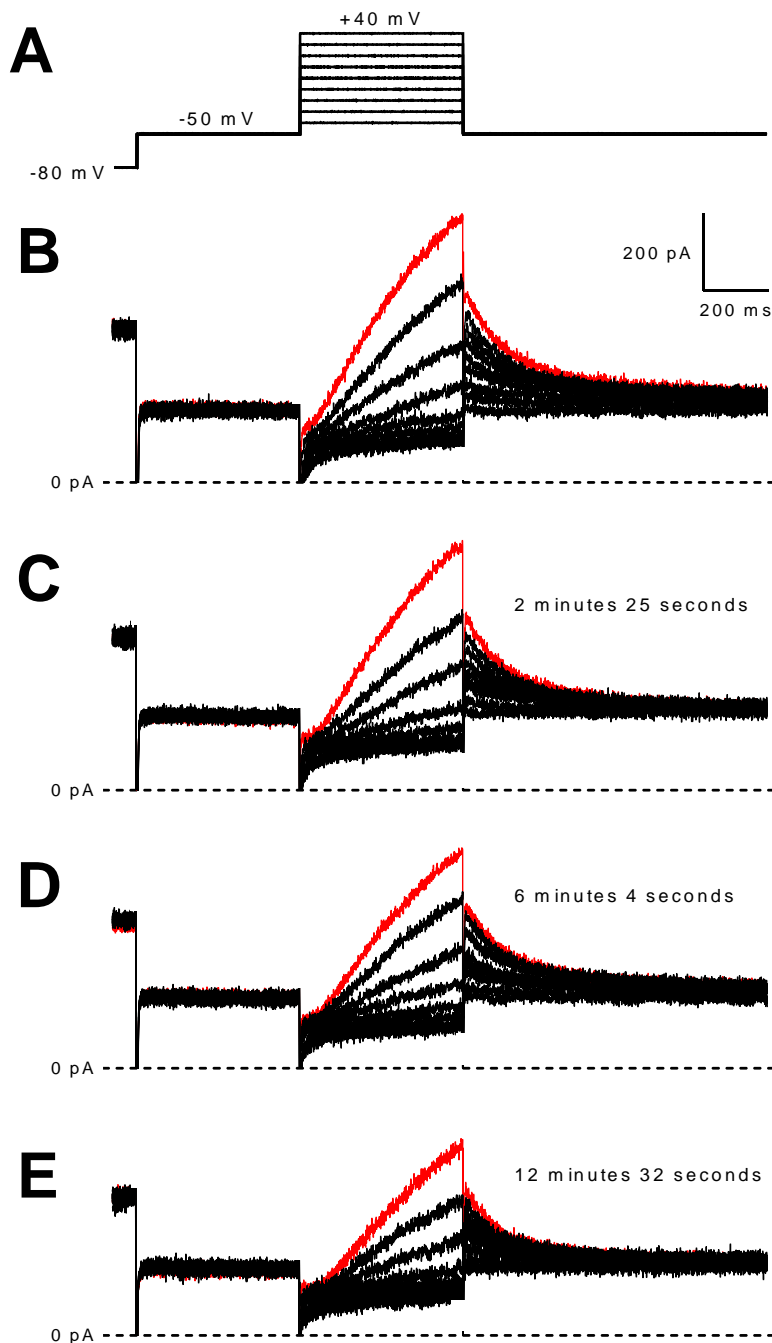
4.2.1.2 Stable currents recorded using a single test potential voltage protocol

Based on the results from the previous section, the decision was taken to use the same voltage protocol, but repetitively step to a single test potential of +40 mV, as opposed to a range of test potentials (refer to Figure 2.6). Stepping to a single test potential enabled the delayed rectifier K^+ current tail current amplitude to be monitored easily throughout the course of an experiment, to ensure that a steady-state was reached prior to and in between superfusion with test reagents. Therefore, the experimental time was also utilised more effectively. This voltage protocol was used in combination with pharmacological inhibitors to selectively record the slow and rapid delayed rectifier K^+ currents, I_{Ks} and I_{Kr}.

I_{Ks} and I_{Kr} were recorded selectively by using, in combination, the voltage protocol described and pharmacological inhibitors which inhibited contaminating currents and isolated each current. In all experiments, current changes were carefully observed during superfusion with pharmacological inhibitors and given time to reach steady-state prior to superfusion with test reagents. $I_{Ca,L}$ was a major contaminating current contributing to test pulse currents. Therefore, myocytes were superfused with 10 µM nisoldipine, a selective $I_{Ca,L}$ inhibitor. In initial experiments, nisoldipine was applied alone and the current was given time to reach a steady-state prior to superfusion with I_{Ks} or I_{Kr} inhibitors. In later experiments, myocytes were superfused from the start with nisoldipine and I_{Ks} or I_{Kr} inhibitors to optimise experimental time. Nisoldipine is a commonly used L-type Ca^{2+} channel blocker and is widely used between 1-10 µM. A study investigating the concentration-dependent effects of nisoldipine on delayed rectifier K^+ currents in guinea pig ventricular myocytes found that nisoldipine inhibited I_{Ks} and I_{Kr} with IC_{50} values of 40 µM and 23 µM respectively (Missan *et al.*, 2003).

4.2.1.2.1 Selective recording of the slow delayed rectifier potassium current

The voltage protocol described previously was applied and myocytes were superfused with control solution followed by nisoldipine and then nisoldipine + 1 µM E4031 (Figure 4.3). E4031 is a widely used selective I_{Kr} inhibitor and was used at a relatively high concentration to ensure complete block of hERG channels. Inhibition of $I_{Ca,L}$ and I_{Kr} in combination with the specifically designed voltage protocol enabled selective recording of I_{Ks}. The outward current at +40 mV was measured by the difference in amplitude between the peak current at +40 mV and the sustained current at -50 mV, prior to the +40 mV test potential. The tail current was measured as described previously. Under control conditions the outward current at +40 mV was 1434 pA and tail current was 649 pA (Figure 4.3, A). The transient inward current at +40 mV was completely inhibited by nisoldipine. Nisoldipine also partially inhibited the outward current at +40 mV and the tail current, which decreased to 811 pA and 377 pA respectively (Figure 4.3. B). Nisoldipine + E4031 inhibited the outward current at +40 mV slightly, to 762 pA, which indicated that I_{Kr} was inactivated and did not contribute much current at this voltage. In contrast, the tail current was dramatically inhibited to 180 pA which indicated that a large proportion of the tail current was equivalent to I_{Kr} (Figure 4.3, C). I_{Ks} tail current density was 1.25 pA/pF. The time course of I_{Ks} deactivation was fitted with a standard exponential curve and tau was measured as 118 ms.

Figure 4.3
Selective recording of I_{Ks}. Representative current traces recorded from a
guinea pig left ventricular myocyte at 37°C in response to an applied voltage
protocol as indicated. (A) Current recorded in control solution. (B) Current
recorded in 10 µM nisoldipine to inhibit $I_{Ca,L}$. (C) Current recorded in nisoldipine
+ 1 µM E4031 to inhibit I_{Kr}. The zero current level is indicated by the horizontal
dashed lines. NB. The Na$^+$ current with the first voltage step is a large amplitude
current and not all of it is shown.
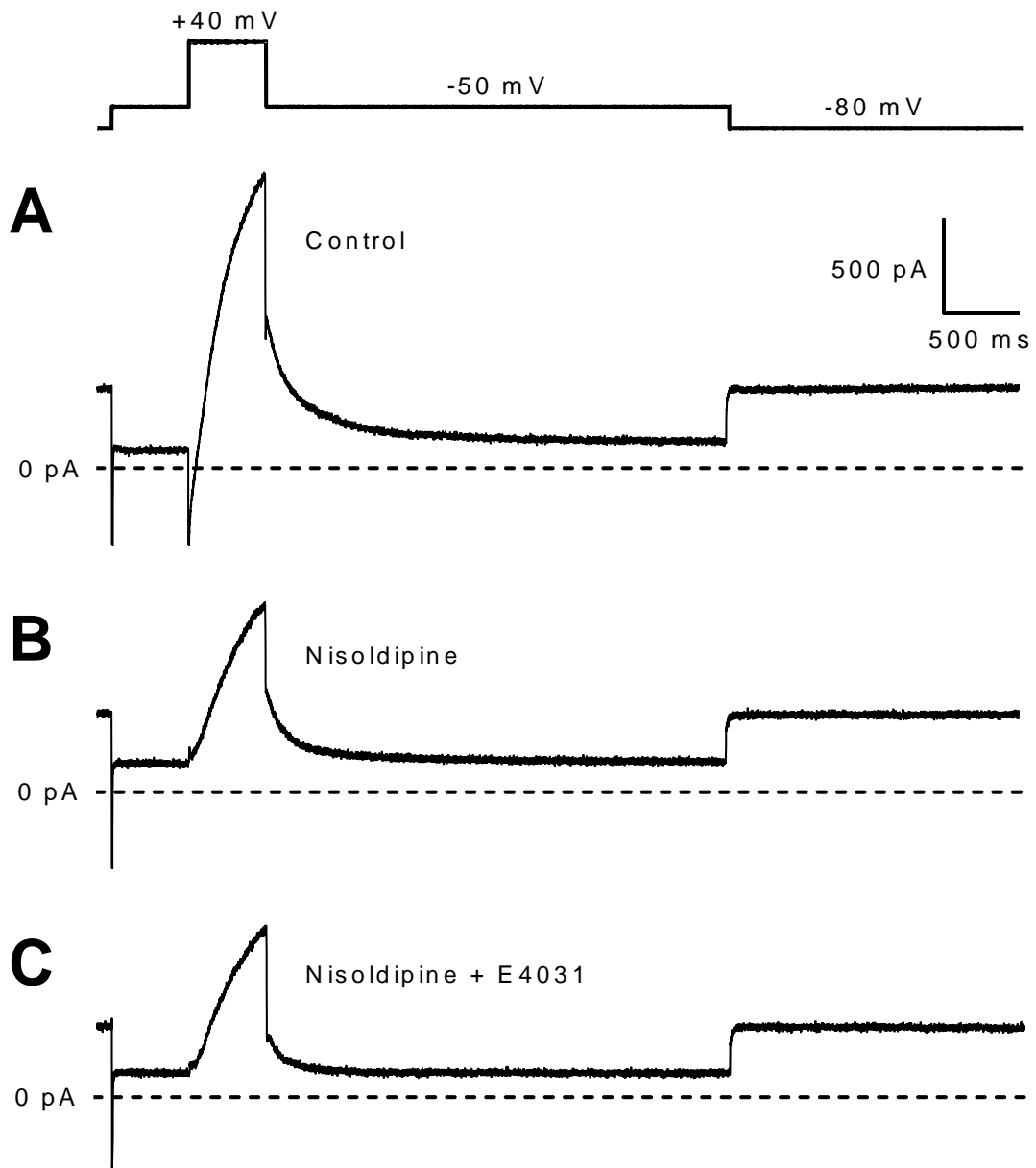
4.2.1.2.2 Selective recording of the rapid delayed rectifier potassium current

In separate experiments, conditions were chosen to selectively record I_{Kr}. The same voltage protocol was applied and $I_{Ca,L}$ was inhibited with nisoldipine as described previously. To enable selective recording of I_{Kr}, I_{Ks} was inhibited with 1 µM JNJ 303. JNJ 303 is a relatively new potent and selective I_{Ks} blocker with an IC_{50} of 64 nM for I_{Ks} and 12.6 µM for I_{Kr} (Towart *et al.*, 2009). Therefore, JNJ 303 was deemed a suitable inhibitor with high selectively for I_{Ks} over I_{Kr}.

The outward current at +40 mV and the tail current were measured as described previously. In nisoldipine the outward current at +40 mV was 238 pA and the tail current was 159 pA (Figure 4.4, A). Nisoldipine + JNJ 303 inhibited the outward current at +40 mV almost completely to 7 pA, which indicated that I_{Ks} contributed most of the current at this voltage. The tail current was also inhibited to 89 pA which indicated that a large proportion of the tail current was equivalent to I_{Ks} (Figure 4.4, B). I_{Kr} tail current density was 0.79 pA/pF. The time course of I_{Kr} deactivation was fitted with a standard exponential curve and tau was measured as 163 ms.

The tail current should be completely inhibited if I_{Ks} and I_{Kr} were effectively inhibited by the concentrations of the inhibitors used and if the tail current consists solely of these currents. Complete inhibition of the tail current was observed with 10 µM nisoldipine + 1 µM JNJ 303 + 1 µM E4031. Upon the step to -50 mV, no tail current was observed and the amplitude was less than at the end of the -50 mV step (Figure 4.5). This indicated that the tail current consisted solely of I_{Ks} and I_{Kr} and that E4031 and JNJ 303 at the concentrations used effectively inhibited these contributing currents.

Figure 4.4

Selective recording of I_{Kr}. Representative current traces recorded from a guinea pig left ventricular myocyte at 37°C in response to an applied voltage protocol (refer to Figure 4.3). (A) Current recorded in 10 µM nisoldipine to inhibit $I_{Ca,L}$. (B) Current recorded in nisoldipine + 1 µM JNJ 303 to inhibit I_{Ks}. The zero current level is indicated by the horizontal dashed lines.

A

Nisoldipine

100 pA

500 ms

0 pA

B

Nisoldipine + JNJ 303

0 pA
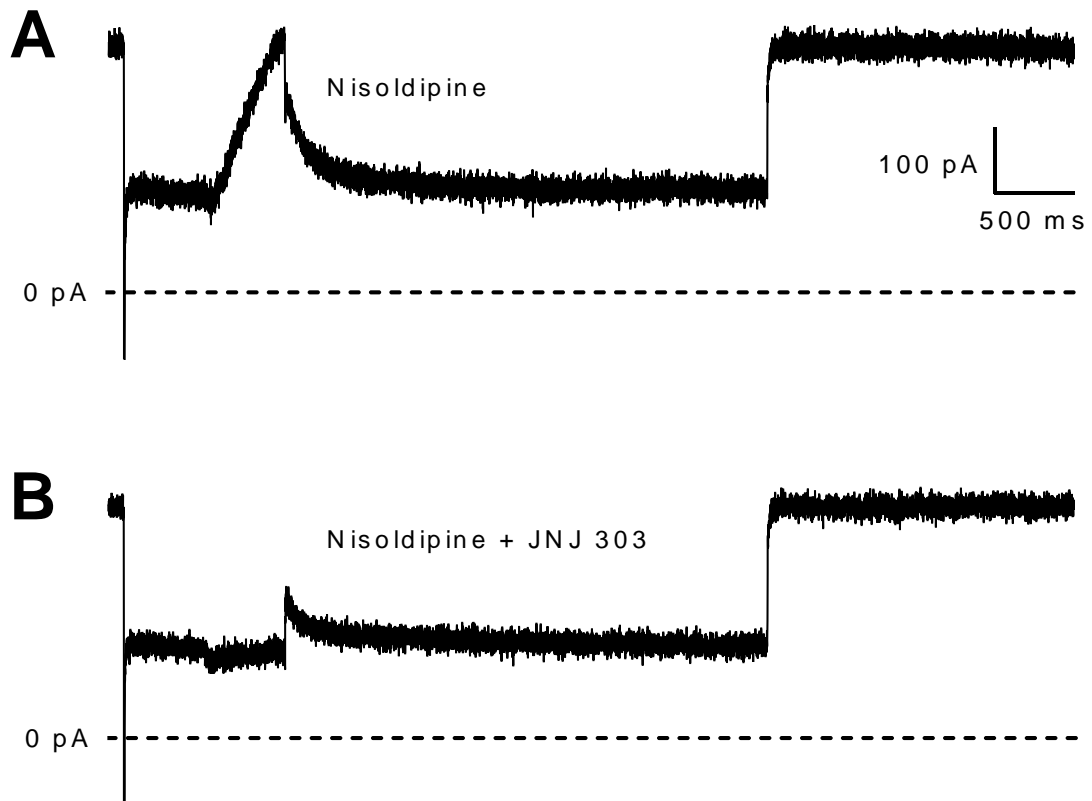
Figure 4.5
Complete inhibition of the tail current contributors I_{Ks} and I_{Kr}.
Representative current trace recorded from a guinea pig left ventricular myocyte at 37°C upon repolarisation to -50 mV in response to an applied voltage protocol (refer to Figure 4.3), in 10 µM nisoldipine + 1 µM JNJ 303 + 1 µM E4031 to inhibit I_{Ks} and I_{Kr}. The zero current level is indicated by the horizontal dashed line.

+40 m V

-50 m V

N isoldipine + JNJ 303 + E4031

0 pA -

100 pA

500 m s
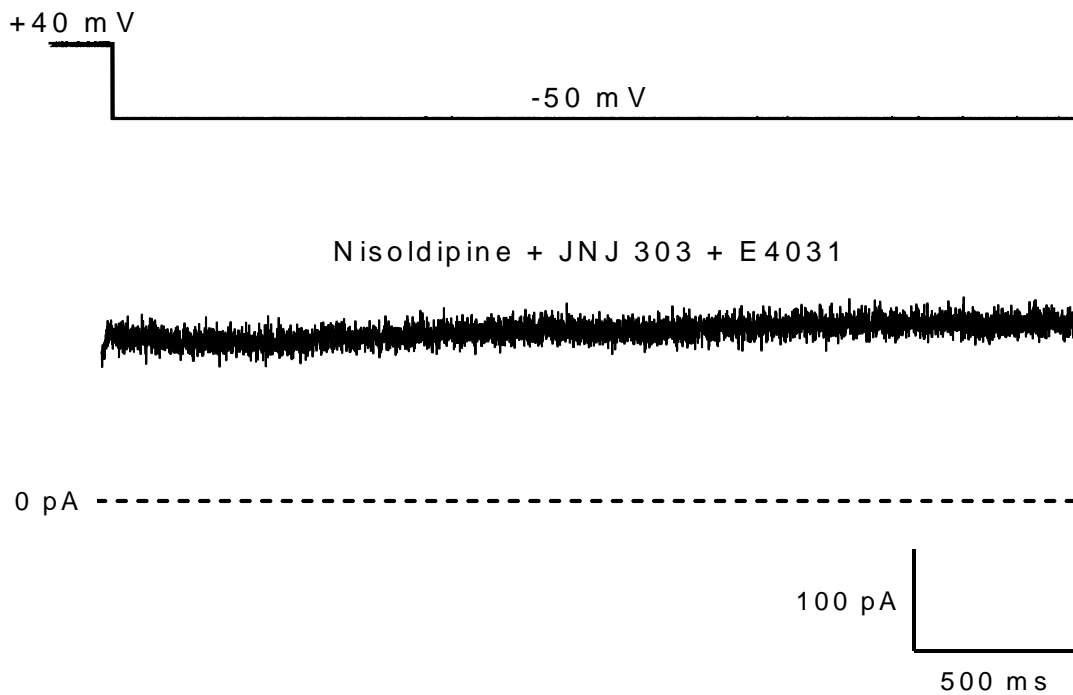
4.2.2 Responses of the slow delayed rectifier potassium current to modulation of cGMP-dependent signalling

4.2.2.1 The effect of soluble guanylyl cyclase activity and phosphodiesterase activity on the slow delayed rectifier potassium current

Results from the previous chapter showed that sGC activation with BAY shortened APD under basal conditions and prolonged APD when PDEs were inhibited. Changes in APD occurred predominantly in the late plateau and repolarisation phases as opposed to the early plateau phase.

The following experiments investigated whether I_{Ks} was modulated under these experimental conditions. Currents were recorded from single guinea pig isolated left ventricular myocytes in response to an applied voltage protocol (Figure 2.6). Pharmacological inhibitors were used to inhibit contaminating currents, in order to isolate and selectively record I_{Ks}. Superfusion with 10 µM nisoldipine + 1 µM E4031, inhibited $I_{Ca,L}$ and I_{Kr} respectively. In all experiments, I_{Ks} tail current was given time to reach steady-state prior to superfusion with test reagents and in between test reagents. I_{Ks} tail current amplitude was measured as described previously and compared between experimental conditions. The aim of these experiments was to investigate the effect of 1 µM BAY on I_{Ks} under basal conditions and when PDEs were inhibited with 100 µM IBMX.

Activation of sGC with BAY did not modulate I_{Ks} under basal conditions. Representative current traces and tail current time course are shown in Figure 4.6. No change in the tail current or the current during the +40 mV test potential was observed in BAY. Steady-state current at -50 mV, typically decreased slightly throughout the course of the majority of experiments (Figure 4.6, A). Tail current amplitude remained relatively stable, with no profound changes observed during BAY application (Figure 4.6, B), Mean tail current amplitude was 85 ± 6.7 pA (n=6) in control, 94 ± 7.4 pA (n=6) in response to BAY and 89 ± 7.3 pA (n=6) in wash off. BAY did not modulate tail current amplitude

compared to control or wash off (P>0.05) (Figure 4.6, D). This suggests sGC activation alone, under basal conditions does not modulate I_{Ks}.

In contrast, BAY inhibited I_{Ks} when PDEs were inhibited with IBMX. Representative current traces and tail current time course are shown in Figure 4.7. Application of IBMX increased the peak tail current and substantially increased the current during the +40 mV test potential. The tail current amplitude rapidly increased within 2 minutes of IBMX application and reached a steady-state within 5 minutes (Figure 4.7, B). Subsequent application of BAY, in the presence of IBMX, partially reversed the increases in current in response to IBMX to a similar amplitude observed in control (Figure 4.7, A). A slow decrease in tail current amplitude was observed within 2 minutes of BAY application which reached a steady-state after 7 minutes (Figure 4.7, B). Mean tail current amplitude increased by 76% from 139 ± 25 pA (n=10) in control to 245 ± 41 pA (n=10) in response to IBMX (P<0.001). Importantly, BAY inhibited 78% of the IBMX response to 162 ± 28 pA (n=10) (P<0.001). Thus, the response to IBMX + BAY was only a 17% increase over control (Figure 4.7, D). In summary, PDE inhibition potentiated I_{Ks} and this effect was inhibited by sGC activation with BAY. Inhibition of PDEs increases cAMP levels and protein kinase A (PKA) activity resulting in potentiation of I_{Ks}. PDE inhibition may also have disrupted compartmentalised cGMP signalling and permitted sGC activation by BAY to inhibit I_{Ks}, in contrast to the lack of modulation with sGC activation alone. In a sub-population of six myocytes, BAY did not modulate I_{Ks} when PDEs were inhibited. Representative current traces and tail current time course are shown in Figure 4.8. IBMX application modulated I_{Ks} as previously described. However, subsequent application of BAY did not modulate the peak tail current or the current during the +40 mV test potential compared to IBMX alone (Figure 4.8, A). This was in contrast to the results shown in Figure 4.7. Mean tail current amplitude increased from 126 ± 22 pA (n=6) in control to 237 ± 38 pA (n=6) in response to IBMX (P<0.01). Importantly, BAY had no effect compared to IBMX alone, at 232 ± 36 pA (n=6) (P>0.05) (Figure 4.8, D). This shows heterogeneity in the modulation of I_{Ks} by BAY when PDEs were inhibited.

Figure 4.6
BAY 60-2770 did not modulate I$_{Ks}$ under basal conditions. (A)
Representative I$_{Ks}$ traces recorded from a guinea pig left ventricular myocyte at
37°C in control, 1 µM BAY and wash off. Currents initiated by a +40 mV test
potential and tail currents upon repolarisation to -50 mV as indicated. Each
current trace was averaged from 5 consecutive traces after reaching steady-
state (indicated by vertical dashed lines in B). The zero current level is indicated
by the horizontal dashed lines. (B) Time course of I$_{Ks}$ tail current amplitude
before, during and after BAY application (indicated by horizontal bar). Individual
symbols represent measurement from a single tail current. (C) I$_{Ks}$ tail current
amplitude from individual myocytes under each condition. Data points from
individual cells linked by lines. (D) Mean ± SEM I$_{Ks}$ tail current amplitude.
Number of cells indicated in each bar. Statistical analysis performed with
repeated measures one-way ANOVA with Sidak's multiple comparisons test.
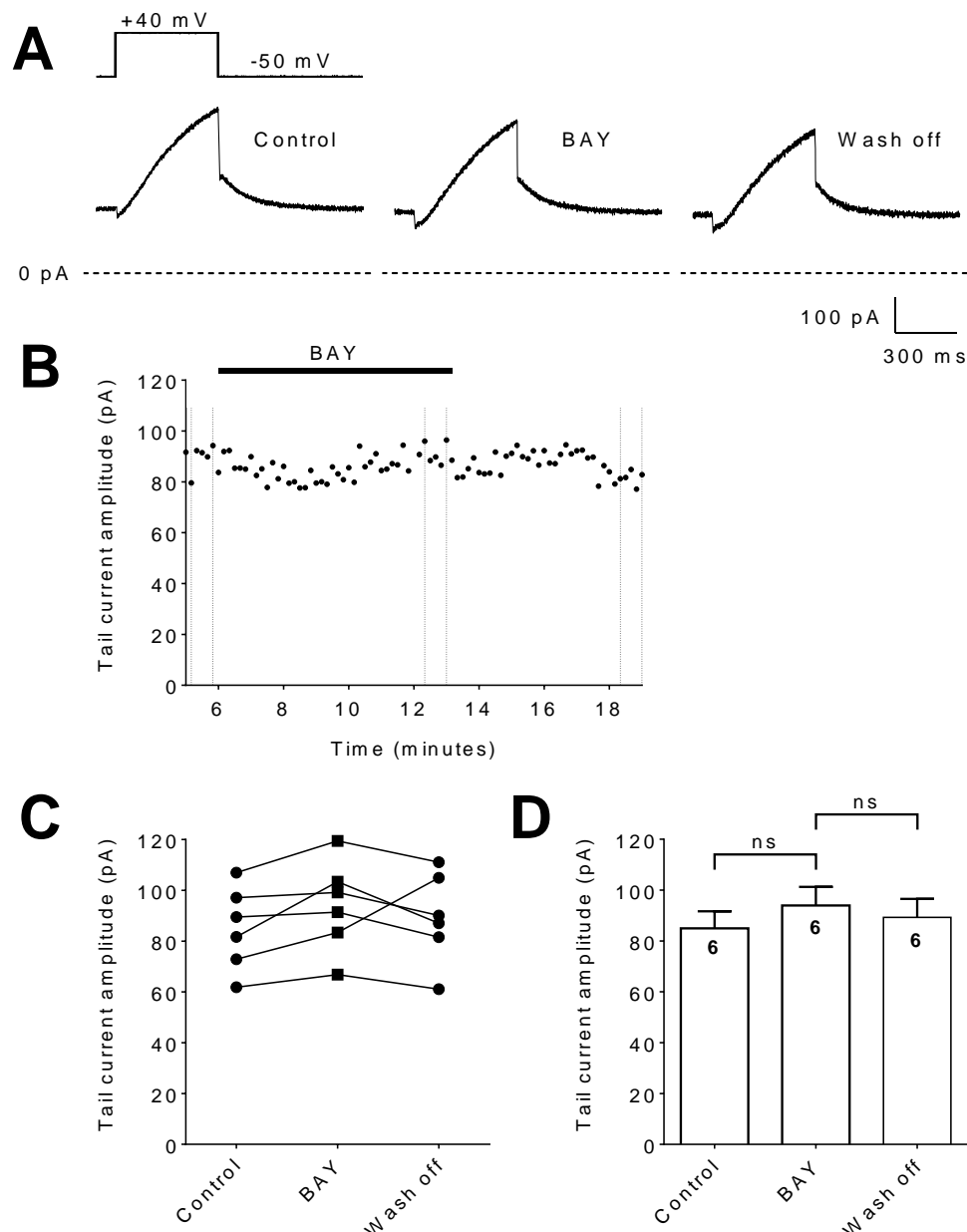
Figure 4.7

BAY 60-2770 inhibited I_{Ks} when PDEs were inhibited. (A) Representative I_{Ks} traces recorded in control, 100 µM IBMX and IBMX + 1 µM BAY. (B) Time course of I_{Ks} tail current amplitude before and during IBMX and BAY application. (C) I_{Ks} tail current amplitude from individual myocytes under each condition. (D) Mean ± SEM I_{Ks} tail current amplitude. Number of cells indicated in each bar. Statistical analysis performed with repeated measures one-way ANOVA with Sidak's multiple comparisons test. (Refer to Figure 4.6 legend for further detail).
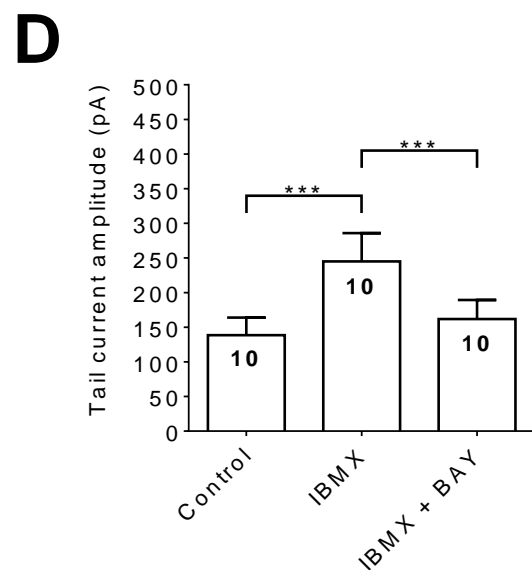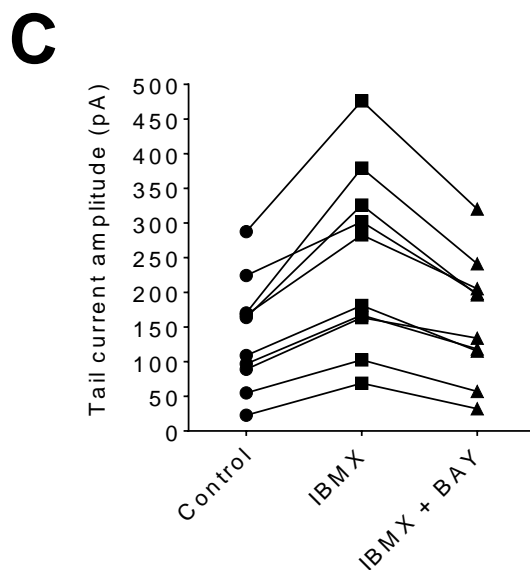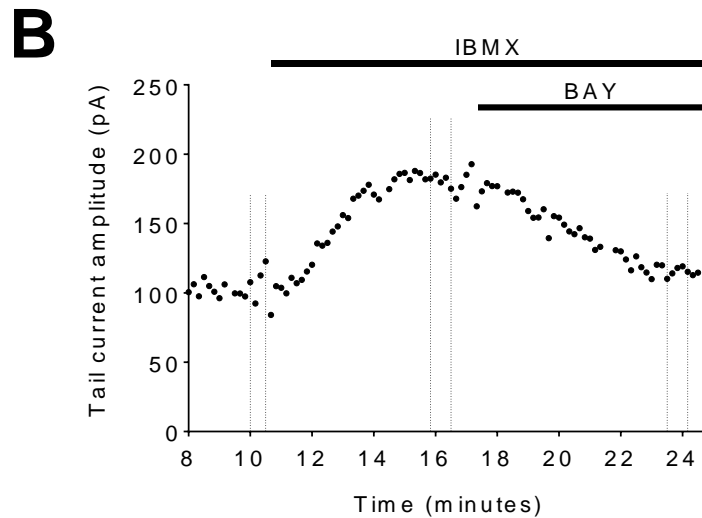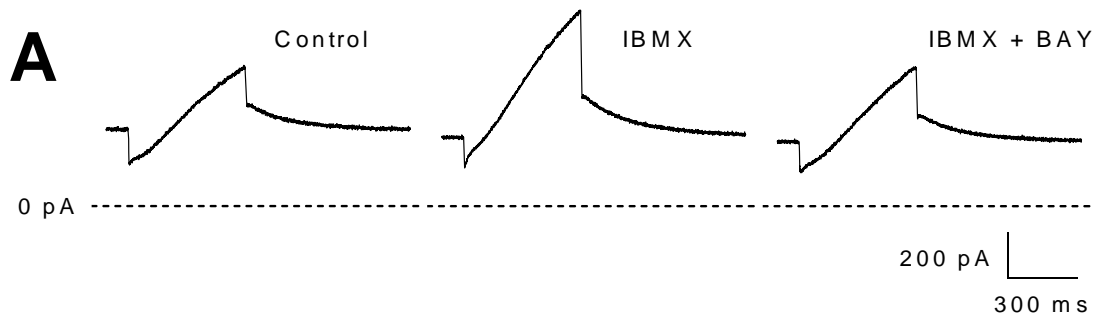
Figure 4.8

In a proportion of myocytes, BAY 60-2770 did not modulate I_{Ks} when PDEs were inhibited. (A) Representative I_{Ks} traces recorded in control, 100 µM IBMX and IBMX + 1 µM BAY. (B) Time course of I_{Ks} tail current amplitude before and during IBMX and BAY application. (C) I_{Ks} tail current amplitude from individual myocytes under each condition. (D) Mean ± SEM I_{Ks} tail current amplitude. Number of cells indicated in each bar. Statistical analysis performed with repeated measures one-way ANOVA with Sidak's multiple comparisons test. (Refer to Figure 4.6 legend for further detail).
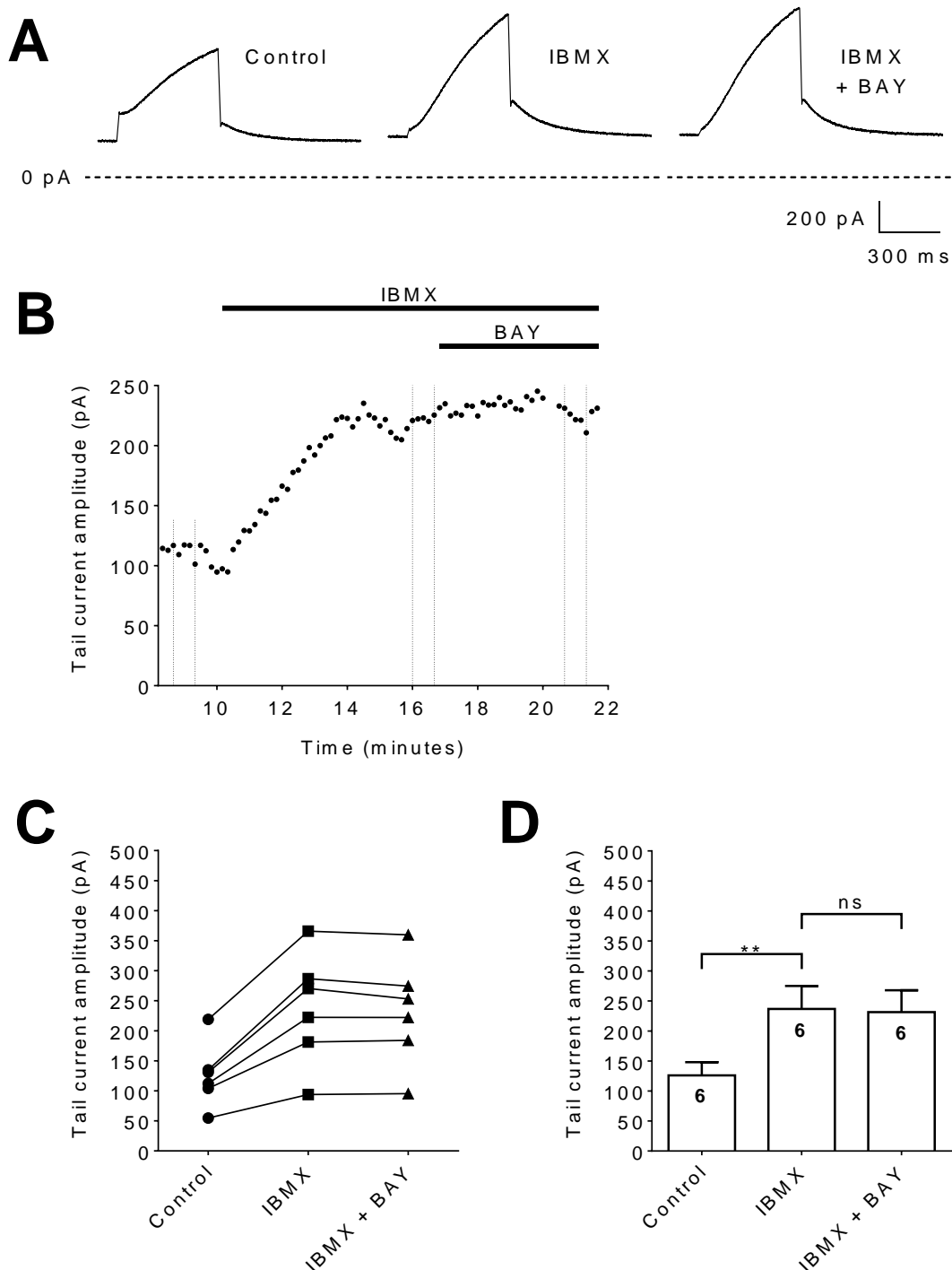
4.2.2.2 The effect of a protein kinase G inhibitor on the modulation of the slow delayed rectifier potassium current by BAY 60-2770

Results from the previous chapter showed that cellular cGMP levels were dramatically increased by IBMX + BAY (Figure 3.2). To investigate whether cGMP is activating protein kinase G (PKG) which could be mediating the effects on I_{Ks}, the PKG inhibitor KT5823 was used. The aim of these experiments was to investigate the effect of 100 nM KT5823 on the modulation of I_{Ks} by BAY when PDEs were also inhibited.

Inhibition of I_{Ks} by IBMX + BAY was not altered by PKG inhibition with KT5823. Representative current traces and tail current time course are shown in Figure 4.9. IBMX application modulated I_{Ks} as described previously. I_{Ks} was not modulated by the subsequent application of KT5823, in the presence of IBMX. No change in the tail current or the current during the +40 mV test potential was observed during KT5823 application (Figure 4.9, A). Application of IBMX + KT5823 + BAY inhibited I_{Ks} as described previously in the absence of KT5823. Mean tail current amplitude was 162 ± 46 pA (n=6) in control, increased to 299 ± 68 pA (n=6) in response to IBMX (P<0.01) and was 276 ± 63 pA (n=6) in response to IBMX + KT5823, which was not significantly different to IBMX alone (P>0.05). Importantly, IBMX + KT5823 + BAY inhibited the mean tail current to 189 ± 41 pA (n=6) which was a significant change over IBMX + KT5823 (P<0.05) (Figure 4.9, D). IBMX increased mean tail current amplitude by 85% over control and BAY inhibited 80% of the IBMX response, thus the response to IBMX + KT5823 + BAY was a 17% increase over control. These responses were similar to those in the absence of KT5823 in Figure 4.7. Whereby, a 76% increase was observed in response to IBMX, BAY inhibited 78% of the IBMX response and the response to IBMX + BAY was a 17% increase over control. In summary, KT5823 did not affect the modulation of I_{Ks} by BAY when PDEs were inhibited. This suggests that modulation of I_{Ks} by BAY occurred independently of PKG, as the response remained in the presence of a PKG inhibitor, therefore BAY is exerting its effect via an alternative signalling mechanism.

Figure 4.9

BAY 60-2770 inhibited I$_{Ks}$ when PDEs were inhibited and a PKG inhibitor was applied. (A) Representative I$_{Ks}$ traces recorded in control, 100 µM IBMX, IBMX + 100 nM KT5823 and IBMX + KT5823 + 1 µM BAY. (B) Time course of I$_{Ks}$ tail current amplitude before and during IBMX, KT5823 and BAY application. (C) I$_{Ks}$ tail current amplitude from individual myocytes under each condition. (D) Mean ± SEM I$_{Ks}$ tail current amplitude. Number of cells indicated in each bar. Statistical analysis performed with repeated measures one-way ANOVA with Sidak's multiple comparisons test. (Refer to Figure 4.6 legend for further detail).
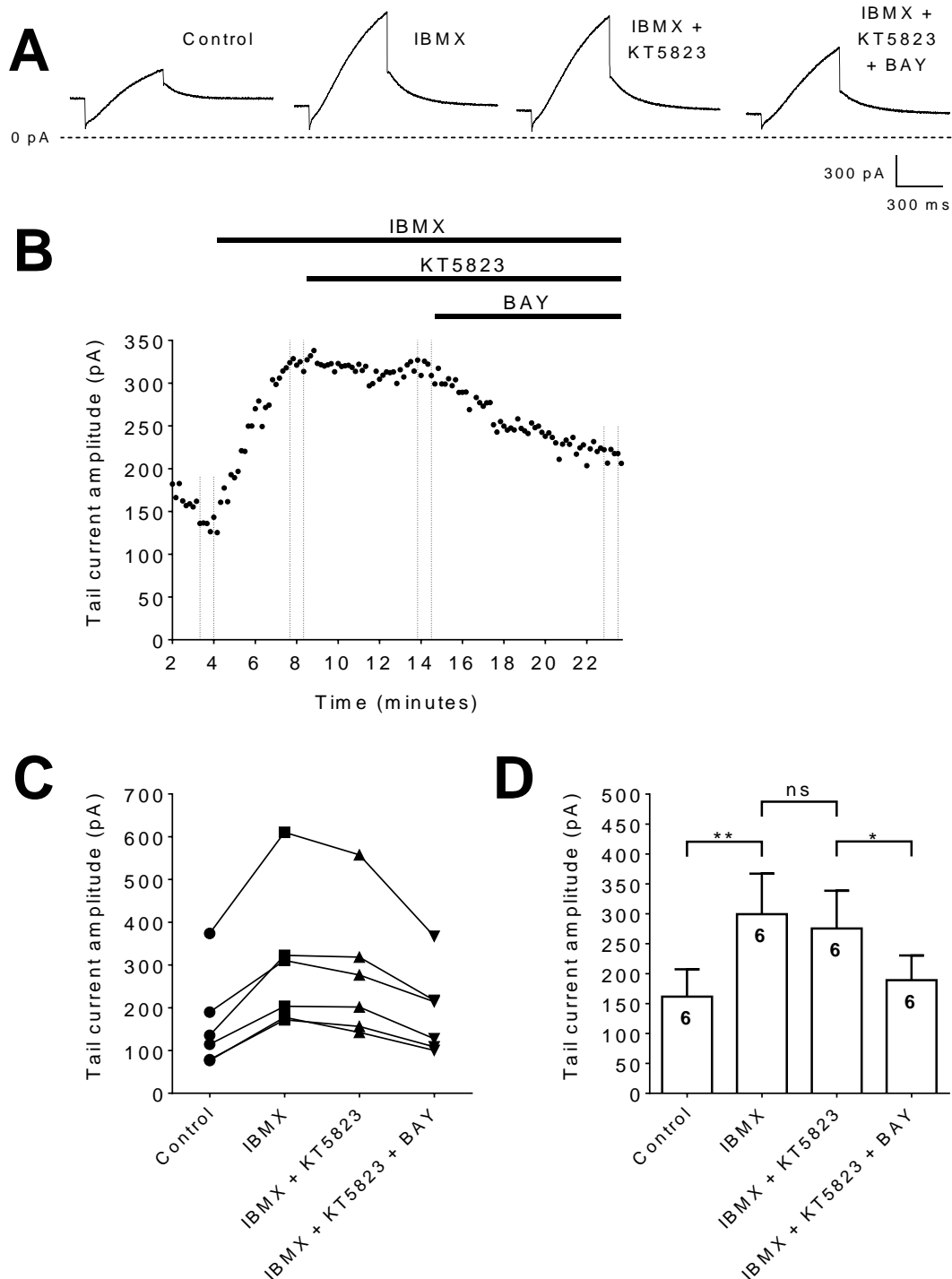
4.2.2.3 The effect of protein kinase G activation on the slow delayed rectifier potassium current

To further investigate the role of PKG in the modulation of I_{Ks} by cGMP-dependent signalling and as an alternative approach to PKG inhibition, PKG was activated with 8-Br-cGMP, the membrane-permeable cGMP analogue. 8-Br-cGMP has a greater resistance to hydrolysis by PDEs compared to cGMP and was initially applied in the absence of PDE inhibitors.

Activation of PKG with 100 µM 8-Br-cGMP did not modulate I_{Ks} under basal conditions or in the presence of PDE inhibition. Representative current traces and tail current time courses are shown in Figures 4.10 and 4.11. Under basal conditions, no change in the tail current or the current during the +40 mV test potential was observed in 8-Br-cGMP (Figure 4.10, A). Tail current amplitude remained relatively stable throughout the course of the experiment, with no profound changes observed during 8-Br-cGMP application (Figure 4.10, B), Mean tail current amplitude was 90 ± 28 pA (n=6) in control, 101 ± 32 pA (n=6) in response to 8-Br-cGMP (P>0.05) and 94 ± 27 pA (n=5) in wash off (Figure 4.10, D).

IBMX application modulated I_{Ks} as described previously. No change in the tail current or the current during the +40 mV test potential was observed in IBMX + 8-Br-cGMP (Figure 4.11, A). Tail current amplitude remained relatively stable with no profound changes observed during 8-Br-cGMP application (Figure 4.11, B). Mean tail current amplitude was 85 ± 16 pA (n=7) in control, 183 ± 27 pA (n=7) in response to IBMX (P<0.01) and 189 ± 28 pA (n=7) in response to IBMX + 8-Br-cGMP, which was importantly not significantly different compared to IBMX alone (P>0.05) (Figure 4.11, D). IBMX and IBMX + 8-Br-cGMP were both significantly different to control (P<0.01). This suggests that PKG activation does not modulate I_{Ks} regardless of PDE inhibition. This is consistent with the PKG inhibitor data (Figure 4.9) suggesting that PKG does not play a role in the regulation of I_{Ks} via cGMP-dependent signalling.

Figure 4.10
PKG activation did not modulate I_{Ks} under basal conditions. (A)
Representative I_{Ks} traces recorded in control, 100 µM 8-Br-cGMP and wash off.
(B) Time course of I_{Ks} tail current amplitude before, during and after 8-Br-cGMP
application. (C) I_{Ks} tail current amplitude from individual myocytes under each
condition. (D) Mean ± SEM I_{Ks} tail current amplitude. Number of cells indicated
in each bar. Statistical analysis performed with a paired two-tailed t test. (Refer
to Figure 4.6 legend for further detail).
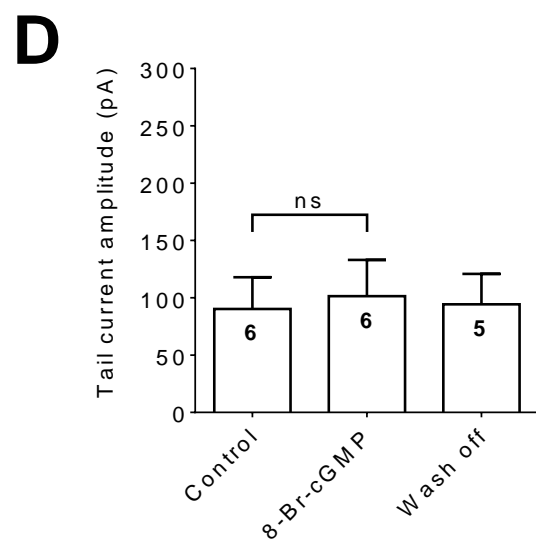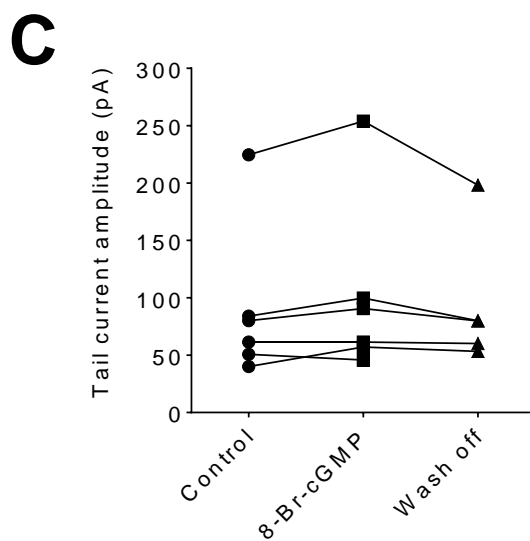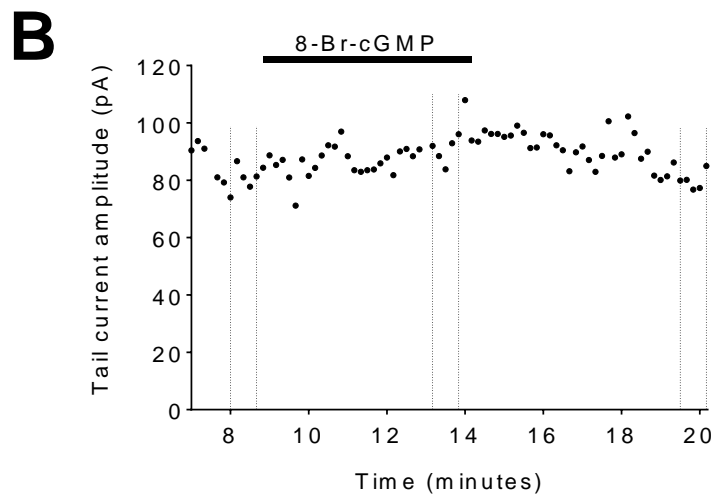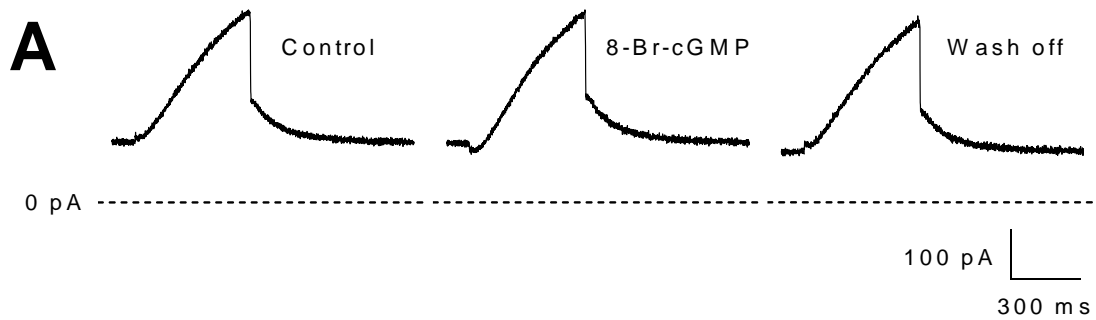
Figure 4.11

PKG activation did not modulate I$_{Ks}$ when PDEs were inhibited. (A)
Representative I$_{Ks}$ traces recorded in control, 100 µM IBMX and IBMX + 100 µM
8-Br-cGMP. (B) Time course of I$_{Ks}$ tail current amplitude before and during
IBMX and 8-Br-cGMP application. (C) I$_{Ks}$ tail current amplitude from individual
myocytes under each condition. (D) Mean ± SEM I$_{Ks}$ tail current amplitude.
Number of cells indicated in each bar. Statistical analysis performed with
repeated measures one-way ANOVA with Sidak's multiple comparisons test.
(Refer to Figure 4.6 legend for further detail).
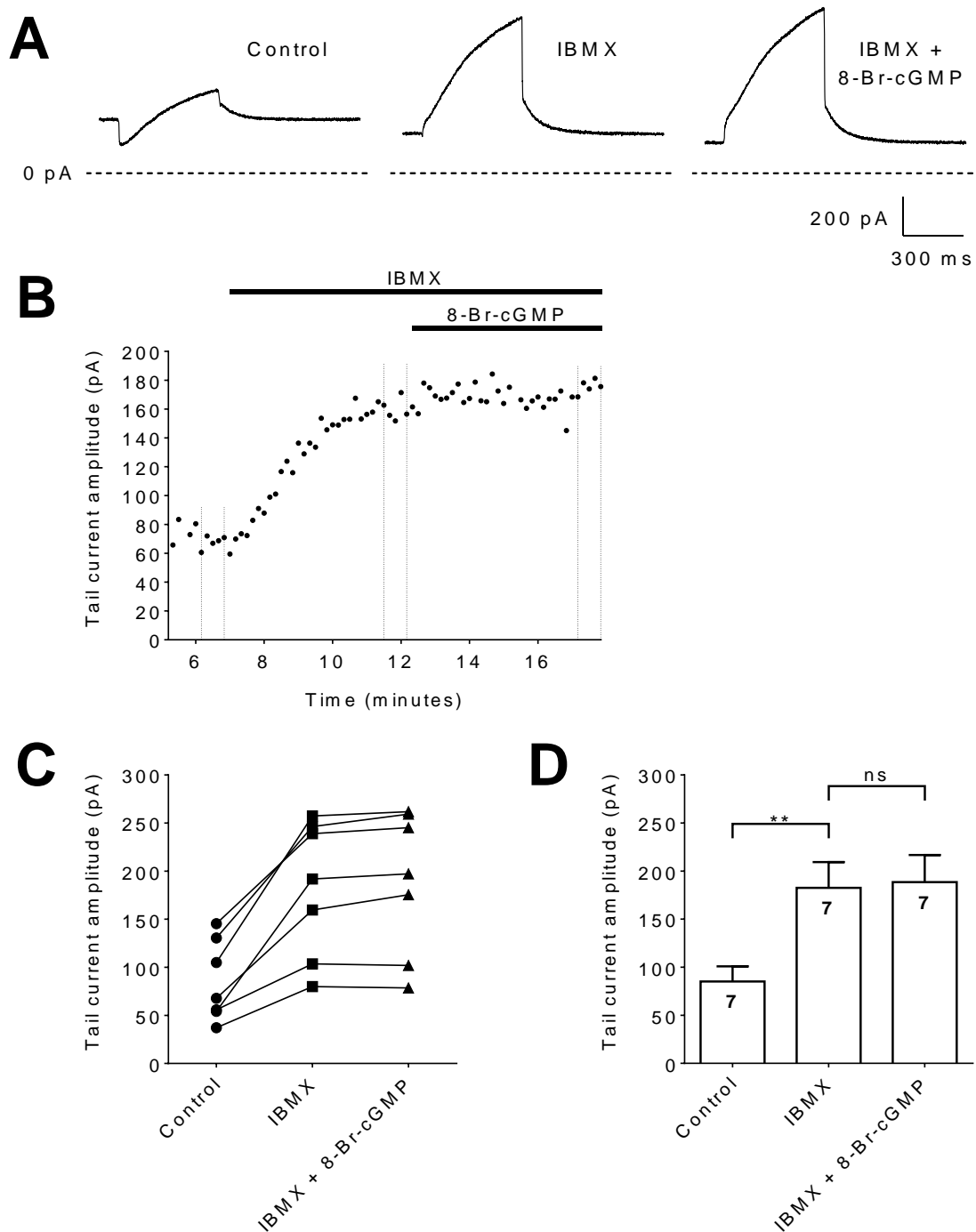
4.2.3 Responses of the rapid delayed rectifier potassium current to modulation of cGMP-dependent signalling

4.2.3.1 The effect of soluble guanylyl cyclase activity and phosphodiesterase activity on the rapid delayed rectifier potassium current

Results from the previous chapter and section showed that BAY shortened APD under basal conditions and prolonged APD when PDEs were inhibited. However, BAY did not modulate I_{Ks} under basal conditions but inhibited I_{Ks} when PDEs were inhibited with IBMX, in the majority of myocytes. I_{Ks} inhibition by IBMX + BAY also occurred in the presence of a PKG inhibitor. Furthermore, activation of PKG with 8-Br-cGMP did not modulate I_{Ks} under basal conditions or in the presence of PDE inhibition.

The following experiments investigated whether I_{Kr} was modulated under these experimental conditions. Currents were recorded from single guinea pig isolated left ventricular myocytes in response to an applied voltage protocol (Figure 2.6). Pharmacological inhibitors were used to inhibit contaminating currents, in order to isolate and selectively record I_{Kr}. Superfusion with 10 µM nisoldipine + 1 µM JNJ 303, inhibited $I_{Ca,L}$ and I_{Ks} respectively. In all experiments, I_{Kr} tail current was given time to reach steady-state prior to superfusion with test reagents and in between test reagents. I_{Kr} tail current amplitude was measured as described previously and compared between experimental conditions. The aim of these experiments was to investigate the effect of 1 µM BAY on I_{Kr} under basal conditions and when PDEs were inhibited with 100 µM IBMX.

Activation of sGC with BAY did not modulate I_{Kr} under basal conditions or when PDEs were inhibited. Representative current traces and tail current time courses are shown in Figures 4.12 and 4.13. Steady-state current at -50 mV prior to the +40 mV test potential (not shown), typically decreased slightly throughout the course of the majority of experiments. Therefore, the tail current

moved towards the zero current level (Figure 4.12 and 4.13, A). However, tail current amplitude remained relatively stable with no profound changes observed during BAY application under basal conditions (Figure 4.12, B) or when PDEs were inhibited (Figure 4.13, B). PDE inhibition alone also did not modulate I_{Kr} (Figure 4.13, A and B). Under basal conditions, mean tail current amplitude was 90 ± 6.1 pA (n=6) in control, 85 ± 4.2 pA (n=6) in response to BAY and 78 ± 5.3 pA (n=6) in wash off. BAY did not modulate tail current amplitude compared to control or wash off (P>0.05) (Figure 4.12, D). This suggests that sGC activation alone, under basal conditions does not modulate I_{Kr}. When PDEs were inhibited, mean tail current amplitude remained unchanged at 96 ± 11 pA (n=8) in response to IBMX, compared to 95 ± 12 pA (n=8) in control (P>0.05). Mean tail current amplitude was 89 ± 9.4 pA (n=8) in response to IBMX + BAY, which was not a significant change over IBMX alone (P>0.05) (Figure 4.13, D). IBMX and IBMX + BAY were not significantly different to control (P>0.05). This suggests that PDE inhibition alone and in combination with sGC activation does not modulate I_{Kr}.

Figure 4.12

BAY 60-2770 did not modulate I_{Kr} under basal conditions. (A)
Representative I_{Kr} tail current traces upon repolarisation to -50 mV, recorded
from a guinea pig left ventricular myocyte at $37^{o}C$ in control, 1 µM BAY and
wash off. Each current trace was averaged from 5 consecutive traces after
reaching steady-state (indicated by vertical dashed lines in B). The zero current
level is indicated by the horizontal dashed lines. (B) Time course of I_{Kr} tail
current amplitude before, during and after BAY application (indicated by
horizontal bar). Individual symbols represent measurement from a single tail
current. (C) I_{Kr} tail current amplitude from individual myocytes under each
condition. Data points from individual cells linked by lines. (D) Mean ± SEM I_{Kr}
tail current amplitude. Number of cells indicated in each bar. Statistical analysis
performed with repeated measures one-way ANOVA with Sidak's multiple
comparisons test.

Figure 4.13

BAY 60-2770 did not modulate I_{Kr} when PDEs were inhibited. (A) Representative I_{Kr} tail current traces recorded in control, 100 µM IBMX and IBMX + 1 µM BAY. (B) Time course of I_{Kr} tail current amplitude before and during IBMX and BAY application. (C) I_{Kr} tail current amplitude from individual myocytes under each condition. (D) Mean ± SEM I_{Kr} tail current amplitude. Number of cells indicated in each bar. Statistical analysis performed with repeated measures one-way ANOVA with Sidak's multiple comparisons test. (Refer to Figure 4.12 legend for further detail).
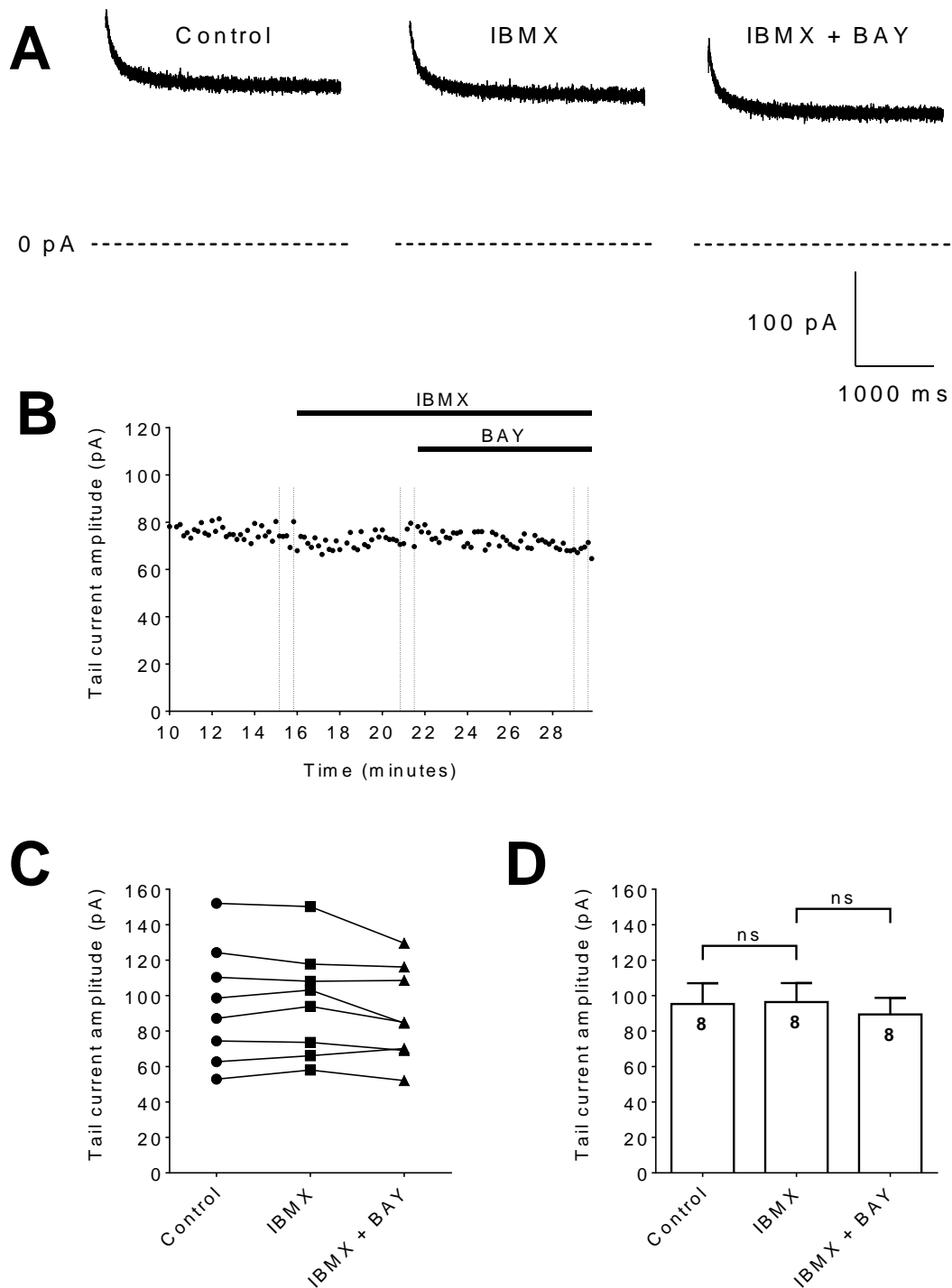
4.2.3.2 The effect of protein kinase G activation on the rapid delayed rectifier potassium current

To further investigate whether I_{Kr} was modulated by cGMP-dependent signalling, and as an alternative approach to sGC activation by BAY, PKG was activated with 8-Br-cGMP. Initially, 8-Br-cGMP was applied in the absence of PDE inhibitors.

Activation of PKG with 8-Br-cGMP did not modulate I_{Kr} under basal conditions or when PDEs were inhibited. Representative current traces and tail current time courses are shown in Figures 4.14 and 4.15. Tail current amplitude remained relatively stable with no profound changes observed during 8-Br-cGMP application under basal conditions (Figure 4.14, A and B) or when PDEs were inhibited (Figure 4.15, A and B). Under basal conditions, mean tail current amplitude was 92 ± 9.4 pA (n=7) in control, 94 ± 9.9 pA (n=7) in response to 8-Br-cGMP and 91 ± 12 pA (n=6) in wash off. BAY did not modulate tail current amplitude over control (P>0.05) (Figure 4.14, D). This suggests that PKG activation alone, under basal conditions does not modulate I_{Kr}. When PDEs were inhibited, mean tail current amplitude remained unchanged at 108 ± 12 pA (n=6) in response to IBMX, compared to 105 ± 13 pA (n=6) in control (P>0.05). Mean tail current amplitude was 108 ± 14 pA (n=6) in response to IBMX + 8-Br-cGMP, which was not a significant change over IBMX alone (P>0.05) (Figure 4.15, D). In addition, IBMX and IBMX + 8-Br-cGMP were not significantly different to control (P>0.05). This suggests that PKG activation does not modulate I_{Kr} regardless of PDE inhibition.

In summary, I_{Kr} was not modulated by sGC activation, PDE inhibition or PKG activation, suggesting that cGMP-dependent signalling does not play a role in the regulation of I_{Kr}.

Figure 4.14

PKG activation did not modulate I$_{Kr}$ under basal conditions. (A)
Representative I$_{Kr}$ tail current traces recorded in control, 100 µM 8-Br-cGMP
and wash off. (B) Time course of I$_{Kr}$ tail current amplitude before, during and
after 8-Br-cGMP application. (C) I$_{Kr}$ tail current amplitude from individual
myocytes under each condition. (D) Mean ± SEM I$_{Kr}$ tail current amplitude.
Number of cells indicated in each bar. Statistical analysis performed with a
paired two-tailed t test. (Refer to Figure 4.12 legend for further detail).
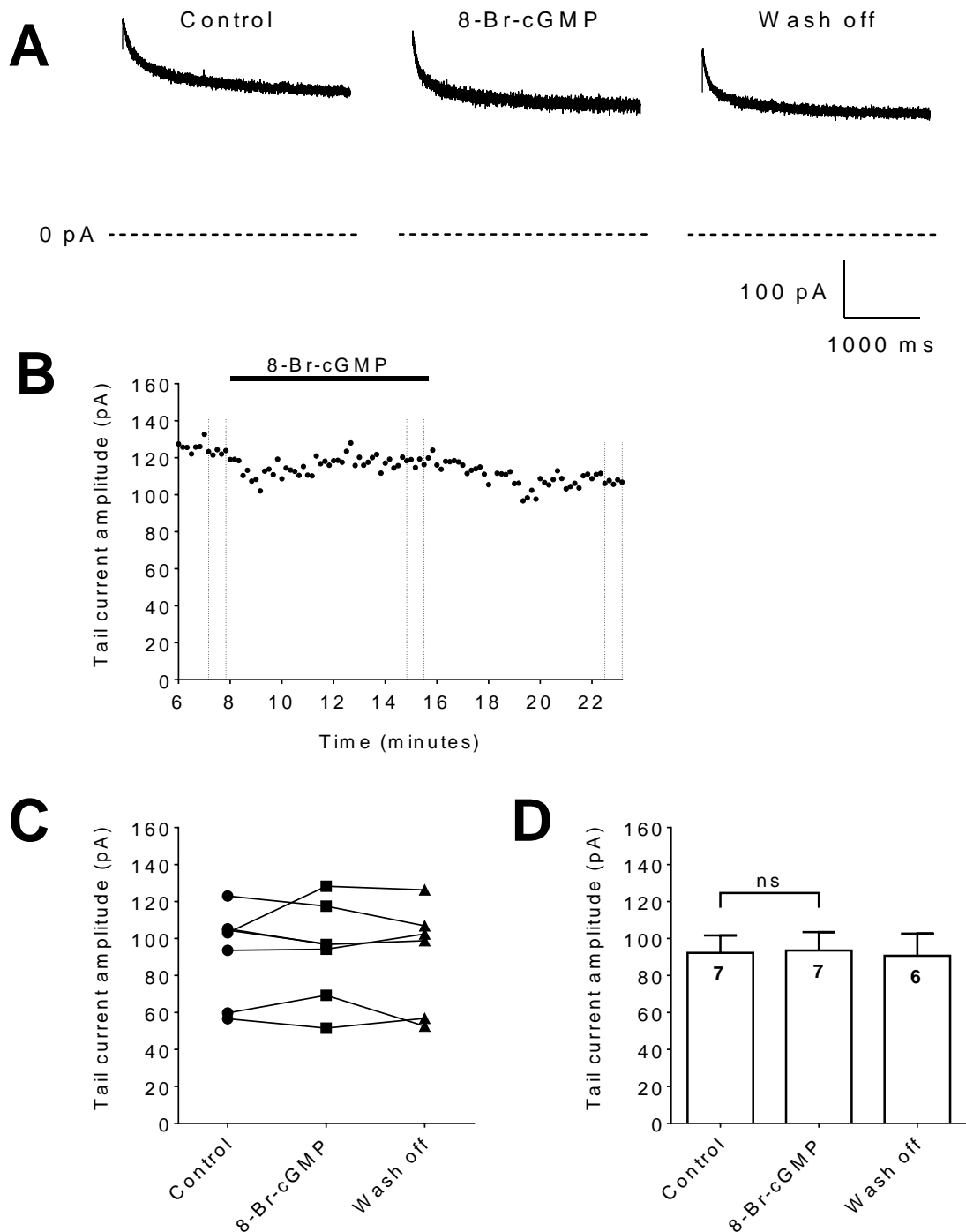
Figure 4.15

PKG activation did not modulate I$_{Kr}$ when PDEs were inhibited. (A)
Representative I$_{Kr}$ tail current traces recorded in control, 100 µM IBMX and
IBMX + 100 µM 8-Br-cGMP. (B) Time course of I$_{Kr}$ tail current amplitude before
and during IBMX and 8-Br-cGMP application. (C) I$_{Kr}$ tail current amplitude from
individual myocytes under each condition. (D) Mean ± SEM I$_{Kr}$ tail current
amplitude. Number of cells indicated in each bar. Statistical analysis performed
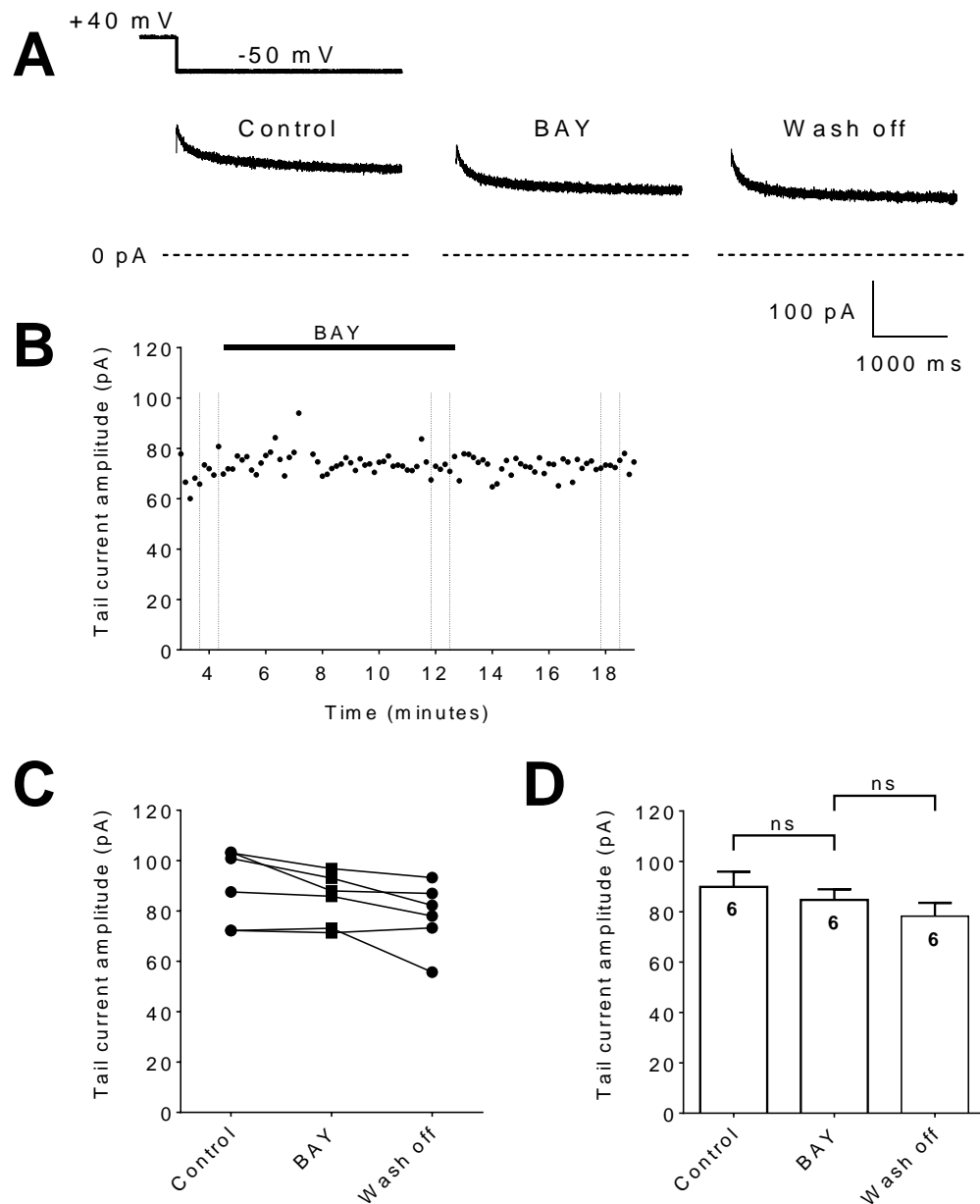with repeated measures one-way ANOVA with Sidak's multiple comparisons
test. (Refer to Figure 4.12 legend for further detail).
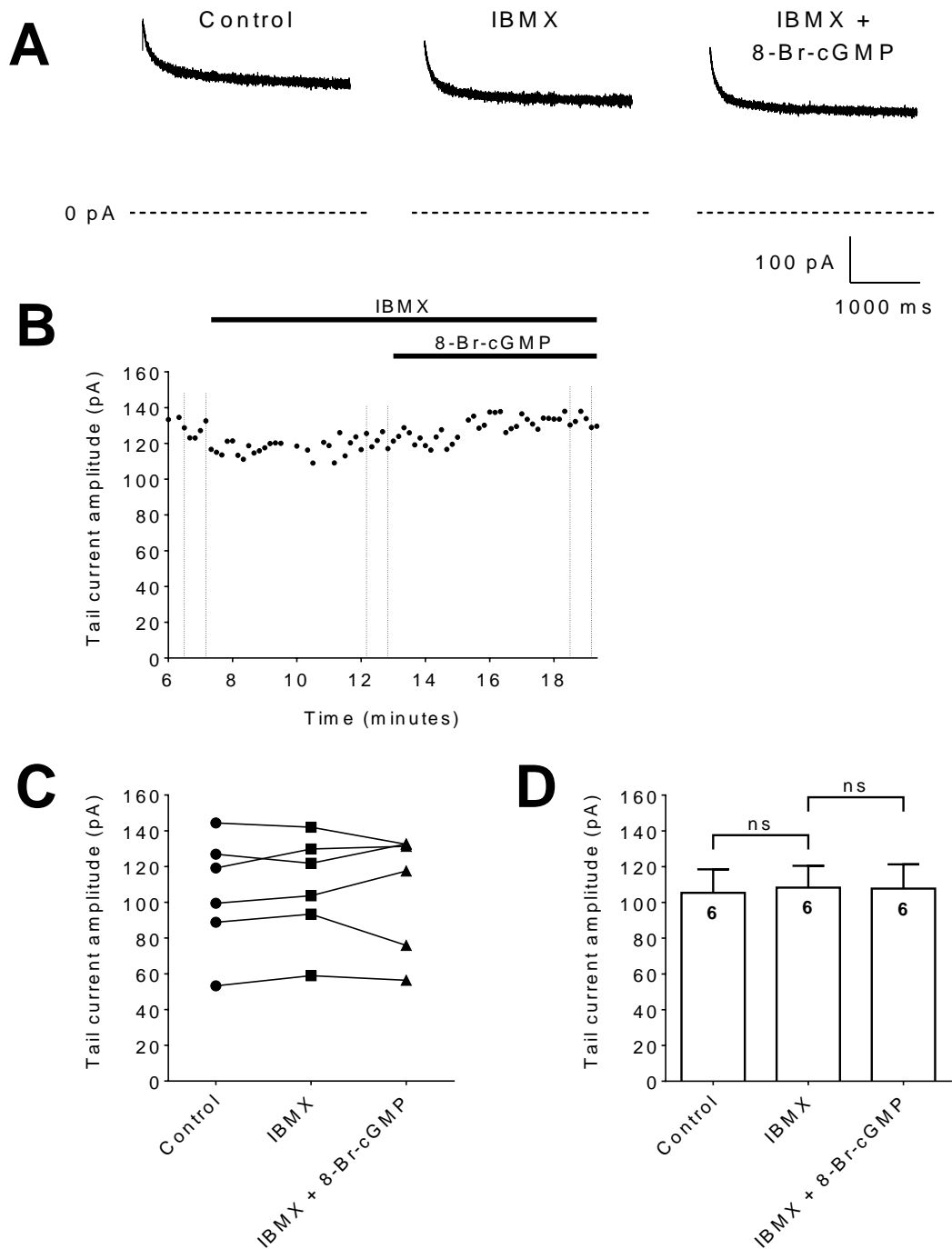
Chapter 5

Do action potentials and cell shortening exhibit diurnal variation in guinea pig left ventricular myocytes?

5.1 Introduction

Many cardiovascular parameters exhibit diurnal variation (Takeda & Maemura, 2011). QT and QT_c intervals have been reported to be longer at night and shorter during the day, with a profound shortening between 6 AM and 9 AM (Hohnloser *et al.*, 1993; Bexton *et al.*, 1986). Diurnal variation of the QT_c interval has been shown to be influenced by the activity of the autonomic nervous system (Bexton *et al.*, 1986). It has been reported that the QT_c interval is prolonged by the parasympathetic nervous system and shortened by the sympathetic nervous system (Honda *et al.*, 2013). Furthermore, the occurrence of arrhythmias and sudden cardiac death is higher in the morning, particularly upon awakening (Muller *et al.*, 1987; Mahmoud *et al.*, 2011). Therefore, an increase in the activity of the sympathetic nervous system during the transition from resting to active may increase the susceptibility to arrhythmias by modulating repolarisation.

Diurnal variation of repolarisation may also be due to alterations in the expression of genes and proteins associated with K^+ channels. Recently, diurnal variation in the expression of a wide variety of genes in the heart have been detected, including those regulating I_{To} and I_{Kur} (refer to section 1.4). Diurnal variation of ECC through regulation of NO signalling has also been demonstrated. Collins & Rodrigo, (2010) showed in rat left ventricular myocytes that, paradoxically, Ca^{2+} transients and cell shortening were larger in resting than active period myocytes and that resting period myocytes also responded more strongly to β-adrenergic receptor stimulation, with more arrhythmic episodes. These effects were largely mediated by a diurnal variation in NO signalling pathways, with a higher expression of nNOS and greater suppression of ECC in active than resting period myocytes (refer to section 1.4).

Studies in this field have been conducted using mouse and rat models in which ventricular APD is short and repolarisation is mediated predominantly by I_{To} and I_{K1}. The first objective of this study was to investigate whether AP and cell shortening under basal conditions and in response to ISO exhibited diurnal variation in guinea pig isolated left ventricular myocytes, which like human myocytes, have an elevated AP plateau and are more dependent on repolarisation by delayed rectifier K^+ currents. The second objective was to determine whether NO signalling played a role in the response to ISO by inhibiting NOS activity with L-NNA.

5.2 Results

5.2.1 Responses of action potentials to isoprenaline in active and resting period myocytes

Diurnal variation of $I_{Ca,L}$ responses to β-adrenergic receptor stimulation in rat left ventricular myocytes has been reported (Collins & Rodrigo, 2010). The objective was to establish whether there was diurnal variation in responses to β-adrenergic receptor stimulation in guinea pig left ventricular myocytes. The response of APs to the β-adrenergic receptor agonist isoprenaline (ISO) was studied.

In order to investigate whether there was diurnal variation of APs under basal conditions and in response to β-adrenergic receptor stimulation, guinea pigs were divided into two groups and housed in opposing 12 hour light cycles prior to use in experiments (refer to Figure 2.1). Therefore, experimental animals were either in an active or resting period when culled at 8:30 AM. APs were recorded from single guinea pig isolated left ventricular myocytes stimulated at 2 Hz. In all experiments, APD was given time to reach steady-state prior to superfusion with test reagents and in between test reagents. APD_{90} was measured and compared between experimental conditions. ISO was applied at 3, 10 and 30 nM in increasing concentration.

ISO shortened APD in a concentration-dependent manner, in both active and resting period myocytes. However, the response to ISO was greater in active compared to resting period myocytes. Representative APs and APD_{90} time courses are shown in Figures 5.1 and 5.2. Application of 3 nM ISO shortened APD by a modest acceleration of repolarisation, known to be due to potentiation of I_{Ks} via AC activation, cAMP production and activation of PKA. The early phases of the AP were marginally altered by 3 nM ISO, whereas 10 nM ISO greatly accelerated repolarisation which resulted in a substantially shortened APD. In addition, the membrane potential of the early plateau phase changed modestly and became more positive compared to APs in 3 nM ISO and control.

This is likely to be due to potentiation of $I_{Ca,L}$. APD was shortened dramatically by 30 nM ISO, which caused a profound acceleration in repolarisation and a profound positive shift in the membrane potential of the plateau (Figures 5.1 and 5.2, A). ISO application at all concentrations typically decreased APD_{90} within 1 minute of application and reached a steady-state within 3 minutes, for both active and resting period myocytes (Figures 5.1 and 5.2, B).

In active and resting period myocytes, mean APD_{90} under basal conditions was not significantly different ($P>0.05$) (Figure 5.3). In contrast, the AP responses to 3 and 10 nM ISO were significantly different between active and resting period myocytes ($P<0.05$) (Figure 5.3). In active period myocytes, mean APD_{90} decreased by 25 ms from 199 ± 4.2 ms (n=25) in control to 174 ± 3.0 ms (n=25) in response to 3 nM ISO ($P<0.001$) (Figure 5.1, D). In comparison, a smaller decrease of 16 ms from 201 ± 3.0 ms (n=33) to 185 ± 2.9 ms (n=33) was observed in resting period myocytes ($P<0.001$) (Figure 5.2, D). Application of 10 nM ISO further decreased mean APD_{90}, to 148 ± 2.8 ms (n=25) in active period myocytes and 160 ± 2.8 ms (n=33) in resting period myocytes ($P<0.001$) (Figures 5.1 and 5.2, D). The AP responses to 10 nM ISO were also significantly greater in active than resting period myocytes ($P<0.05$) (Figure 5.3). Mean APD_{90} decreased further in response to 30 nM ISO, to 129 ± 3.8 ms (n=13) and 139 ± 3.6 ms (n=20) for active and resting period myocytes respectively (Figures 5.1 and 5.2, D). The AP responses to 30 nM ISO were also greater in active than resting period myocytes. However, statistical analysis could not be performed as APD_{90} in 30 nM ISO was not obtained for all cells, as a proportion of cells failed to tolerate this relatively high concentration of ISO and lost AP stability. These results suggest that there is diurnal variation of AP responses to β-adrenergic receptor stimulation, as active period myocytes were more responsive to ISO than resting period myocytes, but there were no differences in APs under basal conditions.

Figure 5.1

AP responses to ISO in active period myocytes. (A) Representative APs recorded from an active period guinea pig left ventricular myocyte at 37°C in control, 3, 10 and 30 nM isoprenaline (ISO). Each AP was averaged from 20 consecutive APs after reaching steady-state (indicated by vertical dashed lines in B). (B) Time course of APD_{90} responses before and during ISO application (indicated by horizontal bars). Individual symbols represent measurement from a single AP. (C) APD_{90} from individual myocytes under each condition. (D) Mean ± SEM APD_{90}. Number of cells indicated in each bar. Statistical analysis performed with repeated measures one-way ANOVA with Dunnett's multiple comparisons test.
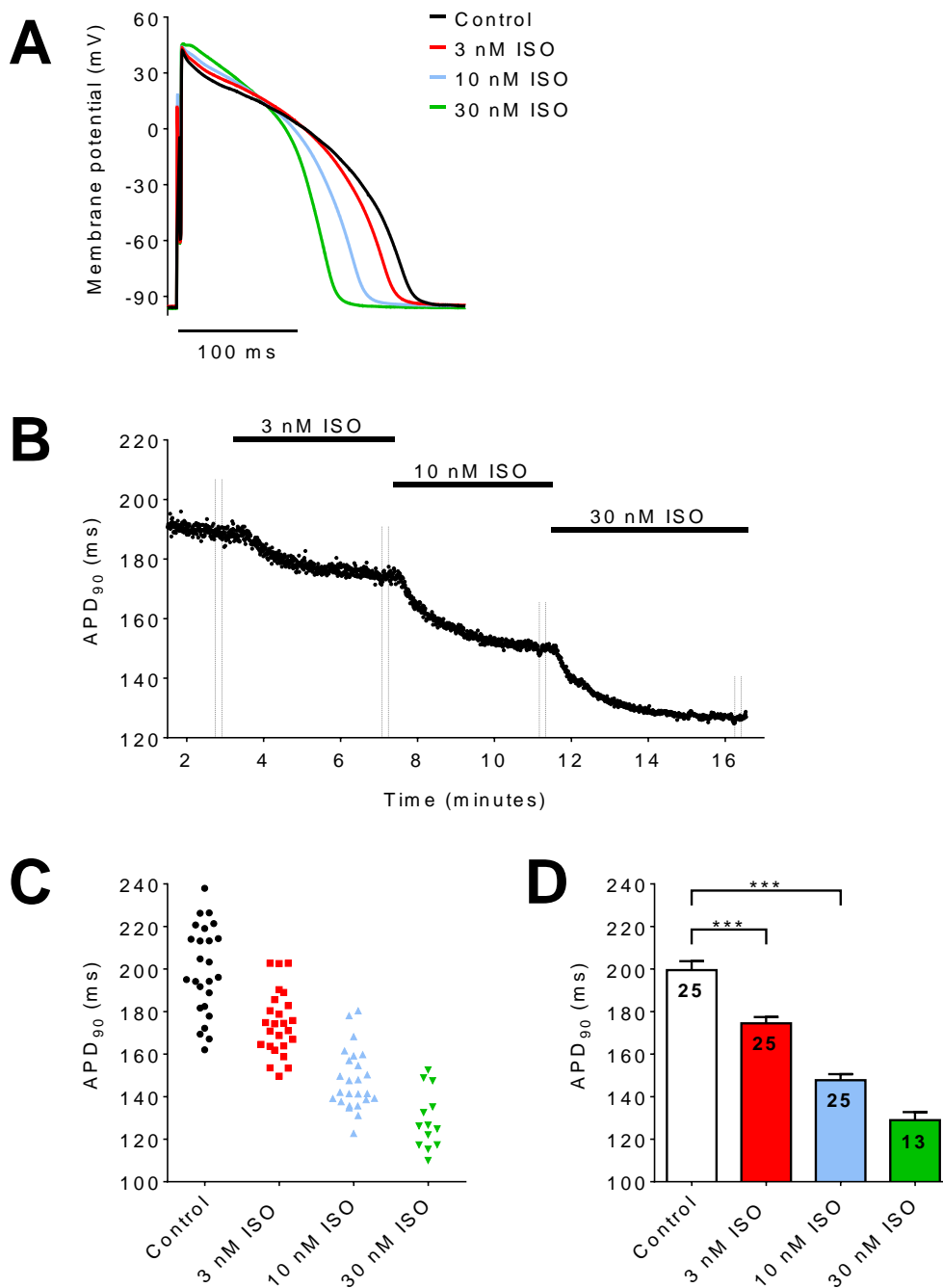
Figure 5.2

AP responses to ISO in resting period myocytes. (A) Representative APs recorded from a resting period guinea pig left ventricular myocyte in control, 3, 10 and 30 nM ISO. (B) Time course of APD_{90} responses before and during ISO application. (C) APD_{90} from individual myocytes under each condition. (D) Mean ± SEM APD_{90}. Number of cells indicated in each bar. Statistical analysis performed with repeated measures one-way ANOVA with Dunnett's multiple comparisons test. (Refer to Figure 5.1 legend for further detail).
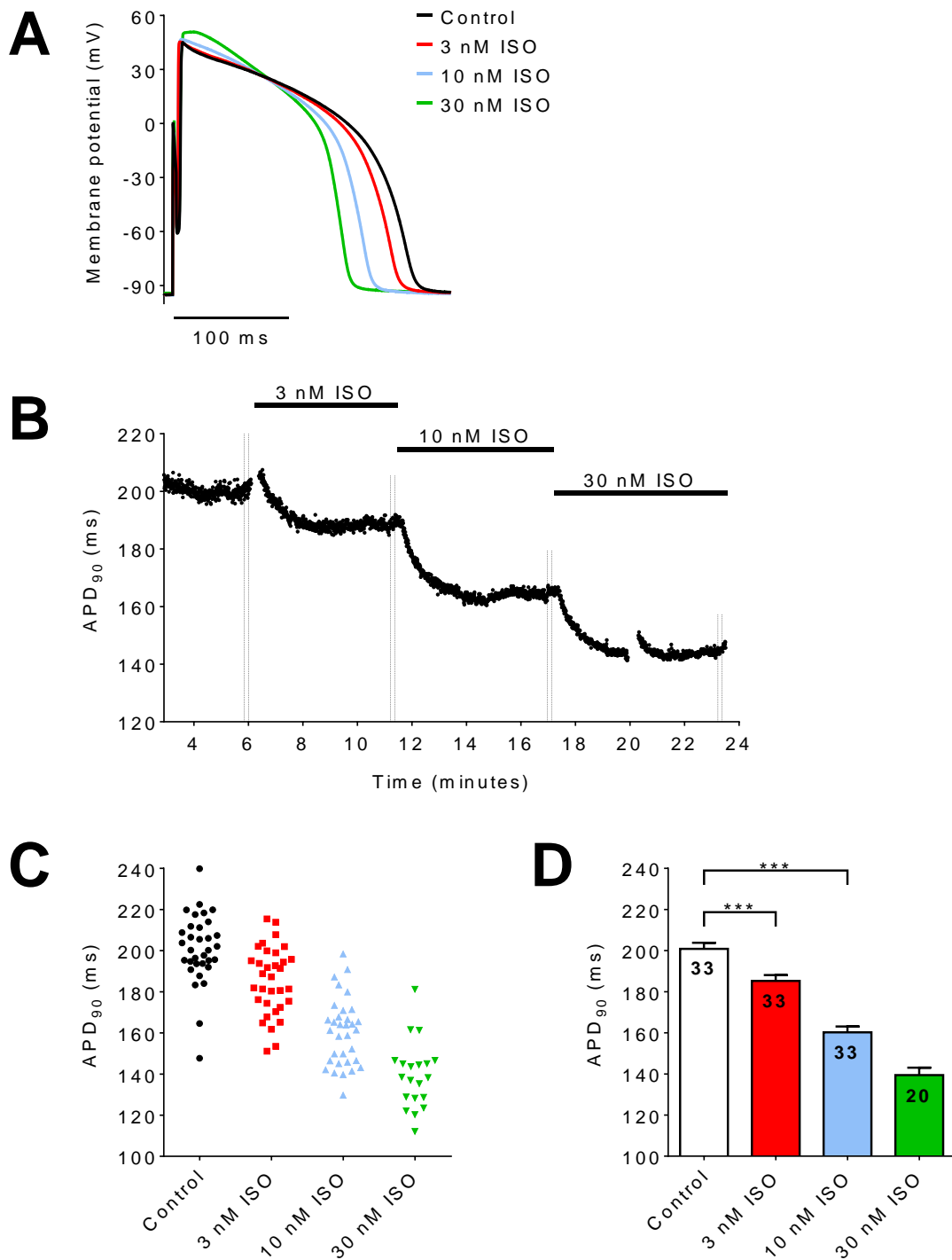
Figure 5.3
AP responses to ISO were greater in active period myocytes than resting period myocytes. Mean ± SEM APD_{90} for active and resting period guinea pig left ventricular myocytes in control, 3, 10 and 30 nM ISO. Number of cells indicated in each bar. Statistical analysis performed with repeated measures two-way ANOVA with Sidak's multiple comparisons test.
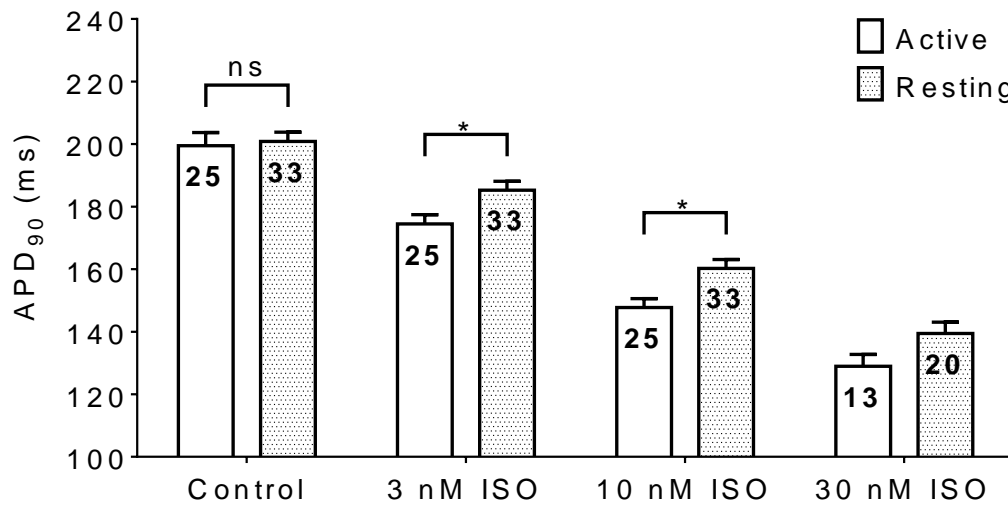
5.2.2 What is the effect of nitric oxide synthase inhibition on the responses of action potentials to isoprenaline in active and resting period myocytes?

Application of ISO may stimulate β_3-adrenergic receptors in addition to β_1- and β_2-adrenergic receptors. Nitric oxide synthase (NOS) is coupled to β_3-adrenergic receptors and activation increases NO production. NOS is also activated by Ca^{2+}-CaM, so increases in intracellular Ca^{2+} with ISO could also activate NOS. Results from previous chapters have shown that cGMP-dependent signalling via NO signalling pathways regulates repolarisation. Therefore, NO signalling might play a role in the AP response to ISO. To address this question, NOS was inhibited with the non-selective inhibitor N-Nitro-L-arginine (L-NNA) and the effect on the AP response to ISO in active and resting period myocytes was investigated. These experiments were performed by returning to 10 nM ISO after the 3, 10 and 30 nM ISO recordings had been made. APs were allowed to reach steady-state in 10 nM ISO before 10 nM ISO + 500 µM L-NNA was applied. This concentration of L-NNA should maximally inhibit nNOS and eNOS.

Inhibition of NOS with L-NNA failed to modulate the AP response to 10 nM ISO in both active and resting period myocytes. Representative APs and APD_{90} time courses are shown in Figures 5.4 and 5.5. No change in APD or AP morphology was observed in L-NNA (Figures 5.4 and 5.5, A). APD_{90} remained relatively stable throughout the course of the experiment, with no profound changes observed during L-NNA application (Figures 5.4 and 5.5, B). Mean APD_{90} was 150 ± 4.8 ms (n=15) in active period myocytes and 152 ± 4.1 ms (n=12) in resting period myocytes in response to ISO, and remained relatively unchanged at 151 ± 5.4 ms (n=15) and 150 ± 4.7 ms (n=12) respectively with L-NNA application (P>0.05) (Figures 5.4 and 5.5, D). The response to ISO and ISO + L-NNA was also not significantly different between active and resting period myocytes (P>0.05) (Figure 5.6). This suggests that the AP response to ISO was not regulated by NOS activity in either active or resting period myocytes.

Figure 5.4

AP responses to ISO were not modulated by NOS inhibition in active period myocytes. (A) Representative APs recorded from an active period guinea pig left ventricular myocyte in 10 nM ISO and ISO + 500 µM L-NNA, to inhibit NOS. (B) Time course of APD_{90} responses before and during L-NNA application. (C) APD_{90} from individual myocytes under each condition. (D) Mean ± SEM APD_{90}. Number of cells indicated in each bar. Statistical analysis performed with a paired two-tailed t test. (Refer to Figure 5.1 legend for further detail).
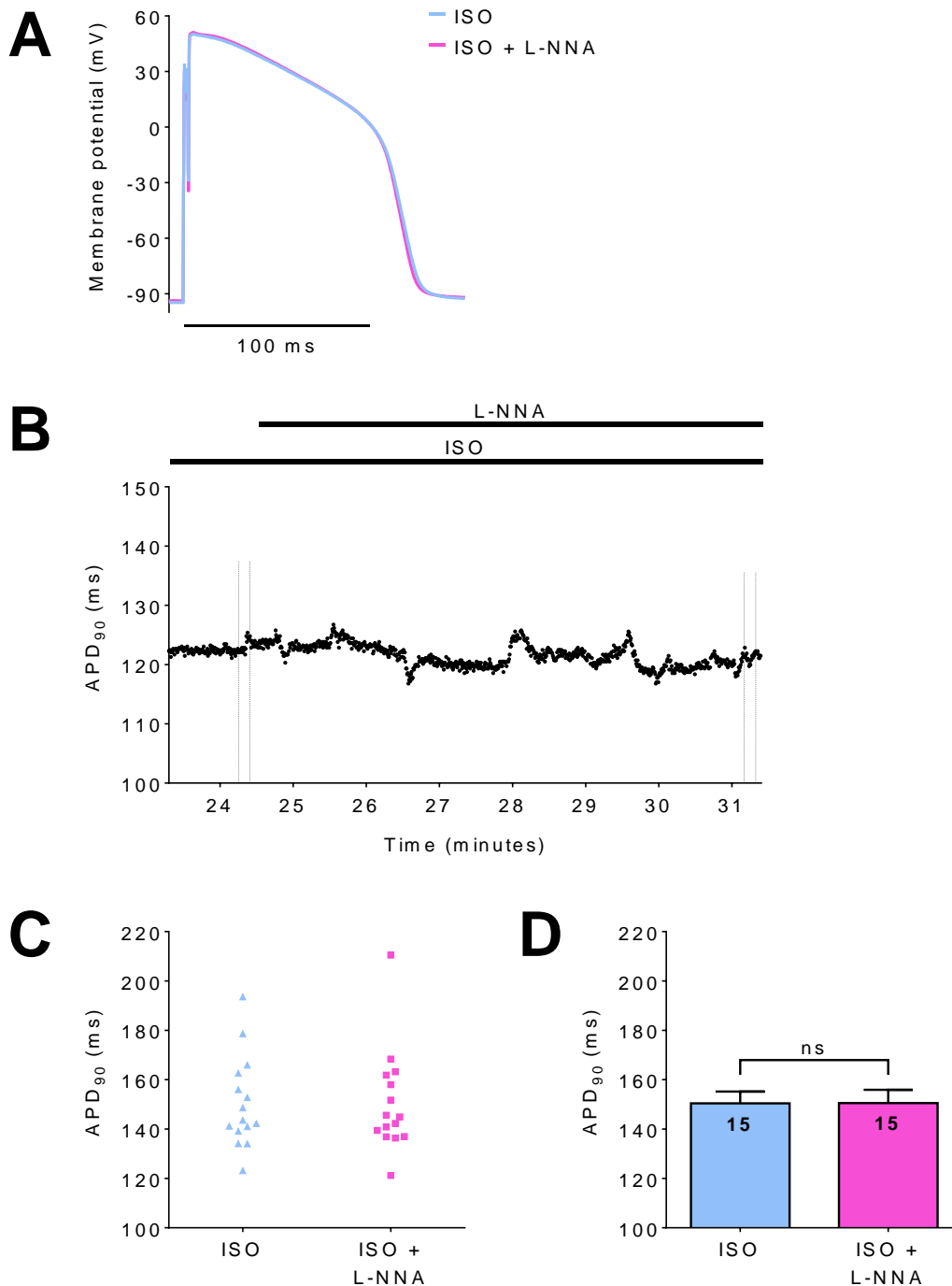
Figure 5.5

AP responses to ISO were not modulated by NOS inhibition in resting period myocytes. (A) Representative APs recorded from a resting period guinea pig left ventricular myocyte in 10 nM ISO and ISO + 500 µM L-NNA. (B) Time course of APD_{90} responses before and during L-NNA application. (C) APD_{90} from individual myocytes under each condition. (D) Mean ± SEM APD_{90}. Number of cells indicated in each bar. Statistical analysis performed with a paired two-tailed t test. (Refer to Figure 5.1 legend for further detail).
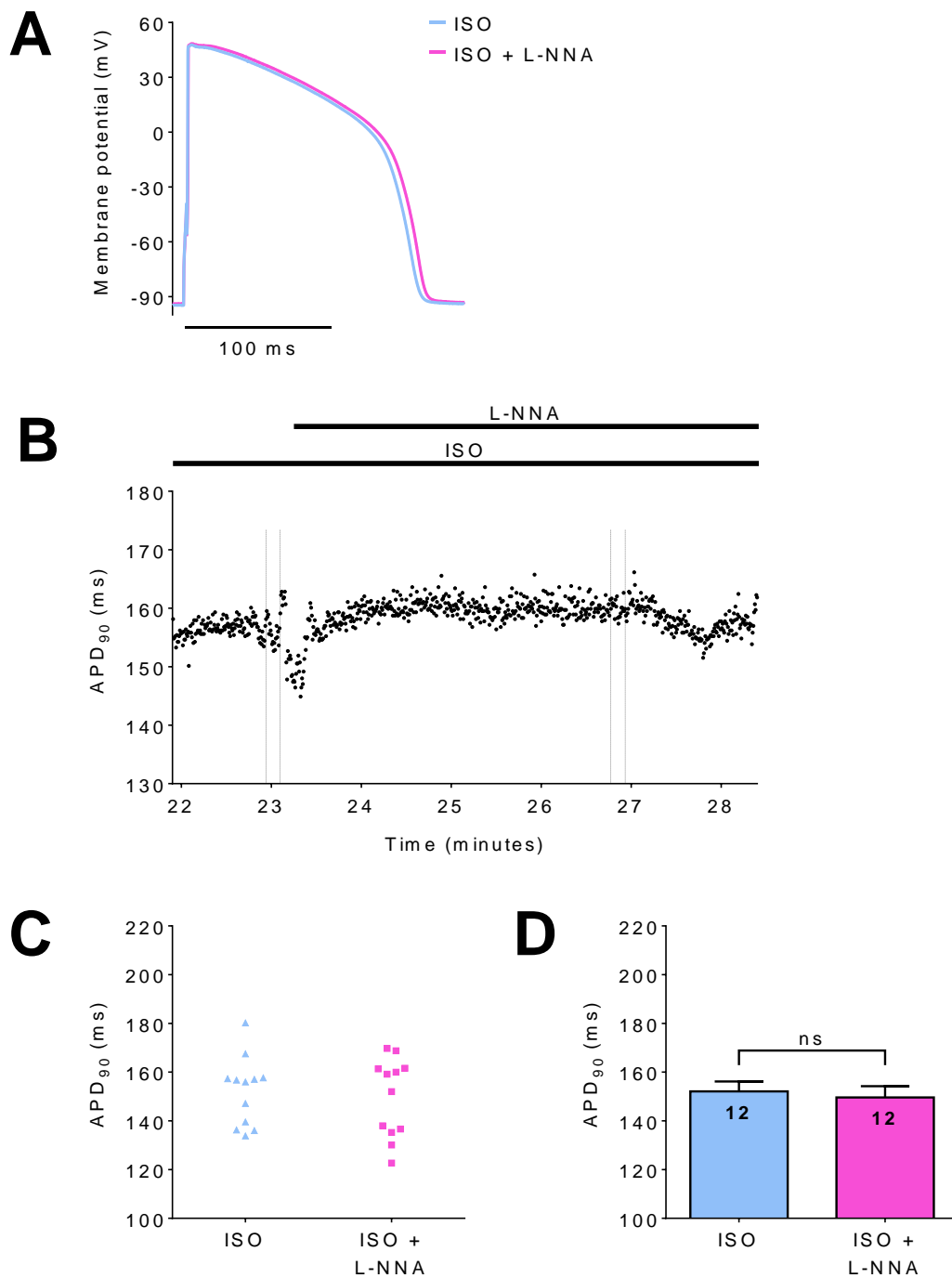
Figure 5.6

AP responses to ISO alone and ISO with NOS inhibition did not differ between active and resting period myocytes. Mean ± SEM APD_{90} for active and resting period guinea pig left ventricular myocytes in 10 nM ISO and ISO + 500 µM L-NNA. Number of cells indicated in each bar. Statistical analysis performed with repeated measures two-way ANOVA with Sidak's multiple comparisons test.
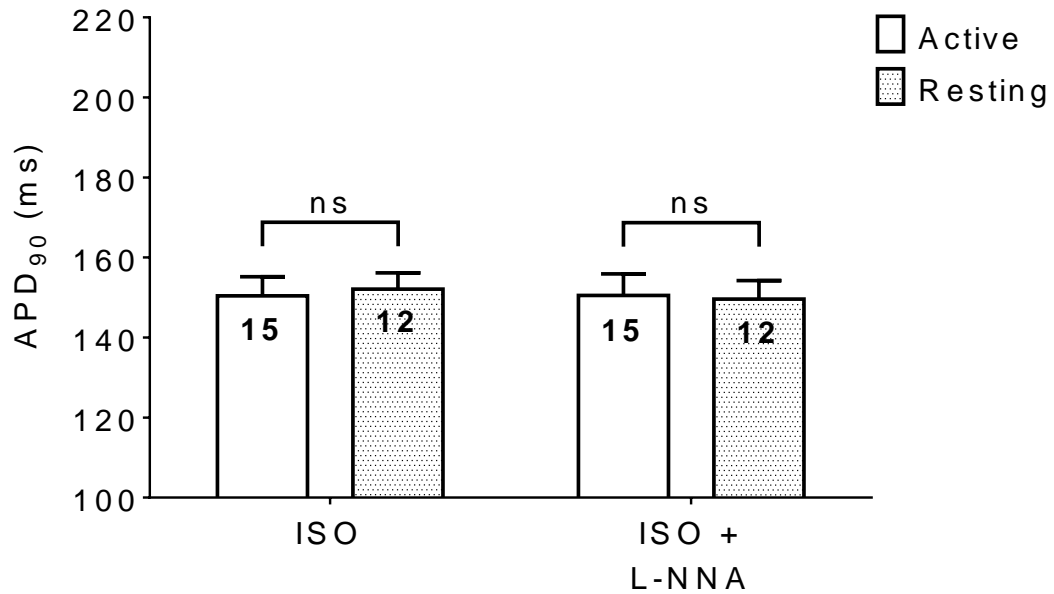
5.2.3 Responses of cell shortening to isoprenaline in active and resting period myocytes

There is a physiologically important interplay between APs and the subsequent contraction of myocytes. Results from a previous section have shown that AP responses to ISO exhibit diurnal variation. In the same experiments I also investigated whether there was diurnal variation of cell shortening responses upon stimulation with ISO.

Video based edge detection was used as a measurement of cell shortening. A stronger contraction corresponded to a greater change in distance moved by the edge of the myocyte and therefore a greater change in cell shortening. The amount of movement at one end of the myocyte was measured as opposed to cell length (edge detection at both ends of the cell) due to limitations in the apparatus (refer to section 2.3.6.3). The edge detection signal was recorded in parallel with the AP and current stimulus signals. The signal increased in amplitude upon contraction, reached a peak and then returned to baseline upon relaxation. The difference in amplitude between the peak and the baseline was measured and compared between experimental conditions.

ISO application at all concentrations typically increased the amplitude of cell shortening within 1 minute of application. However, the pattern of increase in response to ISO application, differed between concentrations, between cells and also within the same cell. In many instances, cell shortening amplitude peaked upon ISO application and then continuously decreased in amplitude. As a result, a steady-state was not reached within the time frame of ISO application, as shown by the response to 10 nM ISO in Figure 5.7, B. In other cases, a peak and decrease to a smaller quasi steady-state level was observed, as shown by the response to 3 nM ISO in Figure 5.7, B. On other occasions, cell shortening amplitude reached a maximum and remained at a relatively steady-state, as shown by the response to 3 nM ISO in Figure 5.8, B. Due to this variation, the cell shortening amplitude was consistently measured at the end of each ISO application and referred to as 'sustained' amplitude. In addition, if a larger amplitude peak was observed initially upon ISO application,

144

this was also measured and referred to as 'peak' amplitude. ISO application modulated the time course as well as the amplitude of cell shortening, in both active and resting period myocytes. Representative cell shortening traces and time courses of maximum amplitudes of each contraction during the course of an experiment are shown in Figures 5.7 and 5.8. Upon ISO application, an acceleration in the onset and decline of cell shortening was typically observed. Increasing the concentration of ISO, further enhanced the accelerated time course and amplitude of cell shortening. The application of 30 nM ISO caused profound changes in many cells. However, some cells failed to tolerate this relatively high concentration of ISO and lost contractile stability. Thus, the cell shortening response to 30 nM ISO could not be obtained for all cells.

Mean cell shortening was normalised to control amplitude and expressed as a fold change over control, as large differences in cell shortening amplitude were observed between cells. Mean sustained and peak cell shortening in response to 3 and 10 nM ISO were marginally larger in active than resting period myocytes, but these changes were not significantly different ($P>0.05$) (Figure 5.9). In active period myocytes, mean sustained cell shortening increased by 1.1 ± 0.04 fold (n=22) ($P<0.05$) and 1.5 ± 0.14 fold (n=22) ($P<0.01$) in response to 3 and 10 nM ISO respectively (Figure 5.7, C). The application of 30 nM ISO increased cell shortening further by 1.7 ± 0.25 fold (n=10). In comparison, 1.1 ± 0.02 fold (n=28) ($P<0.01$) and 1.3 ± 0.05 fold (n=28) ($P<0.001$) increases were observed in response to 3 and 10 nM ISO respectively in resting period myocytes (Figure 5.8, C). 30 nM ISO also further increased sustained cell shortening by 1.7 ± 0.20 fold (n=18). Furthermore, the mean peak cell shortening increased by 1.3 ± 0.07 fold (n=14), 1.7 ± 0.16 fold (n=16) and 1.9 ± 0.42 fold (n=5) in response to 3, 10 and 30 nM ISO respectively in active period myocytes. The fold changes were marginally smaller at 1.2 ± 0.04 fold (n=14) and 1.6 ± 0.10 fold (n=22) in response to 3 and 10 nM ISO and slightly larger at 2.2 ± 0.39 fold (n=12) in response to 30 nM ISO. However, none of these differences were statistically significant ($P>0.05$) (Figure 5.9). These results suggest that cell shortening responses to ISO do not exhibit diurnal variation in guinea pig left ventricular myocytes.

Figure 5.7

Cell shortening responses to ISO in active period myocytes. (A) Representative sustained (S) and peak (P) cell shortening traces recorded from an active period guinea pig left ventricular myocyte at 37°C in control, 3, 10 and 30 nM ISO. Each trace was averaged from 20 consecutive traces, indicated by the vertical dashed lines in B. (B) Time course of cell shortening amplitude before and during ISO application (indicated by horizontal bars). Individual symbols represent maximal amplitude from a single trace. (C) Mean ± SEM sustained cell shortening fold changes over control. Number of cells indicated in each bar. Statistical analysis performed with repeated measures one-way ANOVA with Dunnett's multiple comparisons test. (D) Mean ± SEM sustained and peak cell shortening fold changes over control.
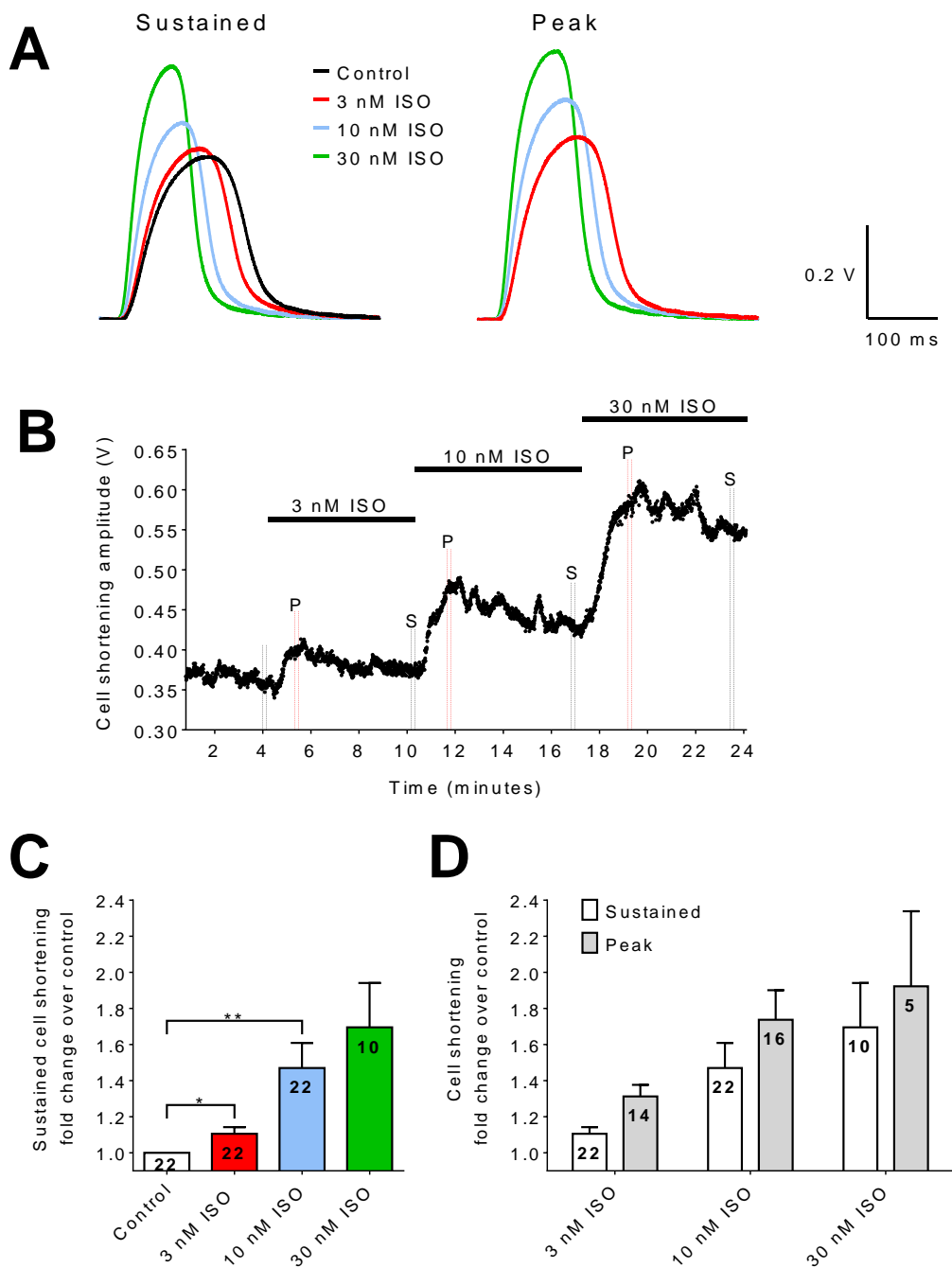
Figure 5.8

Cell shortening responses to ISO in resting period myocytes. (A) Representative sustained (S) and peak (P) cell shortening traces recorded from a resting period guinea pig left ventricular myocyte in control, 3, 10 and 30 nM ISO. (B) Time course of cell shortening amplitude before and during ISO application. (C) Mean ± SEM sustained cell shortening fold changes over control. Number of cells indicated in each bar. Statistical analysis performed with repeated measures one-way ANOVA with Dunnett's multiple comparisons test. (D) Mean ± SEM sustained and peak cell shortening fold changes over control. (Refer to Figure 5.7 legend for further detail).
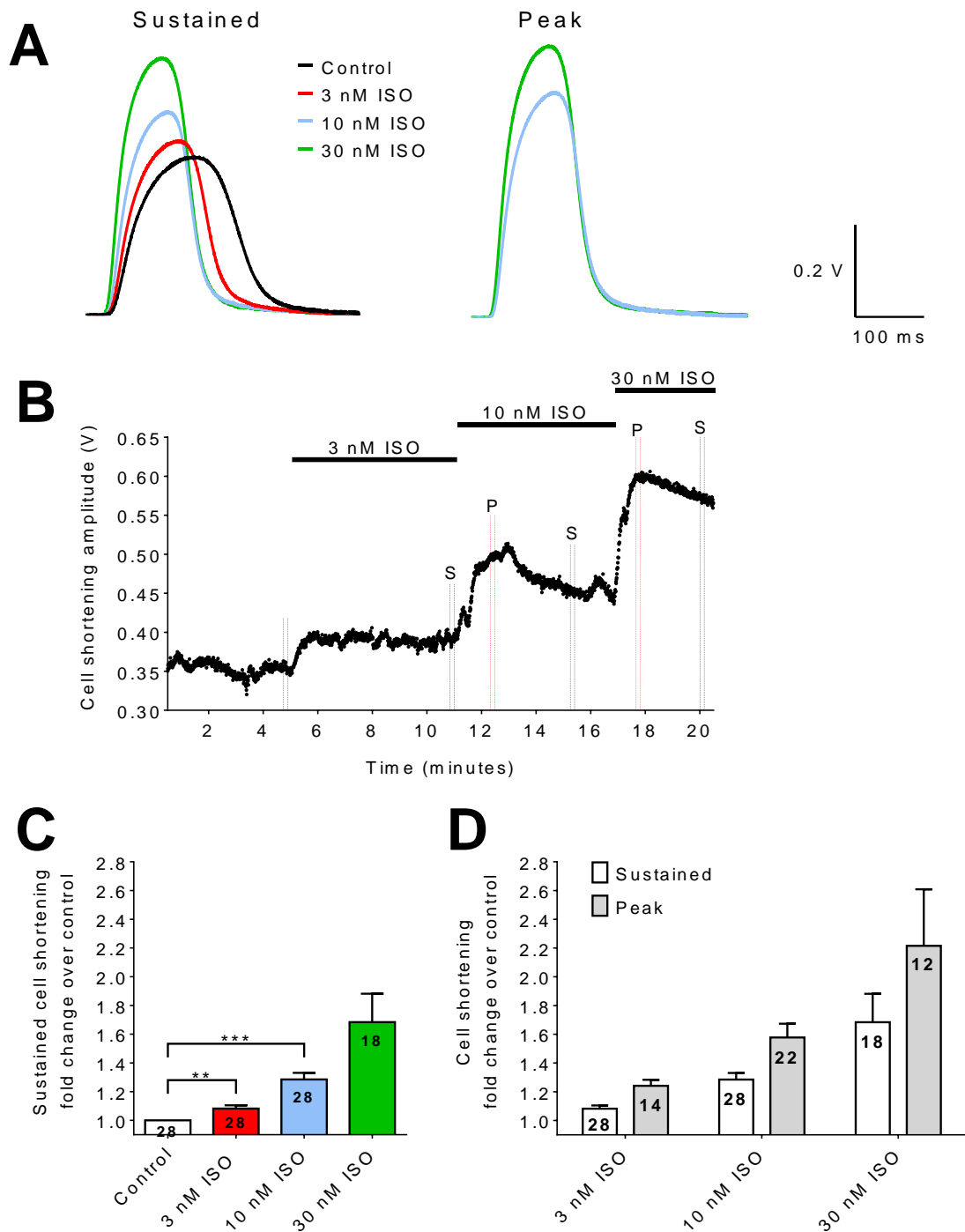
Figure 5.9

Sustained and peak cell shortening responses to ISO did not differ between active and resting period myocytes. Mean ± SEM sustained (A) and peak (B) cell shortening fold changes over control in active and resting period guinea pig left ventricular myocytes in 3, 10 and 30 nM ISO. Number of cells indicated in each bar. Statistical analysis performed with repeated measures two-way ANOVA with Sidak's multiple comparisons test (A) and ordinary two-way ANOVA with Sidak's multiple comparisons test (B).
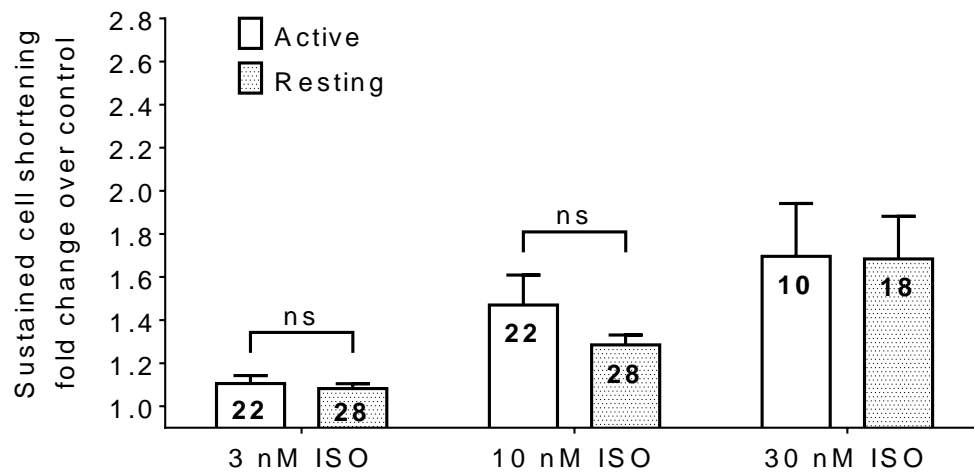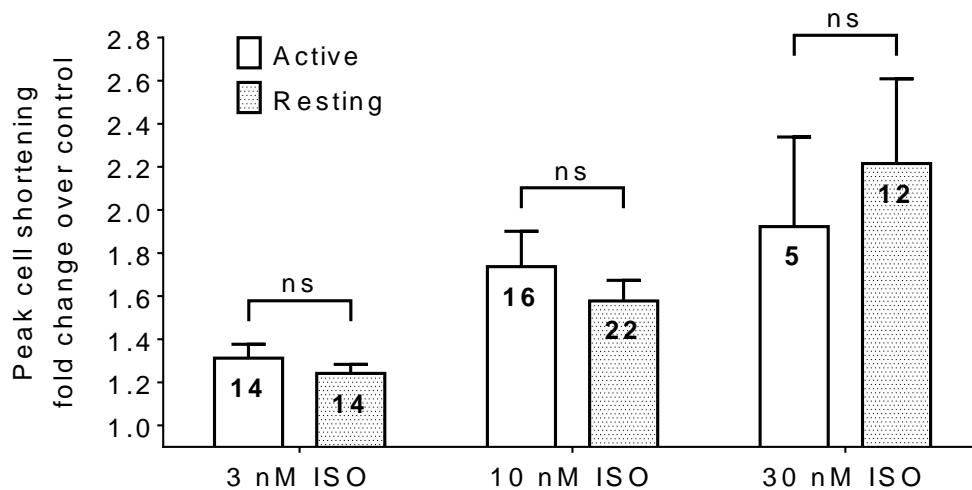
5.2.4 What is the effect of nitric oxide synthase inhibition on the responses of cell shortening to isoprenaline in active and resting period myocytes?

As previously described, ISO is a non-selective β-adrenergic receptor agonist. Stimulation by ISO is reported to produce NO and this may have a negative inotropic effect on myocyte contractility. Some of the response to ISO may be mediated by activation of NOS. Therefore, NO signalling might play a role in the cell shortening responses to ISO. To test this, NOS was inhibited with 500 μM L-NNA and the effect on the cell shortening response to 10 nM ISO in active and resting period myocytes was investigated, as described with AP recordings (refer to section 5.2.2).

L-NNA had no significant effect on the cell shortening responses to ISO in both active and resting period myocytes (Figures 5.10 and 5.11). Furthermore, the response to ISO + L-NNA was not significantly different between active and resting period myocytes (Figure 5.12). Representative cell shortening traces and time courses of maximum amplitudes of each contraction during the course of an experiment are shown in Figures 5.10 and 5.11. Although not statistically significant, a trend was observed in response to L-NNA. Upon L-NNA application, cell shortening typically increased slightly, reached a maximum and remained at a relatively steady-state, as shown in Figure 5.11, B. The increase in cell shortening in response to L-NNA was sustained rather than peaking and then decreasing as was observed in some instances in response to ISO alone. Therefore, all cell shortening amplitudes presented for ISO and ISO + L-NNA are 'sustained'. Mean cell shortening was normalised to the amplitude in ISO and expressed as a fold change over ISO. In ISO + L-NNA, mean cell shortening increased slightly by 1.1 ± 0.04 fold (n=9) and 1.3 ± 0.11 fold (n=8) in active and resting period myocytes respectively (Figure 5.12). However, these fold changes were not significantly different to ISO alone ($P>0.05$). These results suggest that cell shortening responses to ISO in guinea pig left ventricular myocytes are not regulated by NOS activity and also do not exhibit diurnal variation.

Figure 5.10
Cell shortening responses to ISO were not modulated by NOS inhibition in active period myocytes. (A) Representative cell shortening traces recorded from an active period guinea pig left ventricular myocyte in 10 nM ISO and ISO + 500 µM L-NNA. (B) Time course of cell shortening amplitude before and during L-NNA application. (Refer to Figure 5.7 legend for further detail).
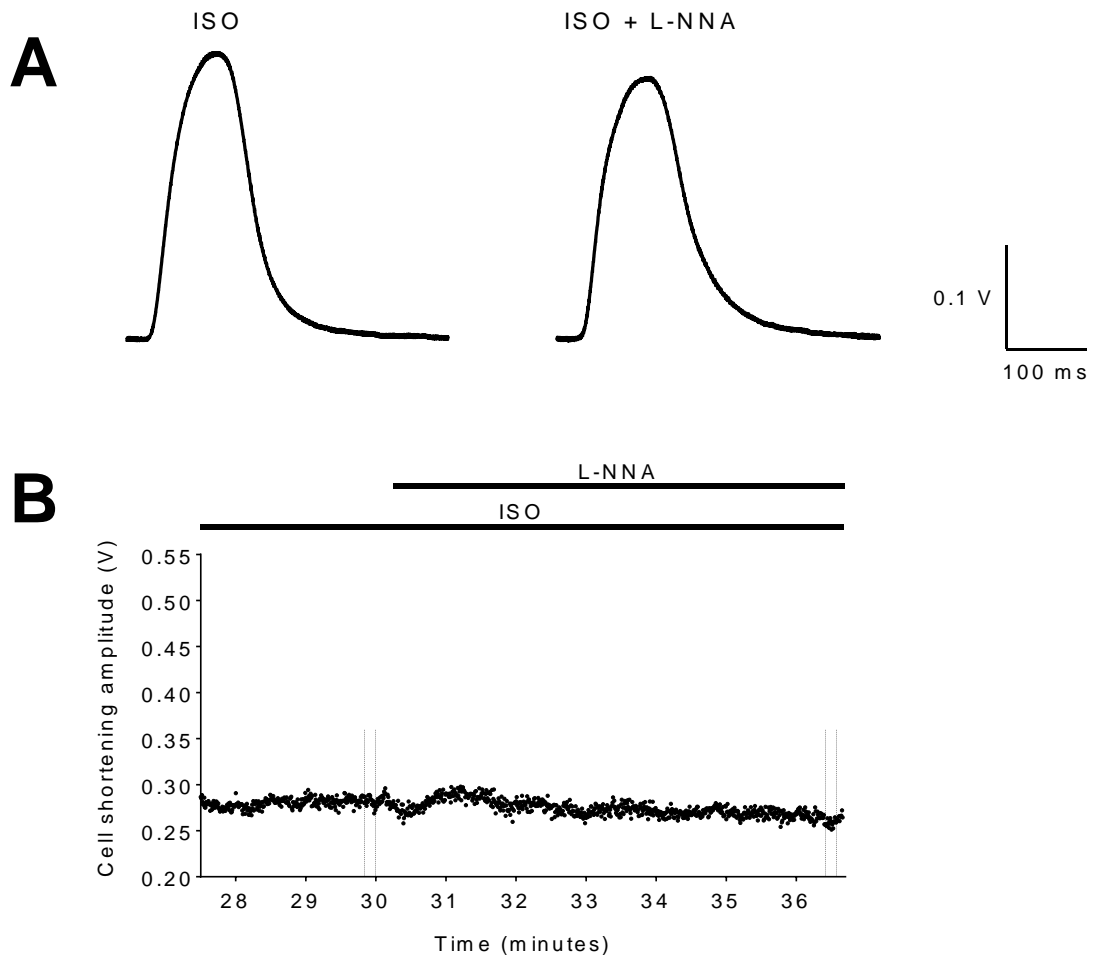
Figure 5.11
Cell shortening responses to ISO were not modulated by NOS inhibition in resting period myocytes. (A) Representative cell shortening traces recorded from a resting period guinea pig left ventricular myocyte in 10 nM ISO and ISO + 500 µM L-NNA. (B) Time course of cell shortening amplitude before and during L-NNA application. (Refer to Figure 5.7 legend for further detail).
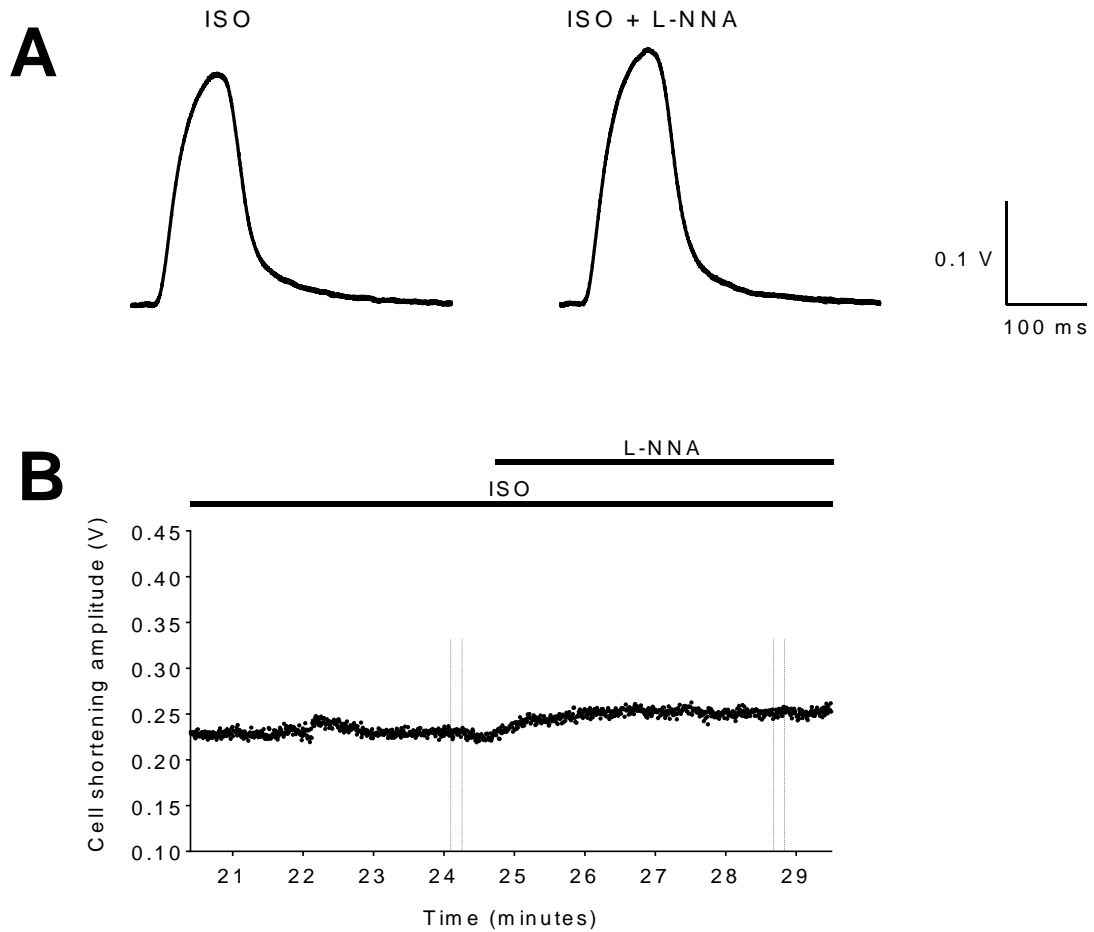
Figure 5.12
Cell shortening responses to ISO with NOS inhibition did not differ between active and resting period myocytes. Mean ± SEM cell shortening fold changes over ISO, in active and resting period guinea pig left ventricular myocytes in 10 nM ISO + 500 µM L-NNA. Number of cells indicated in each bar. Statistical analysis performed with an unpaired two-tailed t test.
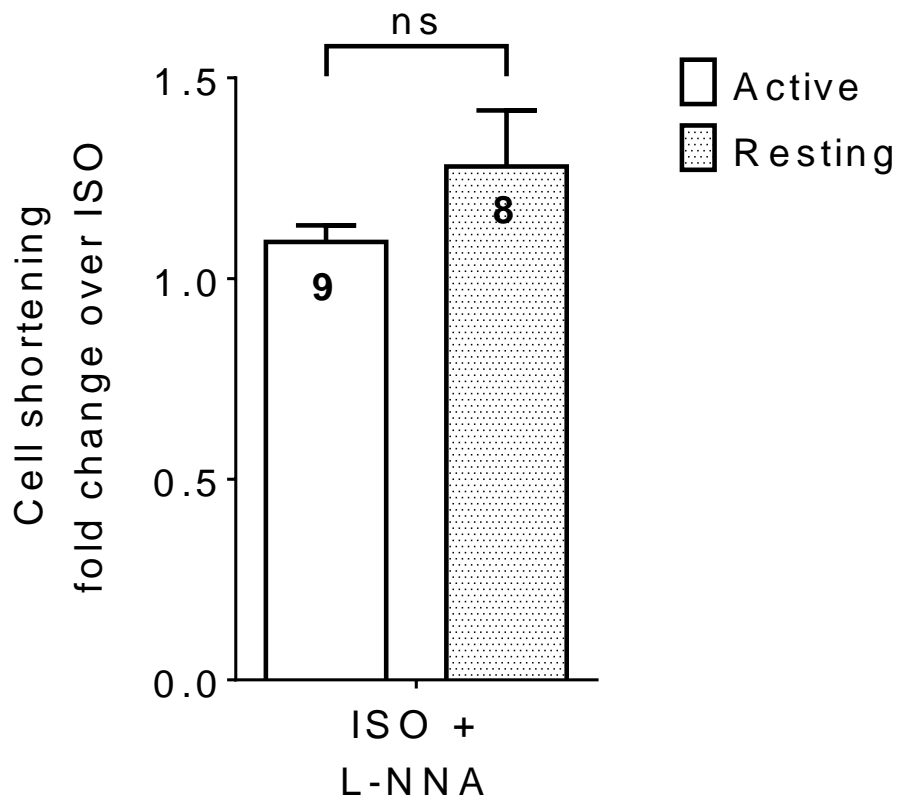
Chapter 6
Discussion

The work detailed in this thesis describes an investigation into the regulation of ventricular repolarisation by cGMP-dependent NO signalling. The effects of the novel NO/haem-independent sGC activator BAY 60-2770 on cellular cGMP levels, APD and delayed rectifier K^+ current amplitude were characterised. Additionally, AP and cell shortening responses to β-adrenergic receptor stimulation and the consequences of NOS inhibition were investigated, with a view as to whether the responses exhibited diurnal variation.

6.1 Pharmacological effects of BAY 60-2770 in guinea pig isolated ventricular myocytes

The overall findings were that BAY 60-2770 modulated cellular cGMP levels, APD and delayed rectifier K^+ current amplitude. BAY 60-2770 had differential effects dependent on the experimental conditions. Under basal conditions, BAY 60-2770 modestly increased cellular cGMP levels, modestly shortened APD but failed to modulate I_{Ks} or I_{Kr}. However, when PDEs were non-selectively inhibited, BAY 60-2770 increased cGMP levels further, prolonged APD, inhibited I_{Ks} but still failed to modulate I_{Kr}. Furthermore, inhibition of I_{Ks} by BAY 60-2770 remained in the presence of a PKG inhibitor. Interestingly, the increase in cellular cGMP levels by BAY 60-2770 was dramatically potentiated by ODQ. Despite this, BAY 60-2770 and ODQ in combination failed to modulate APD more than BAY 60-2770 alone. Finally, the cGMP responses to BAY 60-2770 in the absence and presence of PDE inhibition were found to be comparable with ACh and ISO, which are physiologically relevant modulators of cGMP levels. However, unlike with BAY 60-2770, ODQ did not potentiate ACh, ISO and FSK cGMP responses. BAY 60-2770 was thus a useful pharmacological tool for selectively activating sGC and investigating the role of cGMP-dependent signalling. My results indicate that even large changes in cellular cGMP concentrations have little impact on ventricular repolarisation unless PDEs are

inhibited, further demonstrating the importance of PDEs in compartmentalising cGMP and cAMP signalling.

6.2 Modulators of cellular cGMP levels had minor effects on ventricular action potentials

Cellular cGMP levels were quantified in response to multiple modulators of cGMP signalling, including the novel NO/haem-independent sGC activator BAY 60-2770, the NO donor SNAP and the sGC inhibitor ODQ. These reagents differentially modulated cGMP levels and ventricular APs.

Under basal conditions, BAY 60-2770 modestly increased cellular cGMP in a concentration-dependent manner. Cellular cGMP levels increased by 2.2 fold in response to 1 µM BAY 60-2770. SNAP also increased cGMP in a concentration-dependent manner. However, more substantial increases were measured in response to SNAP compared to BAY 60-2770, although a higher concentration range was used. 100 µM SNAP brought about a 19 fold increase in cellular cGMP. Interestingly, ventricular APs were modulated by BAY 60-2770 but not SNAP. In the case of BAY 60-2770, a 2.2 fold increase in cGMP equated to an 11 ms shortening in APD. Whereas, APD was not altered by SNAP despite a 19 fold increase in cGMP.

A contrasting approach to sGC activation by BAY 60-2770 and SNAP was to use ODQ to inhibit sGC. Under basal conditions, cGMP levels were not modulated by ODQ, which suggests that constitutive activity of sGC is low. Not surprisingly, ODQ also failed to modulate ventricular APs. However, ODQ potentiated the cGMP response to BAY 60-2770, increasing cGMP by 28 fold. When PDEs were non-selectively inhibited, ODQ also potentiated the cGMP response to BAY 60-2770. *In-vitro* studies on purified sGC have demonstrated that ODQ acts synergistically with BAY to potentiate sGC activity (Knorr *et al.*, 2008; Kumar *et al.*, 2013). ODQ inhibits sGC by oxidising the haem group, which renders sGC unresponsive to NO. However, a reduced haem is not a pre-requisite for sGC activators like BAY 60-2770, which have been shown to preferentially activate oxidised/haem-free NO-insensitive sGC (Schmidt *et al.*,

2009). These studies provide an explanation for the mechanism underlying the BAY 60-2770-dependent potentiation of cGMP levels by ODQ. Remarkably, BAY 60-2770 + ODQ failed to modulate ventricular APs further compared to BAY 60-2770 alone, despite a substantial increase in cGMP. The effect of PDE inhibition on the response of ventricular APs to BAY 60-2770 + ODQ was not characterised.

Several studies have quantified cGMP levels in response to ODQ, BAY 60-2770 and SNAP in cardiac tissue and other tissue types. Similar to my findings, Vila-Petroff *et al.* (1999) found that cGMP was not modulated by ODQ under basal conditions in rat cardiac myocytes. Very recently, Bice *et al.* (2014) reported that cGMP levels were elevated by BAY 60-2770 + ODQ but not by BAY 60-2770 alone, in rat cardiac tissue. This result contrasts from my findings, since I found that BAY 60-2770 alone modestly but significantly increased cGMP. The sensitivity of my assay may have been higher since I worked on isolated myocytes rather than tissue containing different cell types. In another study, BAY 60-2770 alone and in the presence of ODQ, increased cGMP levels in a concentration-dependent manner in activated human platelets. ODQ potentiated the cGMP response to BAY 60-2770 as was found in cardiac tissue (Mendes-Silverio *et al.*, 2012). SNAP is well known to increase cGMP levels over control, in rat and human cardiac tissue (Ebihara & Karmazyn, 1996; Ross *et al.*, 2005; Rozmaritsa *et al.*, 2014). Kotlo *et al.* (2011) also demonstrated that SNAP increased cGMP in a concentration-dependent manner in human vascular smooth muscle. Furthermore, SNAP increased cGMP in other tissues, including kidney and platelets (Lu *et al.*, 1998; Kottenberg-Assenmacher *et al.*, 2003; Monteiro *et al.*, 2012). Surprisingly, few studies have investigated the modulation of APs by SNAP. Cameron *et al.* (2003) reported that SNAP shortened APD in goldfish ventricular myocytes, by enhancing K_{ATP} channel activation. Abramochkin *et al.* (2012), however, demonstrated that SNAP prolonged APD in rat atrial tissue by causing a distinct change in AP morphology in which repolarisation was 'hump-like'. In my experiments, SNAP failed to modulate APD. There is no published research investigating the effect of BAY 60-2770 on APs. My results show that sGC activation by BAY 60-2770, but not SNAP, modulates ventricular APs. These findings suggest that the

relative increase in cGMP may not be a defining factor in determining a response, as substantial increases in cGMP levels in response to SNAP failed to modulate ventricular APs, whereas a small increase in cGMP in response to BAY 60-2770 was sufficient to modulate APD. Therefore, other factors must be involved, including the important role of PDEs.

6.3 Phosphodiesterases are important regulators of cyclic nucleotide-dependent signalling

Since PDEs hydrolyse cGMP, it was predicted that PDE activity might suppress the effects of BAY 60-2770. Therefore, PDEs were non-selectively inhibited with IBMX. Under basal conditions, inhibition of PDEs resulted in a modest 2.5 fold increase in cGMP. This suggests that cGMP is constitutively produced, as PDE inhibition alone was sufficient to increase cellular cGMP levels in the absence of exogenous sGC activation. In contrast to my finding, Castro *et al.* (2010) reported that IBMX failed to modulate basal cGMP levels in rat ventricular myocytes. I also found that inhibition of PDEs shortened ventricular APs substantially. This was most likely attributed to an enhancement of I_{Ks} caused by an increase in PKA-mediated phosphorylation of I_{Ks} channels as a result of an increase in cAMP (Marx *et al.*, 2002). Another factor could be faster inactivation of $I_{Ca,L}$ due to channel phosphorylation and increased Ca^{2+}-dependent inactivation. However, this was not investigated in my study.

When PDEs were inhibited, 1 µM BAY 60-2770 increased cGMP levels more than either BAY 60-2770 alone or PDE inhibition alone. The cGMP responses to BAY 60-2770 and PDE inhibition were not additive as a greater increase of 7.1 fold was observed. This suggests that PDE activity suppressed the cGMP response to BAY 60-2270 due to hydrolysis of cGMP. Tsai *et al.* (2012) found that in mouse cardiac tissue, BAY 60-2770, in the presence of IBMX, increased cGMP to similar levels as the NO donor diethylamine NONOate. Similar findings were reported in a subsequent study in canine cardiac tissue (Liu *et al.*, 2013).

Since, BAY 60-2770 modestly shortened ventricular APD, it was predicted that a further shortening would be observed when PDEs were inhibited. However, although BAY 60-2770 still modulated APD when PDEs were inhibited, it had the opposite effect and prolonged APD by 16 ms. Thus, there were differential effects of sGC activation with BAY 60-2770 in the absence and presence of PDE activity. Furthermore, in a small proportion of myocytes, BAY 60-2770 failed to modulate APD when PDEs were inhibited. The reason for this was not apparent and could possibly be due to heterogeneity in the response to BAY 60-2770 between myocytes from different regions of the ventricle. The shortening of APD in response to BAY 60-2770 is possibly due to an increase in cAMP and could be investigated by inhibiting PKA. Changes in cGMP can differentially alter the activity of PDE2 and PDE3, which hydrolyse both cAMP and cGMP. Thus, an increase in cGMP in response to BAY 60-2770 may lead to an increase in cAMP levels by inhibiting the activity of PDE3 and decreasing cAMP degradation. This could be investigated further using selective PDE inhibitors but was not the focus of my study as the feedback mechanisms involved in the modulation of cAMP and cGMP levels by PDEs are highly complex.

PDE5 is a cGMP-specific PDE expressed in cardiac myocytes. Particularly high expression of PDE5 has been reported in guinea pig ventricular myocytes (Johnson *et al.*, 2012). Thus, PDE5 is an important regulator of cGMP levels and was predicted to be a key PDE responsible for suppressing the cGMP response to BAY 60-2770. Therefore, PDE5 was selectively inhibited with sildenafil. Under basal conditions, inhibition of PDE5 failed to modulate cellular cGMP levels, in contrast to the increase observed in response to non-selective PDE inhibition. This suggests that PDE5 was not primarily responsible for the degradation of constitutively produced cGMP. Furthermore, the cGMP response to BAY 60-2770 was not enhanced by PDE5 inhibition as was the case with IBMX. At the cellular level, cGMP synthesised by sGC did not appear to be influenced by PDE5.

6.4 SNAP and BAY 60-2770 both increase cellular cGMP levels but have differential effects on ventricular action potentials

The physiological agonist of sGC is NO. SNAP is a NO donor, whereas BAY 60-2770 is a novel NO/haem-independent sGC activator. Therefore, SNAP and BAY 60-2770 activate sGC in different ways to increase cGMP. As previously discussed, SNAP failed to modulate APD despite a 19 fold increase in cGMP. Similar to BAY 60-2770, cGMP levels in response to SNAP were suppressed by the activity of PDEs but not PDE5. When PDEs were non-selectively inhibited with IBMX, SNAP increased cellular cGMP by 34 fold. Other studies have also demonstrated that PDE activity suppresses increases in cGMP in response to SNAP, in cardiac tissue and other tissue types. Castro *et al.* (2010) found that cGMP levels increased further in response to SNAP with non-selective PDE inhibition compared to SNAP alone, in rat ventricular myocytes. Hamad *et al.* (1997) reported a similar finding in human airway smooth muscle. Importantly, in contrast to BAY 60-2770, ventricular APs were not modulated by SNAP-derived cGMP and PDEs were not an important regulator of this lack of response in my experiments.

In addition, ODQ had opposing effects on the cellular cGMP responses to SNAP and BAY 60-2770. As previously discussed, ODQ potentiated the cGMP response to BAY 60-2770. In contrast, the cGMP response to SNAP was inhibited by ODQ. ODQ binds to the haem group of sGC in competition with NO and oxidises the haem group, which prevents activation by NO (Lies *et al.*, 2013). Studies have demonstrated that SNAP-induced elevations in cGMP were abolished by ODQ, in rat cardiac myocytes (Vila-Petroff *et al.*, 1999; Sandirasegarane & Diamond, 1999). Furthermore, the same effect has been found in cardiac mitochondria and human umbilical vein endothelial cells (Seya *et al.*, 2007; Hoffmann *et al.*, 2003).

6.5 The slow delayed rectifier potassium current was regulated by BAY 60-2770, but only when phosphodiesterases were inhibited

It was anticipated that modulation of repolarisation by BAY 60-2770 was most likely due to modulation of I_{Ks} or I_{Kr}, as the early phases of the AP were not altered during BAY 60-2770 application. Under basal conditions, BAY 60-2770 failed to modulate I_{Ks}. It was hypothesised that PDE activity might suppress the effects of BAY 60-2770, since PDEs hydrolyse cGMP. PDE inhibition increased I_{Ks}. This potentiation was most likely caused by an increase in PKA-mediated phosphorylation of I_{Ks} channels (Marx *et al.*, 2002). When PDEs were inhibited, BAY 60-2770 inhibited I_{Ks}. However, in a proportion of myocytes, BAY 60-2770 had no effect. This heterogeneity in the response of I_{Ks} to BAY 60-2770 is similar to that observed with APD prolongation under the same conditions.

To investigate whether PKG mediated the inhibition of I_{Ks} by BAY 60-2770, experiments were repeated in the presence of the PKG inhibitor KT5823. IBMX-enhancement of I_{Ks} was not altered by KT5823. Furthermore, inhibition of I_{Ks} by BAY 60-2770 remained in the presence of KT5823. Although not significant, a small decrease in I_{Ks} was observed in KT5823 before BAY 60-2770 application, thus the effects of BAY 60-2770 may not solely account for all the inhibition. Since KT5823 failed to prevent I_{Ks} inhibition, the effects of BAY 60-2770 might be mediated by a PKG-independent mechanism. However, the effectiveness of KT5823 as a PKG inhibitor has to be questioned. Bain *et al.* (2003) investigated the efficacy and specificity of multiple commercially available protein kinase inhibitors, including KT5823. KT5823 failed to inhibit PKG activity in a protein kinase assay. Burkhardt *et al.* (2000) demonstrated that KT5823 inhibited purified PKG but failed to inhibit PKG-mediated phosphorylation in response to NO signalling in human platelets and rat mesangial cells. Therefore, determining whether signalling is PKG-dependent using solely KT5823 is not sufficient.

As an alternative approach, PKG was activated with 8-Br-cGMP, a membrane-permeable analogue of cGMP, and I_{Ks} was measured. 8-Br-cGMP, in the absence and presence of PDE inhibition, failed to modulate I_{Ks}, this suggests that PKG does not play a role in modulating I_{Ks}.

In summary, I_{Ks} inhibition by BAY 60-2770 appears to be mediated by a PKG-independent mechanism. In addition, BAY 60-2770-mediated signalling is suppressed and compartmentalised by PDEs. Importantly, it seems likely that sGC and the molecular components of I_{Ks} channels are not found within the same signalling compartment, as no effect was observed unless PDEs were inhibited. The compartmentalisation of cGMP-dependent signalling is discussed in detail in the following section. These findings may be relevant under pathophysiological conditions in which PDE expression or activity is altered. The mechanism underlying the inhibition of I_{Ks} by BAY 60-2770 is unclear, but is unlikely to be a direct effect on I_{Ks} channels as I_{Ks} was not altered by BAY 60-2770 alone. Unfortunately, it was not possible to test whether the effects of BAY 60-2770 were sGC-mediated, as ODQ does not inhibit sGC under these conditions and other inhibitors are not selective enough.

Research investigating the regulation of I_{Ks} by cGMP-dependent signalling is very limited. Shimizu *et al.* (2002) studied I_{Ks} responses, but in guinea pig sinoatrial node cells rather than ventricular cells using ruptured rather than perforated patch techniques. In contrast to what I found, when elevating cGMP (via the pipette or with a membrane-permeable analogue) they observed an increase in I_{Ks} (rather than no effect) and a negative shift in the voltage-dependence of activation under basal conditions. The enhancement of I_{Ks} by 8-Br-cGMP was reversed by KT5823. Furthermore, when PDEs were inhibited, 8-Br-cGMP increased I_{Ks} in their experiments whereas I saw no response to 8-Br-cGMP and a profound inhibition of I_{Ks} in response to BAY 60-2770. In addition, the response to BAY 60-2770 was not blocked by KT5823 in my experiments. Some of these differences could be due to the differential expression of specific PDEs in sinoatrial node versus ventricular cells, but other unidentified factors

must also play a role. However, a similarity exists between this study and my experiments. Surprisingly, PKG appears to partially mediate the enhancement of I_{Ks} by IBMX. They found that when PDEs were inhibited, I_{Ks} enhancement was largely reversed by the PKA inhibitor, Rp-8-Br-cAMPS and modestly reversed by KT5823. In a few preliminary experiments not shown in this thesis, I found that the potentiation of I_{Ks} by IBMX appeared smaller when IBMX and KT5823 were applied at the same time, as opposed to sequentially. A suppressed response might be due to a lack of KT5823 selectivity for PKG over PKA. However, this is unlikely, if this was the case then sequential KT5823 application would be expected to reverse the IBMX-enhancement of I_{Ks}, which is predominantly mediated by PKA, which did not occur in my experiments. Furthermore, this effect of KT5823 suggests that the compound is active, although its effectiveness as a PKG inhibitor was not confirmed by this.

6.6 Phosphodiesterases compartmentalise cyclic nucleotide signalling pathways

In the past, it has been questioned how several different receptors coupled to cyclic nucleotide signalling are able to successfully achieve specific cellular responses. Over time, this has led to the notion that PDEs are important not only in the degradation of cyclic nucleotides but also in organising and compartmentalising intracellular signalling pathways in specific microdomains of the cell (Fischmeister *et al.*, 2006). There is now evidence that, cyclic nucleotide levels rise in specific subcellular locations, as opposed to globally, thus regulating specific targets in different parts of the cell (Castro *et al.*, 2006). Furthermore, this provides a convincing explanation as to why multiple PDE isoforms are expressed within the same cell (Fischmeister *et al.*, 2006). Compartmentalisation of cAMP signalling pathways by PDEs has been extensively studied. In recent years, research has shown that cGMP signalling also appears to be compartmentalised, although the effects are less well established compared to cAMP (Castro *et al.*, 2006). The development of selective PDE inhibitors has been integral to research in this field. The role of PDEs in the compartmentalisation of cGMP signalling is often investigated

using recombinant cyclic nucleotide-gated channels, from the rat olfactory system, which open directly in response to cyclic nucleotides (Rochais *et al.*, 2004; Castro *et al.*, 2006; Castro *et al.*, 2010). Cardiac myocytes are infected with an adenovirus encoding this channel to induce expression at the plasma membrane resulting in a cyclic nucleotide-gated current (I_{CNG}) in response to cyclic nucleotide concentration. Thus, cyclic nucleotide-gated channels act as real-time biosensors of cyclic nucleotide concentration beneath the plasma membrane (Fischmeister *et al.*, 2006).

Castro *et al.* (2006) studied the compartmentalisation of cGMP-dependent NO signalling in rat ventricular myocytes, expressing cyclic nucleotide-gated channels. Channels bound cGMP with over a 10 fold higher affinity than cAMP. Interestingly, they found that 100 µM SNAP had no effect on I_{CNG} under basal conditions, but increased I_{CNG} when PDEs were non-selectively inhibited with IBMX. IBMX alone had no effect on basal I_{CNG}. This indicates that SNAP-derived cGMP was not detected at the plasma membrane unless PDEs were inhibited. This is consistent with my results. I found that under basal conditions SNAP had no effect on APD, which I predicted was because cGMP was unable to reach the plasma membrane. However, SNAP + IBMX also failed to modulate APD, and so this lack of response of APs to cGMP cannot be explained by compartmentalisation of cGMP signalling by PDEs alone. HMR1766, a NO/haem-independent sGC activator also had no effect on I_{CNG} under basal conditions, but increased I_{CNG} in the presence of IBMX. These findings demonstrate that cGMP produced by sGC was unable to reach I_{CNG} channels at the plasma membrane due to rapid degradation by PDEs. Contamination of the I_{CNG} response by cAMP was tested using a cyclic nucleotide-gated channel with a 10 fold higher sensitivity to cAMP. In the presence of IBMX, SNAP and HMR1766, had no effect on cAMP-sensitive I_{CNG}. In relation to my results, I found that under basal conditions BAY 60-2770 modestly shortened APD but had no effect on I_{Ks}. This suggests that cGMP signalling was able to reach some ion channels in the plasma membrane, but not I_{Ks} channels. Whereas, BAY 60-2770 in the presence of IBMX, inhibited I_{Ks},

suggesting that PDE inhibition permitted modulation of I_{Ks} channels by cGMP-dependent signalling.

If PDEs are able to prevent cGMP levels changing around I_{Ks} channels, the next questions are which PDEs are responsible and what is the mechanism for channel specificity? Castro *et al.* investigated the effect of PDE2 and PDE5 inhibition on the I_{CNG} response to SNAP, using the selective inhibitors EHNA and sildenafil respectively. EHNA and sildenafil alone had no effect on basal I_{CNG} but potentiated the effect of SNAP. Sildenafil potentiated the effect of SNAP in a concentration-dependent manner, with a maximal response at 100 nM. This response was almost 2 fold greater than potentiation by EHNA, suggesting that PDE5 is the predominant isoform responsible for SNAP-derived cGMP degradation. SNAP, sildenafil and EHNA in combination, increased I_{CNG} further, and to an extent similar to SNAP + IBMX, which suggests PDEs 2 and 5 are the main PDEs involved in SNAP-derived cGMP degradation. In contrast, I found that sildenafil had no effect on cGMP levels in response to SNAP and therefore was unlikely to be the PDE preventing cGMP reaching I_{Ks} channels. I did not investigate the role of PDE2 in my experiments.

In a subsequent study, Castro *et al.* (2010) studied the role of PKG in the compartmentalisation of cGMP signalling. PDE5 is activated by phosphorylation by PKG. They hypothesised that PKG exerts a negative feedback to regulate the local level and time course of changes in cGMP. A similar negative feedback mechanism has been described for PDE4 regulation by PKA (Rochais *et al.*, 2004). PKG inhibitors KT5823 or DT-2 had no effect on basal I_{CNG}, but potentiated the I_{CNG} response to SNAP. cGMP levels in response to SNAP were also increased by PKG inhibition. The effect of PKG inhibition on I_{CNG} could be blocked by sildenafil, providing evidence that PKG activates PDE5 to decrease cGMP levels via a negative feedback mechanism.

In summary, there is increasing evidence that cGMP-dependent signalling is compartmentalised within cells. There is evidence that, at least in rat ventricular

myocytes, the 'soluble' cGMP pool is compartmentalised by PDE5 predominantly but also by PDE2. This pool of cGMP increases in response to sGC activation and is not accessible to the plasma membrane. In my experiments, cGMP-dependent signalling was compartmentalised, and sGC and I_{Ks} channels did not appear to share the same intracellular signalling compartment.

6.7 The rapid delayed rectifier potassium current was not regulated by cGMP-dependent signalling

In my experiments, I_{Kr} was not modulated by BAY 60-2770 or 8-Br-cGMP, under basal conditions or when PDEs were inhibited. Therefore, I_{Kr} does not appear to be regulated by sGC or PKG. Furthermore, I_{Kr} was not altered by IBMX, which elevates cGMP and cAMP levels. Thus, it seems that I_{Kr} is not regulated by cAMP signalling either. My findings are at odds with other reports in the literature.

Mewe *et al*. (2010) studied the effect of cGMP signalling on rat and guinea pig papillary muscle APD, heterologously expressed ERG1 channels and mouse atrial and ventricular I_{Kr}. They found that in papillary muscle, APD was prolonged by 8-Br-cGMP, in an E4031-dependent manner. They also found that 8-Br-cGMP suppressed ERG1b and ERG1a/1b currents from channels heterologously expressed in human embryonic kidney cells, by accelerating deactivation and inactivation kinetics, and also causing a negative shift in the voltage-dependence of activation. Most of these effects could be blocked by pre-incubation with Rp-8-Br-cGMPS, a PKG inhibitor. Interestingly, ERG1a currents were not modulated by 8-Br-cGMP. Finally, 8-Br-cGMP was found to inhibit atrial I_{Kr}, but consistent with my data, had no effect on ventricular I_{Kr}, possibly because of a lower expression of ERG1b in the ventricle. Although interesting, there were a number of weaknesses of this study. It's unclear why the effects of 8-Br-cGMP were studied on APD in papillary muscle rather than cardiac myocytes, and why there was no consistency in species of experimental models that were chosen. There are marked differences in ventricular APD, AP

morphology and the relative contribution of repolarising currents between species. For example, I_{To} and I_{K1} are the predominant repolarising currents in the mouse, and in contrast to humans, repolarisation has little dependence on I_{Kr}. Therefore, the mouse is not the most suitable model to study I_{Kr}. Guinea pig and rabbit cardiac electrophysiology resembles that of humans more closely.

In the only other relevant study, Taglialatela *et al.* (1999) found that 8-Br-cGMP had no effect on hERG1 currents expressed in Xenopus oocytes. In light of the findings reported by Mewe *et al.* (2010), this could be due to lack of expression of hERG1b.

Furthermore, as PDE inhibition with IBMX increases cAMP as well as cGMP levels, my results suggest that under my experimental conditions (perforated patch and physiologically relevant temperatures) cAMP levels also appear to have no effect on I_{Kr}. This is quite a controversial topic. Several studies have reported that cAMP-dependent signalling modulates I_{Kr}. Heath & Terrar, (2000) demonstrated that using the perforated patch-clamp or switch electrode voltage clamp with sharp electrodes technique, I_{Kr} recorded at $36^{o}C$ was enhanced by ISO and FSK in guinea pig ventricular myocytes. Whereas, ISO had no effect on I_{Kr} recorded using the ruptured patch-clamp technique. However, Harmati *et al.* (2011) found that I_{Kr} recorded at $37^{o}C$ using the ruptured patch-clamp technique, was enhanced by ISO, FSK and several PKA activator analogues in canine ventricular myocytes, with the ISO-enhancement of I_{Kr} being blocked by the PKA inhibitor Rp-8-Br-cAMP. In contrast, Cui *et al.* (2000) demonstrated that the cAMP analogue CPT-cAMP inhibited currents from hERG channels heterologously expressed in Chinese hamster ovary cells, recorded using the ruptured patch-clamp technique (temperature not stated). This effect was blocked when PKA was inhibited by PKI in the electrode.

In summary, my findings showed that I_{Kr} was not regulated by cGMP or cAMP signalling. In contrast, other studies have reported modulation of I_{Kr} by cyclic nucleotide signalling pathways. The reasons for the discrepancies in the

165

literature are not clear, but they could be species-dependent or relate to differences in recording conditions. All the available evidence points to the complexity of the intracellular signalling environment, which can easily be influenced by precisely how the experiment is performed. Factors such as buffering intracellular Ca^{2+} and dialysing cellular contents via the electrode are likely to have an impact. Temperature is also important since it influences reaction rates of kinases, phosphatases and PDEs.

6.8 Diurnal variation of ventricular action potentials and contractile shortening

AP and cell shortening responses to the β-adrenergic receptor agonist ISO, were studied in active and resting period myocytes, with a view as to whether the responses exhibited diurnal variation. Under basal conditions, there was no difference in APD between active and resting period myocytes. The application of ISO shortened APD in a concentration-dependent manner. However, APD shortening was greater in active compared to resting period myocytes. Cell shortening was measured in parallel with AP stimulation as an indication of contraction. Cell shortening amplitude increased and the time course accelerated in response to ISO, but there was no significant difference between active and resting period myocytes, despite APs displaying diurnal variation. Although not significant, a trend was observed. Active period myocytes shortened more than resting period myocytes in response to 3 and 10 nM ISO, although the trend was less obvious for 3 nM ISO. This suggests that diurnal variation exists in the responsiveness to β-adrenergic receptor stimulation, at least in terms of the AP.

β-adrenergic signalling and NO signalling are linked through the coupling of $β_3$-adrenergic receptors and eNOS (Saraiva & Hare, 2006) and by Ca^{2+}-CaM dependent regulation of NOS isoforms. Indeed, I detected a significant increase of cGMP levels in response to ISO stimulation. eNOS has been widely reported to attenuate contractility in response to β-adrenergic receptor stimulation (Barouch *et al.*, 2002; Massion *et al.*, 2004). To investigate if NOS was involved in the diurnal variation of APs and cell shortening, NOS was inhibited with L-

NNA. NOS inhibition failed to significantly modulate ISO-induced AP and cell shortening responses in both active and resting period myocytes, although trends were observed in the cell shortening responses. Although not significant, L-NNA typically caused a small but clear observable increase in cell shortening, which was slightly greater in resting compared to active period myocytes.

The sympathetic nervous system mediates the 'fight or flight' response, which leads to a multitude of physiological changes that prepare an organism for high levels of activity or alertness. Such physiological changes include, increases in heart rate and contractility. Stressful or dangerous encounters are more likely to occur during active rather than resting periods. Therefore it seems logical that physiological parameters would be more responsive to β-adrenergic receptor stimulation during active periods, which was the case for APD responses to ISO. Whereas, during resting periods these encounters are less likely. Although not specifically tested in my experiments, my hypothesis would be that β_3-adrenergic receptors signalling through NO-dependent pathways act to suppress responses to $\beta_{1/2}$-adrenergic receptor stimulation in resting period myocytes to more of an extent than active period myocytes. Zhou *et al.* (2011) found that in left ventricular rat tissue, mRNA and protein levels of β_3-adrenergic receptors displayed a distinct circadian rhythm over 24 hours. Expression was highest during the day (corresponding to the resting period since rats are nocturnal) and lowest during the night (active period). Stimulation of β_3-adrenergic receptors with BRL37344 decreased contractile force substantially during the resting period with minimal effects in the active period, providing evidence that β_3-adrenergic receptor signalling is higher during resting periods and lower during active periods.

My findings also correlate with research studying diurnal variation of the QT_c interval and the influence of the autonomic nervous system in human patients (Bexton *et al.*, 1986). The QT_c interval is shorter during active periods and longer during resting periods. This could be linked to diurnal variation of APD shortening in response to ISO. Furthermore, higher sympathetic nervous system activity occurs during active periods and higher parasympathetic

nervous system activity occurs during resting periods (Honda *et al.*, 2013). In contrast to my results, Shiotani *et al.* (2008) found that in young guinea pigs of a similar age and weight to those used in my experiments, QT_c intervals failed to exhibit diurnal variation and uncorrected QT intervals were shorter as opposed to longer during resting periods. NO signalling has been reported to play an important role in the parasympathetic nervous system, in terms of mediating the protective effects of vagus nerve stimulation against the induction of VF (Brack *et al.*, 2007). Thus, it is possible that NO may be a fundamental signalling molecule in the parasympathetic control of the heart. The precise cellular mechanisms have not yet been determined. Nevertheless, there is now a lot of evidence that an imbalance in the autonomic regulation of the heart and, in particular, the loss of vagal tone, is associated with an increased risk of arrhythmias (refer to reviews by Brack *et al.*, 2013; Zhao *et al.*, 2012).

6.9 The therapeutic potential of targeting nitric oxide signalling pathways in the heart

Since NO signalling and the QT interval have recently been linked through genetic variants in CAPON/NOS1AP (Arking *et al.*, 2006; Crotti *et al.*, 2009; Chang *et al.*, 2008), NO signalling could be a potential therapeutic target for LQTS, if the mechanistic basis for abnormalities in cardiac repolarisation can be determined. Another important therapeutic area is heart failure, which is characterised by excessive $\beta_{1/2}$-adrenergic receptor activity, and might be counteracted by up-regulating β_3-adrenergic receptor/eNOS coupled signalling (Barouch *et al.*, 2002; Massion *et al.*, 2004; Moens *et al.*, 2010).

BAY 58-2667, also known as cinaciguat, is a NO/haem-independent sGC activator that was developed for the treatment of acute heart failure. Current therapy requires improvement, as symptoms commonly remain and outcome is poor in terms of re-hospitalisation and mortality. Loop diuretics and intravenous nitrates are most widely used as treatment, but the latter is only administered in patients without low blood pressure. These drugs result in preferential venous dilation with modest effects on blood pressure. An ideal treatment would reduce

preload, decongest the heart, whilst maintaining cardiac output and having a minimal effect on blood pressure (Voors & van Veldhuisen, 2012). Lapp *et al.* (2009) found that BAY 58-2667 decreased pulmonary capillary wedge pressure (which reflects left atrial pressure), reduced preload and increased cardiac output, in a non-randomised, uncontrolled study on patients with acute heart failure. However hypotension was reported in a number of patients. The phase IIb COMPOSE programme consisted of three randomised, double-blind, placebo-controlled studies (Gheorghiade *et al.*, 2012). These studies aimed to assess the safety and efficacy of a lower dose of intravenous BAY 58-2667, for up to 48 hours, in acute heart failure patients. BAY 58-2667 was hypothesised to be suitable as an add-on to current treatments. In a small group of patients, BAY 58-2667 consistently reduced pulmonary capillary wedge pressure, which is believed to be the predominant mechanism by which symptoms and outcome are improved (Voors & van Veldhuisen, 2012). However, BAY 58-2667 failed to improve dyspnoea (shortness of breath) compared to placebo and decreased blood pressure, even at this lower dosage. Therefore, the beneficial effects were outweighed by the side-effects. Due to multiple cases of hypotension and recruitment difficulties, the study was terminated early. However, this study was criticised due to low dosage time and the suitability of pulmonary capillary wedge pressure and dyspnoea as well defined endpoints (Voors & van Veldhuisen, 2012). Another phase IIb study on acute heart failure patients, demonstrated similar findings, in terms of pulmonary capillary wedge pressure reduction and adverse hypotension (Erdmann *et al.*, 2013). Overall, clinical studies have found that intravenous BAY 58-2667 is not a suitable treatment for acute heart failure as it is not advantageous over current treatments. As BAY 60-2770 has similar properties, it seems unlikely that it would be a suitable intravenous treatment either. However, NO/haem-independent sGC activators may have potential as an oral treatment for acute heart failure.

With regard to the link recently established between LQTS and a common generic variant in the NOS1AP gene that encodes CAPON, a NOS1 adaptor protein (Arking *et al.*, 2006; Crotti *et al.*, 2009; Chang *et al.*, 2008), modulation of NO signalling may have the potential to treat LQTS. Current LQTS therapies include β-adrenergic receptor blockade, left cardiac sympathetic denervation

and the implantable cardioverter-defibrillator. In addition, lifestyle changes can help to manage the condition more effectively. β-adrenergic receptor blockade with propranolol and nadolol is the most widely used therapy for LQTS. The use of β-blockers is a highly effective therapy for LQT1 patients, and has been reported to reduce the risk of cardiac events considerably (Vincent *et al.*, 2009). In contrast, β-blockers appear to be less effective at decreasing the number or severity of cardiac events for LQT2 and 3 patients (Schwartz & Ackerman, 2013). NO signalling is known to modulate β-adrenergic receptor signalling and may therefore be a target for therapeutic agents aimed at treating LQTS. Furthermore, LQT1 which is treated most effectively by β-blockers, is characterised by I_{Ks} channel mutations and my results have shown that I_{Ks} was modulated by cGMP-dependent signalling, but only when PDEs were inhibited.

An alternative therapy is the implantation of a cardioverter-defibrillator. Implantation is recommended in patients who have suffered a cardiac arrest. However, many patients with implanted cardioverter-defibrillators have not suffered cardiac arrest or failure of β-blocker therapy (Schwartz *et al.*, 2010). Another therapy for LQTS is left cardiac sympathetic denervation, which involves removal of the first four thoracic ganglia, resulting in an anti-fibrillatory effect (Schwartz *et al.*, 1976). This procedure is recommended for LQTS patients who have had cardiac events despite β-blocker therapy or are unable to tolerate β-blockers. A study by Schwartz *et al.* (2004) reported a 91% decrease in the risk of cardiac events following left cardiac sympathetic denervation, in a group of high risk LQTS patients. Lifestyle changes can also help to manage LQTS, such as avoiding intense exercise and being woken by sudden noises, which is known to trigger cardiac events due to an increase in the activity of the sympathetic nervous system (Schwartz & Ackerman, 2013). Similar to left cardiac sympathetic denervation, vagus nerve stimulation has been shown to have an anti-fibrillatory effect which is NO-dependent (Brack *et al.*, 2007). There are a number of clinical trials, INOVATE-HF and NECTAR-HF, that are stimulating vagus input into the heart to determine if this improves outcome in heart failure patients (Hauptman *et al.*, 2012; Zannad *et al.*, 2014). Vagus nerve stimulators could also be used to potentially reduce episodes in patients with persistent arrhythmias. Clearly, understanding the cellular

mechanisms that induce the protective effect of vagus nerve stimulation would help in trying to identify a better therapy.

6.10 Conclusions

NO signalling pathways may be able to regulate ventricular repolarisation through a cGMP-dependent mechanism, but PDEs act to limit these responses by compartmentalising cyclic nucleotide signalling in the healthy myocardium. The subcellular location of changes in cGMP appears to be a defining factor, as opposed to the relative increase in cGMP, as substantial increases in cGMP with the NO donor SNAP, failed to modulate ventricular repolarisation. In contrast, the novel NO/haem-independent sGC activator BAY 60-2770, inhibited I_{Ks}, but only when PDEs were inhibited. This indicates that I_{Ks} channels and cGMP-dependent signalling are not in the same signalling compartment. The mechanism for inhibition of I_{Ks} requires further investigation, as it did not involve PKG. In contrast to I_{Ks}, I_{Kr} was not regulated by cGMP- or cAMP-dependent signalling. Furthermore, ventricular repolarisation exhibited diurnal variation in response to ISO. A greater shortening of APD was found in active compared to resting period myocytes. However, this effect was not blocked by NOS inhibition, suggesting NO signalling does not mediate this effect. In conclusion, based on the literature and these findings, NO signalling may be a potential therapeutic target for diseases such as LQTS. However, further research is necessary, to fully elucidate the regulation of ventricular repolarisation by cGMP-dependent NO signalling.

6.11 Future work

To further investigate the mechanisms underlying the regulation of repolarisation by cGMP-dependent NO signalling in guinea pig isolated left ventricular myocytes, I would conduct the following experiments:

- Investigate whether prior application of ODQ potentiates the effect of BAY 60-2770 on APD.

- Investigate whether PDEs suppress the effect of ODQ + BAY 60-2770 on APD by prior application of the non-selective PDE inhibitor IBMX.

- Further investigate whether PKG mediates the inhibition of I_{Ks} in response to BAY 60-2770 by using other PKG inhibitors, such as DT-2.

- Investigate whether any protein kinases mediate the inhibition of I_{Ks} in response to BAY 60-2770 by using staurosporine, a non-selective protein kinase inhibitor.

- Investigate whether phosphatases mediate the inhibition of I_{Ks} in response to BAY 60-2770 by using protein phosphatase inhibitors, such as okadaic acid.

- Investigate the PDEs responsible for compartmentalisation of BAY-60-2770 -dependent signalling by using silencing RNAs to selectively suppress the gene expression of specific PDE isoforms.

Chapter 7

Bibliography

Aarnoudse, A.J., Newton-Cheh, C., de Bakker, P.I., Straus, S.M., Kors, J.A., Hofman, A., Uitterlinden, A.G., Witteman, J.C., Stricker, B.H., 2007. Common NOS1AP variants are associated with a prolonged QTc interval in the Rotterdam Study. *Circulation.* **116,** 10-16.

Abbott, G.W., 2012. KCNE2 and the K (+) channel: the tail wagging the dog. *Channels (Austin, Tex.).* **6,** 1-10.

Abbott, G.W., Sesti, F., Splawski, I., Buck, M.E., Lehmann, M.H., Timothy, K.W., Keating, M.T., Goldstein, S.A., 1999. MiRP1 forms IKr potassium channels with HERG and is associated with cardiac arrhythmia. *Cell.* **97,** 175-187.

Abi-Gerges, N., Fischmeister, R., Mery, P.F., 2001. G protein-mediated inhibitory effect of a nitric oxide donor on the L-type Ca2+ current in rat ventricular myocytes. *The Journal of Physiology.* **531,** 117-130.

Abi-Gerges, N., Hove-Madsen, L., Fischmeister, R., Mery, P.F., 1997. A comparative study of the effects of three guanylyl cyclase inhibitors on the L-type Ca2+ and muscarinic K+ currents in frog cardiac myocytes. *British Journal of Pharmacology.* **121,** 1369-1377.

Abi-Gerges, N., Szabo, G., Otero, A.S., Fischmeister, R., Mery, P.F., 2002. NO donors potentiate the beta-adrenergic stimulation of I(Ca,L) and the muscarinic activation of I(K,ACh) in rat cardiac myocytes. *The Journal of Physiology.* **540,** 411-424.

Abramochkin, D.V., Makarenko, E.Y., Mitrochin, V.M., Tian, B., Kalugin, L.Y., Sutyagin, P.V., Kamkin, A.G., 2012. Effect of nitric oxide on mechanoelectric feedback in rat right atrium. *Bulletin of Experimental Biology and Medicine.* **153,** 32-35.

Ahern, G.P., Hsu, S.F., Klyachko, V.A., Jackson, M.B., 2000. Induction of persistent sodium current by exogenous and endogenous nitric oxide. *The Journal of Biological Chemistry.* **275,** 28810-28815.

Ahmmed, G.U., Xu, Y., Hong Dong, P., Zhang, Z., Eiserich, J., Chiamvimonvat, N., 2001. Nitric oxide modulates cardiac Na(+) channel via protein kinase A and protein kinase G. *Circulation Research.* **89,** 1005-1013.

Akar, F.G., Wu, R.C., Deschenes, I., Armoundas, A.A., Piacentino, V.,3rd, Houser, S.R., Tomaselli, G.F., 2004. Phenotypic differences in transient outward K+ current of human and canine ventricular myocytes: insights into molecular composition of ventricular Ito. *American Journal of Physiology.Heart and Circulatory Physiology.* **286,** H602-9.

Al-Sa'doni, H. & Ferro, A., 2000. S-Nitrosothiols: a class of nitric oxide-donor drugs. *Clinical Science (London, England : 1979).* **98,** 507-520.

Andreopoulos, S. & Papapetropoulos, A., 2000. Molecular aspects of soluble guanylyl cyclase regulation. *General Pharmacology.* **34,** 147-157.

Archer, S.L., Huang, J.M., Hampl, V., Nelson, D.P., Shultz, P.J., Weir, E.K., 1994. Nitric oxide and cGMP cause vasorelaxation by activation of a charybdotoxin-sensitive K channel by cGMP-dependent protein kinase. *Proceedings of the National Academy of Sciences of the United States of America.* **91,** 7583-7587.

Arking, D.E., Pfeufer, A., Post, W., Kao, W.H., Newton-Cheh, C., Ikeda, M., West, K., Kashuk, C., Akyol, M., Perz, S., Jalilzadeh, S., Illig, T., Gieger, C., Guo, C.Y., Larson, M.G., Wichmann, H.E., Marban, E., O'Donnell, C.J., Hirschhorn, J.N., Kaab, S., Spooner, P.M., Meitinger, T., Chakravarti, A., 2006. A common genetic variant in the NOS1 regulator NOS1AP modulates cardiac repolarization. *Nature Genetics.* **38,** 644-651.

Arnold, W.P., Mittal, C.K., Katsuki, S., Murad, F., 1977. Nitric oxide activates guanylate cyclase and increases guanosine 3':5'-cyclic monophosphate levels in various tissue preparations. *Proceedings of the National Academy of Sciences of the United States of America.* **74,** 3203-3207.

Arstall, M.A., Sawyer, D.B., Fukazawa, R., Kelly, R.A., 1999. Cytokine-mediated apoptosis in cardiac myocytes: the role of inducible nitric oxide synthase induction and peroxynitrite generation. *Circulation Research.* **85,** 829-840.

Asada, K., Kurokawa, J., Furukawa, T., 2009. Redox- and calmodulin-dependent S-nitrosylation of the KCNQ1 channel. *The Journal of Biological Chemistry.* **284,** 6014-6020.

Axon Instruments, I., 1999. Axopatch 200B Patch Clamp Theory and Operation. Axon Instruments, Inc.

Bai, C.X., Namekata, I., Kurokawa, J., Tanaka, H., Shigenobu, K., Furukawa, T., 2005. Role of nitric oxide in Ca2+ sensitivity of the slowly activating delayed rectifier K+ current in cardiac myocytes. *Circulation Research.* **96,** 64-72.

Bai, C.X., Takahashi, K., Masumiya, H., Sawanobori, T., Furukawa, T., 2004. Nitric oxide-dependent modulation of the delayed rectifier K+ current and the L-type Ca2+ current by ginsenoside Re, an ingredient of Panax ginseng, in guinea-pig cardiomyocytes. *British Journal of Pharmacology.* **142,** 567-575.

Bain, J., McLauchlan, H., Elliott, M., Cohen, P., 2003. The specificities of protein kinase inhibitors: an update. *The Biochemical Journal.* **371,** 199-204.

Barhanin, J., Lesage, F., Guillemare, E., Fink, M., Lazdunski, M., Romey, G., 1996. K(V)LQT1 and lsK (minK) proteins associate to form the I(Ks) cardiac potassium current. *Nature.* **384,** 78-80.

Barouch, L.A., Harrison, R.W., Skaf, M.W., Rosas, G.O., Cappola, T.P., Kobeissi, Z.A., Hobai, I.A., Lemmon, C.A., Burnett, A.L., O'Rourke, B., Rodriguez, E.R., Huang, P.L., Lima, J.A., Berkowitz, D.E., Hare, J.M., 2002. Nitric oxide regulates the heart by spatial confinement of nitric oxide synthase isoforms. *Nature.* **416,** 337-339.

Bayraktutan, U., Yang, Z.K., Shah, A.M., 1998. Selective dysregulation of nitric oxide synthase type 3 in cardiac myocytes but not coronary microvascular endothelial cells of spontaneously hypertensive rat. *Cardiovascular Research.* **38,** 719-726.

Bellamy, T.C. & Garthwaite, J., 2002. The receptor-like properties of nitric oxide-activated soluble guanylyl cyclase in intact cells. *Molecular and Cellular Biochemistry.* **230,** 165-176.

Bendall, J.K., Damy, T., Ratajczak, P., Loyer, X., Monceau, V., Marty, I., Milliez, P., Robidel, E., Marotte, F., Samuel, J.L., Heymes, C., 2004. Role of myocardial neuronal nitric oxide synthase-derived nitric oxide in beta-adrenergic hyporesponsiveness after myocardial infarction-induced heart failure in rat. *Circulation.* **110,** 2368-2375.

Bender, A.T. & Beavo, J.A., 2006. Cyclic nucleotide phosphodiesterases: molecular regulation to clinical use. *Pharmacological Reviews.* **58,** 488-520.

Bennett, P.B., Yazawa, K., Makita, N., George, A.L.,Jr, 1995. Molecular mechanism for an inherited cardiac arrhythmia. *Nature.* **376,** 683-685.

Bers, D.M., 2002. Cardiac excitation-contraction coupling. *Nature.* **415,** 198-205.

Best, J.M. & Kamp, T.J., 2012. Different subcellular populations of L-type Ca2+ channels exhibit unique regulation and functional roles in cardiomyocytes. *Journal of Molecular and Cellular Cardiology.* **52,** 376-387.

Bexton, R.S., Vallin, H.O., Camm, A.J., 1986. Diurnal variation of the QT interval--influence of the autonomic nervous system. *British Heart Journal.* **55,** 253-258.

Bice, J.S., Keim, Y., Stasch, J.P., Baxter, G.F., 2014. NO-independent stimulation or activation of soluble guanylyl cyclase during early reperfusion limits infarct size. *Cardiovascular Research.* **101,** 220-228.

Brack, K.E., Patel, V.H., Coote, J.H., Ng, G.A., 2007. Nitric oxide mediates the vagal protective effect on ventricular fibrillation via effects on action potential duration restitution in the rabbit heart. *The Journal of Physiology.* **583,** 695-704.

Brack, K.E., Patel, V.H., Mantravardi, R., Coote, J.H., Ng, G.A., 2009. Direct evidence of nitric oxide release from neuronal nitric oxide synthase activation in the left ventricle as a result of cervical vagus nerve stimulation. *The Journal of Physiology.* **587,** 3045-3054.

Brack, K.E., Winter, J., Ng, G.A., 2013. Mechanisms underlying the autonomic modulation of ventricular fibrillation initiation--tentative prophylactic properties of vagus nerve stimulation on malignant arrhythmias in heart failure. *Heart Failure Reviews.* **18,** 389-408.

Brahmajothi, M.V. & Campbell, D.L., 1999. Heterogeneous basal expression of nitric oxide synthase and superoxide dismutase isoforms in mammalian heart : implications for mechanisms governing indirect and direct nitric oxide-related effects. *Circulation Research.* **85,** 575-587.

Brahmajothi, M.V., Campbell, D.L., Rasmusson, R.L., Morales, M.J., Trimmer, J.S., Nerbonne, J.M., Strauss, H.C., 1999. Distinct transient outward potassium current (Ito) phenotypes and distribution of fast-inactivating potassium channel alpha subunits in ferret left ventricular myocytes. *The Journal of General Physiology.* **113,** 581-600.

Budworth, J., Meillerais, S., Charles, I., Powell, K., 1999. Tissue distribution of the human soluble guanylate cyclases. *Biochemical and Biophysical Research Communications.* **263,** 696-701.

Burkhardt, M., Glazova, M., Gambaryan, S., Vollkommer, T., Butt, E., Bader, B., Heermeier, K., Lincoln, T.M., Walter, U., Palmetshofer, A., 2000. KT5823 inhibits cGMP-dependent protein kinase activity in vitro but not in intact human platelets and rat mesangial cells. *The Journal of Biological Chemistry.* **275,** 33536-33541.

Buys, E.S., Raher, M.J., Blake, S.L., Neilan, T.G., Graveline, A.R., Passeri, J.J., Llano, M., Perez-Sanz, T.M., Ichinose, F., Janssens, S., Zapol, W.M., Picard, M.H., Bloch, K.D., Scherrer-Crosbie, M., 2007. Cardiomyocyte-restricted restoration of nitric oxide synthase 3 attenuates left ventricular remodeling after chronic pressure overload. *American Journal of Physiology.Heart and Circulatory Physiology.* **293,** H620-7.

Cameron, J.S., Hoffmann, K.E., Zia, C., Hemmett, H.M., Kronsteiner, A., Lee, C.M., 2003. A role for nitric oxide in hypoxia-induced activation of cardiac KATP channels in goldfish (Carassius auratus). *The Journal of Experimental Biology.* **206,** 4057-4065.

Campbell, D.L., Stamler, J.S., Strauss, H.C., 1996. Redox modulation of L-type calcium channels in ferret ventricular myocytes. Dual mechanism regulation by nitric oxide and S-nitrosothiols. *The Journal of General Physiology.* **108,** 277-293.

Castro, L.R., Schittl, J., Fischmeister, R., 2010. Feedback control through cGMP-dependent protein kinase contributes to differential regulation and compartmentation of cGMP in rat cardiac myocytes. *Circulation Research.* **107,** 1232-1240.

Castro, L.R., Verde, I., Cooper, D.M., Fischmeister, R., 2006. Cyclic guanosine monophosphate compartmentation in rat cardiac myocytes. *Circulation.* **113,** 2221-2228.

Catterall, W.A., Perez-Reyes, E., Snutch, T.P., Striessnig, J., 2005. International Union of Pharmacology. XLVIII. Nomenclature and structure-function relationships of voltage-gated calcium channels. *Pharmacological Reviews.* **57,** 411-425.

Cawley, S.M., Kolodziej, S., Ichinose, F., Brouckaert, P., Buys, E.S., Bloch, K.D., 2011. sGC{alpha}1 mediates the negative inotropic effects of NO in cardiac myocytes independent of changes in calcium handling. *American Journal of Physiology.Heart and Circulatory Physiology.* **301,** H157-63.

Chang, K.C., Barth, A.S., Sasano, T., Kizana, E., Kashiwakura, Y., Zhang, Y., Foster, D.B., Marban, E., 2008. CAPON modulates cardiac repolarization via neuronal nitric oxide synthase signaling in the heart. *Proceedings of the National Academy of Sciences of the United States of America.* **105,** 4477-4482.

Cho, H.S., Takano, M., Noma, A., 2003. The electrophysiological properties of spontaneously beating pacemaker cells isolated from mouse sinoatrial node. *The Journal of Physiology.* **550,** 169-180.

Collins, H.E. & Rodrigo, G.C., 2010. Inotropic response of cardiac ventricular myocytes to beta-adrenergic stimulation with isoproterenol exhibits diurnal variation: involvement of nitric oxide. *Circulation Research.* **106,** 1244-1252.

Corbin, J.D., Turko, I.V., Beasley, A., Francis, S.H., 2000. Phosphorylation of phosphodiesterase-5 by cyclic nucleotide-dependent protein kinase alters its catalytic and allosteric cGMP-binding activities. *European Journal of Biochemistry / FEBS.* **267,** 2760-2767.

Cornwell, T.L., Arnold, E., Boerth, N.J., Lincoln, T.M., 1994. Inhibition of smooth muscle cell growth by nitric oxide and activation of cAMP-dependent protein kinase by cGMP. *The American Journal of Physiology.* **267,** C1405-13.

Crotti, L., Monti, M.C., Insolia, R., Peljto, A., Goosen, A., Brink, P.A., Greenberg, D.A., Schwartz, P.J., George, A.L.,Jr, 2009. NOS1AP is a genetic modifier of the long-QT syndrome. *Circulation.* **120,** 1657-1663.

Cui, J., Melman, Y., Palma, E., Fishman, G.I., McDonald, T.V., 2000. Cyclic AMP regulates the HERG K(+) channel by dual pathways. *Current Biology : CB.* **10,** 671-674.

Curran, M.E., Splawski, I., Timothy, K.W., Vincent, G.M., Green, E.D., Keating, M.T., 1995. A molecular basis for cardiac arrhythmia: HERG mutations cause long QT syndrome. *Cell.* **80,** 795-803.

Damy, T., Ratajczak, P., Robidel, E., Bendall, J.K., Oliviero, P., Boczkowski, J., Ebrahimian, T., Marotte, F., Samuel, J.L., Heymes, C., 2003. Up-regulation of cardiac nitric oxide synthase 1-derived nitric oxide after myocardial infarction in senescent rats. *FASEB Journal : Official Publication of the Federation of American Societies for Experimental Biology.* **17,** 1934-1936.

Damy, T., Ratajczak, P., Shah, A.M., Camors, E., Marty, I., Hasenfuss, G., Marotte, F., Samuel, J.L., Heymes, C., 2004. Increased neuronal nitric oxide synthase-derived NO production in the failing human heart. *Lancet.* **363,** 1365-1367.

de Belder, A.J., MacAllister, R., Radomski, M.W., Moncada, S., Vallance, P.J., 1994. Effects of S-nitroso-glutathione in the human forearm circulation: evidence for selective inhibition of platelet activation. *Cardiovascular Research.* **28,** 691-694.

Decher, N., Uyguner, O., Scherer, C.R., Karaman, B., Yuksel-Apak, M., Busch, A.E., Steinmeyer, K., Wollnik, B., 2001. hKChIP2 is a functional modifier of hKv4.3 potassium channels: cloning and expression of a short hKChIP2 splice variant. *Cardiovascular Research.* **52,** 255-264.

Draijer, R., Vaandrager, A.B., Nolte, C., de Jonge, H.R., Walter, U., van Hinsbergh, V.W., 1995. Expression of cGMP-dependent protein kinase I and phosphorylation of its substrate, vasodilator-stimulated phosphoprotein, in human endothelial cells of different origin. *Circulation Research.* **77,** 897-905.

Drexler, H., Kastner, S., Strobel, A., Studer, R., Brodde, O.E., Hasenfuss, G., 1998. Expression, activity and functional significance of inducible nitric oxide synthase in the failing human heart. *Journal of the American College of Cardiology.* **32,** 955-963.

Du, X.L., Lau, C.P., Chiu, S.W., Tse, H.F., Gerlach, U., Li, G.R., 2003. Effects of chromanol 293B on transient outward and ultra-rapid delayed rectifier potassium currents in human atrial myocytes. *Journal of Molecular and Cellular Cardiology.* **35,** 293-300.

Ebihara, Y. & Karmazyn, M., 1996. Inhibition of beta- but not alpha 1-mediated adrenergic responses in isolated hearts and cardiomyocytes by nitric oxide and 8-bromo cyclic GMP. *Cardiovascular Research.* **32,** 622-629.

Eijgelsheim, M., Newton-Cheh, C., Aarnoudse, A.L., van Noord, C., Witteman, J.C., Hofman, A., Uiterlinden, A.G., Stricker, B.H., 2009. Genetic variation in NOS1AP is associated with sudden cardiac death: evidence from the Rotterdam Study. *Human Molecular Genetics.* **18,** 4213-4218.

Eldstrom, J. & Fedida, D., 2011. The voltage-gated channel accessory protein KCNE2: multiple ion channel partners, multiple ways to long QT syndrome. *Expert Reviews in Molecular Medicine.* **13,** e38.

Erdmann, E., Semigran, M.J., Nieminen, M.S., Gheorghiade, M., Agrawal, R., Mitrovic, V., Mebazaa, A., 2013. Cinaciguat, a soluble guanylate cyclase activator, unloads the heart but also causes hypotension in acute decompensated heart failure. *European Heart Journal.* **34,** 57-67.

Evgenov, O.V., Pacher, P., Schmidt, P.M., Hasko, G., Schmidt, H.H., Stasch, J.P., 2006. NO-independent stimulators and activators of soluble guanylate cyclase: discovery and therapeutic potential. *Nature Reviews.Drug Discovery.* **5,** 755-768.

Fakler, B., Brandle, U., Glowatzki, E., Weidemann, S., Zenner, H.P., Ruppersberg, J.P., 1995. Strong voltage-dependent inward rectification of inward rectifier K+ channels is caused by intracellular spermine. *Cell.* **80,** 149-154.

Feng, J., Wible, B., Li, G.R., Wang, Z., Nattel, S., 1997. Antisense oligodeoxynucleotides directed against Kv1.5 mRNA specifically inhibit ultrarapid delayed rectifier K+ current in cultured adult human atrial myocytes. *Circulation Research.* **80,** 572-579.

Feng, Q., Lu, X., Jones, D.L., Shen, J., Arnold, J.M., 2001. Increased inducible nitric oxide synthase expression contributes to myocardial dysfunction and higher mortality after myocardial infarction in mice. *Circulation.* **104,** 700-704.

Feron, O., Belhassen, L., Kobzik, L., Smith, T.W., Kelly, R.A., Michel, T., 1996. Endothelial nitric oxide synthase targeting to caveolae. Specific interactions with caveolin isoforms in cardiac myocytes and endothelial cells. *The Journal of Biological Chemistry.* **271,** 22810-22814.

Ficker, E., Taglialatela, M., Wible, B.A., Henley, C.M., Brown, A.M., 1994. Spermine and spermidine as gating molecules for inward rectifier K+ channels. *Science (New York, N.Y.).* **266,** 1068-1072.

Fiorucci, S., Mencarelli, A., Meneguzzi, A., Lechi, A., Renga, B., del Soldato, P., Morelli, A., Minuz, P., 2004. Co-administration of nitric oxide-aspirin (NCX-4016) and aspirin prevents platelet and monocyte activation and protects against gastric damage induced by aspirin in humans. *Journal of the American College of Cardiology.* **44,** 635-641.

Fischmeister, R., Castro, L., Abi-Gerges, A., Rochais, F., Vandecasteele, G., 2005. Species- and tissue-dependent effects of NO and cyclic GMP on cardiac ion channels. *Comparative Biochemistry and Physiology.Part A, Molecular & Integrative Physiology.* **142,** 136-143.

Fischmeister, R., Castro, L.R., Abi-Gerges, A., Rochais, F., Jurevicius, J., Leroy, J., Vandecasteele, G., 2006. Compartmentation of cyclic nucleotide signaling in the heart: the role of cyclic nucleotide phosphodiesterases. *Circulation Research.* **99,** 816-828.

Fisher, D.A., Smith, J.F., Pillar, J.S., St Denis, S.H., Cheng, J.B., 1998. Isolation and characterization of PDE9A, a novel human cGMP-specific phosphodiesterase. *The Journal of Biological Chemistry.* **273,** 15559-15564.

Francis, S.H., Busch, J.L., Corbin, J.D., Sibley, D., 2010. cGMP-dependent protein kinases and cGMP phosphodiesterases in nitric oxide and cGMP action. *Pharmacological Reviews.* **62,** 525-563.

Franz, M.R., 2003. The electrical restitution curve revisited: steep or flat slope--which is better? *Journal of Cardiovascular Electrophysiology.* **14,** S140-7.

Fritz, B.G., Hu, X., Brailey, J.L., Berry, R.E., Walker, F.A., Montfort, W.R., 2011. Oxidation and loss of heme in soluble guanylyl cyclase from Manduca sexta. *Biochemistry.* **50,** 5813-5815.

Gaborit, N., Le Bouter, S., Szuts, V., Varro, A., Escande, D., Nattel, S., Demolombe, S., 2007. Regional and tissue specific transcript signatures of ion channel genes in the non-diseased human heart. *The Journal of Physiology.* **582,** 675-693.

Gallo, M.P., Ghigo, D., Bosia, A., Alloatti, G., Costamagna, C., Penna, C., Levi, R.C., 1998. Modulation of guinea-pig cardiac L-type calcium current by nitric oxide synthase inhibitors. *The Journal of Physiology.* **506 (Pt 3),** 639-651.

Gallo, M.P., Malan, D., Bedendi, I., Biasin, C., Alloatti, G., Levi, R.C., 2001. Regulation of cardiac calcium current by NO and cGMP-modulating agents. *Pflugers Archiv : European Journal of Physiology.* **441,** 621-628.

Gambaryan, S., Butt, E., Kobsar, A., Geiger, J., Rukoyatkina, N., Parnova, R., Nikolaev, V.O., Walter, U., 2012. The oligopeptide DT-2 is a specific PKG I inhibitor only in vitro, not in living cells. *British Journal of Pharmacology.* **167,** 826-838.

Gauthier, C., Tavernier, G., Charpentier, F., Langin, D., Le Marec, H., 1996. Functional beta3-adrenoceptor in the human heart. *The Journal of Clinical Investigation.* **98,** 556-562.

Gheorghiade, M., Greene, S.J., Filippatos, G., Erdmann, E., Ferrari, R., Levy, P.D., Maggioni, A., Nowack, C., Mebazaa, A., COMPOSE Investigators and Coordinators, 2012. Cinaciguat, a soluble guanylate cyclase activator: results from the randomized, controlled, phase IIb COMPOSE programme in acute heart failure syndromes. *European Journal of Heart Failure.* **14,** 1056-1066.

Giles, W.R. & Imaizumi, Y., 1988. Comparison of potassium currents in rabbit atrial and ventricular cells. *The Journal of Physiology.* **405,** 123-145.

Gomez, R., Caballero, R., Barana, A., Amoros, I., Calvo, E., Lopez, J.A., Klein, H., Vaquero, M., Osuna, L., Atienza, F., Almendral, J., Pinto, A., Tamargo, J., Delpon, E., 2009. Nitric oxide increases cardiac IK1 by nitrosylation of cysteine 76 of Kir2.1 channels. *Circulation Research.* **105,** 383-392.

Gomez, R., Nunez, L., Vaquero, M., Amoros, I., Barana, A., de Prada, T., Macaya, C., Maroto, L., Rodriguez, E., Caballero, R., Lopez-Farre, A., Tamargo, J., Delpon, E., 2008. Nitric oxide inhibits Kv4.3 and human cardiac transient outward potassium current (Ito1). *Cardiovascular Research.* **80,** 375-384.

Gonzalez, D.R., Beigi, F., Treuer, A.V., Hare, J.M., 2007. Deficient ryanodine receptor S-nitrosylation increases sarcoplasmic reticulum calcium leak and arrhythmogenesis in cardiomyocytes. *Proceedings of the National Academy of Sciences of the United States of America.* **104,** 20612-20617.

Gonzalez, D.R., Treuer, A., Sun, Q.A., Stamler, J.S., Hare, J.M., 2009. S-Nitrosylation of cardiac ion channels. *Journal of Cardiovascular Pharmacology.* **54,** 188-195.

Grossi, L. & D'Angelo, S., 2005. Sodium nitroprusside: mechanism of NO release mediated by sulfhydryl-containing molecules. *Journal of Medicinal Chemistry.* **48,** 2622-2626.

Grushin, K.S., Nenov, M.N., Dynnik, V.V., Semushina, S.G., Pakhomova, I.A., Murashev, A.N., Kokoz, Y.M., 2008. Role of the NO–cGMP Cascade in Regulation of L-Type Ca^{2+} Currents in Isolated Cardiomyocytes. *Biochemistry (Moscow) Supplement Series A: Membrane and Cell Biology.* **2,** 243-252.

Guasti, L., Crociani, O., Redaelli, E., Pillozzi, S., Polvani, S., Masselli, M., Mello, T., Galli, A., Amedei, A., Wymore, R.S., Wanke, E., Arcangeli, A., 2008. Identification of a posttranslational mechanism for the regulation of hERG1 K+ channel expression and hERG1 current density in tumor cells. *Molecular and Cellular Biology.* **28,** 5043-5060.

Guazzi, M., Vicenzi, M., Arena, R., Guazzi, M.D., 2011. PDE5 inhibition with sildenafil improves left ventricular diastolic function, cardiac geometry, and clinical status in patients with stable systolic heart failure: results of a 1-year, prospective, randomized, placebo-controlled study. *Circulation.Heart Failure.* **4,** 8-17.

Hamad, A.M., Range, S., Holland, E., Knox, A.J., 1997. Regulation of cGMP by soluble and particulate guanylyl cyclases in cultured human airway smooth muscle. *The American Journal of Physiology.* **273,** L807-13.

Hammond, J. & Balligand, J.L., 2012. Nitric oxide synthase and cyclic GMP signaling in cardiac myocytes: from contractility to remodeling. *Journal of Molecular and Cellular Cardiology.* **52,** 330-340.

Hancox, J.C., Levi, A.J., Witchel, H.J., 1998. Time course and voltage dependence of expressed HERG current compared with native "rapid" delayed rectifier K current during the cardiac ventricular action potential. *Pflugers Archiv : European Journal of Physiology.* **436,** 843-853.

Harmati, G., Banyasz, T., Barandi, L., Szentandrassy, N., Horvath, B., Szabo, G., Szentmiklosi, J.A., Szenasi, G., Nanasi, P.P., Magyar, J., 2011. Effects of beta-adrenoceptor stimulation on delayed rectifier K(+) currents in canine ventricular cardiomyocytes. *British Journal of Pharmacology.* **162,** 890-896.

Harteneck, C., Koesling, D., Soling, A., Schultz, G., Bohme, E., 1990. Expression of soluble guanylyl cyclase. Catalytic activity requires two enzyme subunits. *FEBS Letters.* **272,** 221-223.

Harteneck, C., Wedel, B., Koesling, D., Malkewitz, J., Bohme, E., Schultz, G., 1991. Molecular cloning and expression of a new alpha-subunit of soluble guanylyl cyclase. Interchangeability of the alpha-subunits of the enzyme. *FEBS Letters.* **292,** 217-222.

Hauptman, P.J., Schwartz, P.J., Gold, M.R., Borggrefe, M., Van Veldhuisen, D.J., Starling, R.C., Mann, D.L., 2012. Rationale and study design of the increase of vagal tone in heart failure study: INOVATE-HF. *American Heart Journal.* **163,** 954-962.e1.

Hausdorff, S.F., Goldstein, S.A., Rushin, E.E., Miller, C., 1991. Functional characterization of a minimal K+ channel expressed from a synthetic gene. *Biochemistry.* **30,** 3341-3346.

Heath, B.M. & Terrar, D.A., 2000. Protein kinase C enhances the rapidly activating delayed rectifier potassium current, IKr, through a reduction in C-type inactivation in guinea-pig ventricular myocytes. *The Journal of Physiology.* **522 Pt 3,** 391-402.

Heath, B.M. & Terrar, D.A., 1996. Separation of the components of the delayed rectifier potassium current using selective blockers of IKr and IKs in guinea-pig isolated ventricular myocytes. *Experimental Physiology.* **81,** 587-603.

Herring, N., Golding, S., Paterson, D.J., 2000. Pre-synaptic NO-cGMP pathway modulates vagal control of heart rate in isolated adult guinea pig atria. *Journal of Molecular and Cellular Cardiology.* **32,** 1795-1804.

Hibino, H., Inanobe, A., Furutani, K., Murakami, S., Findlay, I., Kurachi, Y., 2010. Inwardly rectifying potassium channels: their structure, function, and physiological roles. *Physiological Reviews.* **90,** 291-366.

Hidaka, H. & Kobayashi, R., 1992. Pharmacology of protein kinase inhibitors. *Annual Review of Pharmacology and Toxicology.* **32,** 377-397.

Hoffmann, A., Gloe, T., Pohl, U., Zahler, S., 2003. Nitric oxide enhances de novo formation of endothelial gap junctions. *Cardiovascular Research.* **60,** 421-430.

Hohnloser, S.H., Zabel, M., Just, H., Raeder, E.A., 1993. Relation of diurnal variation of ventricular repolarization to ventricular ectopic activity and modification by sotalol. *The American Journal of Cardiology.* **71,** 475-478.

Honda, M., Komatsu, R., Isobe, T., Tabo, M., Ishikawa, T., 2013. Involvement of the autonomic nervous system in diurnal variation of corrected QT intervals in common marmosets. *Journal of Pharmacological Sciences.* **121,** 131-137.

Honore, E., Attali, B., Romey, G., Heurteaux, C., Ricard, P., Lesage, F., Lazdunski, M., Barhanin, J., 1991. Cloning, expression, pharmacology and regulation of a delayed rectifier K+ channel in mouse heart. *The EMBO Journal.* **10,** 2805-2811.

Huai, Q., Liu, Y., Francis, S.H., Corbin, J.D., Ke, H., 2004. Crystal structures of phosphodiesterases 4 and 5 in complex with inhibitor 3-isobutyl-1-methylxanthine suggest a conformation determinant of inhibitor selectivity. *The Journal of Biological Chemistry.* **279,** 13095-13101.

Iachini Bellisarii, F., Radico, F., Muscente, F., Horowitz, J., De Caterina, R., 2012. Nitrates and other nitric oxide donors in cardiology: current positioning and perspectives. *Cardiovascular Drugs and Therapy / Sponsored by the International Society of Cardiovascular Pharmacotherapy.* **26,** 55-69.

Imai, Y., Jiang, B., Pappano, A.J., 2001. Mechanism for muscarinic inhibition of I(Ca(L)) is determined by the path for elevating cyclic AMP in cardiac myocytes. *Cardiovascular Research.* **51,** 331-343.

Imoto, Y., Ehara, T., Matsuura, H., 1987. Voltage- and time-dependent block of iK1 underlying Ba2+-induced ventricular automaticity. *The American Journal of Physiology.* **252,** H325-33.

IONA Study Group, 2002. Effect of nicorandil on coronary events in patients with stable angina: the Impact Of Nicorandil in Angina (IONA) randomised trial. *Lancet.* **359,** 1269-1275.

Irisawa, H., Brown, H.F., Giles, W., 1993. Cardiac pacemaking in the sinoatrial node. *Physiological Reviews.* **73,** 197-227.

Jansen, J.A., van Veen, T.A., de Bakker, J.M., van Rijen, H.V., 2010. Cardiac connexins and impulse propagation. *Journal of Molecular and Cellular Cardiology.* **48,** 76-82.

Jarchau, T., Hausler, C., Markert, T., Pohler, D., Vanderkerckhove, J., De Jonge, H.R., Lohmann, S.M., Walter, U., 1994. Cloning, expression, and in situ localization of rat intestinal cGMP-dependent protein kinase II. *Proceedings of the National Academy of Sciences of the United States of America.* **91,** 9426-9430.

Jeyaraj, D., Haldar, S.M., Wan, X., McCauley, M.D., Ripperger, J.A., Hu, K., Lu, Y., Eapen, B.L., Sharma, N., Ficker, E., Cutler, M.J., Gulick, J., Sanbe, A., Robbins, J., Demolombe, S., Kondratov, R.V., Shea, S.A., Albrecht, U., Wehrens, X.H., Rosenbaum, D.S., Jain, M.K., 2012. Circadian rhythms govern cardiac repolarization and arrhythmogenesis. *Nature.* **483,** 96-99.

Jiang, M., Xu, X., Wang, Y., Toyoda, F., Liu, X.S., Zhang, M., Robinson, R.B., Tseng, G.N., 2009. Dynamic partnership between KCNQ1 and KCNE1 and influence on cardiac IKs current amplitude by KCNE2. *The Journal of Biological Chemistry.* **284,** 16452-16462.

Jiang, M., Zhang, M., Tang, D.G., Clemo, H.F., Liu, J., Holwitt, D., Kasirajan, V., Pond, A.L., Wettwer, E., Tseng, G.N., 2004. KCNE2 protein is expressed in ventricles of different species, and changes in its expression contribute to electrical remodeling in diseased hearts. *Circulation.* **109,** 1783-1788.

Johnson, W.B., Katugampola, S., Able, S., Napier, C., Harding, S.E., 2012. Profiling of cAMP and cGMP phosphodiesterases in isolated ventricular cardiomyocytes from human hearts: comparison with rat and guinea pig. *Life Sciences.* **90,** 328-336.

Jones, E.M., Roti Roti, E.C., Wang, J., Delfosse, S.A., Robertson, G.A., 2004. Cardiac IKr channels minimally comprise hERG 1a and 1b subunits. *The Journal of Biological Chemistry.* **279,** 44690-44694.

Jonsson, M.K., van der Heyden, M.A., van Veen, T.A., 2012. Deciphering hERG channels: molecular basis of the rapid component of the delayed rectifier potassium current. *Journal of Molecular and Cellular Cardiology.* **53,** 369-374.

Jost, N., Papp, J.G., Varro, A., 2007. Slow delayed rectifier potassium current (IKs) and the repolarization reserve. *Annals of Noninvasive Electrocardiology : The Official Journal of the International Society for Holter and Noninvasive Electrocardiology, Inc.* **12,** 64-78.

Kao, W.H., Arking, D.E., Post, W., Rea, T.D., Sotoodehnia, N., Prineas, R.J., Bishe, B., Doan, B.Q., Boerwinkle, E., Psaty, B.M., Tomaselli, G.F., Coresh, J., Siscovick, D.S., Marban, E., Spooner, P.M., Burke, G.L., Chakravarti, A., 2009. Genetic variations in nitric oxide synthase 1 adaptor protein are associated with sudden cardiac death in US white community-based populations. *Circulation.* **119,** 940-951.

Khan, S.A., Lee, K., Minhas, K.M., Gonzalez, D.R., Raju, S.V., Tejani, A.D., Li, D., Berkowitz, D.E., Hare, J.M., 2004. Neuronal nitric oxide synthase negatively regulates xanthine oxidoreductase inhibition of cardiac excitation-contraction coupling. *Proceedings of the National Academy of Sciences of the United States of America.* **101,** 15944-15948.

Kirstein, M., Rivet-Bastide, M., Hatem, S., Benardeau, A., Mercadier, J.J., Fischmeister, R., 1995. Nitric oxide regulates the calcium current in isolated human atrial myocytes. *The Journal of Clinical Investigation.* **95,** 794-802.

Knorr, A., Hirth-Dietrich, C., Alonso-Alija, C., Harter, M., Hahn, M., Keim, Y., Wunder, F., Stasch, J.P., 2008. Nitric oxide-independent activation of soluble guanylate cyclase by BAY 60-2770 in experimental liver fibrosis. *Arzneimittel-Forschung.* **58,** 71-80.

Koesling, D., 1999. Studying the structure and regulation of soluble guanylyl cyclase. *Methods (San Diego, Calif.).* **19,** 485-493.

Kotlo, K.U., Hesabi, B., Danziger, R.S., 2011. Implication of microRNAs in atrial natriuretic peptide and nitric oxide signaling in vascular smooth muscle cells. *American Journal of Physiology.Cell Physiology.* **301,** C929-37.

Kottenberg-Assenmacher, E., Weber, M., Kojda, G., 2003. The effect of hypercholesterolemia on platelet soluble guanylyl cyclase. *Vascular Pharmacology.* **40,** 141-147.

Krieg, T., Liu, Y., Rutz, T., Methner, C., Yang, X.M., Dost, T., Felix, S.B., Stasch, J.P., Cohen, M.V., Downey, J.M., 2009. BAY 58-2667, a nitric oxide-independent guanylyl cyclase activator, pharmacologically post-conditions rabbit and rat hearts. *European Heart Journal.* **30,** 1607-1613.

Krumenacker, J.S., Hanafy, K.A., Murad, F., 2004. Regulation of nitric oxide and soluble guanylyl cyclase. *Brain Research Bulletin.* **62,** 505-515.

Kumar, V., Martin, F., Hahn, M.G., Schaefer, M., Stamler, J.S., Stasch, J.P., van den Akker, F., 2013. Insights into BAY 60-2770 activation and S-nitrosylation-dependent desensitization of soluble guanylyl cyclase via crystal structures of homologous nostoc H-NOX domain complexes. *Biochemistry.* **52,** 3601-3608.

Kuo, H.C., Cheng, C.F., Clark, R.B., Lin, J.J., Lin, J.L., Hoshijima, M., Nguyen-Tran, V.T., Gu, Y., Ikeda, Y., Chu, P.H., Ross, J., Giles, W.R., Chien, K.R., 2001. A defect in the Kv channel-interacting protein 2 (KChIP2) gene leads to a complete loss of I(to) and confers susceptibility to ventricular tachycardia. *Cell.* **107,** 801-813.

Kupershmidt, S., Snyders, D.J., Raes, A., Roden, D.M., 1998. A K+ channel splice variant common in human heart lacks a C-terminal domain required for expression of rapidly activating delayed rectifier current. *The Journal of Biological Chemistry.* **273,** 27231-27235.

Lapp, H., Mitrovic, V., Franz, N., Heuer, H., Buerke, M., Wolfertz, J., Mueck, W., Unger, S., Wensing, G., Frey, R., 2009. Cinaciguat (BAY 58-2667) improves cardiopulmonary hemodynamics in patients with acute decompensated heart failure. *Circulation.* **119,** 2781-2788.

Larsen, A.P., Olesen, S.P., Grunnet, M., Jespersen, T., 2008. Characterization of hERG1a and hERG1b potassium channels-a possible role for hERG1b in the I (Kr) current. *Pflugers Archiv : European Journal of Physiology.* **456,** 1137-1148.

Lee, M.R., Li, L., Kitazawa, T., 1997. Cyclic GMP causes Ca2+ desensitization in vascular smooth muscle by activating the myosin light chain phosphatase. *The Journal of Biological Chemistry.* **272,** 5063-5068.

Lees-Miller, J.P., Kondo, C., Wang, L., Duff, H.J., 1997. Electrophysiological characterization of an alternatively processed ERG K+ channel in mouse and human hearts. *Circulation Research.* **81,** 719-726.

Levi, R.C., Alloatti, G., Penna, C., Gallo, M.P., 1994. Guanylate-cyclase-mediated inhibition of cardiac ICa by carbachol and sodium nitroprusside. *Pflugers Archiv : European Journal of Physiology.* **426,** 419-426.

Li, Y., Zaydman, M.A., Wu, D., Shi, J., Guan, M., Virgin-Downey, B., Cui, J., 2011. KCNE1 enhances phosphatidylinositol 4,5-bisphosphate (PIP2) sensitivity of IKs to modulate channel activity. *Proceedings of the National Academy of Sciences of the United States of America.* **108,** 9095-9100.

Lies, B., Groneberg, D., Gambaryan, S., Friebe, A., 2013. Lack of effect of ODQ does not exclude cGMP signalling via NO-sensitive guanylyl cyclase. *British Journal of Pharmacology.* **170,** 317-327.

Lima, B., Forrester, M.T., Hess, D.T., Stamler, J.S., 2010. S-nitrosylation in cardiovascular signaling. *Circulation Research.* **106,** 633-646.

Lincoln, T.M., Dills, W.L.,Jr, Corbin, J.D., 1977. Purification and subunit composition of guanosine 3':5'-monophosphate-dependent protein kinase from bovine lung. *The Journal of Biological Chemistry.* **252,** 4269-4275.

Liu, Y., Dillon, A.R., Tillson, M., Makarewich, C., Nguyen, V., Dell'Italia, L., Sabri, A.K., Rizzo, V., Tsai, E.J., 2013. Volume overload induces differential spatiotemporal regulation of myocardial soluble guanylyl cyclase in eccentric hypertrophy and heart failure. *Journal of Molecular and Cellular Cardiology.* **60,** 72-83.

Lokuta, A.J., Maertz, N.A., Meethal, S.V., Potter, K.T., Kamp, T.J., Valdivia, H.H., Haworth, R.A., 2005. Increased nitration of sarcoplasmic reticulum Ca2+-ATPase in human heart failure. *Circulation.* **111,** 988-995.

Loscalzo, J., 2013. The identification of nitric oxide as endothelium-derived relaxing factor. *Circulation Research.* **113,** 100-103.

Lu, M., Wang, X., Wang, W., 1998. Nitric oxide increases the activity of the apical 70-pS K+ channel in TAL of rat kidney. *The American Journal of Physiology.* **274,** F946-50.

Lu, Z., Kamiya, K., Opthof, T., Yasui, K., Kodama, I., 2001. Density and kinetics of I(Kr) and I(Ks) in guinea pig and rabbit ventricular myocytes explain different efficacy of I(Ks) blockade at high heart rate in guinea pig and rabbit: implications for arrhythmogenesis in humans. *Circulation.* **104,** 951-956.

Lu, Z., Xu, X., Hu, X., Lee, S., Traverse, J.H., Zhu, G., Fassett, J., Tao, Y., Zhang, P., dos Remedios, C., Pritzker, M., Hall, J.L., Garry, D.J., Chen, Y., 2010. Oxidative stress regulates left ventricular PDE5 expression in the failing heart. *Circulation.* **121,** 1474-1483.

Mahmoud, K.D., de Smet, B.J., Zijlstra, F., Rihal, C.S., Holmes, D.R.,Jr, 2011. Sudden cardiac death: epidemiology, circadian variation, and triggers. *Current Problems in Cardiology.* **36,** 56-80.

Marx, S.O., Kurokawa, J., Reiken, S., Motoike, H., D'Armiento, J., Marks, A.R., Kass, R.S., 2002. Requirement of a macromolecular signaling complex for beta adrenergic receptor modulation of the KCNQ1-KCNE1 potassium channel. *Science (New York, N.Y.).* **295,** 496-499.

Massion, P.B., Dessy, C., Desjardins, F., Pelat, M., Havaux, X., Belge, C., Moulin, P., Guiot, Y., Feron, O., Janssens, S., Balligand, J.L., 2004. Cardiomyocyte-restricted overexpression of endothelial nitric oxide synthase (NOS3) attenuates beta-adrenergic stimulation and reinforces vagal inhibition of cardiac contraction. *Circulation.* **110,** 2666-2672.

Matsuda, H. & Iyanagi, T., 1999. Calmodulin activates intramolecular electron transfer between the two flavins of neuronal nitric oxide synthase flavin domain. *Biochimica Et Biophysica Acta.* **1473,** 345-355.

Maurice, D.H., Palmer, D., Tilley, D.G., Dunkerley, H.A., Netherton, S.J., Raymond, D.R., Elbatarny, H.S., Jimmo, S.L., 2003. Cyclic nucleotide phosphodiesterase activity, expression, and targeting in cells of the cardiovascular system. *Molecular Pharmacology.* **64,** 533-546.

Mendes-Silverio, C.B., Leiria, L.O., Morganti, R.P., Anhe, G.F., Marcondes, S., Monica, F.Z., De Nucci, G., Antunes, E., 2012. Activation of haem-oxidized soluble guanylyl cyclase with BAY 60-2770 in human platelets lead to overstimulation of the cyclic GMP signaling pathway. *PloS One.* **7,** e47223.

Mery, P.F., Hove-Madsen, L., Chesnais, J.M., Hartzell, H.C., Fischmeister, R., 1996. Nitric oxide synthase does not participate in negative inotropic effect of acetylcholine in frog heart. *The American Journal of Physiology.* **270,** H1178-88.

Mery, P.F., Lohmann, S.M., Walter, U., Fischmeister, R., 1991. $Ca2+$ current is regulated by cyclic GMP-dependent protein kinase in mammalian cardiac myocytes. *Proceedings of the National Academy of Sciences of the United States of America.* **88,** 1197-1201.

Mery, P.F., Pavoine, C., Belhassen, L., Pecker, F., Fischmeister, R., 1993. Nitric oxide regulates cardiac $Ca2+$ current. Involvement of cGMP-inhibited and cGMP-stimulated phosphodiesterases through guanylyl cyclase activation. *The Journal of Biological Chemistry.* **268,** 26286-26295.

Mewe, M., Mauerhofer, M., Wulfsen, I., Szlachta, K., Zhou, X.B., Schwarz, J.R., Bauer, C.K., 2010. Modulation of cardiac ERG1 K(+) channels by cGMP signaling. *Journal of Molecular and Cellular Cardiology.* **49,** 48-57.

Miller, C.L. & Yan, C., 2010. Targeting cyclic nucleotide phosphodiesterase in the heart: therapeutic implications. *Journal of Cardiovascular Translational Research.* **3,** 507-515.

Miller, M.R. & Megson, I.L., 2007. Recent developments in nitric oxide donor drugs. *British Journal of Pharmacology.* **151,** 305-321.

Milstien, S. & Katusic, Z., 1999. Oxidation of tetrahydrobiopterin by peroxynitrite: implications for vascular endothelial function. *Biochemical and Biophysical Research Communications.* **263,** 681-684.

Missan, S., Zhabyeyev, P., Dyachok, O., Jones, S.E., McDonald, T.F., 2003. Block of cardiac delayed-rectifier and inward-rectifier K+ currents by nisoldipine. *British Journal of Pharmacology.* **140,** 863-870.

Moens, A.L., Champion, H.C., Claeys, M.J., Tavazzi, B., Kaminski, P.M., Wolin, M.S., Borgonjon, D.J., Van Nassauw, L., Haile, A., Zviman, M., Bedja, D., Wuyts, F.L., Elsaesser, R.S., Cos, P., Gabrielson, K.L., Lazzarino, G., Paolocci, N., Timmermans, J.P., Vrints, C.J., Kass, D.A., 2008. High-dose folic acid pretreatment blunts cardiac dysfunction during ischemia coupled to maintenance of high-energy phosphates and reduces postreperfusion injury. *Circulation.* **117,** 1810-1819.

Moens, A.L., Yang, R., Watts, V.L., Barouch, L.A., 2010. Beta 3-adrenoreceptor regulation of nitric oxide in the cardiovascular system. *Journal of Molecular and Cellular Cardiology.* **48,** 1088-1095.

Moniotte, S., Kobzik, L., Feron, O., Trochu, J.N., Gauthier, C., Balligand, J.L., 2001. Upregulation of beta(3)-adrenoceptors and altered contractile response to inotropic amines in human failing myocardium. *Circulation.* **103,** 1649-1655.

Monken, C.E. & Gill, G.N., 1980. Structural analysis of cGMP-dependent protein kinase using limited proteolysis. *The Journal of Biological Chemistry.* **255,** 7067-7070.

Monteiro, P.F., Morganti, R.P., Delbin, M.A., Calixto, M.C., Lopes-Pires, M.E., Marcondes, S., Zanesco, A., Antunes, E., 2012. Platelet hyperaggregability in high-fat fed rats: a role for intraplatelet reactive-oxygen species production. *Cardiovascular Diabetology.* **11,** 5-2840-11-5.

Morley, D. & Keefer, L.K., 1993. Nitric oxide/nucleophile complexes: a unique class of nitric oxide-based vasodilators. *Journal of Cardiovascular Pharmacology.* **22 Suppl 7,** S3-9.

Muller, J.E., Ludmer, P.L., Willich, S.N., Tofler, G.H., Aylmer, G., Klangos, I., Stone, P.H., 1987. Circadian variation in the frequency of sudden cardiac death. *Circulation.* **75,** 131-138.

Mungrue, I.N., Gros, R., You, X., Pirani, A., Azad, A., Csont, T., Schulz, R., Butany, J., Stewart, D.J., Husain, M., 2002. Cardiomyocyte overexpression of iNOS in mice results in peroxynitrite generation, heart block, and sudden death. *The Journal of Clinical Investigation.* **109,** 735-743.

Munzel, T., Daiber, A., Ullrich, V., Mulsch, A., 2005. Vascular consequences of endothelial nitric oxide synthase uncoupling for the activity and expression of the soluble guanylyl cyclase and the cGMP-dependent protein kinase. *Arteriosclerosis, Thrombosis, and Vascular Biology.* **25,** 1551-1557.

Nakamura, T.Y., Artman, M., Rudy, B., Coetzee, W.A., 1998. Inhibition of rat ventricular IK1 with antisense oligonucleotides targeted to Kir2.1 mRNA. *The American Journal of Physiology.* **274,** H892-900.

Nakane, M., Arai, K., Saheki, S., Kuno, T., Buechler, W., Murad, F., 1990. Molecular cloning and expression of cDNAs coding for soluble guanylate cyclase from rat lung. *The Journal of Biological Chemistry.* **265,** 16841-16845.

Nerbonne, J.M. & Kass, R.S., 2005. Molecular physiology of cardiac repolarization. *Physiological Reviews.* **85,** 1205-1253.

Ng, G.A., Brack, K.E., Patel, V.H., Coote, J.H., 2007. Autonomic modulation of electrical restitution, alternans and ventricular fibrillation initiation in the isolated heart. *Cardiovascular Research.* **73,** 750-760.

Niwa, N. & Nerbonne, J.M., 2010. Molecular determinants of cardiac transient outward potassium current (I(to)) expression and regulation. *Journal of Molecular and Cellular Cardiology.* **48,** 12-25.

Palmer, R.M., Ferrige, A.G., Moncada, S., 1987. Nitric oxide release accounts for the biological activity of endothelium-derived relaxing factor. *Nature.* **327,** 524-526.

Pokreisz, P., Vandenwijngaert, S., Bito, V., Van den Bergh, A., Lenaerts, I., Busch, C., Marsboom, G., Gheysens, O., Vermeersch, P., Biesmans, L., Liu, X., Gillijns, H., Pellens, M., Van Lommel, A., Buys, E., Schoonjans, L., Vanhaecke, J., Verbeken, E., Sipido, K., Herijgers, P., Bloch, K.D., Janssens, S.P., 2009. Ventricular phosphodiesterase-5 expression is increased in patients with advanced heart failure and contributes to adverse ventricular remodeling after myocardial infarction in mice. *Circulation.* **119,** 408-416.

Post, W., Shen, H., Damcott, C., Arking, D.E., Kao, W.H., Sack, P.A., Ryan, K.A., Chakravarti, A., Mitchell, B.D., Shuldiner, A.R., 2007. Associations between genetic variants in the NOS1AP (CAPON) gene and cardiac repolarization in the old order Amish. *Human Heredity.* **64,** 214-219.

Pourrier, M., Zicha, S., Ehrlich, J., Han, W., Nattel, S., 2003. Canine ventricular KCNE2 expression resides predominantly in Purkinje fibers. *Circulation Research.* **93,** 189-191.

Pyriochou, A. & Papapetropoulos, A., 2005. Soluble guanylyl cyclase: more secrets revealed. *Cellular Signalling.* **17,** 407-413.

Radicke, S., Cotella, D., Graf, E.M., Ravens, U., Wettwer, E., 2005. Expression and function of dipeptidyl-aminopeptidase-like protein 6 as a putative beta-

subunit of human cardiac transient outward current encoded by Kv4.3. *The Journal of Physiology.* **565,** 751-756.

Radomski, M.W., Palmer, R.M., Moncada, S., 1990. An L-arginine/nitric oxide pathway present in human platelets regulates aggregation. *Proceedings of the National Academy of Sciences of the United States of America.* **87,** 5193-5197.

Rameau, G.A., Chiu, L.Y., Ziff, E.B., 2004. Bidirectional regulation of neuronal nitric-oxide synthase phosphorylation at serine 847 by the N-methyl-D-aspartate receptor. *The Journal of Biological Chemistry.* **279,** 14307-14314.

Rapoport, R.M. & Murad, F., 1983. Agonist-induced endothelium-dependent relaxation in rat thoracic aorta may be mediated through cGMP. *Circulation Research.* **52,** 352-357.

Richie-Jannetta, R., Francis, S.H., Corbin, J.D., 2003. Dimerization of cGMP-dependent protein kinase Ibeta is mediated by an extensive amino-terminal leucine zipper motif, and dimerization modulates enzyme function. *The Journal of Biological Chemistry.* **278,** 50070-50079.

Rochais, F., Vandecasteele, G., Lefebvre, F., Lugnier, C., Lum, H., Mazet, J.L., Cooper, D.M., Fischmeister, R., 2004. Negative feedback exerted by cAMP-dependent protein kinase and cAMP phosphodiesterase on subsarcolemmal cAMP signals in intact cardiac myocytes: an in vivo study using adenovirus-mediated expression of CNG channels. *The Journal of Biological Chemistry.* **279,** 52095-52105.

Rosati, B., Dong, M., Cheng, L., Liou, S.R., Yan, Q., Park, J.Y., Shiang, E., Sanguinetti, M., Wang, H.S., McKinnon, D., 2008. Evolution of ventricular myocyte electrophysiology. *Physiological Genomics.* **35,** 262-272.

Rosati, B., Pan, Z., Lypen, S., Wang, H.S., Cohen, I., Dixon, J.E., McKinnon, D., 2001. Regulation of KChIP2 potassium channel beta subunit gene expression underlies the gradient of transient outward current in canine and human ventricle. *The Journal of Physiology.* **533,** 119-125.

Ross, G., Engel, P., Abdallah, Y., Kummer, W., Schluter, K.D., 2005. Tuberoinfundibular peptide of 39 residues: a new mediator of cardiac function via nitric oxide production in the rat heart. *Endocrinology.* **146,** 2221-2228.

Rozmaritsa, N., Christ, T., Van Wagoner, D.R., Haase, H., Stasch, J.P., Matschke, K., Ravens, U., 2014. Attenuated response of L-type calcium current to nitric oxide in atrial fibrillation. *Cardiovascular Research.* **101,** 533-542.

Ruetten, H., Dimmeler, S., Gehring, D., Ihling, C., Zeiher, A.M., 2005. Concentric left ventricular remodeling in endothelial nitric oxide synthase knockout mice by chronic pressure overload. *Cardiovascular Research.* **66,** 444-453.

Russwurm, M., Behrends, S., Harteneck, C., Koesling, D., 1998. Functional properties of a naturally occurring isoform of soluble guanylyl cyclase. *The Biochemical Journal.* **335 (Pt 1),** 125-130.

Sandirasegarane, L. & Diamond, J., 1999. The nitric oxide donors, SNAP and DEA/NO, exert a negative inotropic effect in rat cardiomyocytes which is independent of cyclic GMP elevation. *Journal of Molecular and Cellular Cardiology.* **31,** 799-808.

Sanguinetti, M.C., Curran, M.E., Zou, A., Shen, J., Spector, P.S., Atkinson, D.L., Keating, M.T., 1996. Coassembly of K(V)LQT1 and minK (IsK) proteins to form cardiac I(Ks) potassium channel. *Nature.* **384,** 80-83.

Sanguinetti, M.C., Jiang, C., Curran, M.E., Keating, M.T., 1995. A mechanistic link between an inherited and an acquired cardiac arrhythmia: HERG encodes the IKr potassium channel. *Cell.* **81,** 299-307.

Sanguinetti, M.C. & Mitcheson, J.S., 2005. Predicting drug-hERG channel interactions that cause acquired long QT syndrome. *Trends in Pharmacological Sciences.* **26,** 119-124.

Sanguinetti, M.C. & Tristani-Firouzi, M., 2006. hERG potassium channels and cardiac arrhythmia. *Nature.* **440,** 463-469.

Saraiva, R.M. & Hare, J.M., 2006. Nitric oxide signaling in the cardiovascular system: implications for heart failure. *Current Opinion in Cardiology.* **21,** 221-228.

Schmidt, H.H., Schmidt, P.M., Stasch, J.P., 2009. NO- and haem-independent soluble guanylate cyclase activators. *Handbook of Experimental Pharmacology.* **(191):309-39. doi,** 309-339.

Schmidt, P.M., Schramm, M., Schroder, H., Wunder, F., Stasch, J.P., 2004. Identification of residues crucially involved in the binding of the heme moiety of soluble guanylate cyclase. *The Journal of Biological Chemistry.* **279,** 3025-3032.

Schwartz, P.J. & Ackerman, M.J., 2013. The long QT syndrome: a transatlantic clinical approach to diagnosis and therapy. *European Heart Journal.* **34,** 3109-3116.

Schwartz, P.J., Priori, S.G., Cerrone, M., Spazzolini, C., Odero, A., Napolitano, C., Bloise, R., De Ferrari, G.M., Klersy, C., Moss, A.J., Zareba, W., Robinson, J.L., Hall, W.J., Brink, P.A., Toivonen, L., Epstein, A.E., Li, C., Hu, D., 2004. Left cardiac sympathetic denervation in the management of high-risk patients affected by the long-QT syndrome. *Circulation.* **109,** 1826-1833.

Schwartz, P.J., Snebold, N.G., Brown, A.M., 1976. Effects of unilateral cardiac sympathetic denervation on the ventricular fibrillation threshold. *The American Journal of Cardiology.* **37,** 1034-1040.

Schwartz, P.J., Spazzolini, C., Priori, S.G., Crotti, L., Vicentini, A., Landolina, M., Gasparini, M., Wilde, A.A., Knops, R.E., Denjoy, I., Toivonen, L., Monnig, G., Al-Fayyadh, M., Jordaens, L., Borggrefe, M., Holmgren, C., Brugada, P., De Roy, L., Hohnloser, S.H., Brink, P.A., 2010. Who are the long-QT syndrome patients who receive an implantable cardioverter-defibrillator and what happens to them?: data from the European Long-QT Syndrome Implantable Cardioverter-Defibrillator (LQTS ICD) Registry. *Circulation.* **122,** 1272-1282.

Seya, K., Motomura, S., Furukawa, K., 2007. Cardiac mitochondrial cGMP stimulates cytochrome c release. *Clinical Science (London, England : 1979).* **112,** 113-121.

Shimizu, K., Shintani, Y., Ding, W.G., Matsuura, H., Bamba, T., 2002. Potentiation of slow component of delayed rectifier K(+) current by cGMP via two distinct mechanisms: inhibition of phosphodiesterase 3 and activation of protein kinase G. *British Journal of Pharmacology.* **137,** 127-137.

Shinagawa, Y., Satoh, H., Noma, A., 2000. The sustained inward current and inward rectifier K+ current in pacemaker cells dissociated from rat sinoatrial node. *The Journal of Physiology.* **523 Pt 3,** 593-605.

Shiotani, M., Harada, T., Abe, J., Hamada, Y., Horii, I., 2008. Aging-related changes of QT and RR intervals in conscious guinea pigs. *Journal of Pharmacological and Toxicological Methods.* **57,** 23-29.

Soderling, S.H., Bayuga, S.J., Beavo, J.A., 1998. Identification and characterization of a novel family of cyclic nucleotide phosphodiesterases. *The Journal of Biological Chemistry.* **273,** 15553-15558.

Somlyo, A.P. & Somlyo, A.V., 1994. Signal transduction and regulation in smooth muscle. *Nature.* **372,** 231-236.

Song, T., Hatano, N., Horii, M., Tokumitsu, H., Yamaguchi, F., Tokuda, M., Watanabe, Y., 2004. Calcium/calmodulin-dependent protein kinase I inhibits neuronal nitric-oxide synthase activity through serine 741 phosphorylation. *FEBS Letters.* **570,** 133-137.

Stamler, J.S., 1994. Redox signaling: nitrosylation and related target interactions of nitric oxide. *Cell.* **78,** 931-936.

Stasch, J.P., Pacher, P., Evgenov, O.V., 2011. Soluble guanylate cyclase as an emerging therapeutic target in cardiopulmonary disease. *Circulation.* **123,** 2263-2273.

Stasch, J.P., Schmidt, P., Alonso-Alija, C., Apeler, H., Dembowsky, K., Haerter, M., Heil, M., Minuth, T., Perzborn, E., Pleiss, U., Schramm, M., Schroeder, W., Schroder, H., Stahl, E., Steinke, W., Wunder, F., 2002. NO- and haem-independent activation of soluble guanylyl cyclase: molecular basis and cardiovascular implications of a new pharmacological principle. *British Journal of Pharmacology.* **136,** 773-783.

Stoyanovsky, D., Murphy, T., Anno, P.R., Kim, Y.M., Salama, G., 1997. Nitric oxide activates skeletal and cardiac ryanodine receptors. *Cell Calcium.* **21,** 19-29.

Sun, J., Morgan, M., Shen, R.F., Steenbergen, C., Murphy, E., 2007. Preconditioning results in S-nitrosylation of proteins involved in regulation of mitochondrial energetics and calcium transport. *Circulation Research.* **101,** 1155-1163.

Sun, J. & Murphy, E., 2010. Protein S-nitrosylation and cardioprotection. *Circulation Research.* **106,** 285-296.

Sun, J., Picht, E., Ginsburg, K.S., Bers, D.M., Steenbergen, C., Murphy, E., 2006. Hypercontractile female hearts exhibit increased S-nitrosylation of the L-type Ca2+ channel alpha1 subunit and reduced ischemia/reperfusion injury. *Circulation Research.* **98,** 403-411.

Surks, H.K., 2007. cGMP-dependent protein kinase I and smooth muscle relaxation: a tale of two isoforms. *Circulation Research.* **101,** 1078-1080.

Surks, H.K., Mochizuki, N., Kasai, Y., Georgescu, S.P., Tang, K.M., Ito, M., Lincoln, T.M., Mendelsohn, M.E., 1999. Regulation of myosin phosphatase by a specific interaction with cGMP- dependent protein kinase Ialpha. *Science (New York, N.Y.).* **286,** 1583-1587.

Taglialatela, M., Pannaccione, A., Iossa, S., Castaldo, P., Annunziato, L., 1999. Modulation of the K(+) channels encoded by the human ether-a-gogo-related gene-1 (hERG1) by nitric oxide. *Molecular Pharmacology.* **56,** 1298-1308.

Takeda, N. & Maemura, K., 2011. Circadian clock and cardiovascular disease. *Journal of Cardiology.* **57,** 249-256.

Takimoto, E., 2012. Cyclic GMP-dependent signaling in cardiac myocytes. *Circulation Journal : Official Journal of the Japanese Circulation Society.* **76,** 1819-1825.

Takimoto, E., Champion, H.C., Belardi, D., Moslehi, J., Mongillo, M., Mergia, E., Montrose, D.C., Isoda, T., Aufiero, K., Zaccolo, M., Dostmann, W.R., Smith, C.J., Kass, D.A., 2005. cGMP catabolism by phosphodiesterase 5A regulates cardiac adrenergic stimulation by NOS3-dependent mechanism. *Circulation Research.* **96,** 100-109.

Takimoto, E., Champion, H.C., Li, M., Ren, S., Rodriguez, E.R., Tavazzi, B., Lazzarino, G., Paolocci, N., Gabrielson, K.L., Wang, Y., Kass, D.A., 2005. Oxidant stress from nitric oxide synthase-3 uncoupling stimulates cardiac pathologic remodeling from chronic pressure load. *The Journal of Clinical Investigation.* **115,** 1221-1231.

Tamargo, J., Caballero, R., Gomez, R., Delpon, E., 2010. Cardiac electrophysiological effects of nitric oxide. *Cardiovascular Research.* **87,** 593-600.

Tamargo, J., Duarte, J., Caballero, R., Delpon, E., 2010. Cinaciguat, a soluble guanylate cyclase activator for the potential treatment of acute heart failure. *Current Opinion in Investigational Drugs (London, England : 2000).* **11,** 1039-1047.

Tomas, M., Napolitano, C., De Giuli, L., Bloise, R., Subirana, I., Malovini, A., Bellazzi, R., Arking, D.E., Marban, E., Chakravarti, A., Spooner, P.M., Priori, S.G., 2010. Polymorphisms in the NOS1AP gene modulate QT interval duration and risk of arrhythmias in the long QT syndrome. *Journal of the American College of Cardiology.* **55,** 2745-2752.

Towart, R., Linders, J.T., Hermans, A.N., Rohrbacher, J., van der Linde, H.J., Ercken, M., Cik, M., Roevens, P., Teisman, A., Gallacher, D.J., 2009. Blockade of the I(Ks) potassium channel: an overlooked cardiovascular liability in drug safety screening? *Journal of Pharmacological and Toxicological Methods.* **60,** 1-10.

Toyoda, F., Ueyama, H., Ding, W.G., Matsuura, H., 2006. Modulation of functional properties of KCNQ1 channel by association of KCNE1 and KCNE2. *Biochemical and Biophysical Research Communications.* **344,** 814-820.

Tristani-Firouzi, M. & Sanguinetti, M.C., 2003. Structural determinants and biophysical properties of HERG and KCNQ1 channel gating. *Journal of Molecular and Cellular Cardiology.* **35,** 27-35.

Trudeau, M.C., Warmke, J.W., Ganetzky, B., Robertson, G.A., 1995. HERG, a human inward rectifier in the voltage-gated potassium channel family. *Science (New York, N.Y.).* **269,** 92-95.

Tsai, E.J. & Kass, D.A., 2009. Cyclic GMP signaling in cardiovascular pathophysiology and therapeutics. *Pharmacology & Therapeutics.* **122,** 216-238.

Tsai, E.J., Liu, Y., Koitabashi, N., Bedja, D., Danner, T., Jasmin, J.F., Lisanti, M.P., Friebe, A., Takimoto, E., Kass, D.A., 2012. Pressure-overload-induced subcellular relocalization/oxidation of soluble guanylyl cyclase in the heart modulates enzyme stimulation. *Circulation Research.* **110,** 295-303.

Uhler, M.D., 1993. Cloning and expression of a novel cyclic GMP-dependent protein kinase from mouse brain. *The Journal of Biological Chemistry.* **268,** 13586-13591.

Umar, S. & van der Laarse, A., 2010. Nitric oxide and nitric oxide synthase isoforms in the normal, hypertrophic, and failing heart. *Molecular and Cellular Biochemistry.* **333,** 191-201.

Valdeolmillos, M., O'Neill, S.C., Smith, G.L., Eisner, D.A., 1989. Calcium-induced calcium release activates contraction in intact cardiac cells. *Pflugers Archiv : European Journal of Physiology.* **413,** 676-678.

Van Wagoner, D.R., Pond, A.L., McCarthy, P.M., Trimmer, J.S., Nerbonne, J.M., 1997. Outward K+ current densities and Kv1.5 expression are reduced in chronic human atrial fibrillation. *Circulation Research.* **80,** 772-781.

Vandecasteele, G., Eschenhagen, T., Fischmeister, R., 1998. Role of the NO-cGMP pathway in the muscarinic regulation of the L-type Ca2+ current in human atrial myocytes. *The Journal of Physiology.* **506 (Pt 3),** 653-663.

Vandenberg, J.I., Torres, A.M., Campbell, T.J., Kuchel, P.W., 2004. The HERG K+ channel: progress in understanding the molecular basis of its unusual gating kinetics. *European Biophysics Journal : EBJ.* **33,** 89-97.

Varro, A., Lathrop, D.A., Hester, S.B., Nanasi, P.P., Papp, J.G., 1993. Ionic currents and action potentials in rabbit, rat, and guinea pig ventricular myocytes. *Basic Research in Cardiology.* **88,** 93-102.

Vila-Petroff, M.G., Younes, A., Egan, J., Lakatta, E.G., Sollott, S.J., 1999. Activation of distinct cAMP-dependent and cGMP-dependent pathways by nitric oxide in cardiac myocytes. *Circulation Research.* **84,** 1020-1031.

Vincent, G.M., Schwartz, P.J., Denjoy, I., Swan, H., Bithell, C., Spazzolini, C., Crotti, L., Piippo, K., Lupoglazoff, J.M., Villain, E., Priori, S.G., Napolitano, C., Zhang, L., 2009. High efficacy of beta-blockers in long-QT syndrome type 1: contribution of noncompliance and QT-prolonging drugs to the occurrence of beta-blocker treatment "failures". *Circulation.* **119,** 215-221.

Voors, A.A. & van Veldhuisen, D.J., 2012. Why do drugs for acute heart failure fail? *European Journal of Heart Failure.* **14,** 955-956.

Wahler, G.M. & Dollinger, S.J., 1995. Nitric oxide donor SIN-1 inhibits mammalian cardiac calcium current through cGMP-dependent protein kinase. *The American Journal of Physiology.* **268,** C45-54.

Wang, H., Kohr, M.J., Traynham, C.J., Wheeler, D.G., Janssen, P.M., Ziolo, M.T., 2008. Neuronal nitric oxide synthase signaling within cardiac myocytes targets phospholamban. *American Journal of Physiology.Cell Physiology.* **294,** C1566-75.

Wang, H., Kohr, M.J., Wheeler, D.G., Ziolo, M.T., 2008. Endothelial nitric oxide synthase decreases beta-adrenergic responsiveness via inhibition of the L-type Ca2+ current. *American Journal of Physiology.Heart and Circulatory Physiology.* **294,** H1473-80.

Wang, H., Yan, Z., Yang, S., Cai, J., Robinson, H., Ke, H., 2008. Kinetic and structural studies of phosphodiesterase-8A and implication on the inhibitor selectivity. *Biochemistry.* **47,** 12760-12768.

Wang, Q., Curran, M.E., Splawski, I., Burn, T.C., Millholland, J.M., VanRaay, T.J., Shen, J., Timothy, K.W., Vincent, G.M., de Jager, T., Schwartz, P.J., Toubin, J.A., Moss, A.J., Atkinson, D.L., Landes, G.M., Connors, T.D., Keating, M.T., 1996. Positional cloning of a novel potassium channel gene: KVLQT1 mutations cause cardiac arrhythmias. *Nature Genetics.* **12,** 17-23.

Wang, S., Xu, D.J., Cai, J.B., Huang, Y.Z., Zou, J.G., Cao, K.J., 2009. Rapid component I(Kr) of cardiac delayed rectifier potassium currents in guinea-pig is inhibited by alpha(1)-adrenoreceptor activation via protein kinase A and protein kinase C-dependent pathways. *European Journal of Pharmacology.* **608,** 1-6.

Wang, Y., Wagner, M.B., Joyner, R.W., Kumar, R., 2000. cGMP-dependent protein kinase mediates stimulation of L-type calcium current by cGMP in rabbit atrial cells. *Cardiovascular Research.* **48,** 310-322.

Wang, Y.G., Rechenmacher, C.E., Lipsius, S.L., 1998. Nitric oxide signaling mediates stimulation of L-type Ca2+ current elicited by withdrawal of acetylcholine in cat atrial myocytes. *The Journal of General Physiology.* **111,** 113-125.

Wang, Z., Feng, J., Shi, H., Pond, A., Nerbonne, J.M., Nattel, S., 1999. Potential molecular basis of different physiological properties of the transient outward K+ current in rabbit and human atrial myocytes. *Circulation Research.* **84,** 551-561.

Wedel, B., Harteneck, C., Foerster, J., Friebe, A., Schultz, G., Koesling, D., 1995. Functional domains of soluble guanylyl cyclase. *The Journal of Biological Chemistry.* **270,** 24871-24875.

Wedel, B., Humbert, P., Harteneck, C., Foerster, J., Malkewitz, J., Bohme, E., Schultz, G., Koesling, D., 1994. Mutation of His-105 in the beta 1 subunit yields a nitric oxide-insensitive form of soluble guanylyl cyclase. *Proceedings of the National Academy of Sciences of the United States of America.* **91,** 2592-2596.

Wernet, W., Flockerzi, V., Hofmann, F., 1989. The cDNA of the two isoforms of bovine cGMP-dependent protein kinase. *FEBS Letters.* **251,** 191-196.

West, M.B., Rokosh, G., Obal, D., Velayutham, M., Xuan, Y.T., Hill, B.G., Keith, R.J., Schrader, J., Guo, Y., Conklin, D.J., Prabhu, S.D., Zweier, J.L., Bolli, R., Bhatnagar, A., 2008. Cardiac myocyte-specific expression of inducible nitric oxide synthase protects against ischemia/reperfusion injury by preventing mitochondrial permeability transition. *Circulation.* **118,** 1970-1978.

Willich, S.N., Goldberg, R.J., Maclure, M., Perriello, L., Muller, J.E., 1992. Increased onset of sudden cardiac death in the first three hours after awakening. *The American Journal of Cardiology.* **70,** 65-68.

Wilson, E.M. & Chinkers, M., 1995. Identification of sequences mediating guanylyl cyclase dimerization. *Biochemistry.* **34,** 4696-4701.

Wu, X., Somlyo, A.V., Somlyo, A.P., 1996. Cyclic GMP-dependent stimulation reverses G-protein-coupled inhibition of smooth muscle myosin light chain phosphate. *Biochemical and Biophysical Research Communications.* **220,** 658-663.

Xu, K.Y., Huso, D.L., Dawson, T.M., Bredt, D.S., Becker, L.C., 1999. Nitric oxide synthase in cardiac sarcoplasmic reticulum. *Proceedings of the National Academy of Sciences of the United States of America.* **96,** 657-662.

Xu, L., Eu, J.P., Meissner, G., Stamler, J.S., 1998. Activation of the cardiac calcium release channel (ryanodine receptor) by poly-S-nitrosylation. *Science (New York, N.Y.).* **279,** 234-237.

Yamashita, T., Sekiguchi, A., Iwasaki, Y.K., Sagara, K., Iinuma, H., Hatano, S., Fu, L.T., Watanabe, H., 2003. Circadian variation of cardiac K+ channel gene expression. *Circulation.* **107,** 1917-1922.

Yu, H., Wu, J., Potapova, I., Wymore, R.T., Holmes, B., Zuckerman, J., Pan, Z., Wang, H., Shi, W., Robinson, R.B., El-Maghrabi, M.R., Benjamin, W., Dixon, J., McKinnon, D., Cohen, I.S., Wymore, R., 2001. MinK-related peptide 1: A beta subunit for the HCN ion channel subunit family enhances expression and speeds activation. *Circulation Research.* **88,** E84-7.

Yuen, P.S., Potter, L.R., Garbers, D.L., 1990. A new form of guanylyl cyclase is preferentially expressed in rat kidney. *Biochemistry.* **29,** 10872-10878.

Zaccolo, M. & Movsesian, M.A., 2007. cAMP and cGMP signaling cross-talk: role of phosphodiesterases and implications for cardiac pathophysiology. *Circulation Research.* **100,** 1569-1578.

Zannad, F., De Ferrari, G.M., Tuinenburg, A.E., Wright, D., Brugada, J., Butter, C., Klein, H., Stolen, C., Meyer, S., Stein, K.M., Ramuzat, A., Schubert, B., Daum, D., Neuzil, P., Botman, C., Caste, M.A., D'Onofrio, A., Solomon, S.D., Wold, N., Ruble, S.B., 2014. Chronic vagal stimulation for the treatment of low ejection fraction heart failure: results of the neural cardiac therapy for heart failure (NECTAR-HF) randomized controlled trial. *European Heart Journal.*

Zhang, M., Jiang, M., Tseng, G.N., 2001. minK-related peptide 1 associates with Kv4.2 and modulates its gating function: potential role as beta subunit of cardiac transient outward channel? *Circulation Research.* **88,** 1012-1019.

Zhang, M. & Kass, D.A., 2011. Phosphodiesterases and cardiac cGMP: evolving roles and controversies. *Trends in Pharmacological Sciences.* **32,** 360-365.

Zhang, M., Wang, Y., Jiang, M., Zankov, D.P., Chowdhury, S., Kasirajan, V., Tseng, G.N., 2012. KCNE2 protein is more abundant in ventricles than in atria and can accelerate hERG protein degradation in a phosphorylation-dependent manner. *American Journal of Physiology.Heart and Circulatory Physiology.* **302,** H910-22.

Zhang, P., Xu, X., Hu, X., van Deel, E.D., Zhu, G., Chen, Y., 2007. Inducible nitric oxide synthase deficiency protects the heart from systolic overload-induced ventricular hypertrophy and congestive heart failure. *Circulation Research.* **100,** 1089-1098.

Zhang, Y.H., Jin, C.Z., Jang, J.H., Wang, Y., 2014. Molecular mechanisms of neuronal nitric oxide synthase in cardiac function and pathophysiology. *The Journal of Physiology.* **592,** 3189-3200.

Zhao, M., Sun, L., Liu, J.J., Wang, H., Miao, Y., Zang, W.J., 2012. Vagal nerve modulation: a promising new therapeutic approach for cardiovascular diseases. *Clinical and Experimental Pharmacology & Physiology.* **39,** 701-705.

Zhao, Y., Brandish, P.E., Di Valentin, M., Schelvis, J.P., Babcock, G.T., Marletta, M.A., 2000. Inhibition of soluble guanylate cyclase by ODQ. *Biochemistry.* **39,** 10848-10854.

Zhou, L., Zhang, P., Cheng, Z., Hao, W., Wang, R., Fang, Q., Cao, J.M., 2011. Altered circadian rhythm of cardiac beta3-adrenoceptor activity following myocardial infarction in the rat. *Basic Research in Cardiology.* **106,** 37-50.

Zhou, L. & Zhu, D.Y., 2009. Neuronal nitric oxide synthase: structure, subcellular localization, regulation, and clinical implications. *Nitric Oxide : Biology and Chemistry / Official Journal of the Nitric Oxide Society.* **20,** 223-230.

Zhou, Z., Gong, Q., Ye, B., Fan, Z., Makielski, J.C., Robertson, G.A., January, C.T., 1998. Properties of HERG channels stably expressed in HEK 293 cells studied at physiological temperature. *Biophysical Journal.* **74,** 230-241.

Zicha, S., Moss, I., Allen, B., Varro, A., Papp, J., Dumaine, R., Antzelevich, C., Nattel, S., 2003. Molecular basis of species-specific expression of repolarizing K+ currents in the heart. *American Journal of Physiology.Heart and Circulatory Physiology.* **285,** H1641-9.

Ziolo, M.T., 2008. The fork in the nitric oxide road: cyclic GMP or nitrosylation? *Nitric Oxide : Biology and Chemistry / Official Journal of the Nitric Oxide Society.* **18,** 153-156.

Ziolo, M.T., Kohr, M.J., Wang, H., 2008. Nitric oxide signaling and the regulation of myocardial function. *Journal of Molecular and Cellular Cardiology.* **45,** 625-632.

Zobel, C., Cho, H.C., Nguyen, T.T., Pekhletski, R., Diaz, R.J., Wilson, G.J., Backx, P.H., 2003. Molecular dissection of the inward rectifier potassium current (IK1) in rabbit cardiomyocytes: evidence for heteromeric co-assembly of Kir2.1 and Kir2.2. *The Journal of Physiology.* **550,** 365-372.

Zou, M.H., Shi, C., Cohen, R.A., 2002. Oxidation of the zinc-thiolate complex and uncoupling of endothelial nitric oxide synthase by peroxynitrite. *The Journal of Clinical Investigation.* **109,** 817-826.